

Pharmacological treatments for osteoarthritis

Emerging therapeutic strategies targeting
chondrocyte hypertrophy and inflammation

Mauricio Nicolás Ferrao Blanco

Colofon

ISBN: 978-94-6458-613-8

Copyright © Mauricio Nicolás Ferrao Blanco, 2022

All rights reserved. No part of this thesis may be reproduced, stored in retrieval system or transmitted in any form by any means, without the permission of the author, or when appropriate, of the publisher of the represented published articles.

This research was financially supported by the European Union's Horizon 2020 Research and Innovation program under the Marie Skłodowska-Curie grant agreement no. 7421432 (CarBon) and the Reumafonds under agreement 18-1-202.

Bookdesign/lay-out: Mauricio N. Ferrao Blanco, Marcella van Hoolwerff

Printed by: Ridderprint

Printing of this thesis was financially supported by

Erasmus University Rotterdam

Medical Delta



Pharmacological Treatments for Osteoarthritis

Emerging therapeutic strategies targeting chondrocyte hypertrophy and inflammation

Farmacologische behandeling van artrose

Opkomende therapeutische strategieën gericht op hypertrofie van de kraakbeencel en ontsteking

Thesis

to obtain the degree of Doctor from the
Erasmus University Rotterdam
by command of the
rector magnificus

Prof.dr. A.L. Bredenoord

and in accordance with the decision of the Doctorate Board.

The public defence shall be held on
Friday 28 October 2022 at 13.00 hrs

by

Mauricio Nicolás Ferrao Blanco
born in Salto, Uruguay

Doctoral Committee

Promotor Prof. dr. G.J.V.M. van Osch

Other members Prof. dr. R.W. Hendriks
 Prof. dr. P.M. van der Kraan
 Dr. J.N. Post

Co-promotor Dr. R. Narcisi

*A mis padres
and to every single person that has supported me on this journey*

*Soy porque somos
Ik ben omdat wij zijn
I am because we are*

Contents

Chapter 1	9
General introduction, thesis aim and outline	
Chapter 2	23
Effect of Inflammatory Signaling on Human Articular Chondrocyte Hypertrophy: Potential Involvement of Tissue Repair Macrophages	
Chapter 3	37
Intra-articular injection of triamcinolone acetonide sustains macrophage levels and aggravates osteophytosis during degenerative joint disease in mice	
Chapter 4	61
An integrated <i>in silico-in vitro</i> approach for identification of therapeutic drug targets for osteoarthritis	
Chapter 5	113
Pharmacologic inhibition of EPHA2 decreases inflammation and pathological endochondral ossification in osteoarthritis	
Chapter 6	145
Tyrosine kinases regulate chondrocyte hypertrophy: promising drug targets for osteoarthritis	
Chapter 7	167
General discussion	
Chapter 8	181
Summary	
Chapter 9	187
Appendices	
Nederlandse samenvatting	189
PhD portfolio	191
List of publications	193
Curriculum Vitae	194
Acknowledgements	195

Chapter 1

General introduction,
thesis aim
and outline

Introduction

Osteoarthritis (OA) is the most prevalent musculoskeletal disease worldwide, affecting over 300 million people in 2017 [1]. It is characterized by progressive degeneration of the articular joint, affecting mainly the hands, hips and knees. OA has a great impact on the patient's quality of life that could lead to chronic pain and disability, but also has a considerable economic burden [2]. Knowledge on the pathophysiology of OA is still evolving, from being viewed as a cartilage-limited disease to a multifactorial disease that affects the whole joint. Several factors have been reported to contribute to its clinical presentations, some of which are genetics [3], gender [4], joint mechanics [5, 6], overweight [7], inflammation [8] and age [9, 10]. Recent studies have highlighted the presence of multiple OA subgroups [11]. Disease progression in OA is usually slow; however, some patients manifest rapid disease progression leading to the precocious need for total joint replacement [12]. Identification of OA phenotypes has also been made according to the number of affected joints, biomechanical factors, genome-wide expression analysis and the presence of lesions in the subchondral bone [13, 14]. Moreover, profiles of patients can be defined according to their level of pain, functional disability and presence of comorbidities [15]. Despite its multifactorial origin, the pathological changes of the disease have common features that affect all joint structures, such as degradation of the articular cartilage, osteophyte formation, subchondral bone changes and synovial inflammation (figure 1) [16].

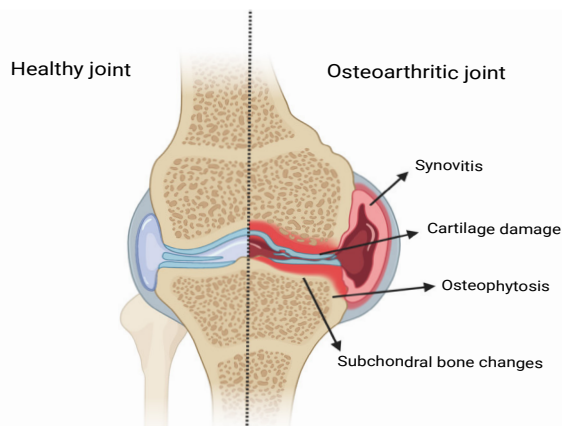


Figure 1 | Schematic representation of a healthy (left) and osteoarthritic (right) joint. Created with BioRender.com

Articular cartilage

Articular cartilage is a specialized connective tissue that provides a lubricated low-friction smooth surface to the joint [17]. It facilitates the transmission of loads and efficiency in movement. Articular cartilage is formed of a 2-4-millimeter-thick hyaline cartilage and, unlike most tissues, it has no nerves, blood and lymphatic vessels. The cellular component

of the tissue are the chondrocytes, cells of mesenchymal origin responsible for the synthesis of extracellular matrix (ECM) proteins [18]. The ECM is mainly composed of water, type-II collagen and proteoglycans. These proteins help to retain the water which is critical to maintain the cartilage mechanical properties [19]. Structurally, different zones have been described with respect to the depth from the articular surface with varying composition in its ECM content and organization [20]. In adult articular cartilage, chondrocytes are in a quiescent state, characterized by a low turnover of cartilage matrix proteins which is the key of cartilage homeostasis.

Endochondral ossification, in homeostasis and pathophysiology

Longitudinal bone development in children is govern by endochondral ossification, a process that takes places in a narrow piece of cartilage in the epiphysis of long bones, namely the growth plate [21]. This tissue is composed of a resting zone formed by skeletal stem progenitor cells that undergo chondrogenesis and provide a column of chondrocytes that form the proliferative and hypertrophic zones [22, 23]. Different from articular chondrocytes, growth plate chondrocytes are on a transition stage, actively undergoing proliferation and differentiation [24]. Hypertrophic differentiation of proliferative chondrocytes leads to the ECM degradation, calcification and vascularization, processes that have a critical role in bone formation [25]. Cell fate of hypertrophic chondrocytes is to either undergo apoptosis or dedifferentiate to a skeletal stem progenitor cell that can further give rise to osteoblasts, osteocytes or adipocytes [23, 26, 27]. This process underlies bone elongation during development and takes place until adolescence [28].

During OA, a gene expression profile similar to the hypertrophic cartilage of the growth plate is observed in the articular cartilage [29], such as upregulation of type X Collagen (*COL10A1*), run-related type II (*RUNX2*), alkaline phosphatase (*ALPL*) and matrix metalloproteinase 13 (*MMP13*). Recent single cell RNA sequencing studies performed in human OA cartilage have confirmed the presence of a distinct population of cells with a hypertrophic phenotype, even in the early stages when the cartilage is macroscopically intact [30, 31]. Given the occurrence of chondrocyte hypertrophy in early stages of osteoarthritis and the catabolic processes that they trigger in the hypertrophic zone of the growth plate, the changes related to hypertrophic differentiation in the articular cartilage are key in the development and the progression of osteoarthritis (figure 2) [32].

In a similar manner, endochondral ossification governs the formation of osseocartilaginous outgrowths at the joint margins, named osteophytes, a characteristic OA feature [33]. In this context, skeletal stem progenitor cells from the periosteum and synovium contribute to the formation of a cartilage template that further undergo hypertrophic differentiation and bone formation via endochondral ossification [34].

Synovium

The synovium is a major contributor to the composition of the synovial fluid. The synovial fluid nourishes chondrocytes, removes metabolites from the joint space and its viscosity provides lubrication [35]. The synovial membrane consists of a thin layer of cells, mainly tissue residence macrophages and fibroblasts, residing on a vascularized connective tissue [36]. Macrophages fulfill indispensable functions in tissue homeostasis and are crucially involved in tissue remodeling and repair in response to damage [37]. They are present in essentially every tissue of the body and provide homeostatic functions to the tissue of residence [38]. Tissue resident macrophages derived from cells that disperse into the tissues during embryonic development and are maintained within the tissue by local proliferation [39, 40]. Tissue resident macrophages in the synovium share many features with epithelial cells, as the expression of tight junction proteins, which provide a protective cellular barrier around the joint that hinders immune cell trafficking in a steady state [41].

Inflammatory microenvironment in the joint

Under inflammatory conditions or aging, blood monocytes can replace embryonic-derived macrophages [42]. Both, tissue resident and monocyte-derived macrophages are highly plastic cells that dynamically respond to changing environmental stimuli and can, therefore, be reprogrammed to varying polarization states [43]. To describe the difference in macrophage activation, a conceptual framework has been developed, which classifies macrophages into classically (M1) or alternatively (M2) activated cells [44]. M1 macrophages are associated with a pro-inflammatory phenotype while M2 with an anti-inflammatory phenotype, representing two polar extremes. These mononuclear phagocytes contribute to the pathogenesis of OA by the production of cytokines and catabolic enzymes, leading to chronic inflammation [45, 46]. The inflammatory microenvironment in the joint is also generated by other immune cells that are recruited to the synovium under inflammatory conditions, such as T cells, mast cells and neutrophils [47-50]. Moreover, articular chondrocytes express numerous cell surface receptors for cytokines, as well as Toll-like receptors. These are activated upon inflammatory stimuli [51-53] and in turn inflammatory factors are secreted by the chondrocytes, leading to a vicious loop of inflammatory signals [54]. Inflammation, that does not resolve becomes chronic and a major driver of OA [55, 56]. Perpetuation of inflammation leads to tissue damage, and vice versa, tissue damage can provoke inflammation. Even though multiple mechanisms normally ensure resolution, when an inflammatory response is either excessive or abnormal it can lead to a non-resolving state [57]. This situation is observed in OA patients, characterized by synovitis and effusion observed in magnetic resonance imaging (MRI), ultrasound or macroscopically as patients might feel it as a swollen joint [58-61].

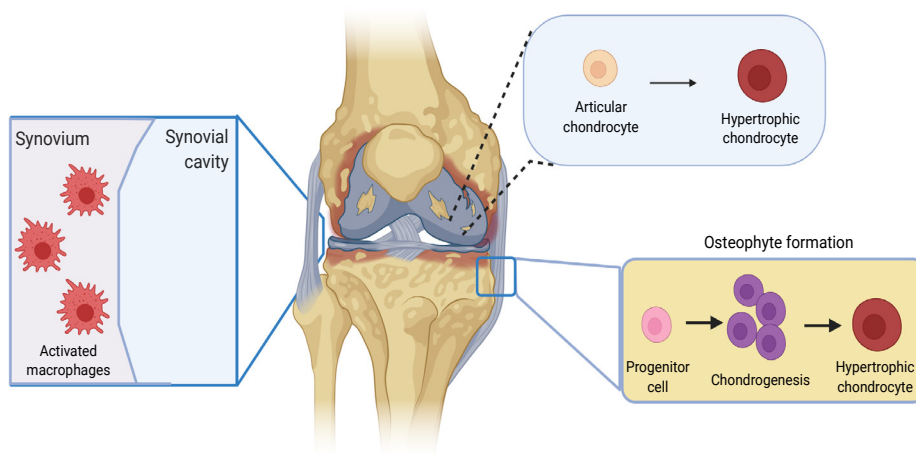


Figure 2 | Graphical representation of the knee of an OA patient. The boxes highlight biological processes occurring in the disease. Created with BioRender.com

Clinical management of OA

The clinical management of OA is complex mainly due to the etiological heterogeneity, individual patient preferences and comorbidities [62]. Several patients with OA have gastrointestinal and/or cardiovascular diseases, frailty, widespread pain and depression. Therefore, the Osteoarthritis Research Society International (OARSI) have developed guidelines to help clinicians to make treatment decisions for the management of OA [62]. These treatments are directed towards reducing joint pain, stiffness and physical disability while maintaining joint mobility and quality of life. When these interventions fail, total joint replacement may be considered. Even though OA is frequently stereotyped as a disease of the elderly, the median age at knee OA diagnosis is estimated to be 55 years [63]. Besides, most patients live with the disease through a large time of their lives, 26 years in average. Therefore, the selection of interventions demands a long-term efficacy and safety, which is not always achievable in such a heterogeneous disease.

First line core treatments are non-pharmacological and consist of exercise, dietary weight management, as well as arthritis education and self-care. Patients are encouraged to follow exercise programs focused on strengthening, cardio, balance and neuromuscular training [64].

Pharmacological therapy in OA

The available therapeutic medication attempts to relief OA symptoms, mainly attenuation of pain. A strong recommended pharmacotherapy is topical non-steroidal anti-inflammatory drugs (NSAIDs), as evidence shows modest benefits with minimal side effects [65]. In case of persistent pain, oral NSAIDs are recommended due to their benefits on pain and functional outcomes [66]. NSAIDs are associated with a heightened cardiovascular risk, therefore, the use of oral NSAIDs is contraindicated for patients with cardiovascular comorbidities [67, 68]. The use of oral or transdermal opioids is not of first choice due to the potential addiction posed by these medications [69, 70]. Intra-articular injections of corticosteroids and hyaluronic acid are conditionally recommended by the OARSI guidelines for knee OA as they provide short-term pain relief [62, 71, 72]. Because of the anti-inflammatory nature of NSAIDs and corticosteroids and its efficiency to reduce pain, it has been proposed that OA pain is linked to inflammation. Nevertheless, next to synovial inflammation, OA pain can originate from bone marrow lesions and alterations in central pain processing pathways have been demonstrated as well [73]. Moreover, robust evidence showing that NSAIDs and corticosteroids effectively decrease synovitis are lacking. Some reports even highlight a potential association of intra-articular corticosteroid treatment with accelerated structural progression of OA [74-76]. Besides, considering the cardiovascular and gastrointestinal risks of NSAIDs, more effective and safe medications are needed for the management of OA. Regulatory agencies worldwide, the Food and Drug Administration (FDA) and the European Medicines Agency (EMA), have pointed out that effective disease-modifying osteoarthritis drugs (DMOADs) should be developed, not merely symptom-relieving but that are able to modify the progression of OA and to prevent long-term disability [77].

Thus, there is an urgent need to discover DMOADs that can alleviate the development of OA.

Thesis aim and outline

The main objective of this thesis is to identify pharmacological targets for Osteoarthritis that will lead to DMOADs, targeting inflammation and chondrocyte hypertrophy. As described in the introduction, inflammation and hypertrophy are main drivers of OA pathogenesis. However, whether inflammation triggers hypertrophic differentiation of human chondrocytes is not clear. Therefore, in **Chapter 2** we evaluate how inflammatory signaling cues modulate chondrocyte hypertrophy. Corticosteroids are potent anti-inflammatory drugs currently used in clinical practice to relieve pain in OA patients. However, how these drugs modulate inflammation and chondrocyte hypertrophy is controversial. Therefore, in **Chapter 3** we investigate how intra-articular injection of the corticosteroid Triamcinolone Acetonide (TAA)

modulates inflammation and pathological endochondral ossification during OA progression *in vivo*.

Using the knowledge acquired in **Chapter 2-3**, we then focus on the discovery of pharmacological targets that could target inflammation and chondrocyte hypertrophy. Hence, in **Chapter 4**, we develop an *in silico* model of articular chondrocyte phenotype, that enables the high throughput testing of promising drug targets. Consequently, in **Chapter 5** we aim to discover a novel pharmacological target for OA, combining transcriptomic datasets, *in silico* (model developed in **Chapter 4**), *in vitro* and *in vivo* studies. Considering the biochemical properties of the target found in **Chapter 5**, in **Chapter 6** we review the role of tyrosine kinases in chondrocyte hypertrophy, as promising targets for OA.

This thesis ends with a general discussion, conclusion and future perspectives of the work presented (**Chapter 7**), followed by a summary in English and Dutch (**Chapter 8**).

References

1. Disease, G.B.D., I. Injury, and C. Prevalence, Global, regional, and national incidence, prevalence, and years lived with disability for 354 diseases and injuries for 195 countries and territories, 1990-2017: a systematic analysis for the Global Burden of Disease Study 2017. *Lancet*, 2018. 392(10159): p. 1789-1858.
2. Kloppenburg, M. and F. Berenbaum, Osteoarthritis year in review 2019: epidemiology and therapy. *Osteoarthritis Cartilage*, 2020. 28(3): p. 242-248.
3. Loughlin, J., Genetic contribution to osteoarthritis development: current state of evidence. *Curr Opin Rheumatol*, 2015. 27(3): p. 284-8.
4. O'Connor, M.I., Osteoarthritis of the hip and knee: sex and gender differences. *Orthop Clin North Am*, 2006. 37(4): p. 559-68.
5. Barr, A.J., et al., The relationship between three-dimensional knee MRI bone shape and total knee replacement-a case control study: data from the Osteoarthritis Initiative. *Rheumatology (Oxford)*, 2016. 55(9): p. 1585-93.
6. Neogi, T. and D.T. Felson, Osteoarthritis: Bone as an imaging biomarker and treatment target in OA. *Nat Rev Rheumatol*, 2016. 12(9): p. 503-4.
7. Felson, D.T., et al., Obesity and knee osteoarthritis. The Framingham Study. *Ann Intern Med*, 1988. 109(1): p. 18-24.
8. Houard, X., M.B. Goldring, and F. Berenbaum, Homeostatic mechanisms in articular cartilage and role of inflammation in osteoarthritis. *Curr Rheumatol Rep*, 2013. 15(11): p. 375.
9. Felson, D.T., et al., Osteoarthritis: new insights. Part 1: the disease and its risk factors. *Ann Intern Med*, 2000. 133(8): p. 635-46.
10. Zhang, Y. and J.M. Jordan, Epidemiology of osteoarthritis. *Clin Geriatr Med*, 2010. 26(3): p. 355-69.
11. Mobasheri, A., et al., Molecular taxonomy of osteoarthritis for patient stratification,

-
- disease management and drug development: biochemical markers associated with emerging clinical phenotypes and molecular endotypes. *Curr Opin Rheumatol*, 2019. 31(1): p. 80-89.
12. Raynauld, J.P., et al., Long term evaluation of disease progression through the quantitative magnetic resonance imaging of symptomatic knee osteoarthritis patients: correlation with clinical symptoms and radiographic changes. *Arthritis Res Ther*, 2006. 8(1): p. R21.
 13. Soul, J., et al., Stratification of knee osteoarthritis: two major patient subgroups identified by genome-wide expression analysis of articular cartilage. *Ann Rheum Dis*, 2018. 77(3): p. 423.
 14. Arden, N., et al., Can We Identify Patients with High Risk of Osteoarthritis Progression Who Will Respond to Treatment? A Focus on Biomarkers and Frailty. *Drugs Aging*, 2015. 32(7): p. 525-35.
 15. Steinberg, J., et al., Linking chondrocyte and synovial transcriptional profile to clinical phenotype in osteoarthritis. *Ann Rheum Dis*, 2021.
 16. Loeser, R.F., et al., Osteoarthritis: a disease of the joint as an organ. *Arthritis Rheum*, 2012. 64(6): p. 1697-707.
 17. Greene, G.W., et al., Adaptive mechanically controlled lubrication mechanism found in articular joints. *Proc Natl Acad Sci U S A*, 2011. 108(13): p. 5255-9.
 18. Goldring, M.B., Chondrogenesis, chondrocyte differentiation, and articular cartilage metabolism in health and osteoarthritis. *Ther Adv Musculoskelet Dis*, 2012. 4(4): p. 269-85.
 19. Poole, A.R., et al., Composition and structure of articular cartilage: a template for tissue repair. *Clin Orthop Relat Res*, 2001(391 Suppl): p. S26-33.
 20. Korhonen, R.K., et al., Importance of collagen orientation and depth-dependent fixed charge densities of cartilage on mechanical behavior of chondrocytes. *J Biomech Eng*, 2008. 130(2): p. 021003.
 21. Kronenberg, H.M., Developmental regulation of the growth plate. *Nature*, 2003. 423(6937): p. 332-6.
 22. Moss-Salentijn, L., et al., Morphological analysis and computer-aided, three dimensional reconstruction of chondrocytic columns in rabbit growth plates. *J Anat*, 1987. 151: p. 157-67.
 23. Mizuhashi, K., et al., Resting zone of the growth plate houses a unique class of skeletal stem cells. *Nature*, 2018. 563(7730): p. 254-258.
 24. Newton, P.T., et al., A radical switch in clonality reveals a stem cell niche in the epiphyseal growth plate. *Nature*, 2019. 567(7747): p. 234-238.
 25. Wuelling, M. and A. Vortkamp, Chondrocyte proliferation and differentiation. *Endocr Dev*, 2011. 21: p. 1-11.
 26. Long, J.T., et al., Hypertrophic chondrocytes serve as a reservoir for marrow-associated skeletal stem and progenitor cells, osteoblasts, and adipocytes during skeletal development. *Elife*, 2022. 11.

27. Yang, L., et al., Hypertrophic chondrocytes can become osteoblasts and osteocytes in endochondral bone formation. *Proc Natl Acad Sci U S A*, 2014. 111(33): p. 12097-102.
28. Hallett, S.A., et al., Chondrocytes in the resting zone of the growth plate are maintained in a Wnt-inhibitory environment. *Elife*, 2021. 10.
29. Singh, P., et al., Phenotypic instability of chondrocytes in osteoarthritis: on a path to hypertrophy. *Ann N Y Acad Sci*, 2019. 1442(1): p. 17-34.
30. Ji, Q., et al., Single-cell RNA-seq analysis reveals the progression of human osteoarthritis. *Ann Rheum Dis*, 2019. 78(1): p. 100-110.
31. Chou, C.H., et al., Synovial cell cross-talk with cartilage plays a major role in the pathogenesis of osteoarthritis. *Sci Rep*, 2020. 10(1): p. 10868.
32. van der Kraan, P.M. and W.B. van den Berg, Chondrocyte hypertrophy and osteoarthritis: role in initiation and progression of cartilage degeneration? *Osteoarthritis Cartilage*, 2012. 20(3): p. 223-32.
33. Gelse, K., et al., Osteophyte development--molecular characterization of differentiation stages. *Osteoarthritis Cartilage*, 2003. 11(2): p. 141-8.
34. Roelofs, A.J., et al., Identification of the skeletal progenitor cells forming osteophytes in osteoarthritis. *Ann Rheum Dis*, 2020. 79(12): p. 1625-1634.
35. Rhee, D.K., et al., The secreted glycoprotein lubricin protects cartilage surfaces and inhibits synovial cell overgrowth. *J Clin Invest*, 2005. 115(3): p. 622-31.
36. Culemann, S., et al., Locally renewing resident synovial macrophages provide a protective barrier for the joint. *Nature*, 2019. 572(7771): p. 670-675.
37. Wynn, T.A., A. Chawla, and J.W. Pollard, Macrophage biology in development, homeostasis and disease. *Nature*, 2013. 496(7446): p. 445-55.
38. Yosef, N., et al., The phenotypic and functional properties of mouse yolk-sac-derived embryonic macrophages. *Dev Biol*, 2018. 442(1): p. 138-154.
39. Gomez Perdiguero, E., et al., Tissue-resident macrophages originate from yolk-sac-derived erythro-myeloid progenitors. *Nature*, 2015. 518(7540): p. 547-51.
40. Sieweke, M.H. and J.E. Allen, Beyond stem cells: self-renewal of differentiated macrophages. *Science*, 2013. 342(6161): p. 1242974.
41. Buckley, C.D., Macrophages form a protective cellular barrier in joints. *Nature*, 2019. 572(7771): p. 590-592.
42. Gentek, R., K. Molawi, and M.H. Sieweke, Tissue macrophage identity and self-renewal. *Immunol Rev*, 2014. 262(1): p. 56-73.
43. Murray, P.J., et al., Macrophage activation and polarization: nomenclature and experimental guidelines. *Immunity*, 2014. 41(1): p. 14-20.
44. Biswas, S.K. and A. Mantovani, Macrophage plasticity and interaction with lymphocyte subsets: cancer as a paradigm. *Nat Immunol*, 2010. 11(10): p. 889-96.
45. Robinson, W.H., et al., Low-grade inflammation as a key mediator of the pathogenesis of osteoarthritis. *Nat Rev Rheumatol*, 2016. 12(10): p. 580-92.

-
46. Smith, M.D., et al., Synovial membrane inflammation and cytokine production in patients with early osteoarthritis. *J Rheumatol*, 1997. 24(2): p. 365-71.
 47. Kulkarni, P., et al., Mast Cells Differentiated in Synovial Fluid and Resident in Osteophytes Exalt the Inflammatory Pathology of Osteoarthritis. *Int J Mol Sci*, 2022. 23(1).
 48. Farinelli, L., et al., Synovial mast cells from knee and hip osteoarthritis: histological study and clinical correlations. *J Exp Orthop*, 2022. 9(1): p. 13.
 49. Zhu, W., et al., Alterations in peripheral T cell and B cell subsets in patients with osteoarthritis. *Clin Rheumatol*, 2020. 39(2): p. 523-532.
 50. de Lange-Brokaar, B.J., et al., Synovial inflammation, immune cells and their cytokines in osteoarthritis: a review. *Osteoarthritis Cartilage*, 2012. 20(12): p. 1484-99.
 51. Zhang, Q., et al., Differential Toll-like receptor-dependent collagenase expression in chondrocytes. *Ann Rheum Dis*, 2008. 67(11): p. 1633-41.
 52. Wang, Y., X. Zhao, and R. Liu-Bryan, Role of TLR2 and TLR4 in regulation of articular chondrocyte homeostasis. *Osteoarthritis Cartilage*, 2020. 28(5): p. 669-674.
 53. Webb, G.R., C.I. Westacott, and C.J. Elson, Chondrocyte tumor necrosis factor receptors and focal loss of cartilage in osteoarthritis. *Osteoarthritis Cartilage*, 1997. 5(6): p. 427-37.
 54. Abramson, S.B., et al., Nitric oxide and inflammatory mediators in the perpetuation of osteoarthritis. *Curr Rheumatol Rep*, 2001. 3(6): p. 535-41.
 55. Nathan, C. and A. Ding, Nonresolving inflammation. *Cell*, 2010. 140(6): p. 871-82.
 56. Serhan, C.N. and J. Savill, Resolution of inflammation: the beginning programs the end. *Nat Immunol*, 2005. 6(12): p. 1191-7.
 57. Buckley, C.D., et al., The resolution of inflammation. *Nat Rev Immunol*, 2013. 13(1): p. 59-66.
 58. Felson, D.T., et al., Synovitis and the risk of knee osteoarthritis: the MOST Study. *Osteoarthritis Cartilage*, 2016. 24(3): p. 458-64.
 59. Neogi, T., et al., Association of Joint Inflammation With Pain Sensitization in Knee Osteoarthritis: The Multicenter Osteoarthritis Study. *Arthritis Rheumatol*, 2016. 68(3): p. 654-61.
 60. Obotiba, A.D., et al., Synovitis and bone marrow lesions associate with symptoms and radiographic progression in hand osteoarthritis: a systematic review and meta-analysis of observational studies. *Osteoarthritis Cartilage*, 2021. 29(7): p. 946-955.
 61. Wang, X., et al., Associations Between Knee Effusion-synovitis and Joint Structural Changes in Patients with Knee Osteoarthritis. *J Rheumatol*, 2017. 44(11): p. 1644-1651.
 62. Bannuru, R.R., et al., OARSI guidelines for the non-surgical management of knee, hip, and polyarticular osteoarthritis. *Osteoarthritis Cartilage*, 2019. 27(11): p. 1578-1589.
 63. Losina, E., et al., Lifetime risk and age at diagnosis of symptomatic knee osteoarthritis in the US. *Arthritis Care Res (Hoboken)*, 2013. 65(5): p. 703-11.
 64. McAlindon, T.E., et al., OARSI guidelines for the non-surgical management of knee

osteoarthritis. *Osteoarthritis Cartilage*, 2014. 22(3): p. 363-88.

65. Underwood, M., et al., Topical or oral ibuprofen for chronic knee pain in older people. *The TOIB study. Health Technol Assess*, 2008. 12(22): p. iii-iv, ix-155.

66. da Costa, B.R., et al., Effectiveness of non-steroidal anti-inflammatory drugs for the treatment of pain in knee and hip osteoarthritis: a network meta-analysis. *Lancet*, 2017. 390(10090): p. e21-e33.

67. Mukherjee, D., S.E. Nissen, and E.J. Topol, Risk of cardiovascular events associated with selective COX-2 inhibitors. *JAMA*, 2001. 286(8): p. 954-9.

68. Trelle, S., et al., Cardiovascular safety of non-steroidal anti-inflammatory drugs: network meta-analysis. *BMJ*, 2011. 342: p. c7086.

69. Deveza, L.A., D.J. Hunter, and W.E. Van Spil, Too much opioid, too much harm. *Osteoarthritis Cartilage*, 2018. 26(3): p. 293-295.

70. Volkow, N.D. and A.T. McLellan, Opioid Abuse in Chronic Pain--Misconceptions and Mitigation Strategies. *N Engl J Med*, 2016. 374(13): p. 1253-63.

71. Juni, P., et al., Intra-articular corticosteroid for knee osteoarthritis. *Cochrane Database Syst Rev*, 2015(10): p. CD005328.

72. He, W.W., et al., Efficacy and safety of intraarticular hyaluronic acid and corticosteroid for knee osteoarthritis: A meta-analysis. *Int J Surg*, 2017. 39: p. 95-103.

73. Sofat, N., V. Ejindu, and P. Kiely, What makes osteoarthritis painful? The evidence for local and central pain processing. *Rheumatology (Oxford)*, 2011. 50(12): p. 2157-65.

74. Kompel, A.J., et al., Intra-articular Corticosteroid Injections in the Hip and Knee: Perhaps Not as Safe as We Thought? *Radiology*, 2019. 293(3): p. 656-663.

75. McAlindon, T.E., et al., Effect of Intra-articular Triamcinolone vs Saline on Knee Cartilage Volume and Pain in Patients With Knee Osteoarthritis: A Randomized Clinical Trial. *JAMA*, 2017. 317(19): p. 1967-1975.

76. Zeng, C., et al., Intra-articular corticosteroids and the risk of knee osteoarthritis progression: results from the Osteoarthritis Initiative. *Osteoarthritis Cartilage*, 2019. 27(6): p. 855-862.

77. Reginster, J.Y., et al., Recommendations for an update of the 2010 European regulatory guideline on clinical investigation of medicinal products used in the treatment of osteoarthritis and reflections about related clinically relevant outcomes: expert consensus statement. *Osteoarthritis Cartilage*, 2015. 23(12): p. 2086-2093.

Chapter 2

Effect of inflammatory signaling on human articular chondrocyte hypertrophy: potential involvement of tissue repair macrophages

Mauricio N. Ferrao Blanco ¹, Yvonne M. Bastiaansen-Jenniskens ¹, Mark G. Chambers ⁴, Andrew A. Pitsillides ⁵, Roberto Narcisi ¹, Gerjo J.V.M. van Osch ^{1,2,3}.

¹ Department of Orthopedics and Sports Medicine, Erasmus MC, University Medical Center Rotterdam, Rotterdam, The Netherlands

² Department of Otorhinolaryngology, Erasmus MC, University Medical Center Rotterdam, Rotterdam, The Netherlands

³ Department of Biomechanical Engineering, TU Delft, Delft, The Netherlands

⁴ Lilly Research Laboratories, Eli Lilly Pharmaceuticals, Indianapolis, USA

⁵ Comparative Biomedical Sciences, Royal Veterinary College, London, United Kingdom

Cartilage. 2021

DOI.10.1177/19476035211021907

Abstract

Objective: In osteoarthritis, chondrocytes tend to acquire a hypertrophic phenotype, which contributes to the modification of the extracellular matrix, resulting in permanent cartilage changes. In mouse chondrocytes, pro-inflammatory macrophages and pro-inflammatory cytokines have been shown to stimulate hypertrophy via the activation of the nuclear factor kappa B (NF κ B) pathway. Whether or not this also occurs in human chondrocytes remains unclear. We therefore aimed to investigate whether hypertrophy-like responses in human cartilage are driven mainly by intrinsic inflammatory signaling or shaped by specific macrophage populations.

Design: Human articular chondrocytes were cultured with pro-inflammatory cytokines or medium conditioned by defined macrophage subsets. Furthermore, the effect of inhibition of NF κ B-dependent gene expression was evaluated using the NF κ B inhibitor SC-514. Hypertrophy was assessed by measuring the transcription level of alkaline phosphatase (*ALPL*), type X collagen (*COL10A1*), Indian hedgehog (*IHH*) and runt-related transcription factor 2 (*RUNX2*).

Results: The expression of hypertrophic genes was not promoted in human chondrocytes by pro-inflammatory cytokines neither pro-inflammatory M(IFN γ +TNF α) macrophages. Inhibition of the NF κ B-dependent gene expression did not affect human articular chondrocyte hypertrophy. However, tissue repair M(IL4) macrophages induced hypertrophy by promoting the expression of *COL10A1*, *RUNX2* and *IHH*.

Conclusion: Intrinsic inflammatory signaling activation is not involved in the hypertrophic shift observed in human articular chondrocytes cultured *in vitro*. However, tissue repair macrophages may contribute to the onset of this detrimental phenotype in human osteoarthritic cartilage, given the effect observed in our experimental models.

Introduction

Osteoarthritis (OA) is characterised by progressive loss of articular cartilage, formation of osteophytes, degeneration of the ligaments and inflammation of the synovium. Even though significant progress has been made in OA research in recent years, advances are still needed to understand the molecular mechanisms of OA in order to develop therapeutic strategies. Articular chondrocytes are responsible for maintaining the balance between catabolic and anabolic processes in the cartilage. In OA, this homeostatic state is lost and chondrocytes acquire an altered phenotype, promoting the degradation of the cartilage and vascularization [1-3]. These hypertrophic-like chondrocytes are characterised by the expression of alkaline phosphatase (*ALPL*), type X collagen (*COL10A1*), Indian hedgehog (*IHH*), matrix metalloproteinase 13 (*MMP13*) and runt-related transcription factor 2 (*RUNX2*) [4, 5].

Increased attention has been paid to the inflammatory process in OA, not only in the symptomatology but also in the pathophysiology of disease initiation and progression [6, 7]. Interestingly, inflammatory signalling activation can direct mouse chondrocytes toward hypertrophic differentiation through the NFκB pathway, which has a major role in the progression of OA in mice models [8, 9]. Macrophages play a prominent role in the progression of OA and are the dominant leukocyte population in inflamed osteoarthritic synovium [10-12]. Macrophages are plastic cells that can acquire a pro- or anti-inflammatory phenotype, depending on environmental cues [13]. Pro-inflammatory macrophages induced the upregulation of catabolic enzymes in human articular chondrocytes [14] and have been shown to promote hypertrophy in mouse chondrocytes [15]. Here we sought to understand whether chondrocyte hypertrophic-like responses in human cartilage are driven mainly by intrinsic inflammatory signalling, as in mouse, or shaped by specific macrophage populations.

Methods

Cartilage explant and chondrocyte isolation

Human articular cartilage was obtained with implicit consent as waste material from patients undergoing total knee replacement surgery (9 females, 5 males, 67 ± 11 years). This protocol was approved by the medical ethical committee of the Erasmus MC, University Medical Center, Rotterdam, protocol number MEC-2004-322. Full thickness cartilage explants ($\varnothing = 5$ mm) were harvested from macroscopically intact areas and washed twice with 0.9% NaCl (Sigma Aldrich St. Louis, MO, USA). To isolate chondrocytes, cartilage chips were subjected to protease (2 mg/ml, Sigma Aldrich) for 2 hours followed by overnight digestion with 1.5 mg/ml collagenase B (Roche Diagnostics, Switzerland) in Dulbecco's Modified Eagle's Medium (DMEM) high glucose supplemented with 10% fetal bovine serum. Single cell suspension was obtained by filtrating the cellular solution by a 100 μ m filter. The isolated chondrocytes were expanded in monolayer at a seeding density of 7,500 cells/cm² in DMEM high glucose

supplemented with 10% fetal bovine serum, 50 µg/ml gentamicin and 1.5 µg/ml fungizone (Gibco, Grand Island, NY, USA). Upon approximately 80% confluency cells were trypsinised and reseeded at 7,500 cells/cm². Cells were used for experiments after three passages.

Preparation of macrophage conditioned medium (MCM)

Monocytes were isolated from two buffy coats (males, 54 and 58 years, Sanquin, Amsterdam, the Netherlands) using Ficoll (GE Healthcare, Little Chalfont, UK) density gradient separation and Cluster of Differentiation (CD)14 magnetic-activated cell sorting microbeads (MACS; Miltenyi, Bergisch Gladbach, Germany). To prepare MCM, monocytes were seeded in culture flasks at 500,000 monocytes/cm² and cultured in X-VIVO TM-15 (Lonza, Verviers, Belgium) containing 20% heat-inactivated fetal calf serum (FCS; Lonza), 50 µg/mL gentamicin (Gibco) and 1.5 µg/mL fungizone (Gibco) at 37°C and 5% CO₂. Monocytes were stimulated with 10 ng/mL Interferon-γ (IFNγ; PeproTech, Rocky Hill, NJ, USA) and 10 ng/mL Tumor Necrosis Factor-α (TNFα, PeproTech) to obtain pro-inflammatory M(IFNγ+TNFα) macrophages. Tissue repair M(IL-4) macrophages were obtained after stimulation with 10 ng/mL Interleukin-4 (IL-4; PeproTech) and anti-inflammatory M(IL-10) macrophages were acquired by stimulation with 10 ng/mL Interleukin (IL)-10 (PeproTech). After 72 hours, medium and stimuli were renewed and after 24 hours the medium was removed, the macrophages were washed twice with 0.9% NaCl and subsequently cultured in serum-free DMEM low glucose supplemented with 1% Insulin- Transferrin-Selenium (ITS premix, BD Biosciences, San Jose, CA, United States), 50 µg/mL gentamicin, 1.5 µg/mL fungizone and 25 µg/mL L-ascorbic acid 2-phosphate (Sigma Aldrich) to obtain MCM. After 24 hours, the MCM was harvested, centrifuged at 200 g and stored at -80°C until use. The media conditioned by M(IFNγ+TNFα), M(IL4), and M(IL10) macrophages were confirmed to contain a higher concentration of IL-6, CCL18, and sCD163, respectively (supplementary figure 1), in accordance with our previous work [16-19]. Non-conditioned DMEM low glucose supplemented with 1% ITS premix, 50 µg/mL gentamicin, 1.5 µg/mL fungizone and 25 µg/mL L-ascorbic acid 2-phosphate was also incubated, centrifuged, and frozen to serve as control medium. Cells were harvested for DNA quantification with a modified CyQUANT assay (Invitrogen, Carlsbad, CA, USA). All MCM used for culture and analysis were frozen and thawed once. For further experiments 50% of MCM or 50% non-conditioned medium was mixed with 50% fresh medium to replenish potentially depleted nutrients.

Exposure of chondrocytes and cartilage explants to inflammatory cytokines and macrophage condition medium

In order to select an inflammatory stimulus, passage three chondrocytes cultured in a six-well plate (BD Falcon, Bedford, MA, USA) at a seeding density of 20,000 cells/cm² were exposed to pro-inflammatory cytokines (IL1-β, TNF-α or IFN-γ) at 1 ng/mL and, alternatively, to a combination of the three cytokines, each at 0.1 ng/mL. The combination of pro-inflammatory

cytokines was selected based on a pilot experiment where nitric oxide was measured in the media as measurement of induction of inflammation (supplementary figure 2). Pro-inflammatory cytokines alone at 1 ng/mL did not significantly increase NO in the medium, which might be due to the basal NO production in OA chondrocytes.

In order to accommodate the likelihood that the acquisition of more fibroblast-like phenotype by these passage three chondrocytes may modify these responses, we examined behavior following redifferentiation. Briefly, redifferentiation of articular chondrocytes was performed using the well-established 3D alginate bead culture model [20], and confirmed by *COL2A1* expression. Moreover, our data shows that OA chondrocytes express the hypertrophic markers *COL10A1* and *RUNX2*, being a suitable model to study chondrocyte hypertrophy. For preparation of alginate beads, chondrocytes after three passages in monolayer were re-suspended in 1.2% (w/v) low viscosity alginate (Kelton LV alginate, Kelco Co, San Diego, CA, USA) in 0.9% NaCl (Sigma Aldrich) at a concentration of 4×10^6 cells/mL. Beads were made by dripping the cell-alginate suspension in 105 mM CaCl₂ (Sigma Aldrich) through a 22-gauge needle. Beads were washed with 0.9% NaCl and DMEM low glucose. Beads with a size that deviated from the average after a visual inspection were not included in the experiment. Redifferentiation of chondrocytes was performed in a 24-well plate (BD Falcon) for two weeks in 100 μ L/bead DMEM low glucose supplemented with 1% ITS fetal (Biosciences), 10 ng/ml transforming growth factor beta one (TGF β 1, recombinant human, R&D systems) 25 μ g/mL l-ascorbic acid 2-phosphate (Sigma Aldrich), 50 μ g/ml gentamicin, and 1.5 μ g/mL fungizone (both Gibco). After two weeks, TGF β 1 was no longer added to the medium and cells were either cultured with 10 μ M of the NF κ B inhibitor SC-514 (Cayman chemicals, Ann Arbor, MI, USA) for 24 hours or with the combination of pro-inflammatory cytokines TNF α , IFN γ , IL1 β at 0.1 ng/mL for one week, refreshing the medium twice.

Cartilage explants were cultured in DMEM low glucose supplemented with 1% ITS premix, 50 μ g/ml gentamicin and 1.5 μ g/ml fungizone and either a combination of pro-inflammatory cytokines TNF α , IFN γ , IL1 β at 0.1 ng/mL each or medium conditioned by macrophages during one week, refreshing the medium twice.

Nitric oxide (NO) assay

NO production was measured in the medium of OA chondrocytes by determining the content of nitrite using the Griess reagent (Sigma Aldrich). The reaction was monitored at 540 nm using a spectrophotometer (VersaMax; Molecular Devices, SunnyVale, USA). Sodium nitrite (NaNO₂; Chemlab, Zedelgem, Belgium) was used as standard.

Gene expression

Alginate beads were dissolved using citrate buffer, centrifuged at 200g and the pellet was resuspended in RLT (Qiagen, Hilden, Germany) buffer containing 1% beta-mercaptoethanol for RNA isolation. RNA was isolated from the cartilage explants by snap freezing in liquid

nitrogen followed by pulverization using a Mikro-Dismembrator (B. Braun Biotech International GmbH, Melsungen, Germany) at 2800 rpm. The tissue was homogenized with 18 μ L/ mg sample RNA-Bee TM (Tel-Test Inc., Friendswood, USA) and 20% chloroform. mRNA isolation was performed according to manufacturer's protocol utilizing the RNeasy Column system (Qiagen, Hilden, Germany). The RNA concentration was determined using a NanoDrop spectrophotometer (Isogen Life Science, Utrecht, the Netherlands). 0.5 μ g RNA was used for cDNA synthesis following the protocol of the manufacturer of the RevertAid First Strand cDNA kit (Thermo Fisher Scientific, Waltham, MA, United States). qPCR was performed on a Bio-Rad CFX96 Real-Time PCR Detection System (Bio-Rad) to assess gene expression, Alkaline phosphatase (*ALPL*; Fw: GACCCTTGACCCCCACAAT; Rev: GCTCGTACTGCATGTCCCCT; Probe: TGGACTACCTATTGGGTCTCTTCGAGCCA), Collagen type 2 (*COL2A1*; Fw: GGCAATAGCAGGTTACGTAC; Rev: CGATAACAGTCTTGCCCCACTT; Probe: CCGGTATGTTTCGTGCAGCCATCCT), Collagen type 10 (*COL10A1*; Fw: CAAGGCACCATCTCCAGGAA; Rev: AAAGGGTATTTGTGGCAGCATATT; Probe: TCCAGCACGCAGAATCCATCTGA), matrix metalloproteinase-13 (*MMP13*; Fw: AAGGAGCATGGCGACTTCT; Rev: TGGCCCAGGAGGAAAAGC; Probe: CCCTCTGGCCTGCGGCTCA), Runt-related transcription factor 2 (*RUNX2*; Fw: ACGTCCCCGTCCATCCA; Rev: TGGCAGTGTCATCATCTGAAATG; Probe: ACTGGGCTTCTGCCATCACCGA), Tumor Necrosis Factor- α (*TNFA*; Fw: GCCGCATCGCCGTCTCTAC; Rev: AGCGCTGAGTCGGTCACCCT). Indian hedgehog (*IHH*) primer was purchased as assays-on-demand from BioRad. Glyceraldehyde-3-phosphate dehydrogenase (*GAPDH*; Fw: ATGGGGAAGGTGAAGGTGC; Rev: TAAAAGCAGCCCTGGTGACC; Probe: CGCCAATACGACCAAATCCGTTGAC) was found stable and therefore used as reference gene. Data were analyzed by the $\Delta\Delta$ Ct method and normalized to the expression of *GAPDH* of each condition and compared to the corresponding gene expression in the control groups. Articular cartilage explants were divided in hypertrophic and non-hypertrophic donors based on the expression of the hypertrophic markers *COL10A1*, *RUNX2* and *IHH* in the basal – control condition, by using a cycle cutoff of 36. Donors with Cq of 36 or higher were classified as non-hypertrophic.

Statistics

Each experiment included at least 3 technical replicates and was repeated with cells/explants derived from at least 3 OA donors. Statistical evaluation was performed using IBM SPSS 22.0. The normal distribution of the data was confirmed using the Kolmogorov-Smirnov test. The linear mixed model was applied using the different conditions as fixed parameters and the donors as random factors.

Results

Pro-inflammatory cytokines did not promote hypertrophy in human chondrocytes *in vitro*

To study the effect of pro-inflammatory signalling activation on chondrocyte hypertrophy, we used a combination of inflammatory cytokines that are secreted by macrophages, IL1 β , TNF α and IFN γ and used two different models, human articular cartilage explants and human articular chondrocytes in alginate. Upon inflammatory stimulation, the expression of the catabolic enzyme *MMP13* was increased in cartilage explants and chondrocytes in alginate (Figure 1 A, B). Interestingly, the expression of the hypertrophic marker *COL10A1* was significantly decreased in both models. *RUNX2* was down-regulated in alginate upon cytokine addition and not detectable in explants. *IHH* and *ALPL* were not detectable in either of the models. To evaluate whether endogenous inflammation present in osteoarthritic chondrocytes influenced hypertrophy, the NF κ B inhibitor SC-514 was added to alginate cultures. SC-514 significantly decreased mRNA expression of the NF κ B-dependent gene *TNFA*, confirming its efficacy (Figure 1 C). However, NF κ B inhibition did not modify *COL10A1*, *RUNX2* nor *MMP13* expression, indicating that hypertrophy is not affected in osteoarthritic chondrocytes when the main inflammatory pathway is inhibited (Figure 1 D). The expression of *MMP13* is related

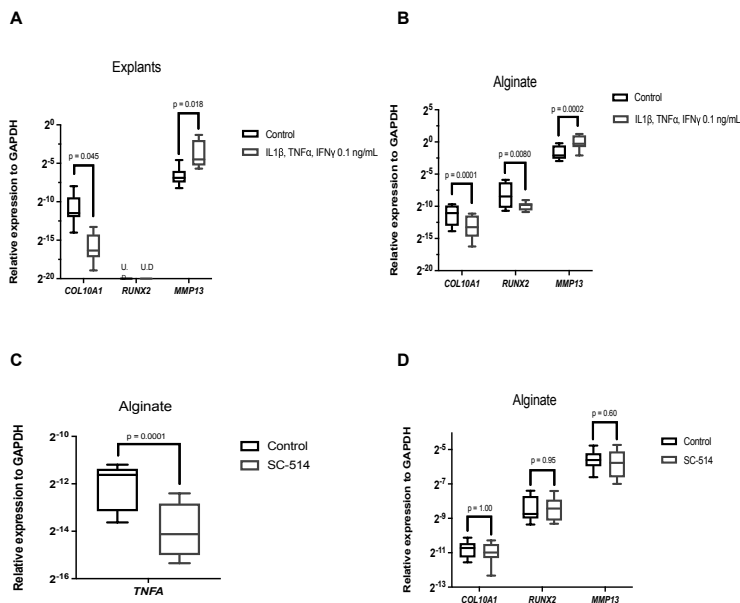


Figure 1 | Effect of pro-inflammatory signal activation in chondrocyte hypertrophy. (A) OA human cartilage explants and (B) chondrocytes encapsulated in alginate stimulated with the combination of the inflammatory cytokines at 0.1 ng/mL for one week (n=3 donors, 3 samples per donor). (C) and (D) OA human chondrocytes encapsulated in alginate cultured with the NF κ B inhibitor, SC-514 at 10 μ M for 24 hours (n=3 donors, 3 samples per donor). UD = Undetectable. Data is shown as Min to Max.

to hypertrophy and to inflammatory signalling in chondrocytes. The absence of an effect of SC-514 on *MMP13* expression thus suggests that *MMP13* in these osteoarthritic chondrocytes is regulated by other transcription factors such as β -Catenin [21, 22]. Summarizing, these data indicate that pro-inflammatory signaling did not stimulate a hypertrophic phenotype in human articular chondrocytes *in vitro*.

Tissue repair M(IL4) macrophages are associated to the onset of human chondrocyte hypertrophy *in vitro*

To better mimic the complex combination of inflammatory factors in the joint, the medium conditioned by different macrophage phenotypes was evaluated for its capacity to modulate chondrocyte hypertrophy. Medium conditioned by pro-inflammatory M(IFN γ +TNF α) or anti-inflammatory M(IL10) macrophages had no effect on expression of *COL10A1*, *RUNX2*, *IHH* nor *ALPL* in cartilage explants (Figure 2). Medium conditioned by tissue repair M(IL4) macrophages, however, significantly upregulated the expression of *COL10A1*, *RUNX2* and *IHH* in explants of two of the five experiments. These two were non-hypertrophic basally, but the remainder three exhibited basal hypertrophy. These data suggest that pro-inflammatory factors do not induce hypertrophic differentiation of human articular chondrocytes but factors secreted by tissue repair macrophages can induce hypertrophy.

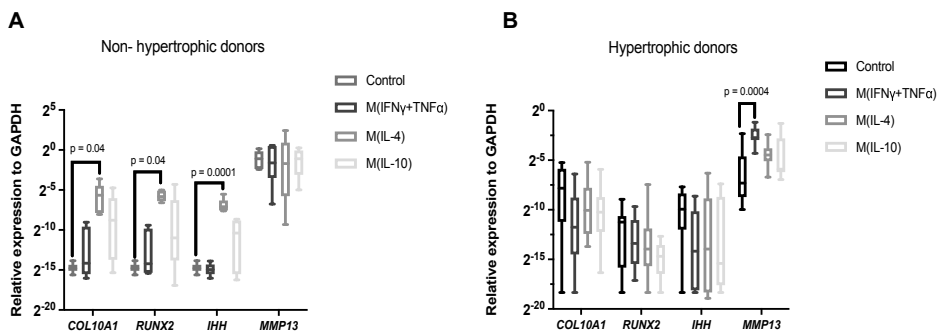


Figure 2 | Effect of macrophage secretome on chondrocyte hypertrophy. (A) Non-hypertrophic OA human cartilage explants stimulated with macrophage condition medium (n=2 donors, 3 samples per donor). (B) Hypertrophic OA human cartilage explants stimulated with macrophage condition medium (n=3 donors, 3 samples per donor) Data is shown as Min to Max. Articular cartilage explants were divided in hypertrophic and non-hypertrophic donors based on the expression of the hypertrophic markers *COL10A1*, *RUNX2* and *IHH* in the basal – control condition, by using a cycle cutoff of 36. Donors with Cq of 36 or higher were classified as non-hypertrophic.

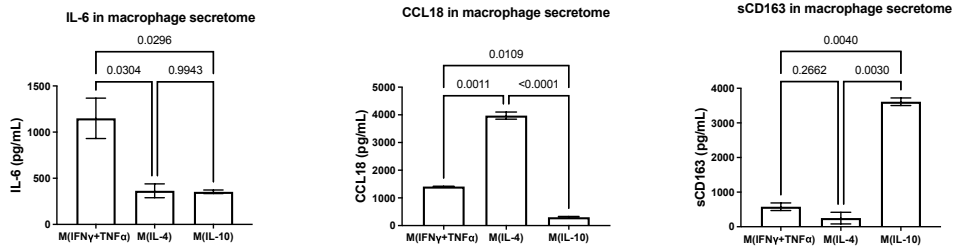
Discussion

Inflammation-induced hypertrophy is a process that has been suggested to play role in the progression of osteoarthritis, but current studies mainly focused on mouse chondrocytes [8, 9]. The findings of our study demonstrate that pro-inflammatory cytokines do not mediate the hypertrophic differentiation of human articular chondrocytes *in vitro*. Inflammatory processes in OA are mainly driven by macrophages, which generate a broad spectrum of cytokines and immune factors. Previous studies in mouse have shown that pro-inflammatory macrophages induced hypertrophy [15]. However, here we show that pro-inflammatory macrophages do not increase hypertrophy of human chondrocytes. In addition, although previous studies in mice chondrocytes have shown that the NF- κ B pathway is responsible for inflammation-induced hypertrophy [23], here we showed that inhibition of NF- κ B did not reduce hypertrophy in human osteoarthritic chondrocytes. These results indicate that, differently from murine chondrocytes, pro-inflammatory signalling cues do not unavoidably induce hypertrophy in human chondrocytes that have been isolated from osteoarthritic knee joints and subsequently maintained *in vitro*.

Macrophages can acquire different phenotypes depending on the environmental stimuli, hence secreting cytokines that lead to various responses in the tissue. Our data suggest that tissue repair macrophages can induce a phenotypic shift in articular chondrocytes towards a hypertrophy state. A limitation of our study is that the number of non-hypertrophic OA donors was low, probably due to the late stage of disease in the majority of OA donors that undergo total knee replacement. These donors had a higher basal MMP13 expression compared with the hypertrophic donors, which might suggest that they had a higher basal inflammatory state. Even though the numbers are low, this demonstrates a proof of principle that macrophages with tissue repair phenotype have the capacity to induce hypertrophy. Interestingly, this macrophage subset secretes the cytokine transforming growth factor beta (TGF β), which has been associated to hypertrophy in aging cartilage as well as in articular chondrocytes in culture [24, 25]. Current literature in the field suggests that M1, also known as pro-inflammatory macrophages are detrimental for the disease while M2, also known as anti-inflammatory & tissue repair macrophages might have a protective role, driving the joint to homeostasis [26]. Moreover, it has been suggested that drugs that alter macrophage phenotype from M1 to M2 would be an effective treatment for OA [27]. However, our findings suggest that not only pro-inflammatory, but also tissue repair macrophages contribute to chondrocyte catabolism.

Here we report that chondrocyte hypertrophy is not necessarily promoted in cultured human chondrocytes by pro-inflammatory signalling cues, as was observed in mice. Attention should be paid to the difference between human and murine chondrocytes when looking for disease modifying drugs, as hypertrophic differentiation might be differently regulated. Our data suggest that targeting tissue repair macrophages might be used as a therapy to inhibit hypertrophy of human chondrocytes.

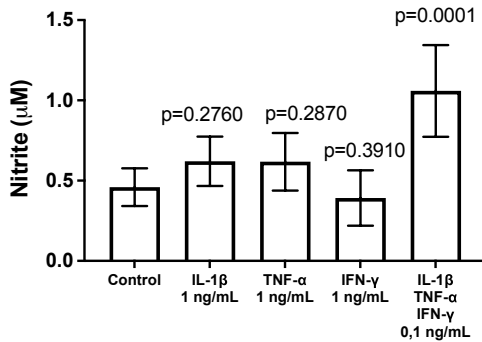
Supplementary figures



Supplementary figure 1 | Characterization of macrophage secretome. Interleukin (IL)- 6, C-C Motif Chemokine Ligand (CCL) 18 and soluble (s) Cluster of differentiation (CD) 163 quantified by enzyme-linked immunosorbent assay (ELISA) in the medium conditioned by monocyte-derived macrophages. Data is shown as mean \pm SD.

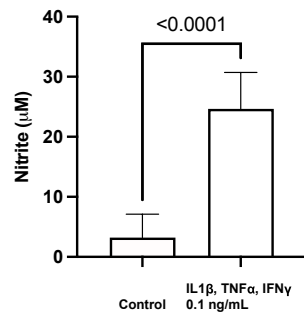
A

OA chondrocytes in 2D



B

OA chondrocytes in alginate



Supplementary figure 2 | Nitrite concentration in the medium of OA human chondrocytes in 2D (A) and in alginate (B) stimulated with pro-inflammatory cytokines for one week (n=3 donors, 3 samples per donor). Data is shown as mean \pm SD.

References

1. Ripmeester, E.G.J., et al., Recent Insights into the Contribution of the Changing Hypertrophic Chondrocyte Phenotype in the Development and Progression of Osteoarthritis. *Front Bioeng Biotechnol*, 2018. 6: p. 18.
2. Pesesse, L., et al., Consequences of chondrocyte hypertrophy on osteoarthritic cartilage: potential effect on angiogenesis. *Osteoarthritis Cartilage*, 2013. 21(12): p. 1913-23.
3. He, Y., et al., Type X collagen levels are elevated in serum from human osteoarthritis patients and associated with biomarkers of cartilage degradation and inflammation. *BMC Musculoskelet Disord*, 2014. 15: p. 309.
4. K. Von Der Mark, A.N., A. Kuss, G. Weseloh, K. Glückert, H. Stöss, Type X collagen synthesis in human osteoarthritic cartilage. Indication of chondrocyte hypertrophy. *Arthritis Rheum*, 1992. 35.
5. Aigner, T., et al., Type X collagen expression in osteoarthritic and rheumatoid articular cartilage. *Virchows Arch B Cell Pathol Incl Mol Pathol*, 1993. 63(4): p. 205-11.
6. Orita, S., et al., Associations between proinflammatory cytokines in the synovial fluid and radiographic grading and pain-related scores in 47 consecutive patients with osteoarthritis of the knee. *BMC Musculoskelet Disord*, 2011. 12: p. 144.
7. Spector, T.D., et al., Low-level increases in serum C-reactive protein are present in early osteoarthritis of the knee and predict progressive disease. *Arthritis Rheum*, 1997. 40(4): p. 723-7.
8. Saito, T., et al., Transcriptional regulation of endochondral ossification by HIF-2alpha during skeletal growth and osteoarthritis development. *Nat Med*, 2010. 16(6): p. 678-86.
9. Yang, S., et al., Hypoxia-inducible factor-2alpha is a catabolic regulator of osteoarthritic cartilage destruction. *Nat Med*, 2010. 16(6): p. 687-93.
10. Daghestani, H.N., C.F. Pieper, and V.B. Kraus, Soluble macrophage biomarkers indicate inflammatory phenotypes in patients with knee osteoarthritis. *Arthritis Rheumatol*, 2015. 67(4): p. 956-65.
11. Kraus, V.B., et al., Direct in vivo evidence of activated macrophages in human osteoarthritis. *Osteoarthritis Cartilage*, 2016. 24(9): p. 1613-21.
12. Klein-Wieringa, I.R., et al., Inflammatory Cells in Patients with Endstage Knee Osteoarthritis: A Comparison between the Synovium and the Infrapatellar Fat Pad. *J Rheumatol*, 2016. 43(4): p. 771-8.
13. Murray, P.J., et al., Macrophage activation and polarization: nomenclature and experimental guidelines. *Immunity*, 2014. 41(1): p. 14-20.
14. Utomo, L., et al., Cartilage inflammation and degeneration is enhanced by pro-inflammatory (M1) macrophages in vitro, but not inhibited directly by anti-inflammatory (M2) macrophages. *Osteoarthritis Cartilage*, 2016. 24(12): p. 2162-2170.
15. Zhang, H., et al., Synovial macrophage M1 polarisation exacerbates experimental

- osteoarthritis partially through R-spondin-2. *Ann Rheum Dis*, 2018. 77(10): p. 1524-1534.
16. Lopa, S., et al., Arthritic and non-arthritic synovial fluids modulate IL10 and IL1RA gene expression in differentially activated primary human monocytes. *Osteoarthritis Cartilage*, 2015. 23(11): p. 1853-7.
 17. Grotenhuis, N., et al., A culture model to analyze the acute biomaterial-dependent reaction of human primary macrophages. *Biochem Biophys Res Commun*, 2013. 433(1): p. 115-20.
 18. Fahy, N., et al., Human osteoarthritic synovium impacts chondrogenic differentiation of mesenchymal stem cells via macrophage polarisation state. *Osteoarthritis Cartilage*, 2014. 22(8): p. 1167-75.
 19. Utomo, L., et al., Guiding synovial inflammation by macrophage phenotype modulation: an in vitro study towards a therapy for osteoarthritis. *Osteoarthritis Cartilage*, 2016. 24(9): p. 1629-38.
 20. Yaeger, P.C., et al., Synergistic action of transforming growth factor-beta and insulin-like growth factor-I induces expression of type II collagen and aggrecan genes in adult human articular chondrocytes. *Exp Cell Res*, 1997. 237(2): p. 318-25.
 21. Zhu, M., et al., Activation of beta-catenin signaling in articular chondrocytes leads to osteoarthritis-like phenotype in adult beta-catenin conditional activation mice. *J Bone Miner Res*, 2009. 24(1): p. 12-21.
 22. Attur, M., et al., Elevated expression of periostin in human osteoarthritic cartilage and its potential role in matrix degradation via matrix metalloproteinase-13. *FASEB J*, 2015. 29(11): p. 4074-84.
 23. Wu, D., et al., Sauchinone inhibits IL-1beta induced catabolism and hypertrophy in mouse chondrocytes to attenuate osteoarthritis via Nrf2/HO-1 and NF-kappaB pathways. *Int Immunopharmacol*, 2018. 62: p. 181-190.
 24. van der Kraan, P.M., et al., Age-dependent alteration of TGF-beta signalling in osteoarthritis. *Cell Tissue Res*, 2012. 347(1): p. 257-65.
 25. Narcisi, R., et al., TGF beta-1 administration during ex vivo expansion of human articular chondrocytes in a serum-free medium redirects the cell phenotype toward hypertrophy. *J Cell Physiol*, 2012. 227(9): p. 3282-90.
 26. Wu, C.L., et al., The role of macrophages in osteoarthritis and cartilage repair. *Osteoarthritis Cartilage*, 2020. 28(5): p. 544-554.
 27. Zhang, H., D. Cai, and X. Bai, Macrophages regulate the progression of osteoarthritis. *Osteoarthritis Cartilage*, 2020. 28(5): p. 555-561.

Chapter 3

Intra-articular injection of triamcinolone acetonide sustains macrophage levels and aggravates osteophytosis during degenerative joint disease in mice

Mauricio N. Ferrao Blanco ¹, Yvonne M. Bastiaansen Jenniskens ¹, Nicole Kops ¹, Athina Chavli ¹, Roberto Narcisi ¹, Sander M. Botter ², Pieter J.M. Leenen ³, Gerjo J.V.M. van Osch ^{1,4,5}, Niamh Fahy ^{1,6}

¹ Department of Orthopaedics and Sports Medicine, Erasmus MC, University Medical Center Rotterdam, Rotterdam, The Netherlands

² Swiss Center for Musculoskeletal Biobanking, Balgrist Campus AG, Zürich, Switzerland

³ Department of Immunology, Erasmus MC, University Medical Center Rotterdam, The Netherlands

⁴ Department of Otorhinolaryngology, Erasmus MC, University Medical Center Rotterdam, Rotterdam, The Netherlands

⁵ Department of Biomechanical Engineering, University of Technology Delft, Delft, The Netherlands

⁶ Department of Oral and Maxillofacial Surgery, Erasmus MC, University Medical Center Rotterdam, Rotterdam, The Netherlands

Abstract

Background and Purpose: Corticosteroids such as triamcinolone acetonide (TAA) are potent drugs administered intra-articularly as an anti-inflammatory therapy to relieve pain associated with osteoarthritis (OA). However, the ability of early TAA intervention to mitigate OA progression and modulate immune cell subsets remains unclear. Here we sought to understand the effect of early intra-articular injection of TAA towards OA progression, local macrophages and peripheral blood monocytes.

Experimental approach: Degenerative joint disease was induced by intra-articular injection of collagenase into the knee joint of C57BL/6 mice. After one week, TAA or saline was injected intra-articularly. Blood was taken throughout the study to analyse monocyte subsets. Mice were euthanised at day 14 and 56 post-induction of collagenase-induced OA (CiOA) to examine synovial macrophages and structural OA features.

Key results: The percentage of macrophages relative to total live cells present within knee joints was increased in collagenase- compared to saline-injected knees at day 14 and was not altered by TAA treatment. However, at day 56 post-induction of CiOA TAA-treated knees had increased levels of macrophages compared with the knees of untreated CiOA-mice. The distribution of monocyte subsets present in peripheral blood was not altered by TAA treatment during the development of CiOA. Osteophyte maturation was increased in TAA-injected knees at day 56.

Conclusion and implications: Intra-articular injection of TAA increases long-term synovial macrophage numbers and osteophytosis. Our findings suggest that TAA accentuates the progression of osteoarthritis-associated features when applied to an acutely inflamed knee.

Introduction

Joint instability as caused by ligament injury, is a risk factor for the development of osteoarthritis (OA) [1-3]. OA is the most common form of arthritis affecting the entire joint, including the articular cartilage, subchondral bone, ligaments, capsule, synovium and peri-articular muscles [4]. Intra-articular injection of glucocorticoids, such as triamcinolone acetonide (TAA), is frequently applied clinically as an anti-inflammatory therapy to alleviate knee pain associated with OA [5-8], and is strongly recommended by the American College of Rheumatology / Arthritis Foundation [9]. However, evidence on the long-term benefit of TAA treatment is conflicting, with reports highlighting a potential association of intra-articular glucocorticoid treatment with accelerated structural progression of OA [10-12]. Interestingly, early intervention with intra-articular TAA treatment following anterior cruciate ligament (ACL) injury has been reported to reduce the levels of cartilage degeneration biomarkers in the synovial fluid of patients [13]. However, the long-term outcome of early TAA treatment following injury and its ability to alleviate OA progression in the knee requires further elucidation.

Low-grade inflammation in OA is associated with progression of structural changes characteristic of knee OA [14]. Macrophages residing within the synovial membrane are considered primary mediators of the inflammatory response and have been recognised as crucial regulators of OA progression [15]. Macrophages are highly plastic cells that exist as diverse phenotypes which dynamically respond to changing environmental stimuli, and can be classified as pro-inflammatory (M1), anti-inflammatory or tissue repair-associated (M2) subsets [16]. TAA is postulated to mediate its therapeutic effect in OA, due to its capacity to modulate inflammatory gene transcription and potential to alter macrophage activation [17, 18]. However, local intra-articular injection of TAA also leads to systemic absorption, with detectable serum plasma concentrations observed in the blood of patients up to 6 weeks post-injection [19]. Interestingly, glucocorticoid treatment has been previously reported to alter the functional profile of peripheral blood monocytes *in vitro* and *in vivo*, inducing an anti-inflammatory, migratory phenotype [20-22]. Blood monocytes which originate in the bone marrow, may migrate from the circulation into tissues under inflammatory conditions and differentiate into macrophages [23, 24]. Like macrophages, monocytes can also be categorised according to their cell surface receptor expression and function, comprising classical and non-classical/intermediate monocyte subsets [25]. Interestingly, circulating non-classical monocytes were shown to be recruited to the joint upon injury driving the development and progression of inflammation in a murine model of rheumatoid arthritis [26]. Intra-articular glucocorticoid injection has been shown to alter blood monocyte phenotype as well as leucocyte trafficking in patients with rheumatoid arthritis [27]. However, the responsiveness of systemic as well as local immune cell subsets to local administration of TAA during OA progression remains unclear.

Knowledge on the impact of an early intervention with short-term TAA treatment towards

local and systemic inflammatory processes, as well as the progression of structural damage following joint injury, could provide important insights for OA therapy. Intra-articular injection of collagenase is a well-known model to study instability-induced OA, characterised by a high synovial inflammatory component [28, 29]. Therefore, the aims of this study were to examine the effect of early intra-articular injection of TAA towards local macrophages and peripheral blood monocytes, as well as cartilage degeneration, subchondral bone changes and osteophyte formation during OA progression in the collagenase-induced OA (CiOA) mouse model.

Methods

Animal model

All animal experimentation procedures were conducted with approval by the Animal Ethical Committee of Erasmus University Medical Center (License number AVD101002015114, protocol number 16-691-03). 11 and 12-week-old male C57BL/6 mice (C57BL/6JolaHsd, 27.66g ± 1.91g; Envigo, Cambridgeshire, UK), were housed in groups of 4 in individually ventilated cages and maintained on a 12h light/dark cycle with ad libitum access to standard diet and water at the Experimental Animal Facility of the Erasmus MC. Mice were randomly divided into three experimental groups (N=12 per time point): Control, untreated CiOA, and TAA-treated CiOA. For all procedures, mice were anaesthetised using 3% isoflurane/0.8 L O₂/min (Pharmachemie BV, Haarlem, the Netherlands) and a 3-4 mm dermal incision was made to the right knee at the height of the patellar tendon. OA was induced unilaterally by 2 intra-articular injections of 3U of highly purified collagenase type VII from *Clostridium histolyticum* (Sigma-Aldrich, St. Louis, USA) in 6 µl of saline (0.9% NaCl; Sigma-Aldrich) at days 0 and 2. Control mice received intra-articular injections of 6 µl of saline only. All intra-articular injections were administered using a 50 µl syringe (Hamilton, Bonaduz, Switzerland) and 30G needle (BD Medical, New Jersey, USA). TAA (Kenacort; Bristol-Myers Squibb, Woerden, The Netherlands) was diluted to a concentration of 4.16 mg/ml with saline. TAA-treated OA mice received an intra-articular injection of 6 µl (containing 25 µg of TAA) to the right knee at day 7 post-induction of CiOA. This dose was based on previous rodent studies and the dose applied in humans considering the volume of the synovial fluid [18, 30]. Untreated CiOA and control mice received an intra-articular injection of 6 µl of saline as a vehicle control. The order of intra-articular injection administration was performed randomly at each time-point. Mice were euthanised in agreement with the Directive 2010/63/EU by cervical dislocation under isoflurane anaesthesia 14 or 56 days following induction of CiOA. A schematic representation of the study is summarised in figure 1.

Flow cytometric analysis of peripheral blood monocytes, synovial tissue and bone marrow

Peripheral blood was harvested from the facial vein of mice 7 days prior to and 9, 14, 28, 42,

49 and 56 days post-induction of OA. Blood sampling order was performed randomly at each time-point. 50 μ l of whole blood was pre-incubated with purified rat anti-mouse CD16/CD32 (Mouse BD Fc Block; BD Biosciences, New Jersey, USA) for 5 mins on ice. Blood was stained for the expression of CD11b, CD115, Ly-6C and CD62L to identify myeloid cells and specific monocyte subsets, as well as CD3, NK1.1, CD19 and Ly-6G to eliminate T cells, natural killer cells, B cells and neutrophils (all antibodies from BioLegend, San Diego, USA; Supplementary table 1). Cells were stained for 30 mins at 4 degrees in the dark, followed by incubation with 2 ml of 1X FACS lysing solution (BD Biosciences) for 10 minutes to lyse red blood cells. Following centrifugation at 400 xg for 10 minutes, supernatant was removed and cells washed and resuspended in FACSFlow buffer (BD Biosciences).

To evaluate macrophage subsets within knee joints at day 14 and 56 post-induction of OA, the patella with surrounding synovial tissue was dissected from the right knee and enzymatically digested. Tissue was incubated with 2 mg/ml collagenase type IV (Life Technologies, California, USA), 2.4 mg/ml dispase II (Roche, Penzberg, Germany) and 0.2 mg/ml DNase I (Sigma-Aldrich) in Hanks' Buffered Salt Solution (Thermo Fisher Scientific, Massachusetts, USA) at 37°C for 60 mins. The resulting cell suspension was filtered through a 100 μ m cell strainer, and cells were washed and resuspended in FACSFlow buffer. Cells were stained for the expression of CD11b, F4/80, CD86, CD206 (all BioLegend; supplementary table 1) and CD163 (Thermo Fisher Scientific) to identify macrophage subsets, and a LIVE/DEAD Fixable Dead Cell Stain (1:1000 dilution; Life Technologies) to exclude dead cells. Cells were stained for 30 mins at 4 degrees in the dark, washed and resuspended in FACSFlow.

Bone marrow was isolated from the contralateral femur at day 14 and 56 post-induction of OA. The femur was cut at both ends, and bone marrow was flushed out over a 100 μ m cell strainer using a 25G needle attached to a 5 ml syringe (All BD Medical) filled with Roswell Park Memorial Institute 1640 (RPMI) media (Thermo Fisher Scientific). The resulting cell suspension was spun at 500 x g for 5 mins, cells were resuspended in FACSFlow and stained for the expression of Ly-6C and CD31 (all Biolegend; supplementary table 1) to assess bone marrow composition as previously described [31], and with a LIVE/DEAD Fixable Dead Cell Stain (1:1000 dilution; Life Technologies). Cells were incubated with antibodies for 30 mins at 4 degrees in the dark, washed and resuspended in FACSFlow.

All samples were analysed using a FACSJazz cytometer (BD Biosciences) and FlowJo software version 10.0.7 (FlowJo LLC, Oregon, USA). The gating strategies applied for blood monocytes, macrophages and bone marrow composition analysis are presented in supplementary figures 1 and 2.

Histological analysis

Knees were fixed in 4 % formalin (v/v) for 1 week and scanned for μ CT analysis. Afterwards, knees were decalcified in 10 % EDTA for 2 weeks and embedded in paraffin. Coronal sections of 6 μ m were cut for analysis and sections were stained with Safranin O & Fast Green. Images were acquired using the NanoZoomer Digital Pathology program (Hamamatsu Photonics,

Ammersee, Germany).

Cartilage damage was evaluated by two observers blinded to the treatment groups using the Osteoarthritis Research Society International (OARSI) scoring system described by Glasson et al. [32]. Briefly, this score ranges from 0, for normal cartilage, to 6, for cartilage with clefts and erosion to the calcified cartilage in > 75 % of the articular surface. For each knee, cartilage quality in the lateral and medial compartment – both femur and tibia – of the knee was scored and averaged with 3 sections at standardised locations in the knee with 180 µm between sections. For each knee, the average score assigned by two blinded observers (MFB and NK) was averaged.

Osteophyte maturation was scored in the lateral and medial compartment of femur and tibiae, from 0 where no osteophyte was observed, 1 for a cartilaginous osteophyte and 2 for an ossified osteophyte, and averaged with 3 sections at standardised locations in the knee with 180 µm between the sections. For each knee, the average score assigned by two blinded observers (MFB and NK) was averaged. Osteophyte size was assessed using the NanoZoomer digital pathology program (Hamamatsu Photonics) by measuring the area of the osteophyte in 3 sections and calculating the average per joint, similarly to the osteophyte maturation score. We selected osteophytes at the medial side of the tibiae plateau, the location where the incidence of osteophytes was highest in CiOA knees.

Micro CT scans and analysis

Knees were imaged using a Quantum GX micro-computed tomography (µCT) scanner (PerkinElmer, Waltham, MA) with the following settings: time = 5 min, voxel size = 7 µm, tube voltage of 90 kV, and tube current = 180 µA. 3D reconstructed images were obtained using software AccuCT 1.0 (PerkinElmer) and the proximal tibia was selected for further analysis. Subchondral bone plate thickness was measured in frontal plane cross sections of the weight-bearing region of the medial tibia plateau.

Data and statistical analysis

The data and statistical analysis comply with the recommendations of the British Journal of Pharmacology on experimental design and analysis in pharmacology (Curtis et al, 2018)

The study was designed to generate groups of equal size, using randomisation and blinded analysis. Statistical analysis was undertaken only for studies where each group size was at least n=5. No values were excluded for the data analysis and presentation, except for the micro CT analysis of the knees at day 56 where n= 8 - 10 per group. In this case, samples were excluded due to low resolution during acquisition that led to inability of image reconstruction. The declared group size is the number of independent values, and statistical analysis was done using these independent values.

Sample size was determined considering a change in peripheral blood monocyte subsets of 30% resulting from treatment to be relevant in our study. As per a power calculation (Using a standard deviation of 25%) with a statistical power level of 0.8 and significance level (α) of

Results

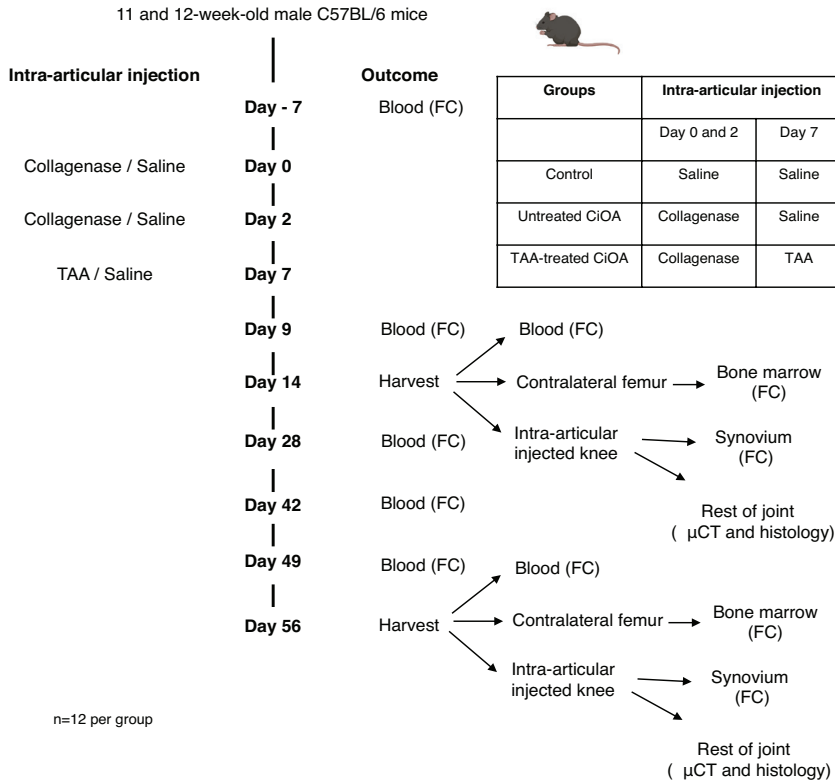


Figure 1 | Experimental set-up of the *in vivo* experiment. The table on the right outlines the intra-articular injection scheme applied to the right knee of mice for each experimental group (n=12). On the left, a timeline showing the outcome measurements. At day 14 a group of 36 mice were euthanised (n=12 per group) to assess the early effects of TAA. Another group of 36 mice was used to assess the long-term effects of TAA at the end point, day 56. TAA= Triamcinolone Acetonide. CiOA= Collagenase-induced osteoarthritis. FC= Flow cytometry. Created with BioRender.com

0.05, our sample size per group for a 2-tailed hypothesis test was 11 mice. One additional mouse per group was included, yielding n=12 mice per treatment group for each time-point, resulting in 72 mice in total. Statistical evaluation was performed using GraphPad Prism 9.0 and IBM SPSS 24 (IBM). Normality testing of data was performed using the Shapiro-Wilk test. For parametric data, a one-way ANOVA with Bonferroni post hoc test was conducted. For nonparametric data, a Kruskal-Wallis test with Bonferroni or Dunn's post-test correction for multiple comparisons was used, depending on the nature of the data. Statistically significant differences of all post hoc tests were found at $P < 0.05$. All post hoc tests were performed only if the F value for the ANOVA achieved statistical significance.

Macrophage-mediated inflammation is sustained in knee joints following TAA treatment

To identify whether TAA affects macrophages after joint injury *in vivo*, the patella with surrounding synovial tissue was isolated from the knee joints of mice and macrophage

composition was examined. At day 14, synovitis was present in this model as observed by a significant increase in macrophages within CiOA-induced knees (Fig. 2A). Intra-articular injection of TAA one week prior to harvesting the knees, however, did not significantly

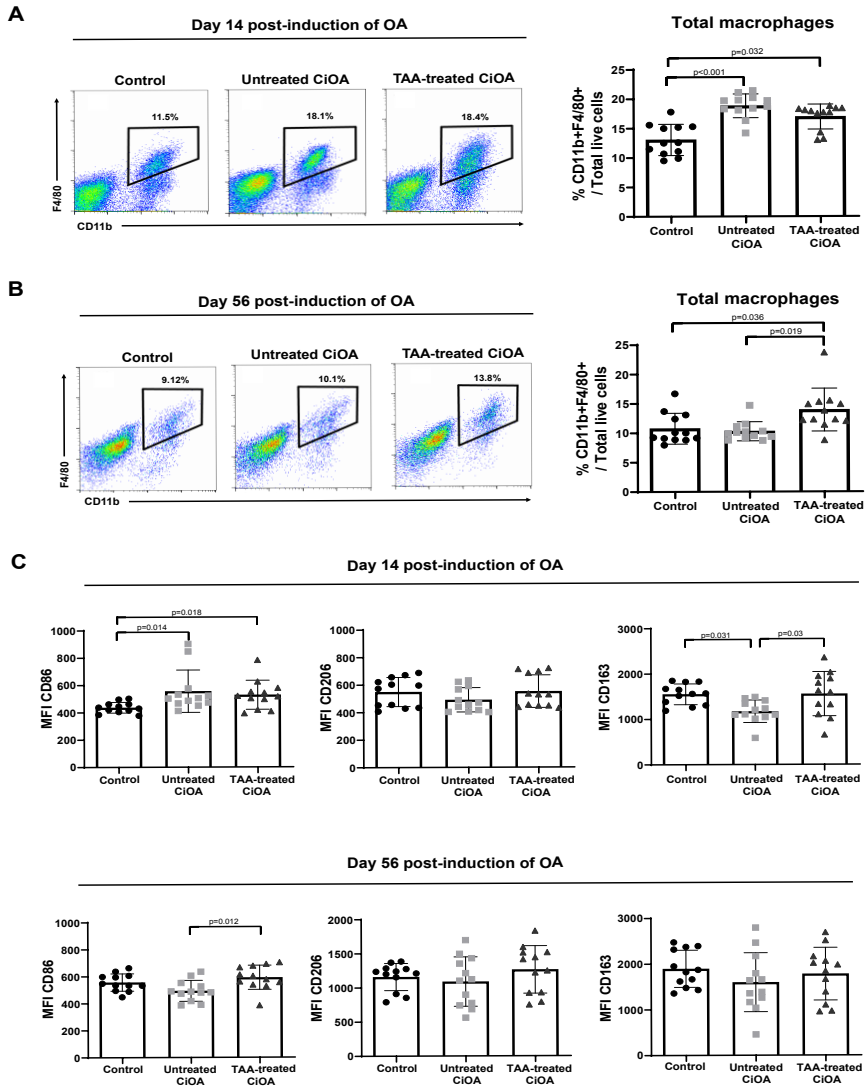


Figure 2 | TAA sustained macrophage-mediated inflammation in the knee joint and altered the expression of macrophage activation markers following induction of collagenase-induced osteoarthritis (CiOA). Analysis of flow cytometry data showing the percentage of CD11b+F4/80+ macrophages present within digested patellar / synovial tissue isolated from the right knee joint of mice at day 14 (A) and day 56 (B) post-induction of CiOA. Data represent the mean \pm SD. (C) Expression of the macrophage activation markers CD86, CD206 and CD163 by macrophages present in the knee joint at day 14 and 56 post-induction of CiOA, as determined by flow cytometry. Values represent the mean \pm SD for median fluorescence intensity (MFI) for each marker. Each dot represents data of an individual mouse (n=12 per timepoint). Non-parametric data were evaluated using a Kruskal-Wallis test with Bonferroni post hoc test. For parametric data a One-way ANOVA with Bonferroni post hoc test was conducted.

affect the proportion of macrophages present at this time point. At day 56 post induction of CiOA, macrophage levels in untreated-CiOA knees did not significantly differ compared to control knees. However, TAA-treated CiOA knees contained significantly higher levels of macrophages compared to both control and untreated CiOA mice at this later time point (Fig. 2B), suggesting that inflammatory processes in CiOA knees were sustained following TAA treatment. To further investigate the disruption of inflammatory responses by TAA, the expression of activation markers by macrophages in the knee joint was examined at each time-point (Fig. 2C). At day 14, flow cytometric analysis identified a significant increase in the expression of the activation marker CD86, associated with a pro-inflammatory phenotype, by macrophages in the knees of CiOA mice compared to control animals, irrespective of TAA treatment. Expression of the marker CD206, indicative of a tissue-repair phenotype, did also not differ between groups at this timepoint. However, expression of the marker CD163, which is associated with an anti-inflammatory phenotype, was significantly decreased by macrophages of untreated-CiOA knees compared to control knees. Interestingly, expression of CD163 was significantly higher in TAA-treated compared with untreated CiOA mice, and did not significantly differ from control animals at this time point. At day 56, macrophages isolated from TAA-treated CiOA joints were associated with higher expression of CD86 compared to untreated-CiOA knees, though it was not different compared to control. The expression of CD206 and CD163 did not differ between experimental groups at this time point. These data suggest that a single intra-articular injection of TAA early in the pathogenic process has long term effects in the joint, sustaining increased levels of macrophages with slightly elevated activation marker expression during OA development.

TAA aggravates osteophyte formation during OA progression

We next interrogated whether TAA injection modulates osteophytosis and cartilage damage in the joint. Cartilage damage was significantly increased at both day 14 and 56 in CiOA knees compared to control knees, and was not altered by TAA injection (Fig. 3 C, H). After two weeks of CiOA, osteophytes were present particularly at the margins of the medial tibia plateau but no differences were observed between untreated and TAA-treated CiOA knees (Fig. 3 D, E). Interestingly, osteophyte maturation was significantly increased in TAA-injected knees at day 56, compared to control and untreated-CiOA joints, though no changes were observed with respect to size (Fig. 3 I, J, K). Together these results show that injection of TAA increased osteophyte maturation in CiOA joints.

Subchondral bone plate thickness is not modulated by TAA

To assess subchondral bone plate (SBP) changes we performed μ CT scans of the knees *ex vivo* at day 14 and 56 and analysed bone morphometry in the medial tibial plateau (Fig. 4A). At day 14 the thickness of the subchondral bone plate was decreased in untreated CiOA knees compared with the knees of control animals, confirming previous studies in this model [33]. Also in TAA-treated CiOA knees the mean subchondral bone plate thickness was diminished

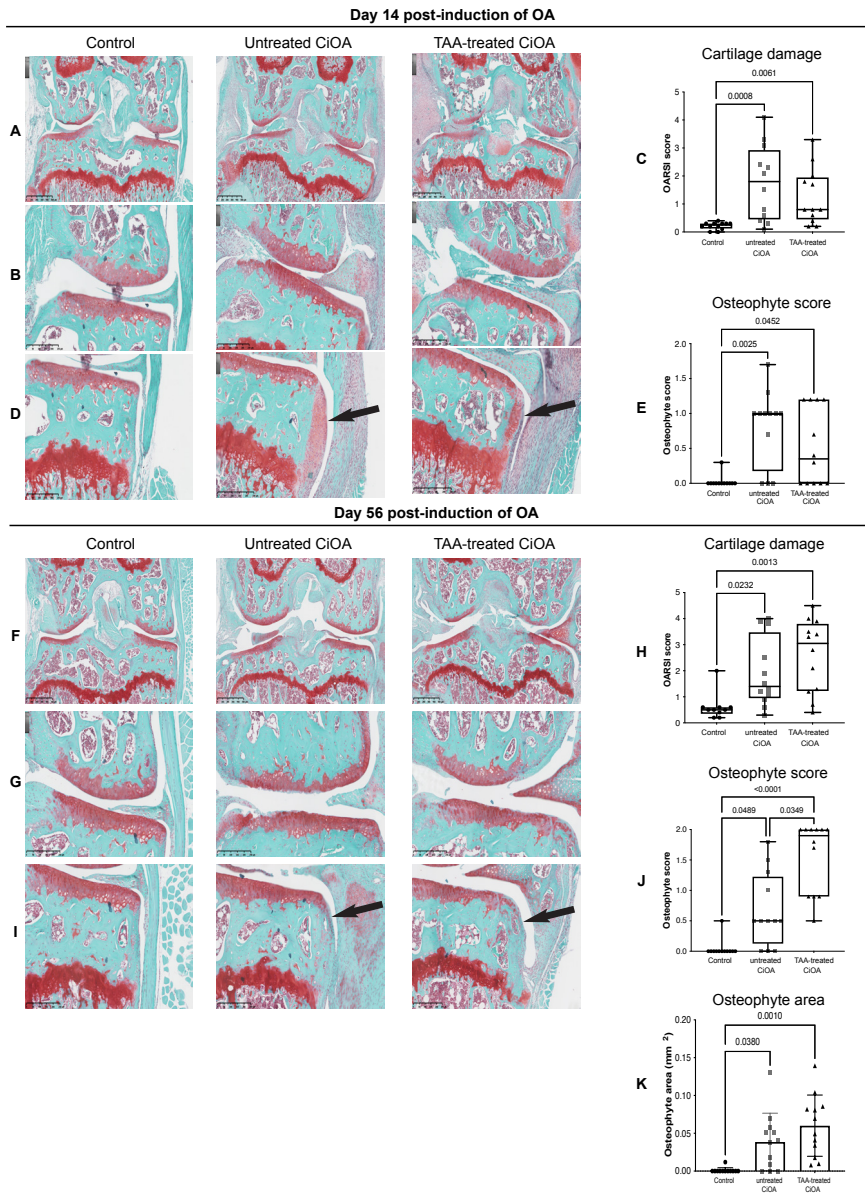


Figure 3 | TAA exacerbated osteophyte formation in CiOA knees. Histological analyses of cartilage damage and osteophyte formation at day 14 and day 56 after induction of CiOA. (A, F) Safranin-O/Fast Green staining of control, untreated CiOA and TAA-treated CiOA knees with magnification of the medial side (B, G), showing osteophyte formation adjacent to the medial tibiae plateau (D, I). Arrows indicate osteophytes. Graphs for cartilage damage (C, H) and osteophyte scores (E, J) are box-and-whiskers plots, with line indicating the median and error bars spanning maximum to minimum values. (K) Osteophyte area adjacent to the medial tibiae plateau is represented by the mean \pm SD. Each dot represents data of an individual mouse (n=12 per timepoint). Kruskal-Wallis test with Dunn's post-test correction for multiple comparisons was used for OARSI and osteophyte score. For osteophyte area, a One-way ANOVA with Bonferroni post hoc test was conducted.

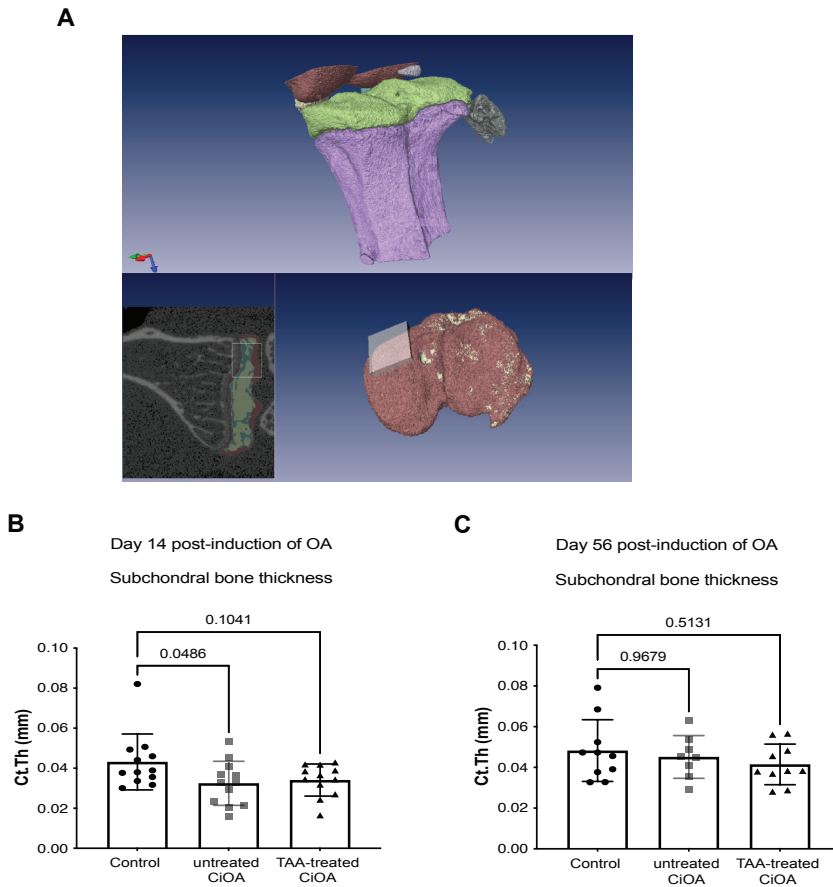


Figure 4 | TAA treatment did not alter subchondral bone plate thickness during CiOA development. (A) Bone morphometric analysis in medial tibiae plateau of the right knee of mice, showing the region of interest (ROI). Cortical thickness (Ct. Th.) in subchondral bone plate at day 14 (B) and day 56 (C). Each dot represents data of an individual mouse, with $n=12$ mice per group at day 14 and $n=8-10$ per group at day 56. Some samples were excluded at day 56 due to low resolution during acquisition that led to inability of image reconstruction. A One-way ANOVA with Bonferroni post hoc test was conducted.

compared with the knees of control mice, but this did not reach statistical difference (Fig. 4B). At day 56 subchondral bone plate thickness was similar between all experimental groups (Fig. 4C). These results suggest that intra-articular TAA injection does not interfere with OA subchondral bone plate changes *in vivo*.

Intra-articular injection of TAA does not exert systemic effects towards monocytes in peripheral blood and bone marrow

Having observed an effect of intra-articular injection of TAA towards local macrophage-mediated inflammation in the joint, we also sought to examine potential systemic effects of TAA treatment. Therefore, we longitudinally assessed the responsiveness of peripheral blood

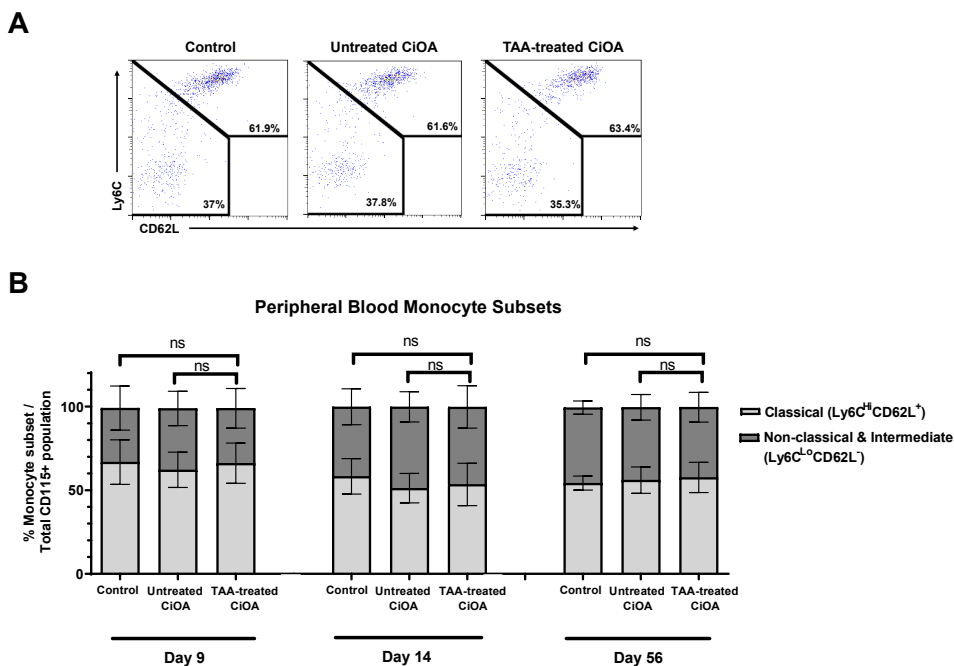


Figure 5 | Intra-articular injection of TAA did not exert systemic effects towards peripheral blood monocyte subsets. (A) Representative dotplots of flow cytometric analysis of peripheral blood monocyte subsets 48 hours following intra-articular injection of TAA (Day 9 post induction of CiOA). (B) Percentage of Classical (Ly6C⁺CD62L⁺) and Non-classical & Intermediate (Ly6C⁻CD62L⁻) monocyte subsets present in the peripheral blood of mice at day 9, 14 and 56 post-induction of CiOA. Data represent the mean \pm SD, with n=24 mice per group at day 9 and 14, and n=12 mice per group at day 56. ns= non-significant. Differences in the percentage of monocyte subsets between experimental groups were evaluated per timepoint using a One-way ANOVA with Bonferroni post hoc test.

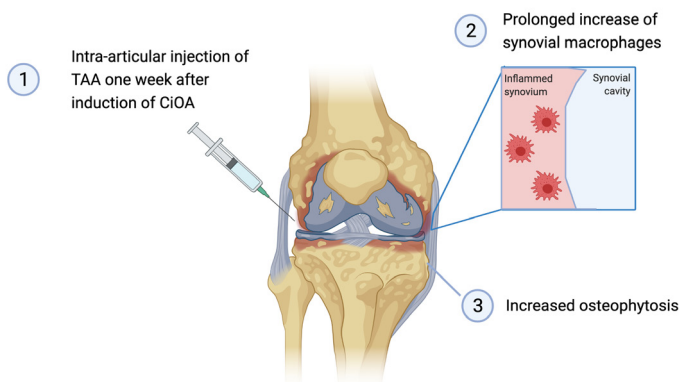


Figure 6 | Graphical representation of main conclusions. Created with BioRender.com

monocyte subsets to intra-articular injection of TAA during the development of CiOA. The distribution of monocyte subsets was not altered in the blood of mice following induction of CiOA compared to control mice, with the exception of day 28 where a significant relative increase in classical monocytes, consequently resulting in a decrease of non-classical/intermediate monocytes, was observed (Supplementary Fig. 3). Intra-articular injection of TAA did not significantly change monocyte subsets in the peripheral blood at an early time point of two days post injection, or at day 14 and 56 (Fig. 5A&B). Finally, the percentage monocytes and myeloid progenitors, granulocytes and lymphocytes in the bone marrow of the contralateral femur of TAA-treated mice, did not significantly differ compared with untreated-CiOA mice or control animals at day 14 and 56 (Supplementary Fig. 4), further indicating that short-term local delivery of TAA does not exert systemic effects at the level of monocyte and bone marrow precursor composition.

Discussion

Despite the long-standing use of intra-articular glucocorticoid injections, there is ongoing debate about their benefits on structural OA features [34]. The dampening activity of TAA towards inflamed synovium following joint injury and progression of OA has been postulated to mediate its therapeutic effect [17, 35]. However, the biological mechanisms underlying the potential impact of TAA towards OA progression are currently not well understood. Additionally, the potential of early TAA treatment following injury to alter OA progression is not clear. The findings of this study identify the presence of sustained macrophage-mediated inflammation as well as increased osteophytosis in the knee joint following short-term local TAA treatment (Fig. 6). These data suggest a negative effect of TAA administration in acutely inflamed joints following trauma, and provide further insight into cellular mechanisms which may govern the balance between therapeutic benefit and potential harm of TAA treatment during OA progression.

Previous studies have highlighted the potential of TAA to alter macrophage activation in the knee joint [18]. Our findings that TAA increased synovial macrophage numbers are in accordance with the data of Siebelt and colleagues, which showed that TAA increased macrophage activation in a rat papain-induced OA model [18]. Rudnik-Jansen et al observed that TAA did not modulate synovitis in an anterior cruciate ligament and medial transection rat model, when administered at 4 weeks-post OA induction [36]. Additionally, intra-articular injection of TAA to the knees of patients with rheumatoid arthritis does not reduce the level of macrophages present within synovial tissue [37]. Therefore, the modulation of synovial inflammation by TAA might be dependent on the pathological environment in the joint and time of administration.

In the present study we also investigated whether TAA modulated the phenotype of macrophages present within the joint following induction of CiOA. In this regard,

macrophage expression of activation markers CD86, CD206 and CD163, which are known markers associated with pro-inflammatory, tissue repair and anti-inflammatory macrophage phenotypes [38-40], respectively, were analysed by flow cytometry. In line with previous reports, macrophage CD163 expression was decreased following induction of CiOA, and significantly increased in response to TAA treatment [18, 41]. Furthermore, macrophages present within the joints of TAA-treated CiOA mice had increased expression of CD86 at the later time-point compared with untreated-CiOA knees, indicating a potential shift towards a pro-inflammatory phenotype. Glucocorticoids are known to induce expression of CD163 and CD206 by human and rodent macrophages *in vitro* [18, 42, 43]. However, discrepancies in the expression of markers associated with polarised macrophage phenotypes between *in vitro*-generated and *in vivo* populations has been previously described [44]. Moreover, expression of M2-associated markers does not indicate anti-inflammatory activity by definition. A human study showed adipose tissue macrophages expressing CD163 and CD206 are capable of high level proinflammatory cytokine production when triggered [45]. Future studies focusing on evaluating the production of mediators and the functionality of macrophage populations present *in vivo* may be required to fully determine their response to TAA treatment and subsequent impact on OA progression.

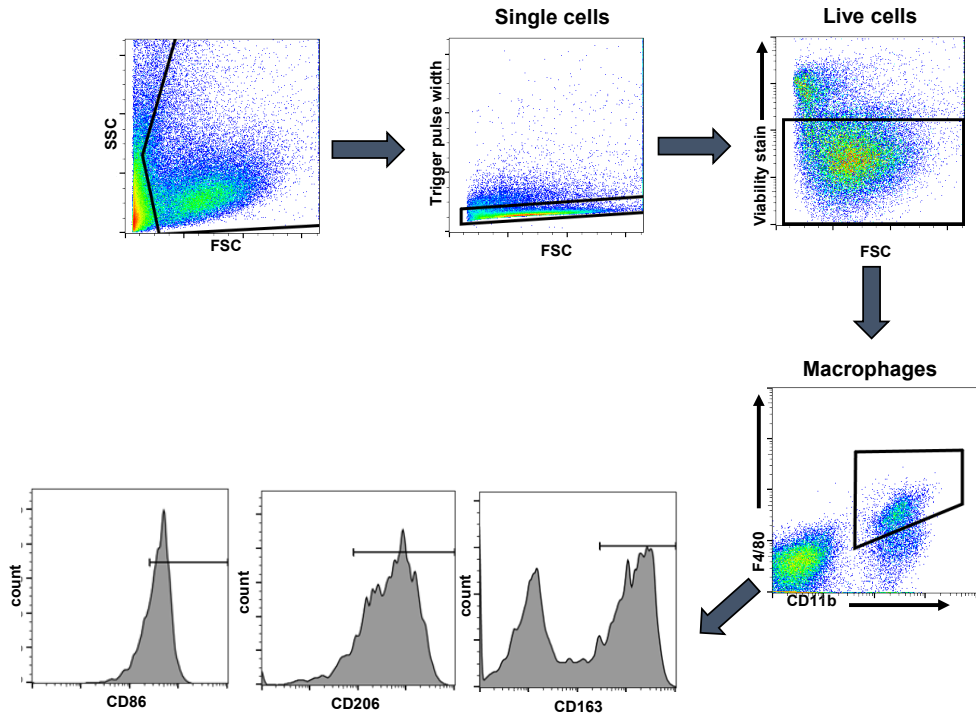
Current clinical reports on the benefit of TAA treatment are conflicting, with previous studies describing accelerated disease progression following repeated intra-articular TAA injections in patients with mild to moderate OA [10, 11]. In line with our findings, Rudnik-Jansen et al. have observed that a single intra-articular bolus injection of TAA did not reduce cartilage damage in an anterior cruciate ligament and medial transection rat model, when administered at 4 weeks-post OA induction [36]. Furthermore, here we have observed increased osteophytosis in TAA-treated CiOA joints. In contrast to our observations, Siebelt et al. found reduced osteophyte formation in rats in response to TAA-treatment. This divergence in outcomes may be due to differences between the models, considering that the use of papain results in cartilage matrix degradation, whereas collagenase initiates joint instability by degrading the ligaments. Furthermore, Siebelt et al. applied a weekly TAA intra-articular injection regime which began at the time of OA induction and continued throughout the duration of the experiment, in contrast to TAA administration at a single early time point post joint injury in the present study. The formation of osteophytes is known to be linked to growth factors which are secreted by macrophages. The increase of osteophyte formation in TAA-treated mice in our study might be associated to the increase of macrophages in the joint, since these cells have been shown to promote osteophytosis in CiOA knees [46, 47]. Additionally, Rudnik-Jansen and colleagues have previously reported increased dystrophic calcification in unstable OA rat knees that were treated with TAA utilising an extended release delivery system [36]. Osteophytes and the abnormal bone formation in the ligaments and tendons are caused by endochondral ossification of skeletal stem cells [48, 49]. Therefore, TAA might accentuate this process on progenitor cells leading to osteophytosis either via a direct effect or via synovial macrophages [50]. In this regard, further studies are needed to investigate the relationship

between the increase of osteophytosis and macrophages due to TAA.

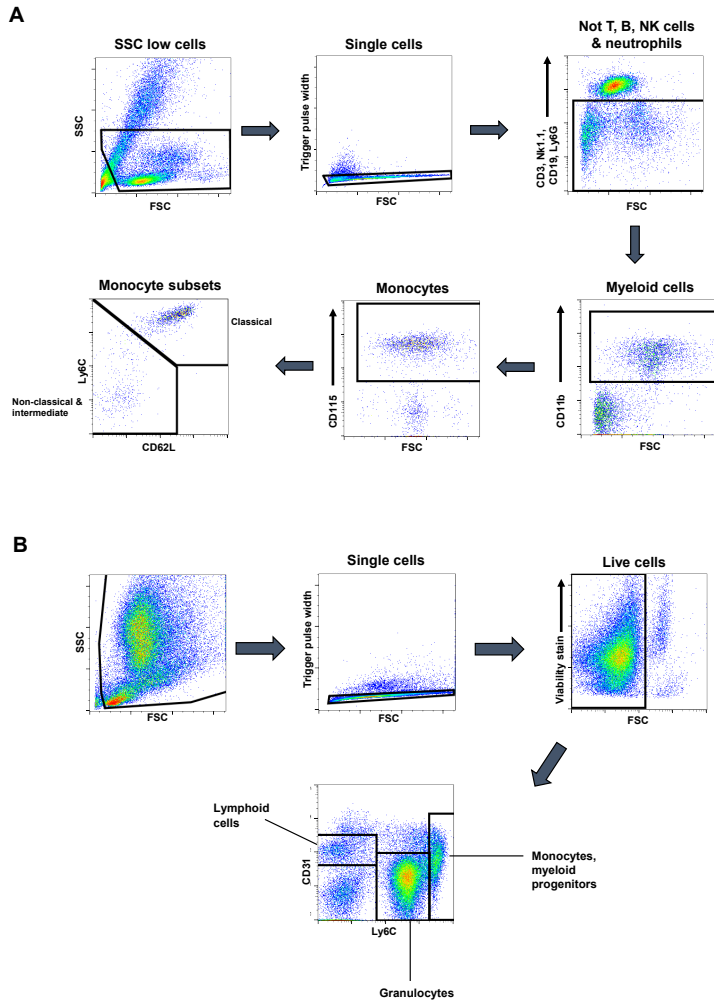
Glucocorticoids are known to modulate bone loss due to increased osteoclastogenesis or induced apoptosis of osteoblasts and osteocytes [51, 52]. However, we found that locally delivered TAA did not alter subchondral bone thickness during CiOA development. Interestingly, non-classical peripheral blood monocytes have been identified as crucial cells for osteoclast differentiation in an experimental model of rheumatoid arthritis [53]. In addition to modulating macrophage behaviour, glucocorticoid treatment has also been reported to alter the functionality of peripheral blood monocytes. Glucocorticoid treatment of human monocytes *in vitro* has been shown to induce an intermediate subset phenotype [54], and *ex vivo* stimulation of monocytes with glucocorticoids reported to induce a distinct monocyte phenotype associated with anti-inflammatory properties [55, 56]. High dose treatment with glucocorticoids induces selective apoptosis of intermediate and non-classical monocytes [57]. Furthermore, intra-articular glucocorticoid injection to patients with rheumatoid arthritis was shown to alter monocyte trafficking [27]. Our findings on the distribution of monocyte subsets in peripheral blood, as well as the abundance of monocytes in the bone marrow, indicate that local short-term intra-articular delivery of TAA at the examined concentration does not induce systemic immune responses *in vivo* during the development of CiOA.

Intra-articular injection of glucocorticoids such as TAA is recommended and routinely applied clinically for the management of OA pain of the knee [8, 58]. A limitation of our study is that we did not perform pain measurements, and therefore further investigation is required to determine the effect of early intervention with TAA towards pain relief during OA progression. Additionally, we did not evaluate the impact of intra-articular TAA administration on a healthy joint. Given that our primary focus was on the modulatory effect of TAA towards an injured joint and TAA will not likely be injected in a healthy joint, this was not a primary aim of our study. Rudnik-Jansen et al., however, previously reported that intra-articular injection of a microsphere-based extended TAA release system to healthy rat knees did not have any deleterious effects within the joint [36]. Interestingly, intramuscular TAA injection into the gluteus muscle has been previously reported to reduce pain compared to placebo injection in patients with hip OA [59]. Furthermore, a clinical trial evaluating the potential of intramuscular TAA injection as an alternative to intra-articular administration for the treatment of knee OA is underway [60]. As suggested by Dorleijn et al. [59], intramuscular injection of TAA may potentially serve as a beneficial therapeutic strategy to reduce joint pain, avoiding the negative local effects of TAA within the injured knee joint observed in our study. In conclusion, the findings of our study suggest that short-term intra-articular TAA treatment may sustain OA-associated local inflammatory processes in the knee mediated by macrophages, which may further contribute to a loss of homeostasis within the joint and exacerbate disease progression. In the context of clinical translation of these findings, caution should be taken when locally applying TAA treatment to an acutely inflamed joint following injury. Further investigation of the impact of TAA towards the behaviour of local immune cell populations during active inflammation in the knee, may enhance therapeutic outcomes for OA.

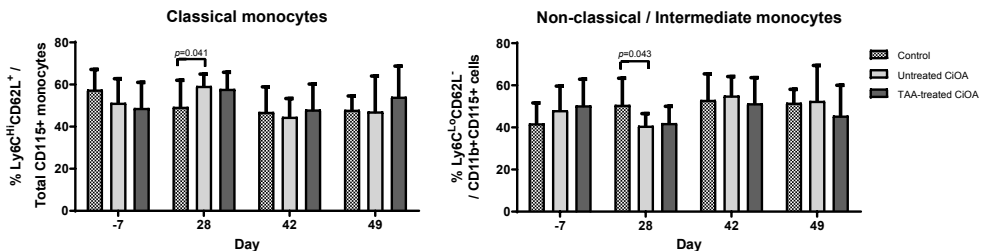
Supplementary figures



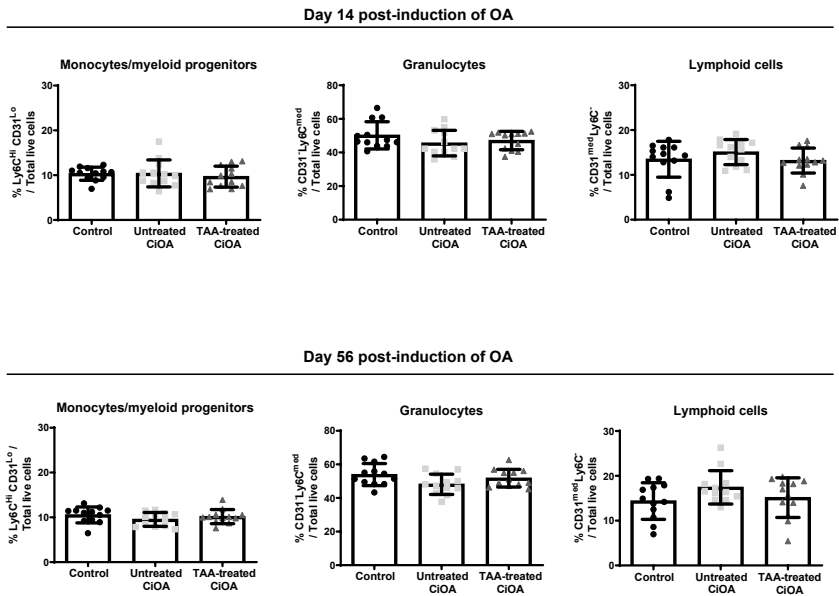
Supplementary figure 1 | Gating strategy applied for flow cytometric analysis of macrophages within knee joints



Supplementary figure 2 | Gating strategy applied for flow cytometric analysis of peripheral blood monocyte subsets (A) and bone marrow composition (B)



Supplementary figure 3 | Longitudinal analysis of the percentage of peripheral blood monocyte subsets in control, untreated CiOA and TAA-treated CiOA mice by flow cytometry. Blood was taken 7 days prior to the induction of CiOA as a baseline measurement (Day -7). Data represent the mean \pm SD. Differences in the percentage of monocyte subsets between experimental groups were evaluated per timepoint using a One-way ANOVA with Bonferroni post hoc test.



Supplementary figure 4 | Flow cytometric analysis of monocytes & myeloid progenitor cells, lymphoid cells and granulocytes within the bone marrow of control, untreated CiOA and TAA-treated CiOA mice at day 14 and day 56. Data represent the mean \pm SD.

Antibody	Clone	Fluorophore
Anti-mouse/human CD11b	M1/70	PerCp-Cy5.5
Anti-mouse CD115	AFS98	PE
Anti-mouse Ly6C	HK1.4	FITC
Anti-mouse CD62L	MEL-14	APC
Anti-mouse Ly6G	1A8	PE-Cy7
Anti-mouse CD3	17A2	PE-Cy7
Anti-mouse NK1.1	PK136	PE-Cy7
Anti-mouse CD19	6D5	PE-Cy7
Anti-mouse F4/80	BM8	FITC
Anti-mouse CD86	GL-1	PE-Cy7
Anti-mouse CD206	C068C2	APC
Anti-mouse CD163	TNKUPJ	PE
Anti-mouse CD31	390	APC

Supplementary table 1 | Flow cytometry antibodies used for markers of interest

References

1. Wilder, F.V., et al., History of acute knee injury and osteoarthritis of the knee: a prospective epidemiological assessment. The Clearwater Osteoarthritis Study. *Osteoarthritis Cartilage*, 2002. 10(8): p. 611-6.
2. Driban, J.B., et al., Association of knee injuries with accelerated knee osteoarthritis progression: data from the Osteoarthritis Initiative. *Arthritis Care Res (Hoboken)*, 2014. 66(11): p. 1673-9.
3. Akhtar, M.A., R. Bhattacharya, and J.F. Keating, Generalised ligamentous laxity and revision ACL surgery: Is there a relation? *Knee*, 2016. 23(6): p. 1148-1153.
4. Bijlsma, J.W., Diagnosis and nonsurgical management of osteoarthritis. *Ann Rheum Dis*, 2001. 60(1): p. 6.
5. Bellamy, N., et al., Intraarticular corticosteroid for treatment of osteoarthritis of the knee. *Cochrane Database Syst Rev*, 2006(2): p. CD005328.
6. Miller, J.H., J. White, and T.H. Norton, The value of intra-articular injections in osteoarthritis of the knee. *J Bone Joint Surg Br*, 1958. 40-B(4): p. 636-43.
7. van Middelkoop, M., et al., The OA Trial Bank: meta-analysis of individual patient data from knee and hip osteoarthritis trials show that patients with severe pain exhibit greater benefit from intra-articular glucocorticoids. *Osteoarthritis Cartilage*, 2016. 24(7): p. 1143-52.
8. McAlindon, T.E., et al., OARSI guidelines for the non-surgical management of knee osteoarthritis. *Osteoarthritis Cartilage*, 2014. 22(3): p. 363-88.
9. Kolasinski, S.L., et al., 2019 American College of Rheumatology/Arthritis Foundation Guideline for the Management of Osteoarthritis of the Hand, Hip, and Knee. *Arthritis Care Res (Hoboken)*, 2020. 72(2): p. 149-162.
10. McAlindon, T.E., et al., Effect of Intra-articular Triamcinolone vs Saline on Knee Cartilage Volume and Pain in Patients With Knee Osteoarthritis: A Randomized Clinical Trial. *JAMA*, 2017. 317(19): p. 1967-1975.
11. Zeng, C., et al., Intra-articular corticosteroids and the risk of knee osteoarthritis progression: results from the Osteoarthritis Initiative. *Osteoarthritis Cartilage*, 2019. 27(6): p. 855-862.
12. Kompel, A.J., et al., Intra-articular Corticosteroid Injections in the Hip and Knee: Perhaps Not as Safe as We Thought? *Radiology*, 2019. 293(3): p. 656-663.
13. Lattermann, C., et al., A Multicenter Study of Early Anti-inflammatory Treatment in Patients With Acute Anterior Cruciate Ligament Tear. *Am J Sports Med*, 2017. 45(2): p. 325-333.
14. Robinson, W.H., et al., Low-grade inflammation as a key mediator of the pathogenesis of osteoarthritis. *Nat Rev Rheumatol*, 2016. 12(10): p. 580-92.
15. Zhang, H., D. Cai, and X. Bai, Macrophages regulate the progression of osteoarthritis. *Osteoarthritis Cartilage*, 2020. 28(5): p. 555-561.
16. Murray, P.J., et al., Macrophage activation and polarization: nomenclature and

experimental guidelines. *Immunity*, 2014. 41(1): p. 14-20.

17. Nixon, M., R. Andrew, and K.E. Chapman, It takes two to tango: dimerisation of glucocorticoid receptor and its anti-inflammatory functions. *Steroids*, 2013. 78(1): p. 59-68.

18. Siebelt, M., et al., Triamcinolone acetonide activates an anti-inflammatory and folate receptor-positive macrophage that prevents osteophytosis in vivo. *Arthritis Res Ther*, 2015. 17: p. 352.

19. Kraus, V.B., et al., Synovial and systemic pharmacokinetics (PK) of triamcinolone acetonide (TA) following intra-articular (IA) injection of an extended-release microsphere-based formulation (FX006) or standard crystalline suspension in patients with knee osteoarthritis (OA). *Osteoarthritis Cartilage*, 2018. 26(1): p. 34-42.

20. Ehrchen, J., et al., Glucocorticoids induce differentiation of a specifically activated, anti-inflammatory subtype of human monocytes. *Blood*, 2007. 109(3): p. 1265-74.

21. Varga, G., et al., Glucocorticoids induce an activated, anti-inflammatory monocyte subset in mice that resembles myeloid-derived suppressor cells. *J Leukoc Biol*, 2008. 84(3): p. 644-50.

22. Varga, G., et al., Immune suppression via glucocorticoid-stimulated monocytes: a novel mechanism to cope with inflammation. *J Immunol*, 2014. 193(3): p. 1090-9.

23. Geissmann, F., S. Jung, and D.R. Littman, Blood monocytes consist of two principal subsets with distinct migratory properties. *Immunity*, 2003. 19(1): p. 71-82.

24. Sunderkötter, C., et al., Subpopulations of mouse blood monocytes differ in maturation stage and inflammatory response. *J Immunol*, 2004. 172(7): p. 4410-7.

25. Ziegler-Heitbrock, L., Monocyte subsets in man and other species. *Cell Immunol*, 2014. 289(1-2): p. 135-9.

26. Misharin, A.V., et al., Nonclassical Ly6C(-) monocytes drive the development of inflammatory arthritis in mice. *Cell Rep*, 2014. 9(2): p. 591-604.

27. Steer, J.H., et al., Altered leucocyte trafficking and suppressed tumour necrosis factor alpha release from peripheral blood monocytes after intra-articular glucocorticoid treatment. *Ann Rheum Dis*, 1998. 57(12): p. 732-7.

28. van Osch, G.J., et al., Relation of ligament damage with site specific cartilage loss and osteophyte formation in collagenase induced osteoarthritis in mice. *J Rheumatol*, 1996. 23(7): p. 1227-32.

29. van Osch, G.J., et al., The relation between cartilage damage and osteophyte size in a murine model for osteoarthritis in the knee. *Rheumatol Int*, 1996. 16(3): p. 115-9.

30. Kroin, J.S., et al., Intraarticular slow-release triamcinolone acetate reduces allodynia in an experimental mouse knee osteoarthritis model. *Gene*, 2016. 591(1): p. 1-5.

31. de Bruijn, M.F., et al., Bone marrow cellular composition in *Listeria monocytogenes* infected mice detected using ER-MP12 and ER-MP20 antibodies: a flow cytometric alternative to differential counting. *J Immunol Methods*, 1998. 217(1-2): p. 27-39.

32. Glasson, S.S., et al., The OARSI histopathology initiative - recommendations for histological assessments of osteoarthritis in the mouse. *Osteoarthritis Cartilage*, 2010. 18

Suppl 3: p. S17-23.

33. Botter, S.M., et al., Osteoarthritis induction leads to early and temporal subchondral plate porosity in the tibial plateau of mice: an in vivo microfocal computed tomography study. *Arthritis Rheum*, 2011. 63(9): p. 2690-9.
34. Juni, P., et al., Intra-articular corticosteroid for knee osteoarthritis. *Cochrane Database Syst Rev*, 2015(10): p. CD005328.
35. Paik, J., S.T. Duggan, and S.J. Keam, Triamcinolone Acetonide Extended-Release: A Review in Osteoarthritis Pain of the Knee. *Drugs*, 2019. 79(4): p. 455-462.
36. Rudnik-Jansen, I., et al., Local controlled release of corticosteroids extends surgically induced joint instability by inhibiting tissue healing. *Br J Pharmacol*, 2019. 176(20): p. 4050-4064.
37. van der Goes, M.C., et al., Intra-articular glucocorticoid injections decrease the number of steroid hormone receptor positive cells in synovial tissue of patients with persistent knee arthritis. *Ann Rheum Dis*, 2012. 71(9): p. 1552-8.
38. Lech, M. and H.J. Anders, Macrophages and fibrosis: How resident and infiltrating mononuclear phagocytes orchestrate all phases of tissue injury and repair. *Biochimica Et Biophysica Acta-Molecular Basis of Disease*, 2013. 1832(7): p. 989-997.
39. Johnston, L.K., et al., Pulmonary Macrophage Subpopulations in the Induction and Resolution of Acute Lung Injury. *American Journal of Respiratory Cell and Molecular Biology*, 2012. 47(4): p. 417-426.
40. Fischer-Riepe, L., et al., CD163 expression defines specific, IRF8-dependent, immune-modulatory macrophages in the bone marrow. *Journal of Allergy and Clinical Immunology*, 2020. 146(5): p. 1137-1151.
41. Khatab, S., et al., Intra-articular Injections of Platelet-Rich Plasma Releasate Reduce Pain and Synovial Inflammation in a Mouse Model of Osteoarthritis. *Am J Sports Med*, 2018. 46(4): p. 977-986.
42. Buechler, C., et al., Regulation of scavenger receptor CD163 expression in human monocytes and macrophages by pro- and antiinflammatory stimuli. *Journal of Leukocyte Biology*, 2000. 67(1): p. 97-103.
43. Shepherd, V.L., M.G. Konish, and P. Stahl, Dexamethasone Increases Expression of Mannose Receptors and Decreases Extracellular Lysosomal-Enzyme Accumulation in Macrophages. *Journal of Biological Chemistry*, 1985. 260(1): p. 160-164.
44. Orecchioni, M., et al., Macrophage Polarization: Different Gene Signatures in M1(LPS+) vs. Classically and M2(LPS-) vs. Alternatively Activated Macrophages. *Frontiers in Immunology*, 2019. 10.
45. Zeyda, M., et al., Human adipose tissue macrophages are of an anti-inflammatory phenotype but capable of excessive pro-inflammatory mediator production. *Int J Obes (Lond)*, 2007. 31(9): p. 1420-8.
46. van Lent, P.L., et al., Crucial role of synovial lining macrophages in the promotion of transforming growth factor beta-mediated osteophyte formation. *Arthritis Rheum*, 2004.

50(1): p. 103-11.

47. Blom, A.B., et al., Synovial lining macrophages mediate osteophyte formation during experimental osteoarthritis. *Osteoarthritis Cartilage*, 2004. 12(8): p. 627-35.
48. van der Kraan, P.M. and W.B. van den Berg, Osteophytes: relevance and biology. *Osteoarthritis Cartilage*, 2007. 15(3): p. 237-44.
49. Roelofs, A.J., et al., Identification of the skeletal progenitor cells forming osteophytes in osteoarthritis. *Ann Rheum Dis*, 2020. 79(12): p. 1625-1634.
50. Ferrao Blanco, M.N., et al., Effect of Inflammatory Signaling on Human Articular Chondrocyte Hypertrophy: Potential Involvement of Tissue Repair Macrophages. *Cartilage*, 2021: p. 19476035211021907.
51. Ahmad, M., et al., A Jack of All Trades: Impact of Glucocorticoids on Cellular Cross-Talk in Osteoimmunology. *Front Immunol*, 2019. 10: p. 2460.
52. Chotiyarnwong, P. and E.V. McCloskey, Pathogenesis of glucocorticoid-induced osteoporosis and options for treatment. *Nat Rev Endocrinol*, 2020. 16(8): p. 437-447.
53. Puchner, A., et al., Non-classical monocytes as mediators of tissue destruction in arthritis. *Annals of the Rheumatic Diseases*, 2018. 77(10): p. 1490-1497.
54. Liu, B.Y., et al., CD14(++)CD16(+) Monocytes Are Enriched by Glucocorticoid Treatment and Are Functionally Attenuated in Driving Effector T Cell Responses. *Journal of Immunology*, 2015. 194(11): p. 5150-5160.
55. Varga, G., et al., Glucocorticoids induce an activated, anti-inflammatory monocyte subset in mice that resembles myeloid-derived suppressor cells. *Journal of Leukocyte Biology*, 2008. 84(3): p. 644-650.
56. Ehrchen, J., et al., Glucocorticoids induce differentiation of a specifically activated, anti-inflammatory subtype of human monocytes. *Blood*, 2007. 109(3): p. 1265-1274.
57. Dayyani, F., et al., Mechanism of glucocorticoid-induced depletion of human CD14+CD16+ monocytes. *J Leukoc Biol*, 2003. 74(1): p. 33-9.
58. Kolasinski, S.L., et al., 2019 American College of Rheumatology/Arthritis Foundation Guideline for the Management of Osteoarthritis of the Hand, Hip, and Knee. *Arthritis Care & Research*, 2020. 72(2): p. 149-162.
59. Dorleijn, D.M.J., et al., Intramuscular glucocorticoid injection versus placebo injection in hip osteoarthritis: a 12-week blinded randomised controlled trial. *Annals of the Rheumatic Diseases*, 2018. 77(6): p. 875-882.
60. Mol, M.F., et al., Effectiveness of intramuscular gluteal glucocorticoid injection versus intra-articular glucocorticoid injection in knee osteoarthritis: design of a multicenter randomized, 24 weeks comparative parallel-group trial. *BMC Musculoskelet Disord*, 2020. 21(1): p. 225.

Chapter 4

An integrated in silico-in vitro approach for identifying therapeutic targets against osteoarthritis

Raphaëlle Lesage ^{1,2}, Mauricio N. Ferrao Blanco ³, Roberto Narcisi ³, Tim Welting ⁴, Gerjo J.V.M. van Osch ^{3,5,6}, Liesbet Geris ^{1,2,7}

¹ Prometheus, Division of Skeletal Tissue Engineering, KU Leuven, Belgium;

² Biomechanics Section, KU Leuven, Belgium;

³ Department of Orthopaedics and Sports Medicine, Erasmus MC, University Medical Center, Rotterdam, Netherlands;

⁴ Orthopedic Surgery Department, UMC+, Maastricht, Netherlands;

⁵ Department of Otorhinolaryngology, Erasmus MC, University Medical Center, Rotterdam, Netherlands;

⁶ Department of Biomechanical Engineering, Delft University of Technology, Delft, Netherlands;

⁷ GIGA In silico medicine, University of Liège, Belgium

Submitted

DOI: 10.1101/2021.09.27.461207

Abstract

Background: Without the availability of disease-modifying drugs, there is an unmet therapeutic need for osteoarthritic patients. During osteoarthritis, the homeostasis of articular chondrocytes is dysregulated and a phenotypical transition called hypertrophy occurs, leading to cartilage degeneration. Targeting this phenotypic transition has emerged as a potential therapeutic strategy. Chondrocyte phenotype maintenance and switch are controlled by an intricate network of intracellular factors, each influenced by a myriad of feedback mechanisms, making it challenging to intuitively predict treatments outcomes, while *in silico* modeling can help unravel that complexity. In this study, we aim to develop a virtual articular chondrocyte to guide experiments in order to rationalize the identification of potential drug targets via screening of combination therapies through computational modeling and simulations.

Results: We developed a signal transduction network model using knowledge-based and data-driven (machine learning) modelling technologies. The *in silico* high-throughput screening of (pairwise) perturbations operated with that network model highlighted conditions affecting the hypertrophic switch. Several combinations were tested in a murine cell line and primary chondrocytes to validate the *in silico* predictions, which notably highlighted a previously unreported synergistic effect between the Protein Kinase A and the Fibroblast Growth Factor Receptor 1.

Conclusions: Here, we provide a virtual articular chondrocyte in the form of a signal transduction interactive knowledge base and of an executable computational model. Our *in silico-in vitro* strategy opens new routes for developing osteoarthritis targeting therapies by refining the early stages of drug targets discovery.

Introduction

Osteoarthritis (OA) is a degenerative disease of the joint increasingly prevalent due to the ageing population. It is a major societal burden as no disease-modifying drugs are currently available on the market (1). OA is characterized by cartilage damage, led by an overall increase of catabolic processes and disturbance of anabolic processes. The joint cartilage is composed of a unique cell type, the chondrocyte, which is responsible for maintaining the tissue homeostasis in an environment mainly composed of water and biomolecules such as proteoglycans and collagen fibers. Many factors, including inflammation, may influence the shift from stable healthy cartilage towards a diseased state (2). Regardless of the exact inducing mechanisms, during that transition, some of the chondrocytes enter a maturation process called hypertrophy (3,4), leading to extracellular matrix (ECM) degradation, mineralization and bone formation. This pathological phenomenon resembles the hypertrophic changes observed in the course of endochondral ossification during growth and development (2,5–8). Therefore, controlling the chondrocyte phenotype to prevent hypertrophic maturation has emerged as a potential therapeutic strategy to treat OA patients (7,9).

Crucial in this approach is the understanding of the process of articular chondrocyte hypertrophy for the identification of key regulators as potential drug targets. Several factors have been associated to the promotion of this phenotypic shift, such as Indian hedgehog (IHH) and inflammatory signalling pathways (10) and routes downstream of various growth factors are thought to be important in the control or disruption of chondrocyte homeostasis, such as the WNT and Bone morphogenic protein (BMP) pathways, the parathyroid hormone related peptide (PTHrP), as well as the insulin-like growth factor (IGF)-I, fibroblast growth factors (FGF) and transforming growth factor (TGF)- β (9,11,12). However, the interplay of intracellular pathways is highly intricate with extensive feedback loops, non-linear pathways, redundancy and intertwinings (11,13,14). This complicates the intuitive prediction of what will happen in case of perturbations of a specific target. For example, it was observed that the *in vitro* activation of the WNT pathway with the WNT3A ligand and the inhibition of that same pathway with Dickkopf1 (DKK1), both induced a reduction of glycosaminoglycan rich ECM in human articular chondrocytes (15). The fact that an activator and an inhibitor of the canonical WNT pathway both lead to the same outcome is surprising and highlights the intricacy of the underlying mechanisms. Hence, the ability to predict the effect of an external perturbation and potential therapies requires a systemic view on the process (13,14).

We propose to unravel the complexity of these regulatory pathways and to rationalize the identification of potential drug targets via screening of (combination) therapies by using a classical engineering approach, namely that of computer modeling and simulation. Contrary to *in vitro* and *in vivo* approaches, having a systemic view of the process using an *in silico* model allows to study the system numerically, in a cost and time efficient way and with less ethical concerns. In addition, it allows to prioritize experiments, thereby refining the traditional funnel of drug targets identification in the drug discovery process. The *in silico*

approach starts with acquiring a systems perspective of the intracellular biological processes. It is necessary to identify the important individual components of the system and to know how they interact and influence each other. A computational model built on this information should generate results consistent with current knowledge but also allow to ask questions that would lead to new insights into yet unexplored situations and interactions (16). Such computational mechanistic approaches were already used in the past to identify influential candidates for cancer therapeutics (17), study the control stem cell fate decision (18) or prioritize personalized combination therapies (19).

In this study, we developed an *in silico* model of the regulatory network capturing articular chondrocyte phenotypic changes during OA. This network is built by combining knowledge-based modeling and data-driven approaches to ensure the mechanistic accuracy of the network whilst taking advantage of current automatic network reconstruction technologies. We characterized the numerical intracellular states of the articular chondrocyte model and looked into consistency with known physiological behaviors, through mathematical model implementation and computer simulations. We subsequently used the model as a ‘virtual chondrocyte’ to perform an *in silico* high throughput screening for early predictions of the best potential therapeutic conditions to be tested in wet lab experiments. Finally, we confirmed *in vitro* the role of predicted factors in the regulation of the phenotypic change, for both single and combinations of factors.

Methods

Network construction

The knowledge-derived networks were built by incorporating fine-grained mechanistic knowledge about signaling pathways and transcriptional regulations. A previously published model of chondrocyte differentiation in the growth plate (21) was used as a basis and was adapted and completed through literature curation of decades of knowledge about articular chondrocyte and osteoarthritis. Reference sources for the experimental evidence (binding assays, clinical observations, etc.) were mostly from mouse and human origin. References used chondrocytes (or related cell lines) and predominantly involved direct protein or promoter binding information, curated pathways or observed phenomenon in cartilage during homeostasis and disease. All references and mechanism descriptions are available through the interactive networks in the online platform Cell Collective (<http://www.cellcollective.org>) (22). See the links for the chondrocyte knowledge bases in the ‘Data availability’ section. Additionally, some gene regulatory interactions were automatically identified with machine learning algorithms using gene expression multi-perturbed data as input. Such informative dataset was achieved by merging six published microarray datasets of mouse articular cartilage (GSE26475, GSE33754, GSE79239, GSE33656, GSE53857, GSE45793). Each dataset had a control or wild type group and an OA-like group, which was either using genetically modified mouse spontaneously developing OA or a DMM-induced OA mouse model. Importantly,

the initial annotations provided by the authors were not necessarily ‘OA’ or ‘WT’ but rather experiment-specific annotations such as ‘DMM’ or ‘SHAM operated’. Therefore the binary annotation as OA-like or WT-like samples was established by hand for the purpose of this study according to the original data annotations published on GEO, as reported Data S1. The datasets were merged applying an in-house developed pipeline adapted from previously published methods (52). Briefly, the datasets were preprocessed first in a platform-specific way prior to assembly as a merged dataset. For the purpose of this study, a sub-dataset was created by restricting ourselves to the genetic profile of 74 genes of interest, being the ones present or closely related to the biological factors from the mechanistic model as listed in Data S1. 41 genes, out of the 5470 from the full dataset, matched our list of interest, based on the Ensembl IDs, and the associated genetic profiles constituted the final sub-dataset (41 genes (or variables) x 109 samples (or observations)). This dataset was quantile normalized and the batch effects were removed through the ComBat algorithm based on Bayes methods (53).

Inference was performed for regulatory interactions within the aforementioned subset of genes. This was achieved employing three different algorithms, being ARACNE, TIGRESS and GENIE3 (54–56); the final retained network was a consensus network of the three algorithms. Typically, an interaction between a transcription factor and a gene was kept if it was present in the three methods’ results. An interaction was called present for a method if the interaction score was higher than a certain threshold for that method. This threshold was set to $m - \sigma$, where m is the average score for the given method and σ is the standard deviation of the scores.

Unless specified, all the aforementioned microarray data analytics were accomplished using the R computational environment (v.3.2.2). Topological parameter analysis of the final network was carried out with the Network Analyzer plug-in of the Cytoscape software v3.7.2 (<https://cytoscape.org/>) (57).

Implementation of the mathematical model and dynamic analysis

The information contained in the network was translated into mathematical equations through an additive formalism with 2 priority classes to distinguish between fast and slow reactions, the importance of which was repeatedly highlighted (58–60). This additive formalism resembles the Boolean threshold networks (61) and was previously implemented with priority classes as described by Kerkhofs and Geris (2015). In this formalism, the nodes or biological component were represented by variables for which the values evolve over pseudo-time steps. The model is semi-quantitative since the nodes or variables could take on a continuous activity values between 0 and 1. The evolution of variables (proteins or genes) was defined by the sum of the upstream activating variables and the subtraction of the upstream inhibitory variables from the network (see definitions in Table S1). Biological interactions could happen at two time scales, reflecting the priority classes: reactions related to slow biological processes such as gene expression, mRNA or protein production, were referred to as slow reactions (lower priority) and those related to fast processes such as protein activation or inhibition, were

referred to as fast reactions (higher priority) (see Table S1 for the definition of fast and slow reactions & variable). A formal description of the mathematical system underlying the model as well as the full list of equations are available in supplementary method SM1.

The asymptotic solutions were evaluated with a Monte Carlo simulation procedure, similar to methods employed for logical models (25,60). When running a simulation (also see section below on Monte Carlo analysis), an initial value in the interval [0,1] was assigned to each variable. Every simulation step, the sub-variables (see definition in Table S1) were updated asynchronously according to the rules given in the equations and following the priority classes, in such a way that fast reactions were always updated before the slow reactions. The order in which variables were updated within a priority class was random, hereby recapitulating the stochasticity inherent to any biological system. See Fig. S4 and S5 for graphical explanations about the algorithm and simulation scheme on a reduced illustrative example network. A stable state (definition in Table S1) was reached whenever the next iteration step did not bring any change for any of the variables up to a tolerance 10^{-2} . In other words, when initializing the system at a random point, it was considered converged when the relations detailed by the system of equations were fulfilled up to a tolerance of 10^{-2} . Thanks to the stochasticity of the model, the same initial point could lead to different types of stable states. Therefore, all computational results of this paper were computed 3 times and standard deviations were evaluated. All implementations and simulations were carried with the MathWorks® suite, MATLAB (2018b).

Monte Carlo analysis and estimation of attractors (or stable states)

The nature and size of the stable states, given the regulatory network provided in the equations, was estimated by a Monte Carlo procedure. In short, all variables were initialized 10.000 times with random values in the interval [0,1]. The amount of initializations reaching each final stable state were computed and reported in terms of percentage of initial states. This number gives a sense of the stable states' size for the unperturbed system, i.e. without constraints (25,60). Then, we performed two other Monte Carlo canalizations in which all variables were randomly initialized, except for seven growth factors that were fixed at values being physiologically relevant in either a normal healthy or a disease environment (profile A and B of Fig.3B, respectively). The networkD3 package from R was used to produce the Sankey diagram for the visualization of the canalization results.

***In silico* target perturbations**

By essence, the attractors are stable, meaning that variables cannot evolve anymore. These states may however be escaped by forcing, computationally, the value of one or several variables to change. Such a perturbation was imposed for a fixed amount of computational iterations, after which the system was left to evolve freely, thereby accounting for the fact that chemical treatments affect biological systems for a finite period of time. The duration of the perturbation was set to 1000 time steps as the perturbed state did not take more than 200

time-steps to be reached, on average. Imposing a perturbation on a stable state forces the system to evolve again, following rules imposed by the equations, and eventually settle down in the same initial or a new attractor (see convergence description above).

The different *in silico* scenarios or treatment experiments that were tested amounted to perturbing one or several variables/nodes, from the healthy or the diseased hypertrophic state and assessing the effect of that perturbation on the state stability. Variables were perturbed by forcing their global activity value to be 0 or 1 for inhibition or activation respectively. Imposing intermediary values between 0 and 1 was also done for some specific questions in which extreme values would be unlikely, such as varying the ratio between different membrane receptors. Each perturbed conditions was imposed starting from the relevant initial stable states (healthy or diseased) and the nature of the final state to which the perturbation led after simulation was documented. We considered that the tested perturbation triggered a state transition when the final state was different from the initial one. Given the stochastic nature of the model, the same perturbation could trigger a different outcome if simulated a second time, therefore the same perturbation was repeated 100 times and we reported the percentage of transition towards each of the possible target states. Standard deviation in the percentage of transition was assessed by repeating that experiment 3 times.

Due to the computational cost associated with the systematic screening of all possible pairwise perturbations, (for each pair there are 4 possible pairwise conditions to be tested either from the healthy state or from the hypertrophic state. The independent simulations were run in parallel using high performance computing infrastructure of the KU Leuven (Vlaams Supercomputer Centrum). Afterwards, we automatically selected combinatorial conditions for which at least 70% of the perturbations triggered transitions from the hypertrophic state towards the healthy one. Among them, we focused on those conditions with more than 70% transition towards the healthy state but less than 5% towards the 'None' state as a first discriminatory factor. Conditions were further selected for their druggability and their ease to be tested in a simple *in vitro* system. For instance, conditions involving the modulation of transcription factors were not considered for the *in vitro* validation since, no small molecule treatment could directly affect transcription factor activity.

Testing treatments *in vitro* with ATDC5 culture

The validation of our *in silico* predicted treatments required *in vitro* testing with small molecules. This was performed with ATDC5, a mouse chondroprogenitor cell line obtained from the Riken Biological Resource Center. Cells were cultured in 2D in proliferation medium containing DMEM/F12 (ThermoFisher, UK), 5% Fetal Bovine Serum (Biowest, Belgium) and 1% antibiotic/antimycotic (Gibco, ThermoFisher Scientific). Chondrogenic differentiation was induced by plating the cells at 6,400 cell/cm² in proliferation medium for 24h, followed by changing the medium to differentiation medium, being proliferation medium supplemented with 10 µg/ml insulin (Sigma-Aldrich), 10 µg/ml transferrin (Sigma-Aldrich) and 30 nM

sodium selenite (Sigma-Aldrich). Cells were incubated in a humid environment at 37°C, 5% CO₂ and differentiation medium was refreshed every other day for the first 10 days, and every day after the 10th day, for longer experiments (i.e. Fig. 5B). Supernatant medium was taken for ALP activity assay and cells were harvested for DNA quantification (0.05% Triton-X reagent). ALP activity was reported relatively to the total DNA quantity to alleviate potential variation in cell number.

To study the correlation between *Col10a1* expression and secreted ALP activity, cells were differentiated for 14 days with or without Ihh supplement (150ng/ml, R&D Systems Europe LTD). The cells were harvested for RNA isolation on day 0, 7, 9, 12 and 14 during differentiation (TRIzol reagent; Thermo Fisher Scientific), in addition to the ALP activity assay and DNA quantification.

To assess the effect of small molecules and growth factors treatments on hypertrophic differentiation, cells were treated on day 8 of ATDC5 chondrogenic differentiation for readout at day 9. Cells were treated with one or a combination of the following compounds: Forskolin (1µM, Axon Medchem), Recombinant Human/Mouse/Rat Activin A Protein (100ng/ml, R&D Systems), Recombinant Mouse IGF-I/IGF-1 Protein (10ng/ml, R&D Systems), Transforming Growth Factor (TGF)β₁ (10ng/ml, PreproTech), PD0325901 (1µM, Axon Medchem), PD161570 (1µM, Axon Medchem), ITSA1 (50µM, Chembridge), LDN-193189 (0.5µM, Axon Medchem), LY294002 (20µM, Axon Medchem) and IWP2 (2µM, Stem cell technology). ALP activity in treated conditions is expressed in terms of fold change with respect to the control medium with appropriate amount of DMSO, which was used as a solvent for most small molecules. Four types of control media were used throughout this study due to sparse solubilities of the compounds. The control medium was with 0.02% DMSO (Medium1) for most treatments, with 0.1% DMSO (Medium2) for the ITSA1 related conditions, without DMSO for the ActivinA treatment (Fig. 5), and with 0.0375% DMSO for the Forskoline/PD161570 synergy study and dose screening (Fig. 6).

Validating treatments effects in primary human chondrocytes culture in alginate beads

Human articular cartilage was obtained with implicit consent as waste material from patients undergoing total knee replacement surgery. This protocol was approved by the medical ethical committee of the Erasmus MC, University Medical Center, Rotterdam, protocol number MEC-2004-322. To isolate chondrocytes, cartilage chips were subjected to protease (2 mg/ml, Sigma Aldrich) for 2 hours followed by overnight digestion with 1.5 mg/mL collagenase B (Roche Diagnostics, Switzerland) in Dulbecco's Modified Eagle's Medium (DMEM) high glucose supplemented with 10% fetal bovine serum. Single cell suspension was obtained by filtrating the cellular solution by a 100 µm filter. The isolated chondrocytes were expanded in monolayer at a seeding density of 7,500 cells/cm² in DMEM high glucose supplemented with

10% fetal bovine serum, 50 µg/ml gentamicin and 1.5 µg/ml fungizone (Gibco, Grand Island, NY, USA). Upon approximately 80% confluency cells were trypsinised and reseeded at 7,500 cells/cm². Cells were used for experiments after three passages. Redifferentiation of articular chondrocytes was performed using a 3D alginate bead culture model. For preparation of alginate beads, chondrocytes after three passages in monolayer were re-suspended in 1.2% (w/v) low viscosity alginate (Kelton LV alginate, Kelco Co, San Diego, CA, USA) in 0.9% NaCl (Sigma Aldrich) at a concentration of 4×10^6 cells/mL. Beads were made by dripping the cell-alginate suspension in 105 mM CaCl₂ (Sigma Aldrich) through a 22-gauge needle. Beads were washed with 0.9% NaCl and DMEM low glucose. Beads with a size that deviated from the average after a visual inspection were not included in the experiment. Re-differentiation of chondrocytes was performed in a 24-well plate (BD Falcon) for two weeks in 100 µL/bead DMEM low glucose supplemented with 1% ITS fetal (Biosciences), 10 ng/ml transforming growth factor beta one (TGFβ₁, recombinant human, R&D systems) 25 µg/mL l-ascorbic acid 2-phosphate (Sigma Aldrich), 50 µg/ml gentamicin, and 1.5 µg/mL fungizone (both Gibco). After two weeks, TGFβ₁ was no longer added to the medium and cells were cultured with and without 1µM of Forskolin for 24h. Each experiment was performed with cells derived from 4 OA donors (3 Females, 1 Male, 65 ± 6 years), in triplicates.

RNA isolation and real time quantitative PCR (RT-qPCR) for ATDC5 samples

Gene expression of *Col10a1* in ATDC5 experiments was evaluated by RT-PCR. For RNA isolation, chloroform was added to the TRIzol samples (TRIzol 5: Chloroform 1), which were subsequently centrifuged for 15min at 15000 rpm (i.e. RCF = 218849) and 4°C. RNA was isolated by collecting the aqueous phase and precipitated with isopropanol (aqueous phase 1: isopropanol 1) for 30min at -80°C. After centrifugation at 15000rpm (i.e. RCF = 218849) and 4°C for 30 min, supernatant was removed and the resulting pellet was washed with 80% Ethanol. RNA pellets were dried for 10min in desiccator and dissolved in 15µl RNase free water. Finally, RNA content and purity was determined with Nanodrop. RNA was converted to cDNA with the Revert Aid H Minus First strand cDNA synthesis kit (Thermo Scientific) according to the manufacturer's protocols. Quantification of gene expression was done using Syber Select Master Mix (Applied Biosystems) adding 400nM forward and reverse oligonucleotides primers as listed in supplementary method SM2.1. The StepOne Plus System (Applied Biosystems) was used for amplification using the following protocol: denaturation cycle at 95°C for 10min followed by 40 cycles of amplification (15 seconds 95°C and 1 min 60°C), followed by a melting curve. Expression levels were analyzed using the 2-ΔCt method and normalized for the expression of the reference gene *Hprt*. This housekeeping (HK) gene was determined after verification of multiple HK genes and selecting the one that remained most constant throughout the procedure.

The specific RNA isolation protocol, RT-qPCR method and oligonucleotides used for measuring gene expression in primary human chondrocytes is reported in supplementary

method SM2.2.

Alkaline Phosphatase assay (ALP)

Enzymatic activity of secreted ALP in the supernatant medium of ATDC5 cultures was determined in a colorimetric assay as previously described (62). Briefly, ALP activity was determined in flat-bottom 96-well plates (Sigma Aldrich, CAT M9410) containing assay buffer (1.5 M Tris-HCl, pH 9.0, 1 mM MgCl₂; 7.5 mM p-nitrophenyl phosphate). The ALP activity was assessed as a function of formed nitrophenyl phosphate (pNp), the reaction colored product, which was measured by spectrophotometry at 405 nm after 30 min of reaction. The reaction was stopped with 1 M NaOH Stop Buffer. A calibration curve containing an increasing concentration of pNp served to determine the absolute amount of ALP-generated pNp. Sample values were normalized to total DNA amount, expressed as μmol of pNp / mg of DNA and reported as fold change with respect to the relevant control medium.

DNA quantification

After harvesting the cells with 350 μl of 0.05% TritonX-100, samples were vortexed and frozen at -80°C for further processing. Samples were sonicated for 5 seconds, centrifuged for 1' at 13000 rpm (i.e. RCF= 164380) and 200 μl of the supernatant was harvested. Samples were diluted with a factor 1/10 with distilled water then DNA content was measured with the Qubit 3.0 fluorometer (Life Technologies). Qubit dsDNA HS (high sensitivity, 0.2 to 500 ng) Assay Kit was used according to the manufacturer's protocols; a sample volume of 5 μl was added to 195 μl of a Qubit working solution.

Statistical analysis

In general, one-tailed statistical tests were used to analyse *in vitro* results and relate them to expected outcomes from the *in silico* model's predictions since the model predicts a directionality of the outcomes. Average effect of Forskoline and Activin treatments were compared to control in one representative experiment with 3 replicates thanks to a one-tailed unpaired t-test with Welch's correction, in Fig5.C. Effect of Forskoline treatment in OA chondrocytes from human donors was performed in triplicates for 4 donors. Comparison of the average effect with the control is done with a linear-mixed effect model to account for donor variability. Graphical visualization and statistical analyses for the semi-high throughput small molecule screening (Fig.5D) were performed by modifying the BraDiPluS package from the Saez Lab (<https://saezlab.github.io/BraDiPluS/>). More precisely, the probability that a treated condition resulted in lower ALP activity z-score than the corresponding control in the ATDC5 screening was estimated with a one-tailed Wilcoxon rank-sum test (the *in vitro* screening dataset was not normally distributed based on Shapiro-Wilk test), with Benjamini-Hochberg correction for multiple testing. Three independent experiments were performed for each condition, and, treatments effects were assessed in triplicates, in each experiment (or run). Probabilities from the independent runs were combined with Fisher's method using

the `combine.test` function from the `survcomp` R package. A treated conditions was considered lower than control for p-value < 0.05 and z-score < 0.

Results

Highly interconnected intracellular networks regulate articular chondrocytes: building a mechanistic model

In order to build an articular chondrocyte model, we gathered known biological mechanisms from the literature into an activity flow graph or network (Fig. 1). In this graphical influence network, or activity flow representation, the nodes represent biological components (proteins or genes, see Table S1) important for chondrocyte biology (9). Directed edges linking two nodes represent interactions or activating/inhibitory influences between source and target proteins or between transcription factor (TFs) and target genes. Information was collected and adapted from a previously published model of growth plate chondrocytes (20,21) as well as from additional deep literature and database curation (see Method section). The annotations, descriptions and cross-references for each network node and its interactions can be consulted in two interactive networks, a protein signaling one and a gene regulatory one. The former goes from the growth factors binding their respective receptors down to the TF entering the nucleus. The latter represents a network of transcription factors regulating the expression of their target genes, coding for the corresponding proteins in the signaling network (Fig. 1). The two networks are interconnected as each biological component is represented by a gene in the gene regulatory network (GRN) and its corresponding protein in the signaling network. The combination of both networks can be regarded as an interactive knowledge base on chondrocyte signaling and is available through the online platform Cell Collective (22). We refer the reader to that interactive knowledge base for the literature support of our network model (see links in data availability Section), while the main pathways that were included are listed below.

Unless stated otherwise, all components of the network and of the *in silico* model are referred to with names in upper cases that designate the numerical variables, which represent neither the protein nor the gene but a product of both. Therefore, neither the gene nor the protein official nomenclatures are used. A list of correspondence between the numerical variable's names and actual mouse gene names is available in Table S2 and reported in the Cell Collective interactive networks, for information.

The regulatory pathways represented in the network include the canonical and non-canonical WNT BMP pathways, the PThrP and IHH pathways, as well as the IGF-I, FGFs and TGF- β pathways since they are all reported to play a role in chondrocyte fate decisions (9,23). The influence of pro-inflammatory cytokines, such as interleukin 1 Beta (IL-1 β) or Tumor Necrosis Factor Alpha (TNF- α), was summarized through a node labelled 'cytokines', in the network (Fig. 1). That node is able to signal through a single receptor (labelled 'Rinfl') that

can activate well known downstream pathways such as the phosphatidylinositol 3-kinase (PI3K)/AKT axis, the nuclear factor kappa B (NFκB) pathway and mitogen-activated protein kinases (MAPK) pathways. These MAPKs in question include extracellular signal-regulated kinase 1&2 (ERK1/2), c-Jun N-terminal kinase (JNK) and P38. For each of the introduced pathways we represented the downstream signaling cascades and known transcription factors as well as their target genes in the nucleus. Examples of important transcription factors that were included are the IHH signal transducer GLI2, the signal transducer and activator of transcription (STAT1), the transcription factor 7 (TCF), the myocyte enhancer factor 2C (MEF2C) as well as SRY-Box Transcription Factor (SOX9), a marker of differentiated healthy chondrocytes, and runt related transcription factor 2 (RUNX2), a hypertrophy marker. All pathways in the model are strongly interconnected as shown by Fig. 1.

In total, there are 60 biological components in the network, which are listed in Table S2. Each component accounts for a different biochemical entity including 8 growth factors, 8 receptors, 20 transcription factors, 4 ECM proteins and 20 signaling molecules of another type. Combining the signal transduction and the gene regulatory networks into one connected network, leads to a total of 264 direct or indirect biochemical interactions. Each node has on average 7.2 direct neighbors (i.e. directly connected node) and the average shortest path (i.e. smaller number of edges) to connect two nodes is 3.01. Hence, all nodes may virtually influence others by means of a couple of intermediary components, supporting the need to represent and study that network mathematically to conclude on key controllers.

Learning from transcriptomic OA data by complementing the mechanistic network with data-inferred interactions

We complemented the knowledge based GRN with data-driven network inference, allowing for identification of de novo regulatory links, introduction of previously unstudied or undiscovered interactions and the reduction of the bias related to human literature curation. To that end, we generated an informative cross-platform merged dataset on mouse osteoarthritic cartilage. It was composed of 109 samples coming from 6 microarray experiments from which we selected a subset corresponding to the expression profile of 41 genes (see Method and full list in Data S1). The selected genes were the ones present in or closely related to the biological factors from the mechanistic model. The purpose was to identify potential regulatory interactions among those genes of interest only (see Method). The sub-dataset was normalized and corrected for batch effects originating from the differences in microarray platform technologies, as described in the Method section. Our data indicate that the gene expression distribution was correctly normalized among the different microarrays (Fig. 2A). The principal component analysis (PCA) showed the inter-array variance was strongly reduced after merging and correction, thereby highlighting successful removal of the batch effect. As a quality control, we applied an unsupervised clustering method to the merged dataset to evaluate whether the biological information was still maintained after merging and correction. The resulting heatmap features the clustering of the 109 samples as well as their prior annotations as “OA” and “WT” (for

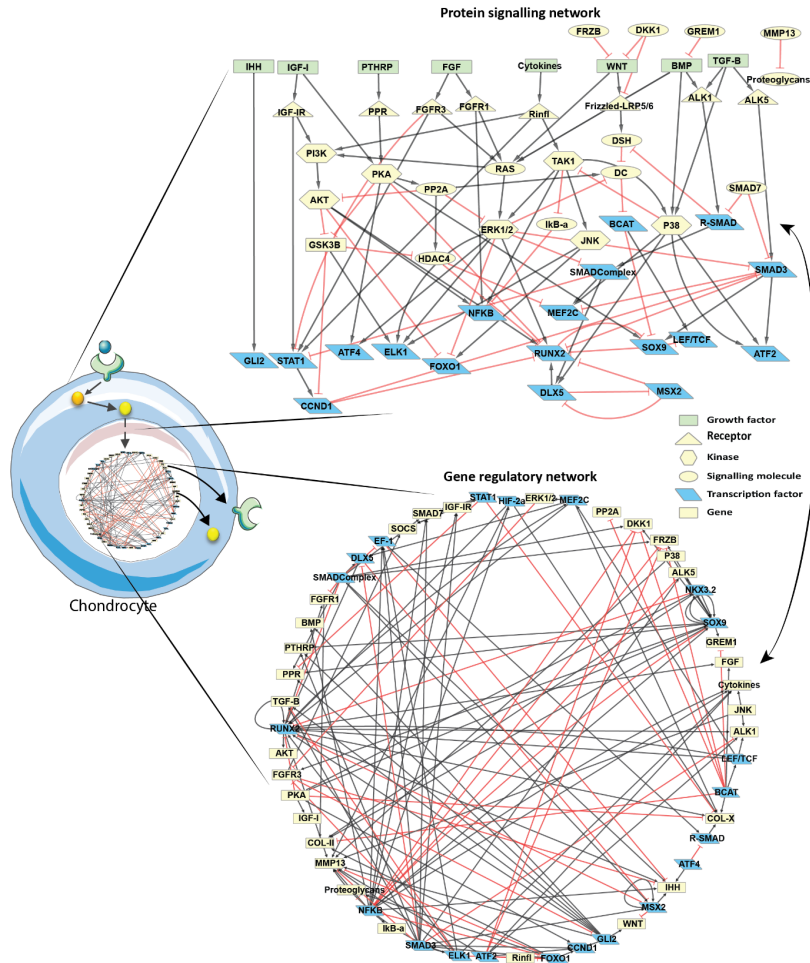


Figure 1 | Influence map of the signaling and gene regulatory networks (GRN) implemented in the model. Red, T-ended arrows represent inhibitory influences and black arrows represent activating influences. On the signaling side, growth factors and pro-inflammatory cytokines are represented by green rectangular nodes, receptors are yellow triangles, kinase proteins are yellow hexagons and other signaling proteins are yellow ellipses. Transcription factors (TFs) are represented in blue both in the signaling network and the GRN. In addition, target genes are represented by yellow rectangles in the GRN and TFs might also be targets of other TFs in the GRN. Each biological component is represented by a gene in the GRN and a protein in the signaling network, except for nodes that are not involved in one of the layers (e.g. NKX3.2 only plays a role in the GRN while COL-II and COL-X do not have upstream or downstream influences in the protein signaling network)

wild-type or control samples) (Fig. 2B). See Method and Data S1 for annotations definition. While splitting the clustering result in three groups, we could identify an OA-like group and a WT-like group as well as a WT-like sample clustering alone. Based on these categories, 81% of the OA tagged samples were correctly identified in the OA group whereas 56% of the WT-tagged samples were correctly located in the WT group. These accuracy levels are similar to the ones achieved when clustering each of the individual microarray experiments

separately, before batch effect removal (Fig. S1). We concluded that, despite the diversity of the technical platforms used in the assembled dataset, most of the variance was not due to the arrays' underlying technology but rather due to the biologically meaningful information usable as input for GRN reconstruction.

In order to complement the GRN with new data-derived hypothetical interactions, we inferred genetic interactions out of this newly assembled dataset. Directed edges between nodes were added in the GRN to account for newly inferred regulatory interactions, as represented in Fig. 2C. We inferred regulatory interactions directed from TFs towards target genes by using three different algorithms to avoid algorithm-specific bias on the inferred edges (see Method) (24). Only interactions predicted by all the three algorithms were implemented in the gene regulation layer of the mechanistic model. In addition, the sign of the Spearman correlation score allowed us to define whether the interactions were genetic activations or inhibitions (Fig. 2C). The inferred interactions are reported with the correlation factors in Fig. 2D. Note that the machine learning methods predicted some TFs as descriptor of a given target gene even for pairs that had not a high correlation score (Fig. 2D). This showed that the ensemble of algorithms we used went beyond the simple correlation for inferring genetic interactions, relying on the concept that some form of covariation is implied by a causal relationship. The inferred interactions were included in the GRN part of the model for all subsequent analyses presented in this study.

The computational model successfully recapitulated two chondrocyte phenotypes and physiologically relevant behaviors

We translated the aforementioned regulatory network into mathematical equations in order to develop an executable numerical model of the articular cartilage chondrocyte. We used a semi-quantitative additive modeling formalism with priority classes as it allows to study large networks without requiring much information on kinetics parameters. Each node takes on a continuous value in the interval $[0,1]$, representing the global functional activity of that node, defined as the multiplication of the gene expression level and the protein activation potential. That way, a protein cannot exert its function on downstream targets unless it is both expressed at the genetic level and activated/not blocked at the post-transcriptional level (global functional activity > 0) (see Method section, supplementary method SM1 and Table S1).

With the above described numerical chondrocyte model, we studied the system free of fixed external cues to identify all potential mathematical stable states that may emerge naturally. These stable states are also called attractors or genetic modules and they equate potentially existing cell phenotypes (see definition of attractors in Table S1). They were evaluated using methodologies similar to those used with logical models (25). Any initial state inputted into the system of equations is like a set of external stimuli that would trigger signal transduction inside a cell, eventually leading to a specific cell state. By randomly initializing the *in silico* model (see method for Monte Carlo analysis) we were able to explore possible model

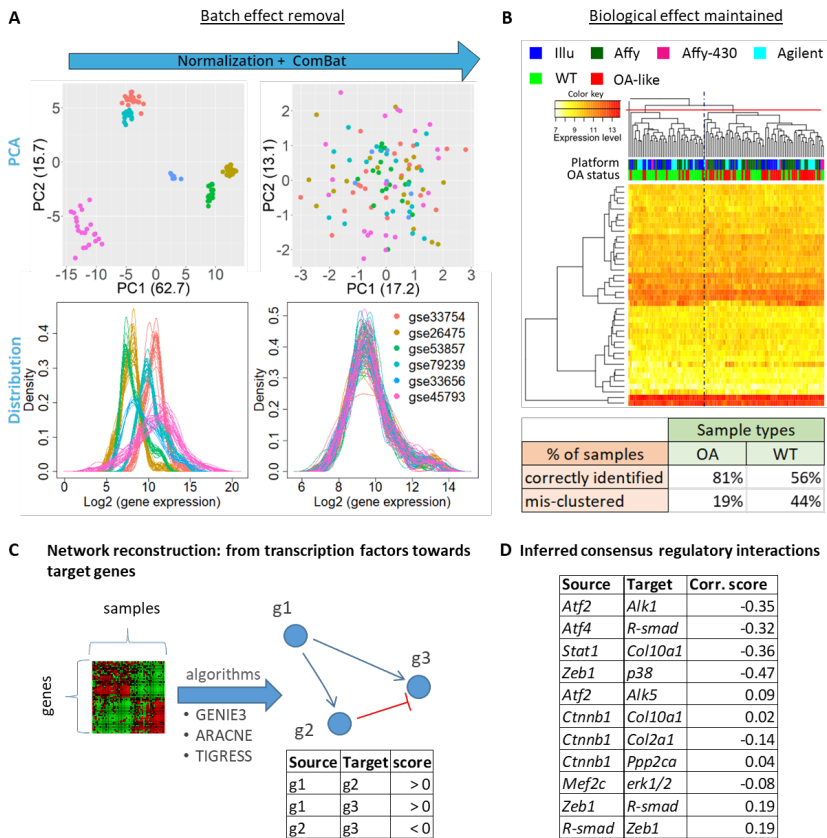


Figure 2 | Microarray integration for GRN inference (A) Assembling and correcting the microarray sub-datasets. PCA plots and gene expression distributions of the assembled dataset colored by arrays (GSE-number), before and after quantile normalization and batch effect correction with the Combat algorithm. (B) Unsupervised clustering with the Euclidian complete method highlights that the samples do not cluster according to the technological platform but rather according to the OA status of the samples. When splitting the hierarchical tree into three branches, a mostly OA group and a mostly WT group stand out. The table summarizes the percentage of true OA (resp. WT) samples correctly grouped in the ‘OA-group’ (resp. ‘WT-group’) highlighting a clustering accuracy in line with what is obtained for the individual sets before correction. (C) Starting from a matrix of gene expression as input, algorithms compute possible regulatory interactions and output a list of possible transcriptional regulatory interactions from a gene coding for a transcription factor to another gene. ‘g1’, ‘g2’ and ‘g3’ denote gene1, 2 and 3, respectively. (D) List of interactions inferred with the merged OA dataset and integrated into the mechanistic model. Inference was run with three algorithms, solely interactions that were present in the results of the three algorithms were reported and integrated. An interaction was considered present for one algorithm if its score was higher than a threshold defined as the difference between the mean and standard deviation of all scores. Corr.score is the spearman correlation coefficient, computed solely to define the interaction sign (activation if positive, inhibition if negative).

outcomes and we observed three emerging attractors. Each of these attractors had a unique global activity profile for the 60 components as reported in Fig. 3A; the details of the protein activation and gene expression level for each component is available in Data S2. Two of the attractor states that we found were biologically relevant, meaning they were comparable to existing chondrocyte phenotypes identified based on known cell state biomarkers such as type II and type X collagen (COL-II and COL-X, respectively), RUNX2 or SOX9. We identified

one of the attractors as a normal healthy articular chondrocyte since markers such as SOX9, NKX.3.2 and COL-II were strongly active and expressed while RUNX2, COL-X and matrix metalloproteinase 13 (MMP13) were inactive or not expressed. In addition, the inflammation-associated nodes had low activity. That correlates with what is known of real chondrocytes during homeostasis. The second attractor corresponded to a hypertrophic-like chondrocyte since RUNX2, COL-X and MMP13 were present or active (i.e. global activities equaling to 1) while SOX9 was not and COL-II and the proteoglycans were degraded and/or not expressed (functional activities nearly zero). In addition, the WNT and inflammation related pathways were active (e.g. WNT =1, DC=0, β -catenin = 1, Cytokines =1, NF κ B = 1, TAK1= 0.76). The third state we found had nearly all protein activities close to zero, consequently, we couldn't associate it with any specific phenotype as it was more likely a trivial mathematical solution. We named it the 'None' attractor as it was neither healthy nor hypertrophic Fig. 3A.

The number of random initializations reaching an attractor during the Monte Carlo simulation gives a sense of the overall attractor's size (attractors are reported in Fig. 3B). Most of the random initial states led to the 'None' final state, reflecting the fact that most of these random initial values might very well be nonsensical from a chondrocyte biology perspective. In addition, about 21% of the initializations led to the healthy state and about 2% to the hypertrophic state (Fig. 3B). These attractors are the spontaneously emerging states arising from the proposed map of biochemical interactions.

We also sampled random initial states while fixing seven growth factors at values that were physiologically relevant in either a normal healthy or a disease environment (profile A and B of Fig.3B, respectively). Interestingly, when imposing the profile A to the growth factors during the Monte Carlo, the system only settled into the healthy state and when imposing profile B it settled into the hypertrophic state, thereby abolishing the 'None' state (Fig. 3B)

With the aim of assessing whether the model could successfully recapitulate relevant physiological behaviors, we established a tool enabling to test experimentally observable scenarios. As a first step to validate our model, we used this tool to test specific scenarios for which the expected outcome was known from literature or hypothesized from clinical observations. For instance, inflammation in the knee is one of the symptoms of OA and has been shown to be one of the drivers of cartilage degradation, possibly by pushing chondrocytes to undergo hypertrophy and produce matrix-degrading enzymes (26,27). For that reason, inflammation-related targets are subject to several investigations for potential OA therapies. Interestingly, *in silico* experiments with our model showed that blocking important transducers of inflammation such as the TGF- β -activating kinase (TAK1) or NF κ B while activating the PTHrP related pathway could push a hypertrophic-like chondrocyte into transitioning towards a more healthy or anabolic state (Data file S2). Moreover, other studies have reported that the TGF- β pathway had a protective effect against inflammation (28–31), a scenario we evaluated with our model too. *In silico* mimicking the presence of inflammation in a healthy chondrocyte by forcing several inflammation related pathways of the model to be set at their highest values led to 100% of transition towards the diseased hypertrophic state

(Fig. 4A). This effect was partially rescued by concomitantly forcing the presence of TGF- β since $5.3\% \pm 1.2$ of the perturbations failed to exit the healthy state, thus, confirming *in silico* that TGF- β could have a protective effect against inflammation through the mechanisms present in the model. Nevertheless, the role of TGF β in OA has been reported to be dual as this growth factor transduces signals in chondrocytes mainly via two receptors, the type I TGF β receptor (ALK5) and the type II TGF β receptor ALK1 (32). They are involved in different intra-signaling routes and depending on which receptor is activated, the downstream-activated signals would be rather anabolic (ALK5) or catabolic (ALK1) (32) and impact chondrocyte maturation differentially (33). Clinical observations reported that the ALK5/ALK1 balance decreased with age and in OA patients (34–36). *In silico* simulations with our model showed that, roughly, the rescue by TGF β was lost when the ratio between the receptors was forced to be $ALK1/ALK5 > 1$ (Fig. 4A and Fig. S2). For higher values of ALK1, ALK1 activity could be as

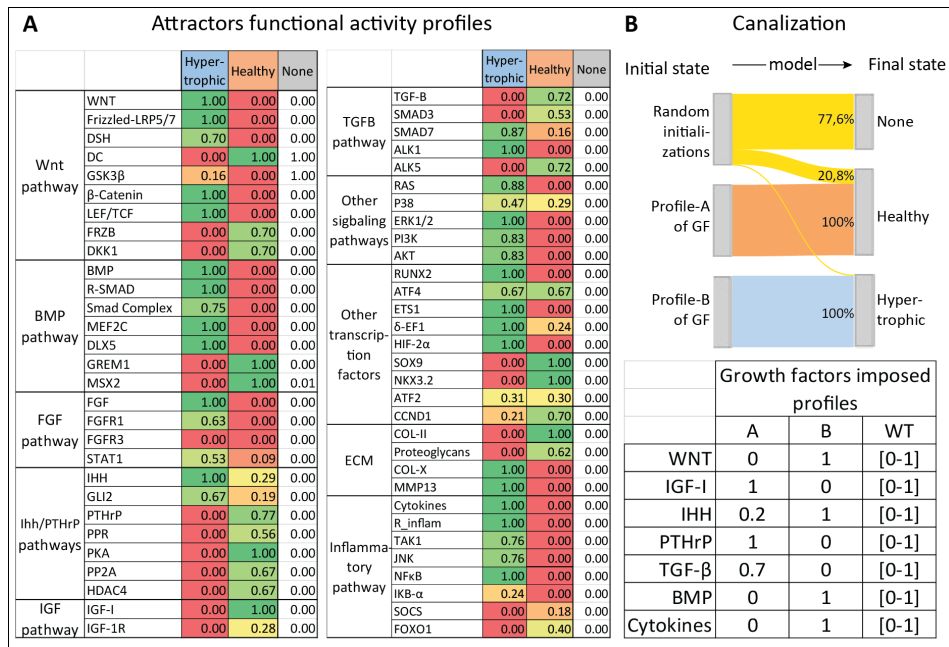


Figure 3 | Predicted chondrocyte profiles and canalization for the three emerging states during Monte Carlo analyses. The Monte Carlo analyses consist in sampling 10.000 random initial states for the variables, with the possibility to impose constraints (similar to external biological cues). (A) The Monte Carlo analysis without constraints highlights the existence of three final states (i.e. attractors) with different activity profiles (in columns). The global activity of a protein is presented in this table as the product of the predicted gene expression and the protein activation level. The table only reports the global activity; a complete table including the gene expression and protein activation levels is available in Data file S2. Rows represent the variables of the model and are grouped by pathways or functional groups. (B) Specific activity profiles were imposed to the growth factors, as reported in the table, while variables other than growth factors were initialized randomly. Profile A represents a possible healthy environment. Profile B represents a more pathological environment. The 'Random' column indicates the case without constraints in which initial activities were randomly sampled within the interval [0,1]. In the Sankey diagram initial states are on the left and final destination states (i.e. attractors) on the right. Strips indicate the percentage of initializations (among the 10.000) that reached each of the possible attractors during the Monte Carlo without constraints ('Random initializations'). That percentage is also reported for the Monte Carlo with constraints (Profile A & B).

low as 0.86*ALK5 and still show the loss of the TGF- β protective effect (Fig. S2). This is in line with what was previously modeled (28), demonstrating that the decrease in that balance could explain why TGF- β loses its protective effect against inflammation in OA patients.

Together, these results show the ability of the articular chondrocyte *in silico* model to behave in a physiologically relevant way and predict emerging effects qualitatively, highlighting the pro- or anti-hypertrophic nature of biological components in specific conditions. The aforementioned tool was further implemented through an executable App (https://github.com/Rapha-L/Insilico_chondro) allowing users, such as biologists, to easily test hypotheses by performing *in silico* experiments on the virtual chondrocyte (see interface Fig. S3).

***In silico* experiments on the modeled system predicted potential important nodes to control chondrocyte fate**

We next decided to exploit further the model by studying the effect of all possible perturbations of each component. Starting either from the healthy or the hypertrophic-like state, variables were individually activated or inhibited in a systematic manner. Over-activation of the FGF receptor 1 (FGFR1) or NF κ B were the most potent conditions to trigger a transition from the healthy towards the hypertrophic state. To a lesser extent, activation of the variables for ERK1/2 kinases, the AKT member of the PI3K/Akt axis, the RUNX2 transcription factor or JNK kinases also promoted this diseased transition (Fig. 4B). On the other hand, transition from the hypertrophic towards the healthy state was mainly triggered by forced activation of the TGF β intracellular effector SMAD3 and partially brought about by activation of the SOX9 transcription factor, IGF-I and members of the PTHrP pathway (i.e. the protein kinase A (PKA), the PTHrP receptor (PPR) and PTHrP). This constitutes a state transition study that can be summarized in the Markov Chain representation (Fig. 4C) with the system's overall probability of transitioning from one state to another under random single node perturbations. Interestingly, despite the small size of the hypertrophic attractor in the random canalization (Fig. 3B), the transition study shows that the total probability of transitioning out of that hypertrophic state under random single node perturbations is 0.11. So, in 89% of the cases, a single node perturbation will not affect this state. This means that even if the hypertrophic state is difficult to reach in the articular cartilage system, it is particularly robust to small single perturbations, and once the numerical system has reached that state, it is unlikely to escape from it, via transitioning to any other state, with a single targeting strategy. For this reason, we also systematically investigated the effect of all possible combinatorial perturbations of two constituents (or pairwise perturbation). The full screening amounted to $(60 \binom{1}{2}) \times 4 = 7080$ tested conditions per attractor. 94% of the variance was explained by the first two components in the PCA reporting the effect (percentage of transition to destination attractors) of the combinatorial treatments on a hypertrophic-like chondrocyte (Fig. 4D). We searched for the most potent conditions to retrieve the healthy state from a hypertrophic chondrocyte (by requiring more than 70% of perturbations input transitioning to the healthy state and less than 5% to the 'None' state), which could point towards potential drug therapies for OA. Based

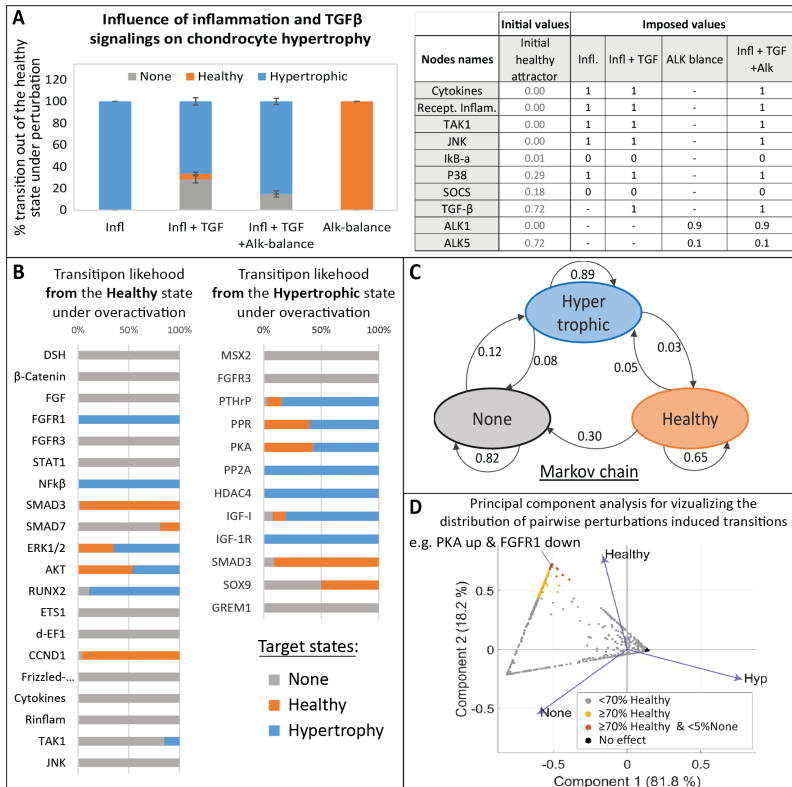


Figure 4 | Study of the virtual chondrocyte state transition and *in silico* screening of target perturbations (A) Relation between Inflammation and TGF β and influence on the chondrocyte state. Perturbations are applied on the healthy attractor, bar height gives the average percentage of transition towards one of the target states, error bar denotes standard deviation. ‘Infl.’ refers to imposed inflammation, ‘TGF’ refers to TGF β over-activation and ‘Alk balance’ to the modification of the ratio between TGF β receptors (ALK1 and ALK5). Conditions were mimicked as described in the table. ‘-’ denotes no modification of the initial value. A transition from ‘healthy’ to ‘healthy’ means no transition. (B) All single node perturbations triggering a state transition from the Healthy (resp. Hypertrophic) state. (C) Markov chain providing the overall probability of transition from one state to another, under single node perturbations. Arrows indicate transitions from an initial state towards a target state with the associated probability. Thus, the total probability of outgoing arrows from any state is 1.0. (D) PCA visualizing the results of the systematic screening of all possible combinatorial perturbations on a hypertrophic-like chondrocyte. Each dot represents one of the 7080 screened conditions. Principal components are computed based on the percentage of transitions towards the 3 attractors, reported as eigenvalues (blue arrows). Dot colors correspond to threshold in the percentage of transition towards the healthy state for potential OA therapies.

on those results, the most efficient way to transition from a hypertrophic towards a healthy chondrocyte in the *in silico* model was with the up-regulation of SMAD3 in combination with activation or inhibition of numerous other targets such as inhibition of the inflammatory mediator NF κ B, inhibition of the DLX5 transcription factor or activation of SOCS, a blocker of pro-inflammatory signals transduction (see complete list in Data S3). Activation of PKA/PPR in combination with inhibition of various targets, such as WNT or FGFR1, also seemed to decrease hypertrophy successfully in the model with 100% of transitions towards the healthy state (Data S3). Therefore, the PKA/PPR axis and SMAD3 seemed to be ‘enablers’ that could ‘unblock’ the *in silico* system, facilitating the effect of other relevant targeting treatments. Moreover, some predictions among the ones triggering more than 70% of transition towards

the healthy state, in Fig. 4D, did not include the two aforementioned enablers. For example, the up-regulation of ALK5 in combination with the down-regulating ALK1, the two receptors of TGF- β in the model, gave more than 90% of transition towards the healthy state. Additionally, inhibition of the WNT pathway while activating ALK5 as well as activation of IGF-1 while activating the destruction complex (DC) involved in the WNT pathway allowed between 70 and 90% of transition towards the healthy state, to mention but a few (Data S3). So, the *in silico* model and associated screening algorithms enabled the prediction of pairwise targeting conditions with a good potential against chondrocyte hypertrophy.

Newly predicted (combinatorial) treatments were validated *in vitro* for their potential to prevent hypertrophy

We used ATDC5s, a chondrogenic murine cell line able to undergo hypertrophy, in order to *in vitro* validate the *in silico* findings obtained from the model. We measured the activity of alkaline phosphatase (ALP), an enzyme typically secreted during hypertrophy and participating to ECM mineralization. It showed that there was a positive linear correlation between the level of ALP activity in the medium and the expression level of the hypertrophic gene *Col10a1* during the ATDC5 differentiation (Fig. 5B). Hypertrophy was further increased when supplementing the differentiation medium with *Ihh*, as expected (Fig. 5B). Indeed this growth factor is known for its pro-hypertrophic effect on ATDC5 (37). These results allowed us to evaluate ALP activity in the medium as a proxy for the level of hypertrophy, significantly increasing the throughput of the experimental set-up for testing small molecule treatments.

This semi-high throughput system was used for validating the *in silico* predictions. *In vitro* experiments evidenced that treatments with Forskolin, an activator of PKA activity or with an activator of the BMP/SMAD3 pathway, were sufficient to prevent the increase in the activity of secreted ALP and thereby were sufficient to block hypertrophy in ATDC5 (Fig. 5C). Additionally, Forskolin treatment decreased *COL10A1* gene expression when applied to primary human OA chondrocytes ($p < 0.01$) (Fig. 5C). Together these results corroborated the *in silico* predictions that activation of PKA was sufficient to block hypertrophic differentiation in chondrocytes (Fig. 5C & D).

Additionally, several combinatorial treatments predicted by the *in silico* screening were tested in ATDC5 and compared to the corresponding individual treatments, to assess their efficacy. In Fig. 5D, ALP activities normalized to total DNA content are reported by means of z-score for all pairwise and single conditions. The ALP activity in the medium during hypertrophic differentiation was lower than the corresponding controls in 6 out of the 8 predicted combinations. The two conditions for which the strongest effect was measured were the inhibition of FGFR1 combined with the activation of PKA ('Forskolin + PD161570', $p = 0.032$) and the inhibition of BMP combined with PKA activation ('LDN-193189 + Forsk', $p = 0.014$). These two combinations seemed to generate an added effect compared to the single drugs. Contrary to *in silico* model predictions, treatment with exogenous IGF-1 combined with BMP inhibition ('IGF-I + LDN-193189', $p = 0.105$) or inhibition of ERK1/2 combined with PKA

activation ('PDO325901 + Forsk', $p = 0.264$) did not show a significantly lower hypertrophic level, based on ALP activity (Fig. 5D).

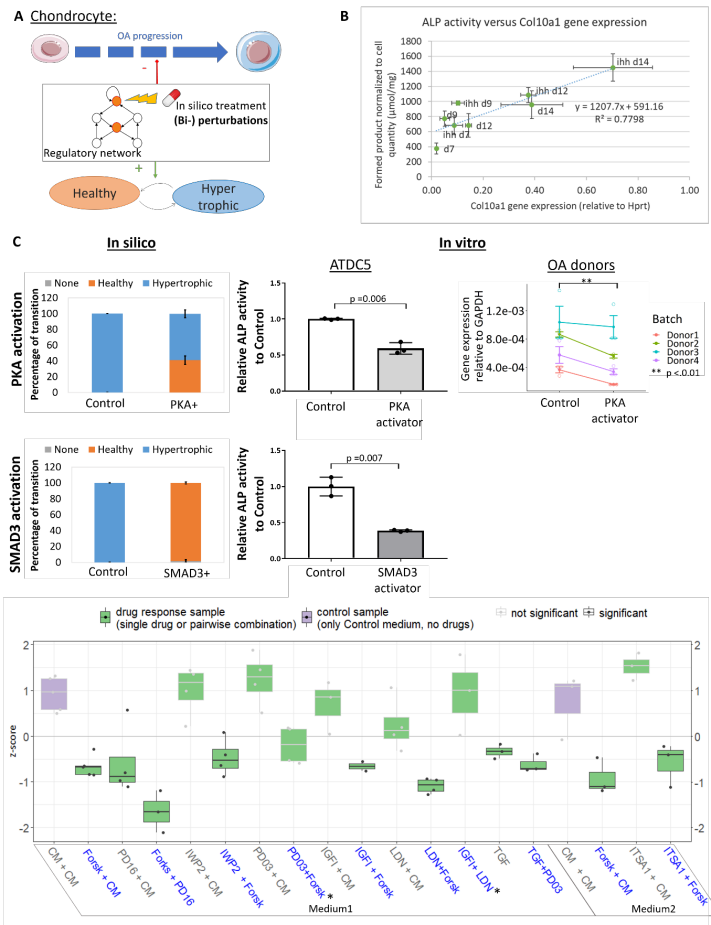


Figure 5 | In vitro validation of in silico predictions on chondrocyte phenotype changes. (A) Concept of *in silico* identification of potential drug targets. (B) Secreted ALP activity, relative to DNA quantity, is positively linearly correlated to *Col10a1* gene expression during hypertrophic differentiation with and without Ihh treatment. Each point is the average of 3 replicates and bars denote standard deviation. (C) Effect of PKA or SMAD3 activation as measured in silico and in vitro in ATDC5 ($N = 3$ replicates, histograms show average fold change in ALP activity relative to control and bars are standard deviations, p -values are computed with one-tailed t -test and welch's correction) and chondrocytes from OA donors ($N = 4$ donors with 3 replicates each, p -value is computed with one-tailed linear mixed effect model). In silico activation was performed by setting the nodes to their maximum value (1.0), in vitro PKA (resp. SMAD3) activation was performed with Forskolin $1\mu\text{M}$ (resp. Activin 100ng/ml) for 24h. (D) Single and combinatorial drug screening in ATDC5 with selected conditions based on in silico predictions. Boxplot of the series of conditions across independent replicates (z -scores of ALP activity fold change) with control conditions in purple. Conditions significantly lower than the control (combined p -value < 0.05) have dark grey borders and dots (Wilcoxon rank-sum test with BH correction) and combined probabilities over independent runs). For each condition, dots are the average of biological triplicates, summary statistics are represented by a horizontal line for the median of independent experimental repetitions and a box for the interquartile range. The whiskers extend to the most extreme data point that is not > 1.5 times the length of the box away from the box. Blue labels indicate potent conditions predicted by the in silico model, grey labeled conditions are added to the experimental set-up for information. CM stands for 'control medium', medium1 has 0.02% of DMSO and medium2 0.035%. *indicates in silico predicted conditions that did not show a significant decrease of ALP activity *in vitro*.

Elaborating one of the conditions that showed the strongest response, PKA activation combined with FGFR1 inhibition, we compared the combinatorial effect with the corresponding single drug treatments. The combinatorial effect was greater than the one for either of the single drug, for both tested concentrations ratios (Fig. 6A). This suggests that activating PKA (resp. inhibiting FGFR1) would potentiate or enable the effect of FGFR1 inhibition (resp.

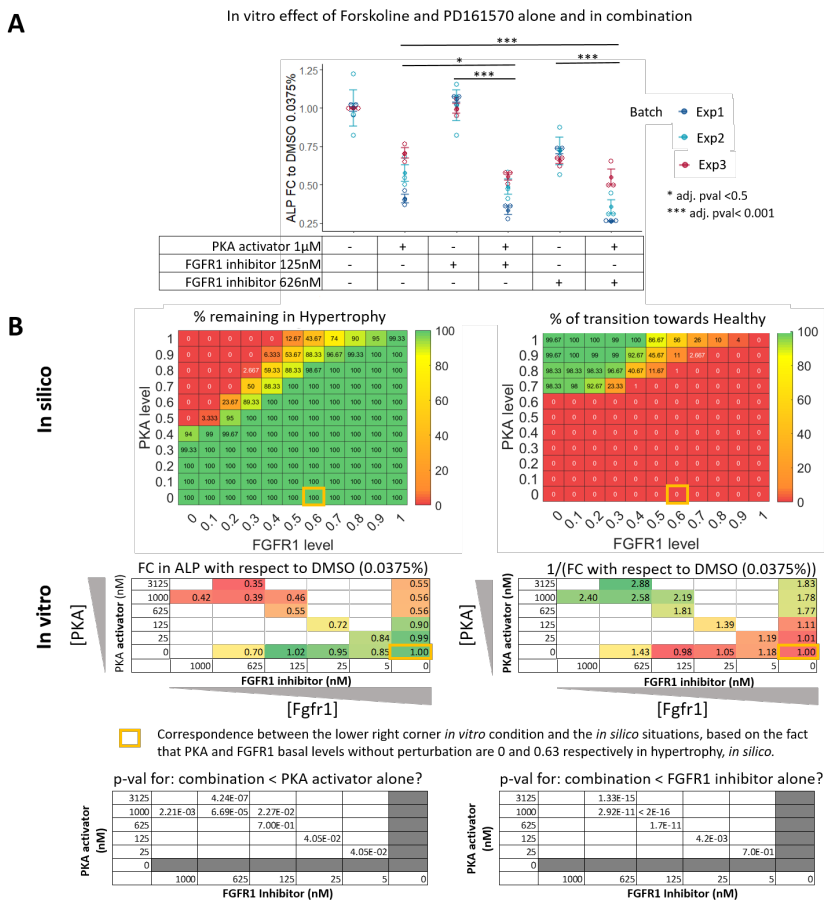


Figure 6 | In silico v.s. In-vitro dose response effect of PKA activation with FGFR1 inhibition. The most potent condition from the screening is investigated further for a potential dose effect. (A) Fold change (FC) in ALP activity, with respect to control, due to PKA activator (Forskoline, 1 μ M) or FGFR1 inhibitor (PD161560, 125nM and 625 nM) or the combination of both. (B) A range of values for PKA and FGFR1 imposed activities is screened in silico with 0 meaning no activity and 1 being the max possible activity. The percentage of transition remaining in the hypertrophic state or transitioning towards the healthy state are reported in the upper panels, the rest of the transitions goes to the 'None' state. In the middle panels, fold change (resp. inverse of fold change) in DNA-normalized ALP activity with respect to control DMSO in ATDC5 is reported for a range of Forskolin and PD161570 concentrations. The in-vitro situation without drugs (yellow rectangle) would correspond to the basal level of PKA and FGFR1 in in-silico hypertrophy but there is no one to one correspondence between the in silico and in vitro ranges. All in vitro results represent n=9 (3 bio-replicates in 3 independent experiments), p-values are computed on log-transformed data with a linear mixed-effect model, user defined contrasts (only combination versus corresponding single doses were compared), one-sided test and adjustment for multiple comparisons with the Holm's method. The combinatorial treatment effects were greater than the ones for either of the single treatment both in silico and in vitro, for all concentrations in the gradient of dose relationships investigated.

PKA activation) by blocking or unblocking key pathways and maintaining the necessary constraints on the system. Dose curve relationships need to be established to confirm that hypothesis. Screening various values of functional activities of PKA and FGFR1 with the virtual chondrocyte and looking at the percentage of transition out of the hypertrophic state, showed that a minimal level of PKA activity (namely about 0.4 on a scale from 0 to 1) was required to achieve any positive effect with this combinatorial treatment (Fig. 6B). In addition, a gradient effect was observed suggesting that the lower the PKA activity, the more we needed to block FGFR1 to achieve an equivalent positive effect (Fig. 6B). *In vitro* validation confirmed this dose effect since the overall gradient shape was very comparable between the *in silico* and *in vitro* situation (Fig. 6B). Comparing the diagonal (combinations of two drugs) to the single drug ranges also highlighted a likely synergistic effect in decreasing hypertrophy between the two drugs, at the tested 1:5 ratio. Taken together, these results support that targeting the regulatory mechanisms at multiple points might be necessary to maintain a physiologically healthy state for a chondrocyte experiencing hypertrophy inducing cues.

Discussion

We report the construction of a mechanistic model of chondrocyte phenotype control in articular cartilage by combining a knowledge-based approach with a data-driven approach. We have leveraged decades of knowledge and data about chondrocyte regulatory pathways and osteoarthritis by integrating that information in a numerical predictive model. This model enables to recapitulate physiologically relevant observations and predict conditional effects resulting from intricate intracellular signalings. It offers the possibility to screen a large amount of (combinatorial) treatments and prioritize subsequent *in vitro* experiments for the identification of molecular drivers and drug targets in OA. The *in silico* targets perturbation screening and the experimental validation of our findings show the potential of *in silico* experiments to identify relevant *in vitro* experiments and refine the early drug discovery pipeline for OA. In particular, our study points towards a likely synergistic effect of PKA and FGFR1 targeting strategies to regulate chondrocyte hypertrophy. Several of our insights have implications both for the network modeling community and for cell and cartilage biology.

We have first built an interactive intracellular network as an online knowledge base and as a reference support for our numerical model. Most network-based models rely on prior mechanistic knowledge. Even current state of the art computational tools meant to reconstruct numerical models automatically from (high-throughput) data often require or offer the possibility to introduce prior knowledge (38). Therefore, there is high need for integrating and curating originally isolated pieces of knowledge, in a comprehensive way. However, biochemical information specifically related to cartilage and osteochondral systems are scarce in public and private pathway databases, in which cancer related cell types tend to be over-represented. The network we provide along with this study, details the prior mechanistic knowledge we have put in the model and that was predominantly chondrocyte or

osteochondral cell type specific, with a focus on articular chondrocytes and osteoarthritis. In our opinion, it is valuable not only for cartilage and OA researchers but also for modelers as it can serve as a basis to derive other models to answer alternative questions.

Combining knowledge and data in a comprehensive network resulted in a systemic view of chondrocyte intracellular regulation. Many independent pieces of information have accumulated over the past decades and many databases have made curated pathways available. Most of the time in literature, these pathway descriptions stop after the (in)activation of the downstream transcription factors while the identity of the target genes downstream these pathways is left obscure. In this study, our strategy was to complement the knowledge based network graph with automatically inferred transcriptional regulations from transcriptomic data through the use of machine learning methods. This usually requires a large multi-perturbed dataset but in absence of such dataset for chondrocytes, we reconstructed one by merging various arrays. Our strategy is supported by a previous study, which reported that equivalent informative data could be successfully achieved by assembling naturally occurring and experimentally generated phenotypic variations of a given cell type (39). Even though relatively few inferred gene regulatory interactions were integrated in the mechanistic model due to the stringency of our selection strategy, we limited the risk of integrating false positive predictions. This data-driven approach allowed us to take advantage of automatic network reconstruction technologies, which are becoming more and more the standard in the state of the art (40,41).

The translation of that network into mathematical rules was then further studied computationally and enabled the prediction of the overall effect of each network component on the virtual chondrocyte. Our perturbation screening approach helped to discover influencer nodes based on the mathematical dynamics, similarly to what had been previously proposed for other diseases (17). Important to mention is that no information was put in the model that directly made one target prevail over the others in being pro- or anti-hypertrophic. The information that fed the mathematical model was about activating or inhibitory influences of one molecule on another molecule, a complex of molecules or a pathway although some edges in the network represented indirect links for the sake of simplification. The advantage of the discrete semi-quantitative mathematical formalisms we employed lies in its ability to reproduce qualitative dynamics using only the activating or inhibitory nature of interactions and additive rules, without any prerequisite about kinetics. This characteristic makes that method perfectly suitable for a large network such as the one of this study. Many biostatistics and machine learning methods that make drug efficacy related predictions solely based on omics data still lack predictability and interpretability (42). In contrast, the numerical approach presented in this study has the advantage of providing mechanistic evidence supporting the predicted effects, thereby increasing the mechanistic interpretability.

Generally, the validation of an *in silico* model to answer questions in a specific context may be achieved in two ways: either by showing its ability to predict non-linear effects that were already reported in literature or by confirming predictions with new experiments. The

relevance of our model to answer osteoarthritis-related questions was first confirmed by its ability to recapitulate earlier described behavior such as the changing role of TGF β signaling in presence of inflammatory stimuli. A recent computational study reporting a quantitative (ODE-based) time dependent model of cartilage breakdown (28) provided more detailed and complexed kinetics underlying the dual role of TGF- β . The fact that our model could lead to equivalent conclusions shows that the more simplifying semi-quantitative formalism that we employed could suffice to capture non-straightforward effects, thereby supporting its credibility for subsequent predictions.

The Monte Carlo analysis of the system without constraints showed that the healthy state was more easily reached than the hypertrophic one. This corroborates with the situation for normal articular cartilage in which chondrocyte hypertrophy does not spontaneously occur unless the homeostasis is disturbed (43). A great part of the state space was occupied by the ‘None’ attractor that is most likely a trivial solution towards which the system converges when an initial state or a trajectory is too far away from a feasible biological state to meet all the constraints imposed by the equations. In such a situation the trivial ‘zero’ solution is more easily reached. An analysis of the ensemble of initial states reaching the ‘None’ state, could possibly spotlight initial states that are unlikely to happen in an *in vivo* physiological environment. Conversely, the analysis of canalization under imposed growth factor profiles have suggested that restricting ourselves to initializing growth factor’s values within biologically ‘feasible’ ranges can decrease prevalence of the ‘None’ state, although the boundaries of those feasible ranges could be further explored. Nevertheless, in the scope of finding potential therapeutic targets, we are less interested in the random canalization of the states than in their robustness to perturbations and capacity of transitioning.

An important result of this study is the highlights that chondrocyte phenotypes are not much sensitive to small, single factor perturbations. Even though, the resistance of the current *in silico* model to single factor perturbation might, in part, be due the omission of some parts of the real world system’s complexity, this trait of robustness to small environmental variations is often considered as a fundamental and ubiquitous trait of biological systems (44). This traits allows systems to function in noisy environments (45) and systems biologists have theorized that disease may establish its own robustness, in some cases (46). In line with that, the Markov chain in our computational model indicates that, for articular chondrocytes, the probability to change phenotypes once it has been reached is rather low. Indeed, due to the very intricate interplay of molecules, it is likely that some pathways play redundant roles and that several factors should be targeted simultaneously to ‘unlock’ the system. Moreover, our *in silico* pairwise perturbation screening confirms that targeting at least two proteins at the same time increase the chance to unlock the hypertrophic commitment. Overall, as its *in vivo* counterpart, the *in silico* articular chondrocyte is unlikely to display hypertrophic signs in normal conditions or even sometimes under inducing treatment (10), but once the hypertrophic transition has been initiated, it is rather difficult to escape that fate.

Another important outcome is the experimental validation of the model predictions on

previously unreported conditions. In practice, as reverting a hypertrophic chondrocyte back to a healthy state has never been observed experimentally, we hypothesize that the *in silico* predicted conditions are, at least, more likely to block hypertrophy. The *in vitro* results that we present here support this hypothesis and open new routes for further testing the suggested combinatorial conditions. Especially, the combination of PKA activation with FGFR1 inhibition is highlighted as good candidate treatment by our integrated *in silico-in vitro* approach. Activation of the PThrP pathway, to which PKA belongs, has already been reported to be rather anti-hypertrophic for growth plate chondrocytes (47). Similarly, genetic inhibition of the *Fgfr1* gene in mouse knee cartilage has been shown to attenuate the degeneration of articular cartilage in mice (48). However, to our knowledge, this combination has never before been investigated nor reported for its synergistic potential against hypertrophy, cartilage degradation or OA.

Validating *in silico* predictions for drug target discovery experimentally is a challenging task. This is especially true when numerical high-throughput screenings, enabled by high computing power, generate a large amount of predictions. We leveraged the evaluation of secreted ALP activity in ATDC5 cell line as a semi-high throughput read-out for validating the *in silico* predictions. Indeed, it served as a convenient experimental system to assess hypertrophy modulation under many screened perturbations (49). Even if that cell line is of mouse origin and cultured in isolation from a physiological environment, we propose to use it within an *in silico-in vitro* pipeline that would act like a funnel for prioritization of candidate drug targets. As shown in our study the main hits can then be further evaluated in more detail using human OA chondrocytes.

We acknowledge that our study has some limitations. A first drawback is the absence of a gold standard to assess the precision of the data-driven network inference. To mitigate this, we used a consensus approach by only integrating predictions made by three different machine learning methods. This reduced the amount of interactions we would integrate but it alleviated each method's weakness and reinforced the strengths of the predictions, as previously proved (24). Secondly, the type of mathematical model we employed comprises almost no numerical parameters but the main one, the saturation constant, was assigned an arbitrary value based on a previous study (20). This constant determines how fast a protein activity or gene expression can saturate to the maximal value depending on the amount of excess positive and negative upstream interactions. It intervenes in the weight of interactions and changing its value might slightly affect the influence of the network's constituents on the system. Finally, we did not experimentally verify the target specificity and dosing regimen for the small molecules employed for our *in vitro* validation since it was out of the scope of this study. However, those small molecules were selected based on their previously reported and well-known *in vitro* action on our targets of interest.

Conclusion

This study is a proof-of-concept that an *in silico* - *in vitro* integrated approach can suggest single and combinatorial target perturbations affecting the hypertrophic transition and help to prioritize therapeutic targets for OA therapy development. In that sense, our model offers the possibility to draw conclusions on the pro- or anti-hypertrophic nature of biochemical pathways and targets based on strict mathematical rules describing the intricate network connectivity. We are convinced that this type of approach can guide the process of therapy development from basic understanding to target selection early on in the drug discovery pipeline while reducing time and cost of experiments as well as the use of animal models in early stages of drug discovery. Furthermore, investigating the effect of a new target that was not present in the current model should be possible by solely informing the model on how the target interacts with and connects to the rest of the network. Typical information on the nature of the upstream activators and inhibitors of the protein's functionality, the nature of downstream proteins modulated by the target under scrutiny as well as information about its transcriptional regulators, from DNA binding assays for instance or reverse engineered from data would be needed. Ideally, this information should be as exhaustive as possible based on current state of the art knowledge, while hypothetical connections could be investigated and compared based on the simulated target's effect. Finally, as scientific research is making progress in the identification OA disease subgroups based on molecular markers and clinical phenotypes (50,51), we foresee data-informed mechanistic models can become more and more patient-type specific. For instance, such knowledge-based network model could serve as a prior and be further optimized with engineering approaches, adjusting the network topology and/or interaction weights, in order to fit chondrocyte baseline profiles of typical patient subgroups. The resulting network models and the effect of targets' perturbations could be compared across the different patient type-specific models.

In conclusion, this work provides a virtual articular chondrocyte in the form of a signal transduction interactive knowledge base and of an executable computational model, and the demonstrated *in silico* - *in vitro* strategy opens new routes for developing osteoarthritis targeting therapies by refining the early stages of drug discovery.

Supplementary Materials

Supplementary computational method SM1

Mathematical framework and system of equations for the articular chondrocyte regulatory network:

Theoretical frame:

The potential function of a component (or node) on its downstream neighbours is called the

global activity. It corresponds to the multiplication of the gene activation level by the protein activation level.

Let's consider the adjacency matrix A of the network whose entries a_{ij} can be 0, 1 or -1. This matrix indicates the presence and the direction of edges in the network. If node j activates node i , then a_{ij} is 1; if node j inhibits node i , a_{ij} is -1. a_{ij} equals 0 when no interaction from node j to node i is present. The vector $L = l_{ij}$ contains a weight for each interaction in the regulatory network. Given A and L , the full system of equations contains equations for both the fast and the slow reactions regulating each variable and can be written as:

$$\begin{cases} z_1^f(t+1) = a_{11}^f l_{11}^f z_1(t) + a_{12}^f l_{12}^f z_2(t) \dots + a_{1n}^f l_{1n}^f z_n(t) \\ \dots \\ z_n^f(t+1) = a_{n1}^f l_{n1}^f z_1(t) + a_{n2}^f l_{n2}^f z_2(t) \dots + a_{nn}^f l_{nn}^f z_n(t) \\ z_1^s(t+1) = a_{11}^s l_{11}^s z_1(t) + a_{12}^s l_{12}^s z_2(t) \dots + a_{1n}^s l_{1n}^s z_n(t) \\ \dots \\ z_n^s(t+1) = a_{n1}^s l_{n1}^s z_1(t) + a_{n2}^s l_{n2}^s z_2(t) \dots + a_{nn}^s l_{nn}^s z_n(t) \end{cases} \quad (\text{eq.1})$$

Or

$$\begin{cases} \mathbf{z}^f(t+1) = A^f L^f \mathbf{z}(t) \\ \mathbf{z}^s(t+1) = A^s L^s \mathbf{z}(t) \end{cases} \quad (\text{eq.2})$$

and the global activity of the component i at the time $t+1$ is defined

as (eq.3)

$$z_i(t+1) = z_i^f(t+1) \times z_i^s(t+1)$$

where n is the total number of nodes in the network, \mathbf{z} is a vector containing the activities for all nodes, $A^v = [a_{ij}^v]$ and $L^v = [l_{ij}^v]$ are matrices with $v \in \{s, f\}$ and $i, j \in [1, n]$. f and s denote fast and slow variables, respectively. \mathbf{z}^f and \mathbf{z}^s and \mathbf{z} are $n \times 1$ vectors filled with the z_i^f , z_i^s or z_i elements respectively. When two nodes are known to act in complex and in synergy, their individual terms are merged. Indeed, a term $a_{i(j,k)} l_{i(j,k)} z_j z_k$ replaces $a_{ij} l_{ij} z_j + a_{ik} l_{ik} z_k$ in the equations (eq.1).

The additive sum includes a weight (l) for each term that assumes a limited amount of saturation whenever there is a majority of stimulatory interactions. The value of that saturation depends on the interactions' signs as defined by Kerkhofs

et al. in (7):

(eq.4)

$$l_{ij} = \begin{cases} 1, & \text{if } \sum_{j \in U} a_{ij} \leq 1 \\ 2 \frac{SC}{\sum_{j \in U} a_{ij}}, & \text{if } \sum_{j \in U} a_{ij} > 1 \end{cases}$$

where U is the set of nodes' indexes that are upstream node i and SC is the saturation constant. If the positive interactions do not outnumber the inhibitory interactions by more than 1, all weights are set to 1. If the number of excess positive interactions is higher than 1, we introduce a saturation factor whose value will determine how fast the node will saturate. The saturation constant was set to $\frac{2}{3}$ in that study based on (1). The table below (**Table sup. text 1**) shows the weights for various values of $\sum_{j \in U} a_{ij}$ (the number of excess positive interactions). We refer the reader to the paper of Kerkhofs et al. (1) for more information pertaining to the implication of the saturation term and sensitivity to the saturation constant value.

$\sum_{j \in U} a_{ij}$ (excess positive interactions)	2	3	4	5
l_{ij} (weight)	$\frac{2}{3} \approx 0.66$	$\frac{4}{9} \approx 0.44$	$\frac{1}{3} \approx 0.33$	$\frac{4}{15} \approx 0.267$

Table sup. text 1: Weight for various values of the number of excess positive interactions and for the saturation constant set to $2/3$.

Overall, while these rules cover a standard situation, incorporation of relevant biological facts should always prevail over these a priori rules. For that reason, some adaptations to the weights in the chondrocyte network were introduced to better reflect natural expression profiles in the WT situation.

Importantly, this additive model was semi-quantitative since the nodes or variables could take on a continuous activity value between 0 and 1. For a given sub-variable (i.e. fast or slow) if the sum and subtraction of activator and inhibitory influences was higher than 1 (respectively lower than 0), then the component was considered as fully activated (resp. inhibited) and the value was brought back to exactly 1 (resp. 0). In mathematical terms:

(eq.5)

$$z^v(t) = \begin{cases} 0, & \text{if } z^v(t) \leq 0 \\ 1, & \text{if } z^v(t) \geq 1 \end{cases}$$

with $v \in \{s, f\}$.

- *Application to the chondrocyte network:*

In the articular chondrocyte regulatory network (c.f. **Fig. 1**), the global activity of a variable i is defined as follow (c.f. **eq.3**) :

$$z_i(t) = z_i^f(t) \times z_i^s(t) \quad (\text{eq.6})$$

with $i \in [1, 60]$, indicating the variable number.

The full system of reaction is provided in two parts: (a) the fast reactions, (b) the slow reactions, the variable index refers to the index provided in **Table S2**.

a) Fast reactions (protein signaling network)

$$z_1^f(t+1) = 1 - z_{49}(t) - z_{48}(t)$$

$$z_2^f(t+1) = z_{50}(t) - 0.3 * z_4(t)$$

$$z_3^f(t+1) = 1$$

$$z_4^f(t+1) = z_{52}(t) - 0.5 * z_{25}(t) + z_{52}(t)$$

$$z_5^f(t+1) = 1$$

$$z_6^f(t+1) = \frac{2}{3} * z_5(t)$$

$$z_7^f(t+1) = 1 - z_{36}(t)$$

$$z_8^f(t+1) = z_7(t) - z_{10}(t)$$

$$z_9^f(t+1) = z_{38}(t) + z_{22}(t) + z_{32}(t) - z_{10}(t) - z_{14}(t) - z_{26}(t) \times z_{30}(t) - z_{31}(t) - z_{43}(t)$$

$$z_{10}^f(t+1) = z_{14}(t) + z_{26}(t) - z_7(t) - z_{19}(t)$$

$$z_{11}^f(t+1) = 1$$

$$z_{12}^f(t+1) = z_{11}(t)$$

$$z_{13}^f(t+1) = 1$$

$$z_{14}^f(t+1) = (z_{12}(t) + z_3(t)) \times s_2$$

$$z_{15}^f(t+1) = z_{34}(t) + z_{19}(t) - z_{30}(t) - z_{26}(t)$$

$$z_{16}^f(t+1) = 1$$

$$z_{17}^f(t+1) = z_{16}(t)$$

$$z_{18}^f(t+1) = \frac{2}{3} \times \left(\frac{2}{3} \times z_{17}(t) + \frac{2}{3} \times z_{27}(t) \right) + \frac{1}{3} \times z_{42}(t) - z_{19}(t) + z_{54}(t) \times (1 - z_{17}(t))$$

$$z_{19}^f(t+1) = z_4(t) - 0.25 \times z_{22}(t)$$

$$z_{20}^f(t+1) = 1$$

$$z_{21}^f(t+1) = 1$$

$$z_{22}^f(t+1) = z_{41}(t) - z_{37}(t) + z_{55}(t)$$

$$z_{23}^f(t+1) = 1$$

$$z_{24}^f(t+1) = 1$$

$$z_{25}^f(t+1) = 1$$

$$z_{26}^f(t+1) = z_{53}(t) - 0.5 \times \left((z_{22}(t) + z_{31}(t) + z_{25}(t)) \times s_3 \right)$$

$$z_{27}^f(t+1) = z_{16}(t)$$

$$z_{28}^f(t+1) = (z_{34}(t) + z_{34}(t) \times z_{26}(t)) \times s_2$$

$$z_{29}^f(t+1) = (z_{27}(t) + z_{38}(t) + z_{55}(t) - z_{58}(t)) \times s_2$$

$$z_{30}^f(t+1) = z_{37}(t) - z_{35}(t)$$

$$z_{31}^f(t+1) = 1 - 0.5 \times (z_{35}(t) + z_{18}(t))$$

$$z_{32}^f(t+1) = z_{34}(t) + z_{19}(t) - z_{43}(t)$$

$$z_{33}^f(t+1) = 1 - z_{47}(t)$$

$$z_{34}^f(t+1) = (z_{23}(t) + z_{33}(t) + z_{55}(t)) \times s_3$$

$$z_{35}^f(t+1) = 1 - z_{14}(t) - z_{38}(t)$$

$$z_{36}^f(t+1) = 1 + z_{37}(t) - z_2(t) - 0.5 \times z_{22}(t)$$

$$z_{37}^f(t+1) = z_{14}(t)$$

$$z_{38}^f(t+1) = z_{39}(t) - 0.5 \times z_{37}(t)$$

$$z_{39}^f(t+1) = (z_{41}(t) + z_{42}(t) + z_{54}(t)) \times s_3$$

$$z_{40}^f(t+1) = (z_{22}(t) + z_{56}(t)) \times s_2$$

$$z_{41}^f(t+1) = (z_1(t) + z_{33}(t) + z_{17}(t) + z_{27}(t)) \times s_4$$

$$z_{42}^f(t+1) = z_3(t)$$

$$z_{43}^f(t+1) = 1 - z_{32}(t)$$

$$z_{44}^f(t+1) = 1$$

$$z_{45}^f(t+1) = (z_{14}(t) + z_{22}(t)) \times s_2$$

$$z_{46}^f(t+1) = 1$$

$$z_{47}^f(t+1) = 1$$

$$z_{48}^f(t+1) = 1$$

$$z_{49}^f(t+1) = 1$$

$$z_{50}^f(t+1) = z_1(t) - z_{49}(t)$$

$$z_{51}^f(t+1) = 1$$

$$z_{52}^f(t+1) = z_{23}(t) - z_{33}(t)$$

$$z_{53}^f(t+1) = z_{23}(t)$$

$$z_{54}^f(t+1) = z_{51}(t) - z_{59}(t)$$

$$z_{55}^f(t+1) = z_{54}(t) - 0.5 \times z_{34}(t)$$

$$z_{56}^f(t+1) = z_{55}(t)$$

$$z_{57}^f(t+1) = 1 - z_{24}(t)$$

$$z_{58}^f(t+1) = 1 - z_{55}(t)$$

$$z_{59}^f(t+1) = 1$$

$$z_{60}^f(t+1) = 0.75 + z_{56}(t) - z_{38}(t) - z_{22}(t)$$

a) Slow reactions (gene regulatory network)

$$z_1^s(t+1) = 2 \times z_6(t) - z_{43}(t)$$

$$z_2^s(t+1) = 1$$

$$z_3^s(t+1) = z_{14}(t)$$

$$z_4^s(t+1) = 1 - z_{45}(t) + z_{44}(t)$$

$$z_5^s(t+1) = (z_9(t) + z_{19}(t) + z_{29}(t) + z_{45}(t) - z_{44}(t) - z_{17}(t)) \times s_2$$

$$z_6^s(t+1) = 1 - z_{17}(t)$$

$$z_7^s(t+1) = 1$$

$$z_8^s(t+1) = (1 + z_9(t) + z_7(t)) \times s_3$$

$$z_9^s(t+1) = (z_{46}(t) + z_8(t) + z_9(t) + z_{15}(t) + z_{32}(t) - z_{21}(t) \times z_{19}(t) - z_{43}(t) + z_6(t) - z_{14}(t) + z_{40}(t)) \times s_4$$

$$z_{10}^s(t+1) = (z_{14}(t) - z_{29}(t) + z_{34}(t) + z_{29}(t) + z_{10}(t) + z_{21}(t)) \times s_4$$

$$z_{11}^s(t+1) = (z_6(t) \times z_{10}(t) + z_{10}(t) + z_{26}(t)) \times s_3$$

$$z_{12}^s(t+1) = (z_6(t) + z_{10}(t) + z_{19} - z_{18}(t)) \times s_2$$

$$z_{13}^s(t+1) = (z_9(t) + z_4(t) + z_{15}(t) - z_{14}(t) - z_{11}(t) + z_{46}(t) - z_{18}(t) + z_7(t)) \times s_2$$

$$z_{14}^s(t+1) = 1$$

$$z_{15}^s(t+1) = (z_9(t) + z_{19}(t)) \times s_2$$

$$z_{16}^s(t+1) = (z_7(t) + z_9(t)) \times s_2$$

$$z_{17}^s(t+1) = z_{10}(t) - z_{40}(t) \times z_{22}(t)$$

$$z_{18}^s(t+1) = 1$$

$$z_{19}^s(t+1) = 1$$

$$z_{20}^s(t+1) = (z_{10}(t) + z_{27}(t) + z_{21}(t) - z_7(t) + z_{60}(t)) \times s_3$$

$$z_{21}^s(t+1) = (z_{10}(t) + z_{14}(t)) \times s_2$$

$$z_{22}^s(t+1) = z_{15}(t)$$

$$z_{23}^s(t+1) = z_6(t) - z_{40}(t) + z_{26}(t)$$

$$z_{24}^s(t+1) = z_9(t) + z_{29}(t) + z_{46}(t) + z_6(t) + z_{46}(t) \times z_9(t) \times z_{34}(t) + z_{19}(t) + z_{40}(t) - z_{26}(t) + z_{40}(t) \times z_{28}(t) \times z_{56}(t) - \frac{1}{5}z_{60}(t)$$

$$z_{25}^s(t+1) = (z_{18}(t) + z_{19}(t) + z_{26}(t) + 2 \times z_{29}(t)) \times s_5$$

$$z_{26}^s(t+1) = 1$$

$$z_{27}^s(t+1) = z_9(t) - 0.5 \times z_{19}(t)$$

$$z_{29}^s(t+1) = 1$$

$$z_{30}^s(t+1) = 1$$

$$z_{31}^s(t+1) = (z_{28}(t) + z_6(t) + 1.5 \times z_{14}(t) + z_{60}(t) \times z_{26}(t)) \times s_4$$

$$z_{32}^s(t+1) = z_{15}(t) + z_{19}(t) - z_{26}(t)$$

$$z_{33}^s(t+1) = (z_6(t) + z_{29}(t)) \times s_2$$

$$z_{34}^s(t+1) = 1 - 0.4 \times z_{44}(t)$$

$$z_{35}^s(t+1) = 1$$

$$\begin{aligned}
z_{36}^s(t+1) &= 1 \\
z_{37}^s(t+1) &= (1 - z_7(t)) \times s_2 \\
z_{38}^s(t+1) &= z_0(t) \\
z_{39}^s(t+1) &= z_0(t) \\
z_{40}^s(t+1) &= 1 \\
z_{41}^s(t+1) &= 1 \\
z_{42}^s(t+1) &= (z_{26}(t) + z_{29}(t) + z_{18}(t)) \times s_3 \\
z_{43}^s(t+1) &= (z_{19}(t) + z_{26}(t) + z_{43}(t) - z_{32}(t)) \times s_2 \\
z_{44}^s(t+1) &= (z_{26}(t) + z_{29}(t) + z_{40}(t) - z_{19}(t) + z_4(t)) \times s_3 \\
z_{45}^s(t+1) &= 1 \\
z_{46}^s(t+1) &= z_{29}(t) \\
z_{47}^s(t+1) &= z_{10}(t) - z_7(t) \\
z_{48}^s(t+1) &= 0.5 \times z_{19}(t) - z_7(t) + z_{10}(t) - z_{29}(t) - z_{28}(t) \\
z_{49}^s(t+1) &= 0.5 \times z_{19}(t) - z_7(t) + z_{10}(t) - z_{29}(t) - z_{28}(t) \\
z_{50}^s(t+1) &= 1 \\
z_{51}^s(t+1) &= z_{40}(t) \times z_{28}(t) \times z_{56}(t) + z_{29}(t) \\
z_{52}^s(t+1) &= (0.4 + z_{18}(t) - z_{26}(t) + z_9(t) + z_{28}(t) \times z_{56}(t)) \times s_3 \\
z_{53}^s(t+1) &= (0.4 + z_{26}(t) - z_{29}(t) + z_{10}(t)) \times s_2 \\
z_{54}^s(t+1) &= 1 - z_{60}(t) \\
z_{55}^s(t+1) &= 1 \\
z_{56}^s(t+1) &= 1 \\
z_{57}^s(t+1) &= (z_{10}(t) + z_{60}(t) - z_{29}(t)) \times s_3 \\
z_{58}^s(t+1) &= z_{29}(t) \\
z_{59}^s(t+1) &= (z_{42}(t) + z_{17}(t)) \times s_3 \\
z_{60}^s(t+1) &= z_{26}(t) - z_{40}(t) \times z_{28}(t) - z_{29}(t)
\end{aligned}$$

With $s_p = 2 \frac{SC}{p}$, where SC is the saturation constant set to $2/3$ and p is the number of excess positive interactions (see equation **eq.4**).

Supplementary experimental method SM2

RT-qPCR protocol for samples from human primary OA chondrocytes cultured in alginate beads: Alginate beads were dissolved using citrate buffer, centrifuged at 200g and the pellet was resuspended in RLT (Qiagen, Hilden, Germany) buffer containing 1% beta-mercaptoethanol for RNA isolation. mRNA isolation was performed according to manufacturer's protocol utilizing the RNeasy Column system (Qiagen, Hilden, Germany). The RNA concentration was determined using a NanoDrop spectrophotometer (Isogen Life Science, Utrecht, the Netherlands). 0.5 µg RNA was used for cDNA synthesis following the protocol of the manufacturer of the RevertAid First Strand cDNA kit (Thermo Fisher Scientific, Waltham, MA, United States). qPCR was performed on a Bio-Rad CFX96 Real-Time PCR Detection System (Bio-Rad) to assess gene expression, Collagen type 10 (*COL10A1*) and Glyceraldehyde-3-phosphate dehydrogenase (*GAPDH*), which was found stable and therefore used as reference gene. Data were analyzed by the $\Delta\Delta C_t$ method and normalized to the expression of *GAPDH* of each condition and compared to the corresponding gene expression in the control groups

Human oligonucleotides used for qRT-PCR reaction with primary chondrocytes:

Gene	Forward primer	Reverse primer	Probe
<i>GAPDH</i>	ATGGGGAAAGGTGAAGGTCG	TAAAAGCAGCCCTGGTGACC	CGCCAATACGACCAATC CGTTGAC
<i>COL10A1</i>	CAAGGCACCATCTCCAGGAA	AAAGGGTATTTGTGGCAGCATATT	TCCAGCACGCAGAATCCAT CTGA

Mouse oligonucleotides used for qRT-PCR reaction with ATDC5 samples.

Primers were designed by the Primer Design tool of NCBI:

Gene	Forward primer	Reverse primer
<i>mHrpt</i>	GAGCGTTGGGCTTACCTCAC	ATCGTAATCACGACGCTGG
<i>mCol10a1</i>	TCCCAGCACGAGAATCTATCTGA	TTATGCCTGTGGCGTTTGG

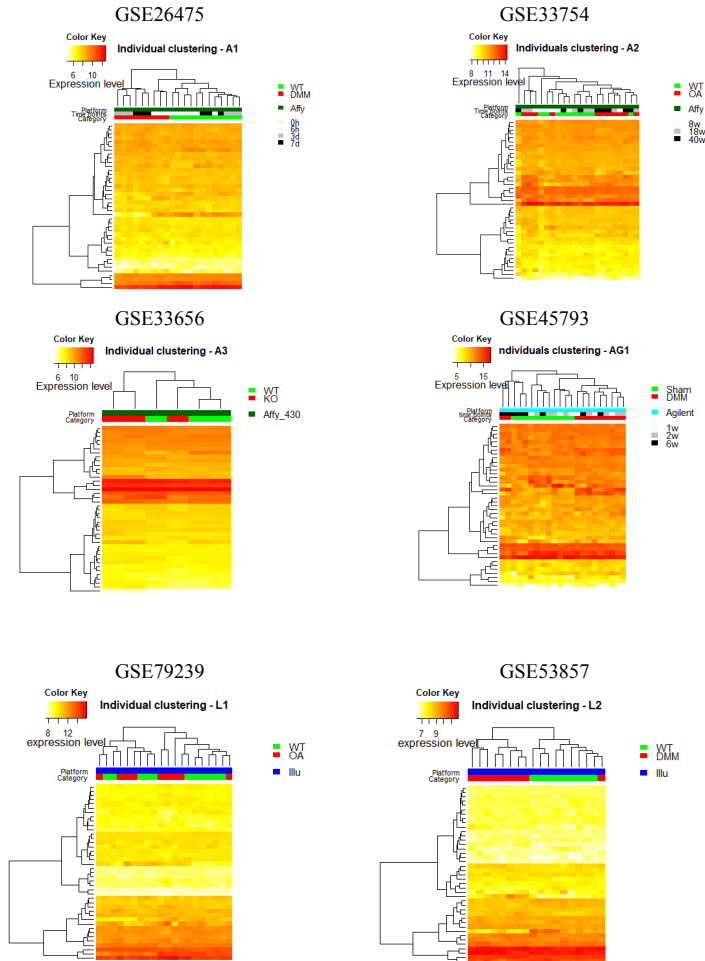


Figure S1 | Heatmap with unsupervised clustering on individual dataset.

The microarray sub-datasets, used in the merged dataset, were also investigated individually. They were pre-processed (i.e. processing steps before merging and correcting for batch effect) in the same way as the merged dataset but the unsupervised clustering analysis was done on each sub-dataset separately in order to compare the biological or OA related information content before and after the data merging. The heatmaps show the expression profile of the same list of genes of interest than for the merged dataset (see Data S3.). These expression datasets were submitted to unsupervised clustering with the Euclidean distance method and the Complete aggregation method in R thanks to the heatmap3 function from the github repository <https://github.com/obigriffith/biostar-tutorials/tree/master/Heatmaps>. The headers indicate the GEO accession numbers of the 6 original datasets. Samples labeled as 'WT', for wild type, are in green, samples labeled as 'OA', for osteoarthritis, in red. The pre-labelling is the same as for the merged dataset (see Data S3). When applicable, a grey scale indicate the time points (w stands for weeks, in the legend). For some datasets (e.g. GSE26475, GSE33656, GSE53857) the OA and the WT samples are well separated in different clusters, while for other the separation is not so clear. For instance, in GSE45793 the variance due the time point 6weeks is greater than the OA induced variance, while for weeks 1 and 2 OA and WT samples are well separated due to the OA condition.

Effect of ALK1/ALK5 ratio on TGF-β protective effect against inflammation induced hypertrophy

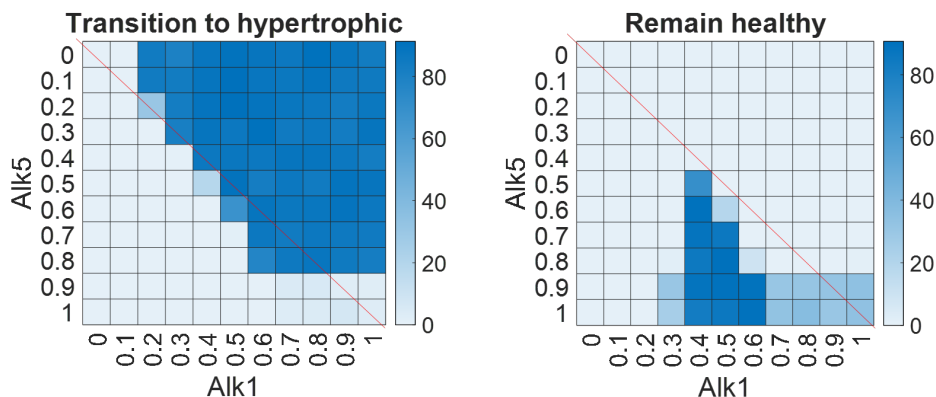


Figure S2 | Role of the ratio between receptors ALK1 and ALK5 in the effect of inflammation and TGFβ signaling on chondrocyte hypertrophy

Percentage of perturbations remaining in the healthy state (right) or transitioning towards the hypertrophic one (left) during inflammatory pathway activation with TGF-B treatment while changing the ratio between ALK1 and ALK5. The inflammatory and TGF-B profiles that were imposed are the same as in Fig.4A except that the value imposed for ALK1 and ALK5 are varying between 0 and 1 with a 0.1 increment. ALK1=ALK5 on the red diagonals and ALK1>ALK5 in the upper right corner. Roughly, the rescue of the healthy state by TGF-B is lost when ALK1 is greater than ALK5. If ALK1 is high enough and that the difference between ALK1 and ALK5 is not greater than 10-20% then the protective effect of TGF-B is also disturbed for ALK1<ALK5

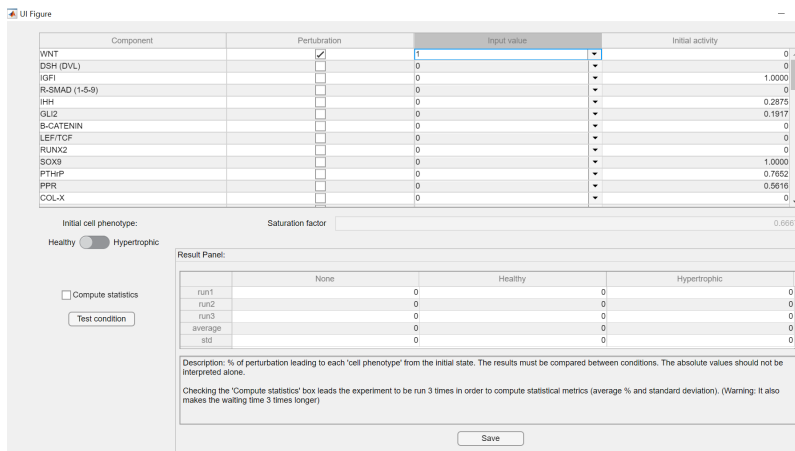


Figure S3 | Screenshot of the user-friendly interface for the virtual chondrocytes App

The standalone Matlab-based applications can be launched and used without Matlab license, provided that the compiler Matlab Runtime is installed (<https://nl.mathworks.com/products/compiler/matlab-runtime.html>). The virtual chondrocyte initial state can be set as healthy or hypertrophic, allowing the user to test any scenarios. All the 60 components may be perturbed alone or in any sort of combination by forcing the variables to take a value in the interval [0;1], with a step of 0.1. The most left column indicate the value of the variable in the selected initial state, for information. Obviously, applying a perturbation that is equal to the initial value of the variable will not affect the system. Once the setting are done, the user can apply the experimental condition by pushing the button 'Test condition' and the percentage of transition towards each of the possible basal stable states (i.e. 'None', 'Healthy' and 'Hypertrophic') is computed. If the 'Compute statistics' box is ticked, then the experiment is repeated 3 times and the average and standard deviations are displayed (variation occurs due to the stochastic nature of the model). The results may be exported and saved in an excel file via the 'Save' button.

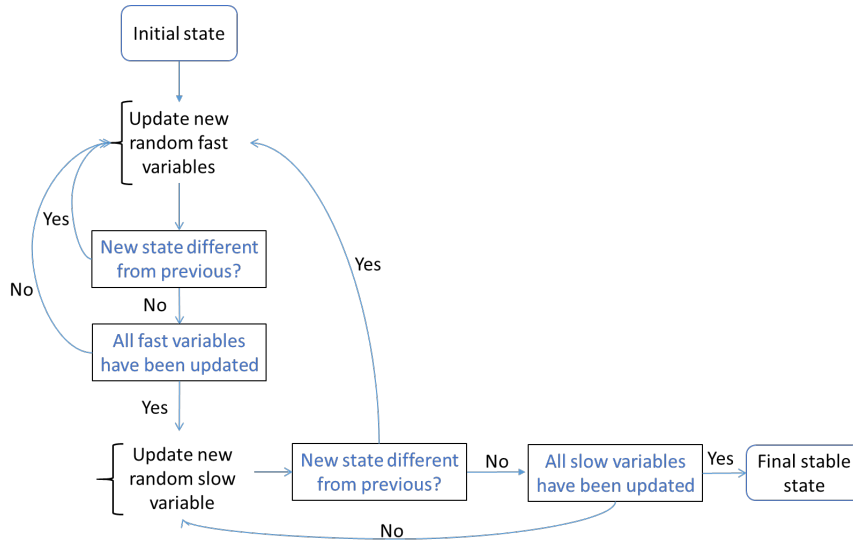


Figure S4 | Decision tree summarizing the variable updating scheme employed in algorithm to simulate the in silico chondrocyte

Each biological component is represented by the gene expression level (slow variable) and the protein activity potential (fast variable). Variables are updated based on the rules stored in the model's equations. First, fast variables are updated in random order, when a pseudo-stable state is reached and that all fast variables have been updated, the next random chosen slow variable is updated. This goes on until a state that is stable both at the fast and slow level is reached. This is the final stable state. A state is considered stable if further variable updates do not bring further changes for any of the variables, more or less a predefined tolerance. The order in which variables are updated is random, thereby generating some stochasticity in the model. Within the fast (resp. slow) updating loops, variables are updated asynchronously (meaning the one after the others) according to the rules defined in the system of equations (see Supplementary text S1) and in a random order.

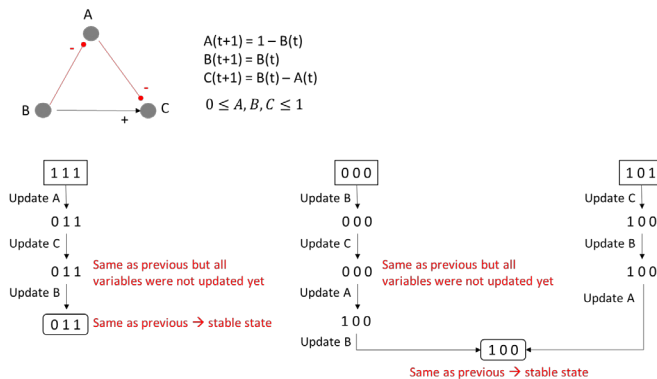


Figure S5 | Illustration of the algorithm for the asynchronous updating of variables with a simplified example network. The network represents interactions happening in one of the layers (protein= fast reactions or genetic = slow reactions). Inhibitory influences are represented in Red and activator influences are in black. The mathematical rules corresponding to the network are displayed. If the rules result in a value lower than 0 (resp. higher than 1), the value is brought back to 0 (resp. 1). For this example, 3 different initial states are inputted and each of the three variables is updated asynchronously. The order in which variables are updated is random. The system reaches a stable state when the next update gives the same state as in the previous time step and that all variables were screened in the random ordering list. That state is a pseudo-stable state if the rules were describing fast reactions, in that case, a new slow variable can be updated (see Fig. S3.). It is a final stable state if the rules were describing slow interactions since it would mean that the system had first reached a pseudo-stable state at the fast level and would now be stable at the slow level too.

Table S1 | Table of definitions. Modelling terms and concepts relative to the current additive regulatory network model are defined.

Definitions
<p>Additive model: A network of protein or gene interactions is modeled with an additive method if the evolution of variables (proteins or genes) at the next time step is defined by the sum of the upstream activating variables and the subtraction of the upstream inhibitory variables of the network. For instance, in a GRN, if a transcription factor A activates a gene P while B inhibits gene P, then the evolution of the P expression level at the next time step is defined as: $P(t + 1) = A(t) - B(t)$ (eq. 1)</p>
<p>Node or component (variable): The nodes of a regulatory network are located at the intersections of multiple interactions (edges) in the network. They represent biological components such as proteins or genes. In mathematical models, such as the additive models, components' evolutions are described with variables (e.g. A, P or B in (eq.1)).</p>
<p>Fast and Slow reactions & variables: All reactions related to slow biological processes such as gene expression, mRNA or protein production, were referred to as slow reactions (lower priority) and those related to fast processes such as protein activation (e.g. post transcriptional modification) or degradation, were referred to as fast reactions (higher priority).</p> <p>This priority order plays a role in the simulation since any network component could be regulated both at the protein and gene level, as in real life. Therefore, each network component or variable was split into a fast and a slow subpart, also called sub-variables. Let's consider that the gene P from (eq.1) produces a protein that is both activated post-transcriptionally by another protein kinase K and blocked by an inhibitory protein I. The global functional activity of the protein P is actually the multiplication of the slow by the fast subparts:</p> $P(t + 1) = [A(t) - B(t)] \times [K(t) - I(t)]. \text{ (eq2)}$ <p>When simulating the system, the sub-variables are updated asynchronously following the priority classes in such a way that fast reactions are always updated before the slow reactions (20).</p>
<p>Stable state (or attractors): A stable state is an ensemble of values, one for each variable/component of the model, that meet all the rules/constraints imposed by the equations. When variables do not evolve anymore after a certain time of simulation, the system has reached a stable state. The nature of such a state depends on the system of equations and on which initial state was used. Given the ensemble of interconnected signaling pathways, it is likely that only a finite number of states can fulfil all the constraints imposed by the network structure (i.e. by the equations).</p>

Table S2 | Table of correspondence between the variable names in the model corresponding real world mouse gene. All mathematical variables and the corresponding node in the network have names written in upper cases and do not reflect the official human or mouse nomenclature. To relate those variables to actual genes more easily, we provide this table of correspondence. A related mouse gene name and NCBI ID is indicated for each variable. Nevertheless, it is not exhaustive since some variables represents a group of factors or a family of ligands rather than a single factor.

Variable index	Variable name	Example representative mouse gene	
		Name	NCBI ID
1	WNT	<i>Wnt3a</i>	22416
2	DSH	<i>Dvl1</i>	20423
3	IGF-I	<i>Igf1</i>	16000
4	R-SMAD	<i>Smad5</i>	17129
5	IHH	<i>Ihh</i>	16147
6	GLI2	<i>Gli2</i>	14633
7	β -Catenin	<i>Cttnb1</i>	12387
8	LEF/TCF	<i>Tcf7</i>	21414
9	RUNX2	<i>Runx2</i> or <i>Cbfa1</i>	12393
10	SOX9	<i>Sox9</i>	20682
11	PTHrP	<i>Pthlh</i>	19227
12	PPR	<i>Pth1r</i>	19228
13	COL-X	<i>Col10a1</i>	12813
14	PKA	<i>Prkaca</i>	18747
15	MEF2C	<i>Mef2c</i>	17260
16	FGF	<i>Fgf2</i>	14173
17	FGFR3	<i>Fgfr3</i>	14184
18	STAT1	<i>Stat1</i>	20846

19	Smadcomplex	<i>Smad4 & R-Smads</i>	17128
20	COL II	<i>Col2a1</i>	12824
21	NKX3.2	<i>Nkx3-2</i> or <i>Bapx1</i>	12020
22	ERK1/2	<i>Mapk3</i>	26417
23	TGFβ	<i>Tgfb1</i>	21803
24	MMP13	<i>Mmp13</i>	17386
25	SMAD7	<i>Smad7</i>	17131
26	SMAD3	<i>Smad3</i>	17127
27	FGFR1	<i>Fgfr1</i>	14182
28	ATF2	<i>Atf2</i>	11909
29	NFκB	<i>Nfkb1</i>	18033
30	HDAC4	<i>Hdac4</i>	208727
31	CCND1	<i>Ccnd1</i>	12443
32	DLX5	<i>Dlx5</i>	13395
33	BMP	<i>Bmp2</i>	12156
34	P38	<i>Mapk14</i>	26416
35	GSK3β	<i>Gsk3b</i>	56637
36	DC	<i>Apc</i>	11789
37	PP2A	<i>Ppp2ca</i>	19052
38	AKT	<i>Akt1</i>	11651
39	PI3K	<i>Pi3kr1</i>	18708

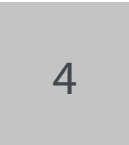
40	ETS1	<i>Ets1</i>	23871
41	RAS	<i>Kras</i>	16653
42	IGF-IR	<i>Igf1r</i>	16001
43	MSX2	<i>Msx2</i>	17702
44	δEF-1	<i>Zeb1</i>	21417
45	ATF4	<i>Atf4 or Creb</i>	11911
46	HIF-2α	<i>Epas1</i>	13819
47	GREM1	<i>Grem1</i>	23892
48	DKK1	<i>Dkk1</i>	13380
49	FRZB	<i>Frzb</i>	20378
50	Frizzled-LRP5/7	<i>Lrp5</i>	16973
51	Cytokines	<i>Il1b</i>	16176
52	ALK1	<i>Acvr11</i>	11482
53	ALK5	<i>Tgrb1</i>	21812
54	R-Infl (Receptor inflammation)	<i>Tlr1</i>	21897
55	TAK1	<i>Map3k7</i>	26409
56	JNK	<i>Mapk8</i>	26419
57	Proteoglycans	<i>Acan</i>	11595
58	IκB-a	<i>Nfkb1</i>	18035
59	SOCS	<i>Socs1</i>	12703
60	FOXO1	<i>Foxo1</i>	56458

Data S1 | Description of the GEO microarray dataset used in the present study. It contains the datasets GSE number with details such as the type of platform, authors, date of first publication, the list of samples, their biological descriptions as well as the binary categorization as OA or WT sample made for the purpose of this study

ID	GEO ID	GEO accession number	Title	Authors & date	sample names	description (according to authors)	Manual annotation for clustering
A	GSE56475	[MGI:Gene_1_0] Affymetrix Mouse Gene 1.0 ST Array (transcript (gene version))	Microarray expression data from whole murine knee joints at early time points post surgery the destabilization of medial meniscus (DMM) model of OA	Burleigh A, Vincent TL, Saklatvala J. (2011)	GSM49331_2.G275_0HNR18_01.CEL.gz	Murine knee joint; Naive; 6hr; rep1	WT
					GSM49338_G275_0HNR18_02.CEL.gz	Murine knee joint; Naive; 6hr; rep2	WT
					GSM49352_G275_0HNR18_03.CEL.gz	Murine knee joint; Naive; 6hr; rep3	WT
					GSM49493_G275_3A0519_14.CEL.gz	Murine knee joint; Operated (DMM); 3day; rep1	OA
					GSM49494_G275_3A0519_17.CEL.gz	Murine knee joint; Operated (DMM); 3day; rep2	OA
					GSM49495_G275_3A0519_18.CEL.gz	Murine knee joint; Operated (DMM); 3day; rep3	OA
					GSM51266_G275_3A0519_08.CEL.gz	Murine knee joint; Operated (Sham); 3day; rep1	WT
					GSM51267_G275_3A0519_09.CEL.gz	Murine knee joint; Operated (Sham); 3day; rep2	WT
					GSM51268_G275_3A0519_10.CEL.gz	Murine knee joint; Operated (Sham); 6hr; rep1	OA
					GSM51269_G275_3A0519_14.CEL.gz	Murine knee joint; Operated (DMM); 6hr; rep1	OA
					GSM51270_G275_3A0519_15.CEL.gz	Murine knee joint; Operated (DMM); 6hr; rep2	OA
					GSM51271_G275_3A0519_04.CEL.gz	Murine knee joint; Operated (Sham); 6hr; rep3	WT
					GSM51272_G275_3A0519_05.CEL.gz	Murine knee joint; Operated (Sham); 6hr; rep2	WT
					GSM51273_G275_3A0519_06.CEL.gz	Murine knee joint; Operated (Sham); 6hr; rep1	WT
					GSM51274_G275_7A0519_19.CEL.gz	Murine knee joint; Operated (DMM); 7days; rep1	OA
					GSM51275_G275_7A0519_20.CEL.gz	Murine knee joint; Operated (DMM); 7days; rep2	OA
					GSM51276_G275_7A0519_21.CEL.gz	Murine knee joint; Operated (DMM); 7days; rep3	OA
					GSM51289_G275_7A0519_10.CEL.gz	Murine knee joint; Operated (Sham); 7days; rep1	WT
					GSM51289_G275_7A0519_11.CEL.gz	Murine knee joint; Operated (Sham); 7days; rep2	WT
					GSM51289_G275_7A0519_12.CEL.gz	Murine knee joint; Operated (Sham); 7days; rep3	WT
B	GSE37954	[MGI:Gene_1_0] Affymetrix Mouse Gene 1.0 ST Array (transcript (gene version))	Erosion data of cartilage from CBA and STR (DRT) mice	Poulet B, Ulici V (2012)	GSM834973.CEL.gz	CBA; 8 weeks old; rep1	WT
					GSM834974.CEL.gz	CBA; 8 weeks old; rep2	WT
					GSM834975.CEL.gz	CBA; 8 weeks old; rep3	WT
					GSM834976.CEL.gz	Str/ort; 8 weeks old; rep1	OA
					GSM834977.CEL.gz	Str/ort; 8 weeks old; rep2	OA
					GSM834978.CEL.gz	Str/ort; 8 weeks old; rep3	OA
					GSM834979.CEL.gz	CBA; 18 weeks old; rep1	WT
					GSM834980.CEL.gz	CBA; 18 weeks old; rep2	WT
					GSM834981.CEL.gz	Str/ort; 18 weeks old; rep1	OA
					GSM834982.CEL.gz	Str/ort; 18 weeks old; rep2	OA
					GSM834983.CEL.gz	Str/ort; 18 weeks old; rep3	OA
					GSM834984.CEL.gz	Str/ort; 18 weeks old; rep4	OA
					GSM834985.CEL.gz	CBA; 40 weeks old; rep1	WT
					GSM834986.CEL.gz	CBA; 40 weeks old; rep2	WT
					GSM834987.CEL.gz	CBA; 40 weeks old; rep3	WT
					GSM834988.CEL.gz	CBA; 40 weeks old; rep4	WT
					GSM834989.CEL.gz	Str/ort; 40 weeks old; rep1	OA
					GSM834990.CEL.gz	Str/ort; 40 weeks old; rep2	OA
					GSM834991.CEL.gz	Str/ort; 40 weeks old; rep3	OA
					GSM834992.CEL.gz	Str/ort; 40 weeks old; rep4	OA
C	GSE39239	Illumina MouseWc-v6 v2.0 expression heatmap	Aberrant Calcium signaling in particular cartilage of aged deficient mice	Borner N, Cornelis FM, Ramos YF, den Hollander W, van der Breggen R, Storms L, Slagboom PE, Lories RJ, Meuwinkel I. (2016)	Sample 20	WT; run	OA
					Sample 21	WT; run	OA
					Sample 22	WT; run	OA
					Sample 27	WT; run	OA
					Sample 12	WT; notrun	WT
					Sample 14	WT; notrun	WT
					Sample 15	WT; notrun	WT
					Sample 16	DiO-F; run	WT
					Sample 17	DiO-F; notrun	WT
					Sample 19	DiO-F; notrun	WT
					Sample 23	WT; run	OA
					Sample 30	WT; run	OA
					Sample 31	WT; run	OA
					Sample 32	DiO-F; run	WT
D	GSE33867	Illumina MouseWc-v2 expression heatmap	Medial Tibial Plateau arthritis results in cartilage changes in OA and involves the DMM	Chanalaris A, Gardiner M. (2014)	2w; ctrl; 2'	Treatment; control'	WT
					2w; ctrl; 2'	Treatment; control'	WT
					2w; ctrl; 1'	Treatment; control'	WT
					2w; ctrl; 1'	Treatment; destabilization of the medial meniscus (DMM)	OA
					2w; ctrl; 1'	Treatment; destabilization of the medial meniscus (DMM)	OA
					2w; ctrl; 1'	Treatment; destabilization of the medial meniscus (DMM)	OA
					4w; ctrl; 2'	Treatment; control'	WT
					4w; ctrl; 2'	Treatment; control'	WT
					4w; ctrl; 1'	Treatment; destabilization of the medial meniscus (DMM)	OA
					4w; ctrl; 1'	Treatment; destabilization of the medial meniscus (DMM)	OA
E	GSE33866	[MGI:Gene_2_0] Affymetrix Mouse Genome 4.0 2.0 Array	Gene expression in particular subchondral bone	Lodewyckx L, Calletto F, Thyssen S, Luyten FP, Lories RJ. (2012)	GSM832358	6-1; 8; 16; 32	WT
					GSM832370	6-1; 8; 16; 32	WT
					GSM832372	6-1; 8; 16; 32	WT
					GSM832369	6-16; AC; FR2B; KO	OA
					GSM832373	14-16; AC; FR2B; KO	OA
F	GSE45793	Agilent-014888 Whole Mouse Genome Microarray 4x44k_G1122F	Differential gene expression in cartilage from the mouse DMM	Bateman J, Rowley L, Belluscio D, Chen B, Bell C, Fosang A, Little C. (2013)	GSM1120018_1.WK; RP1	Sham; 2wk	WT
					GSM1120018_1.WK; RP1	DMM; 2wk	OA
					GSM1120019_1.WK; RP2	Sham; 2wk	WT
					GSM1120019_1.WK; RP2	DMM; 2wk	OA
					GSM1120020_1.WK; RP3	Sham; 2wk	WT
					GSM1120020_1.WK; RP3	DMM; 2wk	OA
					GSM1120021_1.WK; RP1	Sham; 2wk	WT
					GSM1120021_1.WK; RP1	DMM; 2wk	OA
					GSM1120022_2.WK; RP2	Sham; 2wk	WT
					GSM1120022_2.WK; RP2	DMM; 2wk	OA
					GSM1120023_2.WK; RP3	Sham; 2wk	WT
					GSM1120023_2.WK; RP3	DMM; 2wk	OA
					GSM1120024_2.WK; RP4	Sham; 2wk	WT
					GSM1120024_2.WK; RP4	DMM; 2wk	OA
					GSM1120025_6.WK; RP1	Sham; 6wk	WT
					GSM1120025_6.WK; RP1	DMM; 6wk	OA
					GSM1120026_6.WK; RP2	Sham; 6wk	WT
					GSM1120026_6.WK; RP2	DMM; 6wk	OA
					GSM1120027_6.WK; RP3	Sham; 6wk	WT
					GSM1120027_6.WK; RP3	DMM; 6wk	OA
GSM1120028_6.WK; RP4	Sham; 6wk	WT					
GSM1120028_6.WK; RP4	DMM; 6wk	OA					

Data S2 | Complete profile of computed attractors. 3 attractors were identified for the system of equations described in Supplementary text and computed with the algorithm described in Fig. S3. For each attractor, the protein activation level (fast variable), the gene expression level (slow variable) and the global activity (product of the two previous) are indicated for all components of the model.

Complete expression profiles of the 3 WT attractors. Global = protein x gene												
	Attractor1				Attractor2				Attractor3			
	global	protein	gene		global	protein	gene		global	protein	gene	
WNT	0,00	1,00	0,00	WNT	0,00	0,00	0,00	WNT	1,00	1,00	1,00	
DSH	0,00	0,00	1,00	DSH	0,00	0,00	1,00	DSH	0,70	0,70	1,00	
IGFI	0,00	1,00	0,00	IGFI	1,00	1,00	1,00	IGFI	0,00	1,00	0,00	
R-SMAD	0,00	0,00	1,00	R-SMAD	0,00	0,00	0,57	R-SMAD	1,00	1,00	1,00	
IGG	0,00	1,00	0,00	IGG	0,29	1,00	0,29	IGG	1,00	1,00	1,00	
GLI2	0,00	0,00	1,00	GLI2	0,19	0,19	1,00	GLI2	0,67	0,67	1,00	
B-Catenin	0,00	0,00	1,00	B-Catenin	0,00	0,00	1,00	B-Catenin	1,00	1,00	1,00	
LEF/TCF	0,00	0,00	0,44	LEF/TCF	0,00	0,00	0,44	LEF/TCF	1,00	1,00	1,00	
RUNX2	0,00	0,00	0,00	RUNX2	0,00	0,00	0,00	RUNX2	1,00	1,00	1,00	
SOX9	0,00	0,00	0,00	SOX9	1,00	1,00	1,00	SOX9	0,00	0,00	0,16	
PTHRP	0,00	1,00	0,00	PTHRP	0,77	1,00	0,77	PTHRP	0,00	1,00	0,00	
PPR	0,00	0,00	0,00	PPR	0,56	0,77	0,73	PPR	0,00	0,00	0,59	
COL-X	0,00	1,00	0,00	COL-X	0,00	1,00	0,00	COL-X	1,00	1,00	1,00	
PKA	0,00	0,00	1,00	PKA	1,00	1,00	1,00	PKA	0,00	0,00	1,00	
MEF2C	0,00	0,00	0,00	MEF2C	0,00	0,00	0,00	MEF2C	1,00	1,00	1,00	
FGF	0,00	1,00	0,00	FGF	0,00	1,00	0,00	FGF	1,00	1,00	1,00	
FGFR3	0,00	0,00	0,00	FGFR3	0,00	0,00	1,00	FGFR3	0,00	1,00	0,00	
STAT1	0,00	0,00	1,00	STAT1	0,09	0,09	1,00	STAT1	0,53	0,53	1,00	
SMAD	0,00	0,00	1,00	SMAD	0,00	0,00	1,00	SMAD	0,75	0,75	1,00	
complex				complex				complex				
COL-II	0,00	1,00	0,00	COL-II	1,00	1,00	1,00	COL-II	0,00	1,00	0,00	
NKX3.2	0,00	1,00	0,00	NKX3.2	1,00	1,00	1,00	NKX3.2	0,00	1,00	0,00	
ERK1/2	0,00	0,00	0,00	ERK1/2	0,00	0,00	0,00	ERK1/2	1,00	1,00	1,00	
TGFβ	0,00	1,00	0,00	TGFβ	0,72	1,00	0,72	TGFβ	0,00	1,00	0,00	
MMP13	0,00	1,00	0,00	MMP13	0,00	1,00	0,00	MMP13	1,00	1,00	1,00	
SMAD7	0,00	1,00	0,00	SMAD7	0,16	1,00	0,16	SMAD7	0,87	1,00	0,87	
SMAD3	0,00	0,00	1,00	SMAD3	0,53	0,53	1,00	SMAD3	0,00	0,00	1,00	
FGFR1	0,00	0,00	0,00	FGFR1	0,00	0,00	0,00	FGFR1	0,63	1,00	0,63	
ATF2	0,00	0,00	1,00	ATF2	0,30	0,30	1,00	ATF2	0,31	0,31	1,00	
NFKB	0,00	0,00	1,00	NFKB	0,00	0,00	1,00	NFKB	1,00	1,00	1,00	
HDAC4	0,00	0,00	1,00	HDAC4	0,67	0,67	1,00	HDAC4	0,00	0,00	1,00	
CCND1	0,00	0,50	0,00	CCND1	0,70	0,95	0,73	CCND1	0,21	0,66	0,33	
DLX5	0,00	0,00	0,00	DLX5	0,00	0,00	0,00	DLX5	1,00	1,00	1,00	
BMP	0,00	1,00	0,00	BMP	0,00	0,00	0,13	BMP	1,00	1,00	1,00	
P38	0,00	0,00	1,00	P38	0,29	0,32	0,91	P38	0,47	0,78	0,60	
GSK	1,00	1,00	1,00	GSK	0,00	0,00	1,00	GSK	0,16	0,16	1,00	
DC	1,00	1,00	1,00	DC	1,00	1,00	1,00	DC	0,00	0,00	1,00	
PP2A	0,00	0,00	0,67	PP2A	0,67	1,00	0,67	PP2A	0,00	0,00	0,00	
AKT	0,00	0,00	0,00	AKT	0,00	0,00	0,00	AKT	0,83	0,83	1,00	
PI3K	0,00	0,00	0,00	PI3K	0,00	0,12	0,00	PI3K	0,83	0,83	1,00	
ETS1	0,00	0,00	1,00	ETS1	0,00	0,00	1,00	ETS1	1,00	1,00	1,00	
RAS	0,00	0,00	1,00	RAS	0,00	0,00	1,00	RAS	0,88	0,88	1,00	
IGF-IR	0,00	0,00	0,00	IGF-IR	0,28	1,00	0,28	IGF-IR	0,00	0,00	0,68	
MSX2	0,01	1,00	0,01	MSX2	1,00	1,00	1,00	MSX2	0,00	0,00	0,00	
EF-1	0,00	1,00	0,00	EF-1	0,24	1,00	0,24	EF-1	1,00	1,00	1,00	
ATF4	0,00	0,00	1,00	ATF4	0,67	0,67	1,00	ATF4	0,67	0,67	1,00	
HIF-2α	0,00	1,00	0,00	HIF-2α	0,00	1,00	0,00	HIF-2α	1,00	1,00	1,00	
GREM1	0,00	1,00	0,00	GREM1	1,00	1,00	1,00	GREM1	0,00	1,00	0,00	
FRZB	0,00	1,00	0,00	FRZB	0,70	1,00	0,70	FRZB	0,00	1,00	0,00	
DKK1	0,00	1,00	0,00	DKK1	0,70	1,00	0,70	DKK1	0,00	1,00	0,00	
Frizzled-LRP5/6	0,00	0,00	1,00	Frizzled-LRP5/6	0,00	0,00	1,00	Frizzled-LRP5/6	1,00	1,00	1,00	
Cytokines	0,00	1,00	0,00	Cytokines	0,00	1,00	0,00	Cytokines	1,00	1,00	1,00	
ALK1	0,00	0,00	0,18	ALK1	0,00	0,72	0,00	ALK1	1,00	1,00	1,00	
ALK5	0,00	0,00	0,27	ALK5	0,72	0,72	1,00	ALK5	0,00	0,00	0,00	
R_inflamm	0,00	0,00	1,00	R_inflamm	0,00	0,00	0,60	R_inflamm	1,00	1,00	1,00	
TAK1	0,00	0,00	1,00	TAK1	0,00	0,00	1,00	TAK1	0,76	0,76	1,00	
JNK	0,00	0,00	1,00	JNK	0,00	0,00	1,00	JNK	0,76	0,76	1,00	
Proteoglycans	0,00	1,00	0,00	Proteoglycans	0,62	1,00	0,62	Proteoglycans	0,00	0,00	0,00	
IkBa	0,00	1,00	0,00	IkBa	0,00	1,00	0,00	IkBa	0,24	0,24	1,00	
SOC5	0,00	1,00	0,00	SOC5	0,18	1,00	0,18	SOC5	0,00	1,00	0,00	
FOXO1	0,00	0,75	0,00	FOXO1	0,40	0,75	0,53	FOXO1	0,00	0,00	0,00	



Data S3 | Predictions data from the in silico screening. All possible pairwise perturbations (i.e. activation or inhibition) were imposed to the hypertrophic state and likelihood of transition was evaluated. All conditions that led to a percentage of transition higher than a threshold (70% here) towards the healthy state are reported in this data file. Predicted conditions of interest for further experimental validation based on the following criteria: the condition does not involve a transcription factor since their functional activity might be more difficult to target pharmacologically.

Conditions predicted to decrease hypertrophy (excluding TF)			
Transition rate	perturbation	Names	
100%	down-up	WNT - PPR	
	down-up	WNT - PKA	
	down-up	DSH - PKA	
	up-down	PPR - ERK1/2	
	up-down	PPR - FGFR1	
	up-up	PPR - HDAC4	
	up-down	PPR - BMP	
	up-up	PPR - p38	
	up-down	PPR - p38	
	up-up	PPR - DC	
	up-up	PPR - PP2A	
	up-down	PPR - AKT	
	up-down	PPR - PI3K	
	up-down	PPR - RAS	
	up-up	PPR - GREM1	
	up-up	PPR - FRZB	
	up-up	PKA - DKK1	
	up-down	PPR - ALK1	
	up-down	PPR - Rinflam	
	up-down	PPR - TAK1	
	up-up	PPR - IKBA	
	up-down	PKA - ERK1/2	
	up-down	PKA - FGFR1	
	up-up	PKA - HDAC4	
	up-down	PKA - BMP	
	up-up	PKA - p38	
	up-down	PKA - p38	
	up-up	PKA - DC	
	up-up	PKA - PP2A	
	up-down	PKA - PI3K	
	up-down	PKA - RAS	
	up-up	PKA - IGF-IR	
	up-up	PKA - FRZB	
	up-up	PKA - DKK1	
	up-down	PKA - Frizzled-LRP5/6	
	up-down	PKA - ALK1	
	up-down	PKA - Rinflam	
	up-down	PKA - TAK1	
	up-up	PKA - IKBA	
	down-up	DSH - PPR	
	down-up	IHH - PKA	
	up-up	PPR - IGF-IR	
	up-down	PPR - Frizzled-LRP5/6	
	99-90%	up-up	PPR - SOCS
		up-down	PKA - AKT
up-up		PKA - GREM1	
up-up	PKA - SOCS		
89-80%	down-up	ALK5 - ALK5	
	down-up	ERK1/2 - ALK5	
	down-up	DSH - ALK5	
	down-up	IHH - PPR	
	down-up	IHH - ALK5	
	up-down	PTHrP - FGFR1	
	up-up	PTHrP - p38	
	up-down	PTHrP - p38	
	up-down	PTHrP - AKT	
	up-down	PTHrP - PI3K	
	up-down	PTHrP - RAS	
	up-down	PTHrP - Rinflam	
	up-down	PTHrP - TAK1	
	up-up	PTHrP - IKBA	
	up-up	PTHrP - SOCS	
	up-down	PPR - Cytokines	
	up-down	PKA - Cytokines	
	down-up	ERK1/2 - ALK5	
	up-up	DC - ALK5	
	down-up	PI3K - ALK5	
	down-up	RAS - ALK5	
down-up	Frizzled-LRP5/6 - ALK5		
down-up	WNT - PTHrP		
79-70%	down-up	DSH - IGF1	
	down-up	DSH - PTHrP	
	up-up	IGF1 - HDAC4	
	up-down	IGF1 - BMP	
	up-up	IGF1 - DC	
	up-up	IGF1 - FRZB	
	up-down	IGF1 - ALK1	
	up-down	PTHrP - ERK1/2	
	up-up	PTHrP - HDAC4	
	up-up	PTHrP - DC	
	up-up	PTHrP - PP2A	
	up-up	PTHrP - FRZB	
	up-up	PTHrP - DKK1	
	up-down	PTHrP - Frizzled-LRP5/6	
	up-down	PPR - FGF	
	up-up	PPR - ALK5	
	up-down	PKA - FGF	
	up-up	PKA - ALK5	
	up-up	HDAC4 - ALK5	
	down-up	BMP - ALK5	
	up-up	PP2A - ALK5	
down-up	AKT - ALK5		
up-up	GREM1 - ALK5		
up-up	FRZB - ALK5		
up-up	DKK1 - ALK5		
up-down	ALK5 - Rinflam		
up-up	ALK5 - IKBA		
up-up	ALK5 - SOCS		

References

1. Karsdal MA, Michaelis M, Ladel C, Siebuhr AS, Bihlet AR, Andersen JR, et al. Disease-modifying treatments for osteoarthritis (DMOADs) of the knee and hip: lessons learned from failures and opportunities for the future. *Osteoarthr Cartil.* 2016 Dec;24(12):2013–21.
2. Raman S, FitzGerald U, Murphy JM. Interplay of Inflammatory Mediators with Epigenetics and Cartilage Modifications in Osteoarthritis. *Front Bioeng Biotechnol.* 2018 Mar 14;6:22.
3. Ji Q, Zheng Y, Zhang G, Hu Y, Fan X, Hou Y, et al. Single-cell RNA-seq analysis reveals the progression of human osteoarthritis. *Ann Rheum Dis.* 2019 Jan 1;78(1):100–10.
4. Von Der Mark K, Kirsch T, Nerlich A, Kuss A, Weseloh G, Glückert K, et al. Type x collagen synthesis in human osteoarthritic cartilage. indication of chondrocyte hypertrophy. *Arthritis Rheum.* 1992;35(7):806–11.
5. Tchetina E V, Poole AR, Zaitseva EM, Sharapova EP, Kashevarova NG, Taskina EA, et al. Differences in Mammalian Target of Rapamycin Gene Expression in the Peripheral Blood and Articular Cartilages of Osteoarthritic Patients and Disease Activity. *Arthritis.* 2013 Jun 25 ;2013:46148.
6. Poehling GG. Osteoarthritis: Diagnosis and medical/surgical management, third edition: Ronald W. Moskowitz, Davis S. Howell, Roy D. Altman, Joseph A. Buckwalter, and Víctor M. Goldberg. Philadelphia, W. B. Saunders, 2001, 685 pp., \$189.00. *Arthrosc J Arthrosc Relat Surg.* 2002 Jul 1 ;18(6):678.
7. Tchetina E V. Developmental Mechanisms in Articular Cartilage Degradation in Osteoarthritis. *Arthritis.* 2011 Dec 29 ;2011:68397:1–16.
8. van der Kraan PM, van den Berg WB. Chondrocyte hypertrophy and osteoarthritis: role in initiation and progression of cartilage degeneration? *Osteoarthr Cartil.* 2012 Mar 1 ;20(3):223–32.
9. Ripmeester EGJ, Timur UT, Caron MMJ, Welting TJM. Recent Insights into the Contribution of the Changing Hypertrophic Chondrocyte Phenotype in the Development and Progression of Osteoarthritis. *Front Bioeng Biotechnol.* 2018 ;6:18.
10. Ferrao Blanco MN, Bastiaansen-Jenniskens YM, Chambers MG, Pitsillides AA, Narcisi R, van Osch GJVM. Effect of Inflammatory Signaling on Human Articular Chondrocyte Hypertrophy: Potential Involvement of Tissue Repair Macrophages. *Cartilage.* 2021 Jun 24
11. Cleary MA, Osch GJVM van, Brama PA, Hellingman CA, Narcisi R. FGF, TGF β and Wnt crosstalk: embryonic to in vitro cartilage development from mesenchymal stem cells. *J Tissue Eng Regen Med.* 2015 Apr 1 ;9(4):332–42.
12. Monteagudo S, Lories RJ. Cushioning the cartilage: A canonical Wnt restricting matter. *Nat Rev Rheumatol.* 2017 Oct 12;13(11):670–81.
13. Green S, Şerban M, Scholl R, Jones N, Brigandt I, Bechtel W. Network analyses in systems biology: new strategies for dealing with biological complexity. *Synthese.* 2018 Apr 1 ;195(4):1751–77.
14. Rationalizing combination therapies. *Nat Med.* 2017 Oct 6 ;23(10):1113.
15. Nalesso G, Sherwood J, Bertrand J, Pap T, Ramachandran M, de Bari C, et al. WNT-3A modulates articular chondrocyte phenotype by activating both canonical and noncanonical pathways. *J Cell Biol.* 2011 May;193(3):551–64.

16. Kitano H. Systems biology: A brief overview. *Science* (80-). 2002 Mar 1;295(5560):1662–4.
17. Puniya BL, Allen L, Hochfelder C, Majumder M, Helikar T. Systems Perturbation Analysis of a Large-Scale Signal Transduction Model Reveals Potentially Influential Candidates for Cancer Therapeutics. *Front Bioeng Biotechnol.* 2016 Feb 11;4:10.
18. Herberg M, Roeder I. Computational modelling of embryonic stem-cell fate control. *Development.* 2015 Jul 1 ;142(13):2250–60.
19. Eduati F, Jaaks P, Wappler J, Cramer T, Merten CA, Garnett MJ, et al. Patient specific logic models of signaling pathways from screenings on cancer biopsies to prioritize personalized combination therapies. *Mol Syst Biol.* 2020;16(2):1–13.
20. Kerkhofs J, Geris L. A Semiquantitative Framework for Gene Regulatory Networks: Increasing the Time and Quantitative Resolution of Boolean Networks. *PLoS One.* 2015;10(6):e0130033.
21. Kerkhofs J, Leijten J, Bolander J, Luyten FP, Post JN, Geris L. A qualitative model of the differentiation network in chondrocyte maturation: A holistic view of chondrocyte hypertrophy. *PLoS One.* 2016;11(8):1–27.
22. Helikar T, Kowal B, McClenathan S, Bruckner M, Rowley T, Madrahimov A, et al. The Cell Collective: Toward an open and collaborative approach to systems biology. *BMC Syst Biol.* 2012;6.
23. Thielen N, van der Kraan P, van Caam A. TGF β /BMP Signaling Pathway in Cartilage Homeostasis. *Cells.* 2019 Aug 24;8(9):969.
24. Marbach D, Costello JC, Küffner R, Vega NM, Prill RJ, Camacho DM, et al. Wisdom of crowds for robust gene network inference. *Nat Methods.* 2012 Jul 15 ;9(8):796–804.
25. Abou-Jaoudé W, Traynard P, Monteiro PT, Saez-Rodriguez J, Helikar T, Thieffry D, et al. Logical Modeling and Dynamical Analysis of Cellular Networks. *Front Genet.* 2016 May 31 ;7:94.
26. Rowan A, Hui W, Cawston TE, Richards CD. Adenoviral gene transfer of interleukin-1 in combination with oncostatin M induces significant joint damage in a murine model. *Am J Pathol.* 2003 Jun 1;162(6):1975–84.
27. Saito T, Fukai A, Mabuchi A, Ikeda T, Yano F, Ohba S, et al. Transcriptional regulation of endochondral ossification by HIF-2 α during skeletal growth and osteoarthritis development. *Nat Med.* 2010 Jun 23;16(6):678–86.
28. Hodgson D, Rowan AD, Falciani F, Proctor CJ. Systems biology reveals how altered TGF β signalling with age reduces protection against pro-inflammatory stimuli. Saucerman JJ, editor. *PLOS Comput Biol.* 2019 Jan 24;15(1):e1006685.
29. Proctor CJ, Macdonald C, Milner JM, Rowan AD, Cawston TE. A computer simulation approach to assessing therapeutic intervention points for the prevention of cytokine-induced cartilage breakdown. *Arthritis Rheumatol.* 2014 Apr;66(4):979–89.
30. Hui W, Rowan AD, Cawston T. Transforming growth factor- β 1 blocks the release of collagen fragments from bovine nasal cartilage stimulated by oncostatin M in combination with IL-1 α . *Cytokine.* 2000 Jun ;12(6):765–9.
31. Shull MM, Ormsby I, Kier AB, Pawlowski S, Diebold RJ, Yin M, et al. Targeted disruption of the mouse transforming growth factor- β 1 gene results in multifocal inflammatory disease. *Nature.* 1992;359(6397):693–9.

-
32. Van Der Kraan PM. The changing role of TGF β in healthy, ageing and osteoarthritic joints. *Nat Rev Rheumatol*. 2017 Mar 1;13(3):155–63.
33. CM F, EM S, PR R, JE P, RN R, RJ O. Smad2 and 3 mediate transforming growth factor-beta1-induced inhibition of chondrocyte maturation. *Endocrinology*. 2000; 141(12):4728–35.
34. Hui W, Young DA, Rowan AD, Xu X, Cawston TE, Proctor CJ. Oxidative changes and signalling pathways are pivotal in initiating age-related changes in articular cartilage. *Ann Rheum Dis*. 2016 Feb 1;75(2):449–58.
35. van der Kraan P, Matta C, Mobasheri A. Age-Related Alterations in Signaling Pathways in Articular Chondrocytes: Implications for the Pathogenesis and Progression of Osteoarthritis - A Mini-Review. *Gerontology*. 2017 Dec 1;63(1):29–35.
36. Blaney Davidson EN, Remst DFG, Vitters EL, van Beuningen HM, Blom AB, Goumans M-J, et al. Increase in ALK1/ALK5 Ratio as a Cause for Elevated MMP-13 Expression in Osteoarthritis in Humans and Mice. *J Immunol*. 2009 Jun 15;182(12):7937–45.
37. Akiyama H, Shigeno C, Iyama KI, Ito H, Hiraki Y, Konishi J, et al. Indian hedgehog in the late-phase differentiation in mouse chondrogenic EC cells, ATDC5: Upregulation of type X collagen and osteoprotegerin ligand mRNAs. *Biochem Biophys Res Commun*. 1999 Apr 21;257(3):814–20.
38. Terfve C, Cokelaer T, Henriques D, MacNamara A, Goncalves E, Morris MK, et al. CellNOptR: A flexible toolkit to train protein signaling networks to data using multiple logic formalisms. *BMC Syst Biol*. 2012 Oct 18;6(1):133.
39. Basso K, Margolin AA, Stolovitzky G, Klein U, Dalla-Favera R, Califano A. Reverse engineering of regulatory networks in human B cells. *Nat Genet*. 2005 Apr 20;37(4):382–90.
40. Liu A, Trairatphisan P, Gjerga E, Didangelos A, Barratt J, Saez-Rodriguez J. From expression footprints to causal pathways: contextualizing large signaling networks with CARNIVAL. *npj Syst Biol Appl*. 2019;5(1):1–10.
41. Türe D, Korcsmáros T, Saez-Rodriguez J. OmniPath: Guidelines and gateway for literature-curated signaling pathway resources. *Nat Methods*. 2016;13(12):966–7.
42. Yang M, Simm J, Lam CC, Zakeri P, Van Westen GJP, Moreau Y, et al. Linking drug target and pathway activation for effective therapy using multi-Task learning. *Sci Rep*. 2018 Dec 1;8(1):1–10.
43. Binette F, McQuaid DP, Haudenschild DR, Yaeger PC, McPherson JM, Tubo R. Expression of a stable articular cartilage phenotype without evidence of hypertrophy by adult human articular chondrocytes in vitro. *J Orthop Res*. 1998 Mar ;16(2):207–16.
44. Kitano H. Biological robustness. *Nat Rev Genet* 2004 511 [Internet]. 2004 Nov [cited 2021 Jul 28];5(11):826–37. Available from: <https://www-nature-com.kuleuven.e-bronnen.be/articles/nrg1471>
45. Kærn M, Elston TC, Blake WJ, Collins JJ. Stochasticity in gene expression: from theories to phenotypes. *Nat Rev Genet* 2005 66. 2005 May 10 ;6(6):451–64.
46. Kitano H. The Theory of Biological Robustness and Its Implication in Cancer. *Ernst Schering Res Found Workshop*. 2007 ;(61):69–88.
47. Kozhemyakina E, Cohen T, Yao T-P, Lassar AB. Parathyroid Hormone-Related Peptide Represses Chondrocyte Hypertrophy through a Protein Phosphatase 2A/Histone Deacetylase 4/MEF2 Pathway. *Mol Cell Biol*. 2009 Nov 1;29(21):5751–62.

48. Weng T, Yi L, Huang J, Luo F, Wen X, Du X, et al. Genetic inhibition of fibroblast growth factor receptor 1 in knee cartilage attenuates the degeneration of articular cartilage in adult mice. *Arthritis Rheum.* 2012 Dec 1 ;64(12):3982–92.
49. Thysen S, Luyten FP, Lories RJU. Targets, models and challenges in osteoarthritis research. *DMM Dis Model Mech.* 2015 Jan 1 ;8(1):17–30.
50. Luyten FP, Bierma-Zeinstra S, Dell’Accio F, Kraus VB, Nakata K, Sekiya I, et al. Toward classification criteria for early osteoarthritis of the knee. *Semin Arthritis Rheum.* 2018 Feb 1;47(4):457–63.
51. Mobasheri A, van Spil WE, Budd E, Uzieliene I, Bernotiene E, Bay-Jensen A-C, et al. Molecular taxonomy of osteoarthritis for patient stratification, disease management and drug development. *Curr Opin Rheumatol.* 2019 Jan ;31(1):80–9.
52. Turnbull AK, Kitchen RR, Larionov AA, Renshaw L, Dixon JM, Sims AH. Direct integration of intensity-level data from Affymetrix and Illumina microarrays improves statistical power for robust reanalysis. *BMC Med Genomics.* 2012 Aug 21;5:35.
53. Johnson WE, Li C, Rabinovic A. Adjusting batch effects in microarray expression data using empirical Bayes methods. *Biostatistics.* 2007 Jan;8(1):118–27.
54. Huynh-Thu VA, Irrthum A, Wehenkel L, Geurts P. Inferring regulatory networks from expression data using tree-based methods. Isalan M, editor. *PLoS One.* 2010 Sep 28 ;5(9):e12776.
55. Margolin AA, Nemenman I, Basso K, Wiggins C, Stolovitzky G, Favera R, et al. ARACNE: An Algorithm for the Reconstruction of Gene Regulatory Networks in a Mammalian Cellular Context. *BMC Bioinformatics.* 2006 ;7(Suppl 1):S7.
56. Haury A, Mordelet F, Vera-licona P, Vert J. Open Access TIGRESS : Trustful Inference of Gene REgulation using Stability Selection. *BMC Syst Biol.* 2012;
57. Shannon P, Andrew M, Owen O, Nitin S B, Jonathan T W, Daniel R, et al. Cytoscape: A Software Environment for Integrated Models of Biomolecular Interaction Networks. *Genome Res.* 2003 Nov 1;13(11):2498–504.
58. Fauré A, Naldi A, Chaouiya C, Thieffry D. Dynamical analysis of a generic Boolean model for the control of the mammalian cell cycle. *Bioinformatics.* 2006;22(14):124–31.
59. Alon U. An introduction to systems biology: Design principles of biological circuits. *An Introduction to Systems Biology: Design Principles of Biological Circuits.* Chapman and Hall/CRC Press; 2006. 1–605 p.
60. Chaouiya C, Naldi A, Thieffry D. Logical modelling of gene regulatory networks with GINsim. *Methods Mol Biol.* 2012;804:463–79.
61. Zañudo JGT, Aldana M, Martínez-Mekler G. Boolean threshold networks: Virtues and limitations for biological modeling. *Intell Syst Ref Libr.* 2011;11:113–51.
62. Caron MMJ, Emans PJ, Cremers A, Surtel DAM, Coolsen MME, van Rhijn LW, et al. Hypertrophic differentiation during chondrogenic differentiation of progenitor cells is stimulated by BMP-2 but suppressed by BMP-7. *Osteoarthr Cartil.* 2013 Apr 1;21(4):604–13.
63. Lesage R. Github - Rapha-L/Insilico_chondro: Scripts & data used to run the analyses done in the publication [Internet]. Git Hub. 2021 [cited 2021 Sep 29]. Available from: <https://github.com/>

64. Lesage R, Geris L. PPI network- Interactive Modeling of Biological Networks | Cell Collective [Internet]. Cell Collective. 2021 [cited 2021 Sep 29]. Available from: <https://cellcollective.org/#a5b66073-6769-4c88-bf6b-37ca1aa8f766>
65. Lesage R, Geris L. GRN - Interactive Modeling of Biological Networks | Cell Collective [Internet]. Cell Collective. 2021 [cited 2021 Sep 29]. Available from: <https://cellcollective.org/#474de240-8752-4c3b-aa63-23640e50bf7a>
66. Burleigh A, Chanalaris A, Gardiner MD, Driscoll C, Boruc O, Saklatvala J, et al. Joint immobilization prevents murine osteoarthritis and reveals the highly mechanosensitive nature of protease expression in vivo. *Arthritis Rheum.* 2012 Jul ;64(7):2278–88.
67. B P, V U, T C S, M P, V G, E C, et al. Time-series transcriptional profiling yields new perspectives on susceptibility to murine osteoarthritis. *Arthritis Rheum.* 2012;64(10):3256–66.
68. Bomer N, Cornelis FMF, Ramos YF, Den Hollander W, Storms L, Van Der Breggen R, et al. The effect of forced exercise on knee joints in Dio2^{-/-} mice: Type II iodothyronine deiodinase-deficient mice are less prone to develop OA-like cartilage damage upon excessive mechanical stress. *Ann Rheum Dis.* 2016 Mar 1 ;75(3):571–7.
69. Lodewyckx L, Cailotto F, Thysen S, Luyten FP, Lories RJ. Tight regulation of wingless-type signaling in the articular cartilage - subchondral bone biomechanical unit: Transcriptomics in Frzb-knockout mice. *Arthritis Res Ther.* 2012 Jan 20 ;14(1).
70. Gardiner MD, Vincent TL, Driscoll C, Burleigh A, Bou-Gharios G, Saklatvala J, et al. Transcriptional analysis of micro-dissected articular cartilage in post-traumatic murine osteoarthritis. *Osteoarthr Cartil.* 2015 Apr 1 ;23(4):616–28.
71. Bateman JF, Rowley L, Belluoccio D, Chan B, Bell K, Fosang AJ, et al. Transcriptomics of wild-type mice and mice lacking adams-5 activity identifies genes involved in osteoarthritis initiation and cartilage destruction. *Arthritis Rheum.* 2013 Jun 1;65(6):1547–60.

Chapter 5

Pharmacologic inhibition of EPHA2 decreases inflammation and pathological endochondral ossification in osteoarthritis

Mauricio N. Ferrao Blanco ¹, Raphaelle Lesage ^{2,3}, Nicole Kops ¹, Niamh Fahy ^{1,4}, Fjodor T. Bekedam¹, Athina Chavli ¹, Yvonne M. Bastiaansen-Jenniskens ¹, Liesbet Geris ^{2,3,5}, Mark G. Chambers ⁶, Andrew A. Pitsillides ⁷, Roberto Narcisi ¹, Gerjo J.V.M. van Osch ^{1,8,9}

¹ Department of Orthopaedics and Sports Medicine, Erasmus MC, University Medical Center, Rotterdam, Netherlands;

² Prometheus, Division of Skeletal Tissue Engineering, KU Leuven, Belgium;

³ Biomechanics Section, KU Leuven, Belgium;

⁴ Department of Otorhinolaryngology, Erasmus MC, University Medical Center, Rotterdam, Netherlands;

⁵ GIGA In silico medicine, University of Liège, Belgium;

⁶ Lilly Research Laboratories, Eli Lilly Pharmaceuticals, Indianapolis, USA;

⁷ Comparative Biomedical Sciences, Royal Veterinary College, London, United Kingdom;

⁸ Department of Otorhinolaryngology, Erasmus MC, University Medical Center Rotterdam, Rotterdam, The Netherlands;

⁹ Department of Biomechanical Engineering, University of Technology Delft, Delft, The Netherlands.

Submitted

DOI: 10.1101/2022.06.12.495737

Abstract

Pathological endochondral ossification (EO) in the joint underlies the progression of osteoarthritis (OA), a prevalent degenerative joint disease for which no disease-modifying drugs are currently available. Hypertrophic chondrocytes are key players in endochondral ossification driving catabolic processes in articular cartilage and contributing to the formation of osteophytes, the characteristic bony spurs formed at the joint margins in OA. Low-grade inflammation is another hallmark of OA that has been linked with chondrocyte hypertrophy. Therefore, we hypothesized that targeting inflammation and hypertrophy could lead to an effective OA therapy. To identify an appropriate target, we analyzed transcriptomic datasets and identified the erythropoietin-producing hepatocellular carcinoma A2 (EPHA2), a tyrosine kinase receptor associated with osteoarthritis, inflammation and chondrocyte hypertrophy. Computational mechanistic modeling of cellular signaling networks revealed that the activation of EPHA2 triggers an inflammatory response and lead to chondrocyte hypertrophy. Pharmacologic inhibition of EPHA2 reduced both inflammation and hypertrophy in human chondrocytes. Interestingly, systemic administration of the EPHA2 inhibitor ALW-II-41-27 attenuated joint degeneration in a murine OA model, evidenced by significantly reduced synovial inflammation and osteophytosis. Collectively, our interdisciplinary approach - combining *in silico*, *in vitro* and *in vivo* models - suggests that pharmacological inhibition of EPHA2 with ALW-II-41-27 is a promising disease-modifying treatment that paves the route for a novel drug discovery pipeline for osteoarthritis.

Introduction

Osteoarthritis (OA) is the most prevalent and disabling musculoskeletal disease worldwide [1], characterized by progressive joint changes leading to pain and disability [2, 3]. In OA the joint is inflamed, the cartilage lining the joint surface is lost and bony spurs (called osteophytes) are formed at the joint margins. Current pharmacologic treatments are palliative, predominantly pain killers, that do not halt disease progression. Thus, there is an urgent need to discover disease-modifying OA drugs (DMOADs) that can alleviate the development of OA.

Chondrocyte hypertrophy is a chondrocyte phenotype that precedes cartilage calcification and ultimately its replacement by bone. Under physiological conditions, articular chondrocytes are resistant to hypertrophy. During OA, however, the onset of hypertrophic differentiation drives cartilage breakdown [4]. In a similar way, joint margins are established through the growth of an initial cartilage template that undergoes endochondral ossification and is replaced by bone [5]. Inflammation present during OA is characterized by synovitis, encompassing an increase in macrophage activation and the production of inflammatory cytokines such as tumor necrosis factor alpha (TNF- α) [6, 7]. Inflammatory signaling activation is known to trigger cartilage extracellular matrix degradation, and has been proposed to induce chondrocyte hypertrophy [8, 9].

Therefore, we hypothesize that blocking a key target regulating both chondrocyte hypertrophy and inflammation would be an effective therapeutic strategy for OA. Thus, in this study we aim to identify a druggable target for OA associated with chondrocyte hypertrophy and inflammation, and determine the efficacy of its pharmacologic inhibition combining *in silico*, *in vitro* and *in vivo* models.

Methods

Study design

The objective of this study was to identify a drug target for osteoarthritis and further validate a disease modifying osteoarthritic drug. This study consisted of *in silico*, *in vitro* and *in vivo* experiments using available transcriptomic data in cartilage, a computational model of chondrocyte phenotype, patient-derived chondrocytes and mesenchymal stromal cells and C57BL/6 mice. The exact number of replicates used in each experiment are indicated in the respective figure legends. All animals and human tissue were randomized for treatment. The investigators performing the surgeries, injections, hind limb weight distribution and blood extractions were blinded to the animal identity. All mice and their collected samples and human tissue samples were coded and analyzed in a blinded manner until data were obtained and quantification was completed. Data were then decoded and matched to the corresponding groups, results were charted, and statistical analysis was performed.

Data mining of microarray datasets

Three previously published datasets were leveraged for the purpose of the current study. To identify a target associated with chondrocyte hypertrophy, we used a dataset previously generated in different zones of the growth plate of 14 days old female Swiss White mice [10], using a 44k whole genome oligo microarrays (G4122A; Agilent Technologies, Santa Clara, CA, United States). A list of differently expressed genes between the proliferative (PR) and hypertrophic (H) layer was obtained from the supplementary data of the publication, generated via paired t-test and selected factors with a cut off value of 3-fold change in the expression of genes. To identify a target associated with osteoarthritis, we used a dataset previously generated in 10-week-old male C57BL/6 mice by surgical destabilization of the medial meniscus (DMM) [11] using a 44k whole genome oligo microarrays (G4122A; Agilent Technologies). A list of differently expressed genes from cartilage of DMM- or sham-operated mouse joints was obtained from the supplementary data of the publication, generated via paired t-test and selected factors with a cut off value of 2-fold change in the expression of genes. To identify targets associated with human osteoarthritic cartilage we used a microarray dataset previously generated [12], performed using Affymetrix oligonucleotide microarray HG-U133plus2.0 (Affymetrix, Santa Clara, CA). Differently expressed genes in articular cartilage from OA and healthy donors were obtained from the supplementary data of the publication, generated via paired t-test and considering genes that displayed a mean fold change greater than 2. An online resource from Gene Ontology (GO) was used to obtain a list of genes associated with inflammation, namely GO: 0006954 Inflammatory response [13, 14]. The selected lists of uniquely expressed factors were then overlapped utilizing the Funrich software [15], to select for genes associated with osteoarthritis, inflammation and chondrocyte hypertrophy.

In silico experiments (simulations)

A computational model of the intracellular signaling pathways regulating articular chondrocyte phenotypes [16, 17], was leveraged and completed with information about EPHA2. This mechanistic model represents 62 molecular entities (growth factors, receptors, transcription factors, extracellular matrix proteins and signaling) and the way they regulate each other, at protein and genetic level, to transduce external signals into new cellular states. Connections of EPHA2 with the rest of the signaling network were added according to information found in literature (Fig 2A and supplementary table 1) with supporting references featuring different cell types, given that EPHA2 is still understudied in cartilage. The mathematical implementation consists of additive equations in which each variable (i.e. biomolecule) is regulated at protein (fast) and genetic (slow) level with values continuously ranging between 0 (fully repressed) and 1 (fully expressed and activated). An asynchronous updating scheme with priority classes (i.e. fast variables updated first) was employed, resulting in semi-quantitative stochastic simulations [18]. A Monte Carlo approach (10,000 random initializations) was used to compute the model's stable states, equating to possible molecular states of the cell

(i.e. chondrocyte phenotypes). The stable states were characterized regarding the variable (i.e. biomolecules' activity) as markers. *In silico* experiments were initially executed using the model's stable state resembling the most a regular healthy chondrocyte. *In silico* experimental conditions were applied by (simultaneously) forcing the targeted variables to be set to 0 (for inhibition) or 1 (for activation). The *in silico* conditions were applied for 1,000 computing steps after which all variables were left free to evolve until reaching a new stable state, thereby simulating a bolus treatment effect. This was repeated 100 times and the various outcomes, or final states, (due to the model stochasticity) were averaged to compute the final profiles, standard deviations were also computed. When a final state is different from the initial state before perturbation, this is called a state transition. The percentage of transition to each emerging final state was also computed over the 100 repetitions. The following 4 conditions were applied: (1) activation of EPHA2, (2) activation of pro-inflammatory cytokines and their receptors, (3) the combination of the two previous conditions and (4) blockage of EPHA2 while activating the pro-inflammatory cytokines and their receptors.

Evaluation of ALW-II-41-27 in OA chondrocytes

In vitro target validation was performed using chondrocytes isolated from human articular cartilage from OA donors (2 females, one male, age 61, 64 and 69 years). The cartilage was obtained with implicit consent as waste material from patients undergoing total knee replacement surgery. This protocol was approved by the medical ethical committee of the Erasmus MC, University Medical Center, Rotterdam, protocol number MEC-2004-322. Cartilage chips were subjected to protease (2 mg/ml, Sigma Aldrich) in saline for 2 hours followed by overnight digestion with 1.5 mg/ml collagenase B (Roche Diagnostics, Switzerland) in Dulbecco's Modified Eagle's Medium (DMEM) high glucose supplemented with 10% fetal bovine serum. Single cell suspension was obtained by filtrating the cellular solution through a 100 μm filter. The isolated chondrocytes were expanded in monolayer at a seeding density of 7,500 cells/cm² in DMEM high glucose supplemented with 10% fetal bovine serum, 50 $\mu\text{g}/\text{ml}$ gentamicin and 1.5 $\mu\text{g}/\text{mL}$ fungizone (Gibco, Grand Island, NY, USA). Upon attaining approximately 80% confluency, cells were trypsinized and reseeded at 7,500 cells/cm². Cells were used for experiments after three passages. To re-differentiate the expanded articular chondrocytes, a 3D alginate bead culture model was used [19, 20]. Alginate beads were prepared by mixing passage three chondrocytes and re-suspended them in 1.2% (w/v) low viscosity alginate (Kelton LV alginate, Kelco Co, San Diego, CA, USA) in 0.9% NaCl (Sigma Aldrich) at a concentration of 4×10^6 cells/mL. Beads were made by dripping the cell-alginate suspension in 105 mM CaCl₂ (Sigma Aldrich) through a 22-gauge needle. Beads were washed with 0.9% NaCl and DMEM low glucose. Beads with a size that deviated from the average after a visual inspection were not included in the experiment. Re-differentiation of chondrocytes was performed in a 24-well plate (BD Falcon) for two weeks in 100 $\mu\text{L}/\text{bead}$ DMEM low glucose supplemented with 1% v/v Insulin-Transferrin-Selenium (ITSTM+ Premix, Corning, Bedford, MA, USA), 10 ng/ml transforming growth factor beta-1 (TGF- β -1, recombinant

human, R&D systems) 25 µg/mL l-ascorbic acid 2-phosphate (Sigma Aldrich), 50 µg/ml gentamicin, and 1.5 µg/mL fungizone (both Gibco). After two weeks, TGF-β-1 was no longer added to the medium and cells were cultured with 10 µM of ALW-II-41-27 (MedChemExpress, Ann Arbor, MI, USA), vehicle (DMSO) and/or with the pro-inflammatory cytokine TNF-α 10 ng/mL for 24 hours. Preliminary experiments were performed using two doses of ALW-II-41-27, 1 and 10 µM, being 10 µM more effective. Medium and alginate beads were harvested for further analyses.

Nitric oxide (NO) assay

NO production was measured in the medium of OA chondrocytes by determining the content of nitrite using the Griess reagent (Sigma Aldrich). The reaction was monitored at 540 nm using a spectrophotometer (VersaMax; Molecular Devices, Sunnyvale, USA). Sodium nitrite (NaNO₂; Chemlab, Zedelgem, Belgium) was used as standard for the calibration curve.

Interleukin-6 assay

A commercially available enzyme-linked immunosorbent assay (ELISA) kit was used to determine the concentration of IL-6 in the medium of OA chondrocytes as per manufacturer's instructions (R&D systems, Minneapolis, MN, USA).

Evaluation of ALW-II-41-27 in chondrogenically differentiated MSCs

Human MSCs were isolated from surplus iliac crest bone chip material harvested from pediatric patients undergoing alveolar bone graft surgery. All human samples were obtained with the approval of the Erasmus MC, University Medical Center Medical Research Ethics Committee (MEC-2014-16). Written consent was not required in accordance with the national code regarding the use of waste surgical material for scientific research (www.coreon.org), and an opt-out option was available. Iliac crest bone chips were washed with expansion medium composed of Minimum Essential Medium (MEM)-α (containing nucleosides) supplemented with heat inactivated 10% v/v fetal bovine serum (FBS) (both Thermo Fisher Scientific, Waltham, MA, USA), 1.5 µg/mL fungizone (Gibco), 50 µg/ml gentamicin (Gibco), 25 µg/ml L-ascorbic acid 2-phosphate (Sigma-Aldrich, St. Louis, MO, USA), and 1 ng/mL fibroblast growth factor-2 (Instruchemie, Delfzijl, The Netherlands), and the resulting cell suspension was seeded in T75 flasks. Cells were washed twice with phosphate buffered saline (Thermo Fisher Scientific) supplemented with 2% v/v heat inactivated FBS 24 h following seeding to remove non-adherent cells. MSCs were cultured at 37°C and 5% carbon dioxide under humidified conditions, with expansion medium refreshed every 3–4 days. MSCs were sub-cultured upon reaching 80–90% confluency using 0.25% w/v trypsin-EDTA (Thermo Fisher Scientific) and reseeded at a cell density of 2,300 cells/cm². MSCs were used at passage 3 for chondrogenic pellet cultures.

For chondrogenic differentiation, 2×10^5 MSCs were suspended in 500 µl of chondrogenic differentiation medium composed of high glucose Dulbecco's Modified Eagle Medium

supplemented with 1.5 µg/mL fungizone (Gibco), 50 µg/ml gentamicin (Gibco), 1 mM sodium pyruvate (Thermo Fisher Scientific), 1% v/v Insulin-Transferrin-Selenium (ITSTM+ Premix, Corning, Bedford, MA, USA), 40 µg/ml proline (Sigma-Aldrich), 25 µg/ml L-ascorbic acid 2-phosphate (Sigma-Aldrich), 100 nM dexamethasone (Sigma-Aldrich), and 10 ng/ml TGF-β-1 (R&D systems). The cell suspension was added to 15 ml conical polypropylene tubes (TPP, Radnor, PA, USA) and centrifuged at 300 g for 8 min to facilitate pellet formation. Chondrogenic MSC pellets were cultured at 37°C and 5% carbon dioxide in a humidified atmosphere. After 24 h, pellets were tapped to enhance pellet formation and the medium was renewed with chondrogenic medium with 100 nM of ALW-II-41-27 (MedChemExpress, Ann Arbor, MI, USA) or vehicle (DMSO). Afterwards the medium was renewed two times per week for a period of 3 weeks.

Histological analysis of chondrogenic pellets

After 3 weeks of chondrogenic induction, pellets were fixed with 4% (v/v) formaldehyde in phosphate buffered saline, embedded in paraffin and sectioned (6 µm). Glycosaminoglycan (GAG) was stained with 0.04% thionine solution and collagen type II was immunostained using a primary antibody II-II6B3 (Developmental Studies Hybridoma Bank, Iowa City, IA, USA) 0.4 µg/mL in PBS/1% bovine serum albumin (BSA; Sigma-Aldrich), collagen type X using primary antibody 14-9771-82, 5 µg/mL in PBS/1% BSA (Thermofisher, Waltham, MA, USA). Antigen retrieval for collagen type II was performed with 1 mg/mL pronase (Sigma-Aldrich) in PBS for 30 min at 37°C, followed by incubation with 1% hyaluronidase (Sigma-Aldrich) in PBS for 30 min at 37°C to improve antibody penetration. Antigen retrieval for collagen type X was done by a 2h incubation in 1 mg/mL pepsin in 0.5M acetic acid followed by incubation with 1% hyaluronidase (Sigma-Aldrich) in PBS for 30 min at 37°C. The slides were pre-incubated with 10% normal goat serum (Sigma-Aldrich) in PBS with 1% BSA (Sigma-Aldrich). Next, the slides were incubated for 1 h (for collagen type II) or overnight (for collagen type X) with the primary antibody, and then with a biotin-conjugated secondary antibody (HK-325-UM, Biogenex, Fremont, CA, USA), alkaline phosphatase-conjugated streptavidin (HK-321-UK, Biogenex), and the Neu Fuchsin chromogen (B467, Chroma Gesellschaft). An IgG1 isotype antibody (X0931, Dako Cytomation, Santa Clara, CA, USA) was used as negative control.

Gene expression

Alginate beads were dissolved using citrate buffer, centrifuged at 200 g and the pellet was resuspended in RLT (Qiagen, Hilden, Germany) buffer containing 1% beta-mercaptoethanol for RNA isolation. The MSCs chondrogenic pellets were homogenized in RNA-Bee TM (Tel-Test Inc., Friendswood, USA) and 20% chloroform was added to extract RNA. mRNA isolation was performed according to manufacturer's protocol utilizing the RNeasy Column system (Qiagen, Hilden, Germany). The RNA concentration was determined using a NanoDrop spectrophotometer (Isogen Life Science, Utrecht, The Netherlands).

0.5 µg RNA was used for cDNA synthesis following the protocol of the manufacturer of the RevertAid First Strand cDNA kit (Thermo Fisher Scientific, Waltham, MA, United States). qPCR was performed on a Bio-Rad CFX96 Real-Time PCR Detection System (Bio-Rad) to assess gene expression, Alkaline phosphatase (ALPL, Fw: GACCCTTGACCCCAACAAT; Rev: GCTCGTACTGCATGTCCCCT; Probe: TGGACTACCTATTGGGTCTCTTCGAGCCA), Collagen type 2 (COL2A1; Fw: GGCAATAGCAGGTTACGTACA ; Rev: CGATAACAGTCTTGCCCCACTT; Probe: CCGGTATGTTTCGTGCAGCCATCCT), Collagen type 10 (COL10A1; Fw: CAAGGCACCATCTCCAGGAA; Rev: AAAGGGTATTTGTGGCAGCATATT; Probe: TCCAGCACGCAGAATCCATCTGA), matrix metalloproteinase-13 (MMP13; Fw: AAGGAGCATGGCGACTTCT; Rev: TGGCCCAGGAGGAAAAGC; Probe: CCCTCTGGCCTGCGGCTCA), Runt-related transcription factor 2 (RUNX2; Fw: ACGTCCCCGTCCATCCA; Rev: TGGCAGTGTATCATCTGAAATG; Probe: ACTGGGCTTCTTGCCATCACCGA), Tumor Necrosis Factor- α (TNF α ; Fw: GCCGCATCGCCGTCTCTACT; Rev: AGCGCTGAGTCGGTCACCCT). Glyceraldehyde-3-phosphate dehydrogenase (GAPDH; Fw: ATGGGGAAGGTGAAGGTGC; Rev: TAAAAGCAGCCCTGGTGACC; Probe: CGCCAATACGACCAAATCCGTTGAC) was found stable and therefore used as reference gene. Data were analyzed by the $\Delta\Delta C_t$ method and normalized to the expression of GAPDH of each condition and compared to the corresponding gene expression in the control groups.

Animal model

All animal experimentation procedures were conducted with approval by the Animal Ethical Committee of Erasmus University Medical Center (License number AVD101002015114, protocol number 16-691-06). 12-week-old male C57BL/6 mice (C57BL/6JolaHsd, 27.01 g \pm 2.05 g; Envigo, Cambridgeshire, UK), were housed in groups of 8 in individually ventilated cages and maintained on a 12 h light/dark cycle with ad libitum access to standard diet and water at the Experimental Animal Facility of the Erasmus MC. Mice were randomly divided into two experimental groups (N=8 per group): Control and ALW-II-41-27-treated mice. For all procedures, mice were anesthetized using 3% isoflurane/0.8 L O₂/min (Pharmachemie BV, Haarlem, the Netherlands). OA was induced unilaterally by intra-articular injections of 60 µg Monoiodoacetate (MIA) (Sigma-Aldrich, St. Louis, USA) in 6 µl of saline (0.9% NaCl; Sigma-Aldrich) at day 0. Injections were performed after a 3-4 mm dermal incision was made to the right knee at the height of the patellar tendon. All intra-articular injections were administered using a 50 µl syringe (Hamilton, Bonaduz, Switzerland) and 30G needle (BD Medical, New Jersey, USA). ALW-II-41-27 was delivered using Alzet micro-osmotic pumps (Durect Corporation, CA, USA) model 1004, delivery rates of 0.11 µL/ hour, that were implanted subcutaneously on the back of the mice, slightly posterior to the scapulae, immediately after the intra-articular injections. Osmotic pumps were filled with dimethyl sulfoxide: polyethylenglicol alone (55:45 ratio, vehicle-treated group, N=8 mice) or containing 6 mg of ALW-II-41-27 dissolved in vehicle (treated group, N=8 mice) which leads to a dose

of 6.6 µg/ hour. A third group of N=8 mice received the implantation of osmotic pumps delivering a dose of 1.7 µg/ hour of ALW-II-41-27. In the figures 5 and 6 we report the 6.6 µg/ hour dose of ALW-II-41-27. Synovial thickness, Krenn score and osteophyte size for all groups can be found in supplementary figure 6. Mice were euthanized in agreement with the Directive 2010/63/EU by cervical dislocation under isoflurane anesthesia 14 days following MIA injection. After which knees were fixed in 4 % formalin (v/v) for 1 week, decalcified in 10 % EDTA for 2 weeks and embedded in paraffin. Coronal sections of 6 µm were cut for analyses.

Flow cytometric analysis of peripheral blood monocytes

Peripheral blood was harvested from the facial vein of mice on days 2- and 12 post-induction of OA, as previously described [21]. Blood sampling order was performed randomly at each time-point. 50 µl of whole blood was pre-incubated with purified rat anti-mouse CD16/CD32 (BD Biosciences Cat# 553140, New Jersey, USA) for 5 mins on ice. Blood was stained for the expression of CD11b (BioLegend, San Diego, USA, Cat# 101228), CD115 (BioLegend, Cat# 135505), Ly-6C (BioLegend Cat# 128005) and CD62L (BioLegend, Cat# 104412) to identify myeloid cells and specific monocyte subsets, as well as CD3 (BioLegend, Cat# 100220), NK1.1 (BioLegend, Cat# 108713), CD19 (BioLegend, Cat# 115520) and Ly-6G (BioLegend, Cat# 127618) to eliminate T cells, natural killer cells, B cells and neutrophils (Supplementary table 2). Cells were stained for 30 mins at 4°C in the dark, followed by incubation with 2 ml of 1X FACS lysing solution (BD Biosciences) for 10 minutes to lyse red blood cells. Following centrifugation at 400 g for 10 minutes, supernatant was removed and cells washed and resuspended in FACSFlow buffer (BD Biosciences).

All samples were analyzed using a FACSJazz cytometer (BD Biosciences) and FlowJo software version 10.0.7 (FlowJo LLC, Oregon, USA). The gating strategies applied for blood monocytes analysis are presented in supplementary figure 5.

Histological analyses of murine knee joints

To evaluate cartilage damage, sections were stained with Safranin O & Fast Green. To evaluate synovial inflammation and osteophyte area, sections were stained with Hematoxylin & Eosin. Images were acquired using the NanoZoomer Digital Pathology program (Hamamatsu Photonics, Ammersee, Germany). For each knee, 3 sections of the patellofemoral compartment, taken at standardized locations in the knee with 180 µm distance in between were evaluated by two independent well trained evaluators that were blinded for the treatment (MNFB and NK). For each knee, the average value of the three sections was calculated and the values of two observers were averaged and used for representation and statistical analyses.

Cartilage damage was evaluated with the Osteoarthritis Research Society International (OARSI) scoring system [22].

Osteophyte size was assessed by measuring the area of the osteophyte at the lateral side of the patella, the location where the incidence of osteophytes was highest, using the NanoZoomer digital pathology program.

Synovial thickness was measured from the capsule to the superficial layer of the synovial membrane at the medial and lateral sides of the parapatellar recesses (three positions per section).

Synovitis was evaluated using the Krenn score [23] which considers three features of chronic synovitis (enlargement of lining cell layer, cellular density of synovial stroma, leukocytic infiltrate) and grade each feature from 0 (absent) to 3 (strong). The sum provided the synovitis score, which is interpreted as follows: 0–1, no synovitis; 2–4, low-grade synovitis; 5–9, high-grade synovitis.

To evaluate macrophages in the synovial membrane, F4/80 was used as a marker. For this purpose, an antigen retrieval was performed by placing the slides in a 20 µg/mL proteinase K solution for 30 minutes at 37°C. Blocking of specific binding was performed with 10 % goat serum (Southern Biotech, Birmingham, AL, USA) for 30 min. Hereafter, sections were incubated for 1 h with 1 µg/mL primary antibody F4/80 (eBioscience #14-4801-82, Waltham, MA, USA), followed by 30 min incubation with a biotinylated rabbit anti-rat IgG1 (Vector, BA-4000, Burlingame, CA, USA) 6 µg/mL in PBS/1 % BSA. Thereafter, sections were incubated with an alkaline-phosphatase- conjugated streptavidin label (HK-321-UK, Biogenex) concentration not stated, diluted 1:50 in PBS/1 % BSA. To reduce background, endogenous alkaline phosphatase activity was inhibited with levamisole (Sigma-Aldrich Chemie). New Fuchsin (Fisher Scientific) and Naphthol AS-MX phosphate (Sigma-Aldrich Chemie) substrates were used for color development and counterstaining was performed with hematoxylin. As a negative control, a rat IgG2a antibody (#14-4321-82, eBioscience Inc. San Diego, CA, USA) was used.

To evaluate type X collagen in mice knees, a pre-coupling step was performed 24 hours before the staining using a 1:10 dilution of collagen type X antibody (Quartett, #X53) with fluorescent goat anti-rat IgG (H+L) (Cross-Adsorbed Secondary Antibody, Alexa Fluor 546, #A11081, Fisher Scientific, Landsmeer, The Netherlands). Mouse IgG1 antibody (Dako Cytomation #X0931) dilution 1:10, was used as a negative control. Antigen retrieval was performed using Pepsin (Sigma #P7000) 1 mg/mL in 0.5M acetic acid pH2 for 2 hours following 10 mg/ml hyaluronidase (Sigma #H3506) for 30 minutes. Slides were incubated with 10% normal goat serum (Southern Biotech #0060-01) for 30 minutes. Slides were incubated overnight with the pre-coupled antibodies and following day slides were mounted using ProLong Diamond Antifade Mountant with DAPI (#P36966, Fisher Scientific, Landsmeer, The Netherlands).

Pain measurement: hind limb weight distribution

Hind limb weight distribution was monitored as a surrogate pain indicator using an Incapacitance Tester (Linton Instrumentation, Norfolk, UK). Mice were positioned on the Incapacitance Tester with each hind limb resting on a separate force plate. Animals were habituated to the apparatus, three times per week, starting 2 weeks prior to the experiments. The examiner performing the measurements was blinded for treatment condition (MNFB). A baseline measurement was performed at day – 1, just before the induction of the OA.

Follow up measurements were performed at day 1, 2, 3, 5, 7, 9 and 12. For data analyses, measurements with a registration below 10 g (< 30 % of total body weight) in total on both hind limbs were excluded. 10 measurements were recorded per mouse per time point, of which at least 7 measurements were available on average. For each time point per mouse, the average of these measurements was used to calculate the percentage of weight on the affected limb as an indication of pain in the affected limb.

Data and statistical analyses

Statistical evaluation was performed using GraphPad Prism 9.0 and IBM SPSS 24 (IBM). Each *in vitro* experiment included at least 3 biological replicates and was repeated with cells derived from 3 donors. The *in vivo* study was designed to generate groups of equal size, used randomization and blinded analyses. The declared group size is the number of independent values that were used for statistical analysis. Sample size for the *in vivo* study was calculated considering the weight distribution over the hind limbs, as readout parameter. Based on previous studies, we consider an increase of 13% (standard deviation of 10%) in weight distribution on the affected limb in time in the therapy groups as relevant in our study [24]. Sample size was calculated with a statistical power of 80% and significance level of 0.05, which led to N=8. For statistical analysis, the linear mixed model with Bonferroni's multiple comparisons test was performed.

Results

EPHA2 is as an inflammation-related gene upregulated in hypertrophic chondrocytes and osteoarthritic cartilage

To identify a novel therapeutic target for OA associated with chondrocyte hypertrophy and inflammation, we performed data mining on two previously published murine microarray data sets [10, 11]. Differentially expressed genes (DEG) in articular cartilage of mice where OA was induced by destabilization of the medial meniscus (DMM) compared to cartilage of mice that had sham surgery were considered as OA-related genes. By getting the intersection of this set with another set of DEG in the hypertrophic compared to the proliferative zone of the mouse growth plate, we identified 172 genes differently expressed in OA that were also associated with chondrocyte hypertrophy. Nine of these genes overlapped with the gene ontology inflammatory response [13] (Fig. 1A, B). We then analyzed the expression of these 9 genes in a human microarray dataset obtained from OA and healthy articular cartilage [12], and found that 3 genes were also upregulated in human OA cartilage (Fig. 1C). Among these genes, GJA1 and PTGS2 had already been studied in the context of OA [25], while EPHA2, which encodes the tyrosine kinase receptor EPHA2, has a currently unknown role in OA. Epha2 expression was 30-fold upregulated in OA versus sham mouse articular cartilage (adjusted p-value= 2×10^{-2}) [11], and 3-fold upregulated in human OA versus healthy cartilage (adjusted p-value= $1 \times$

10^{-8}) [12]. Moreover, expression of EphA2 was found to be 19-fold higher in the hypertrophic compared to the proliferative zone of the murine growth plate (adjusted p-value= 1×10^{-7}) [10].

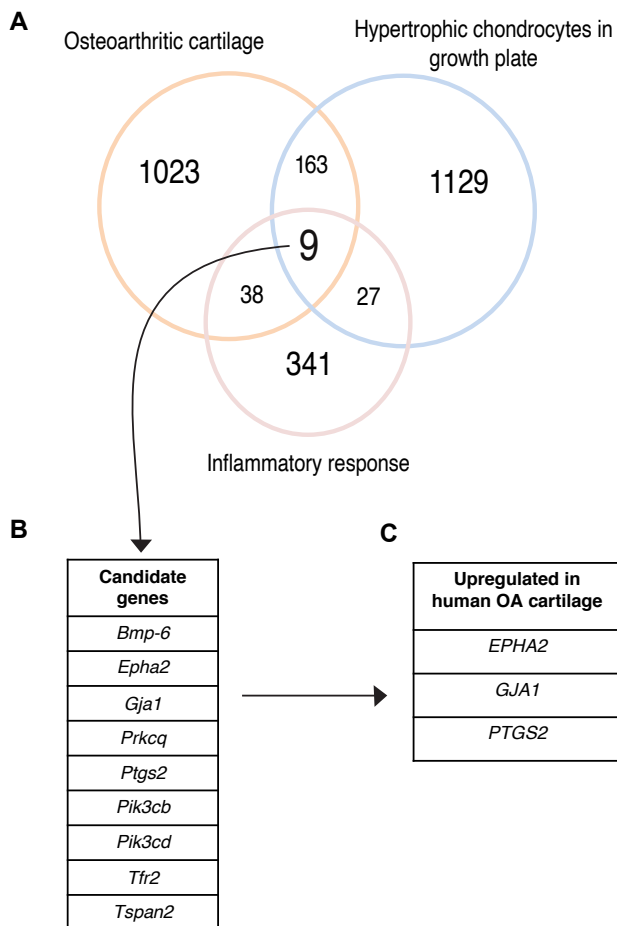


Figure 1 | Identification of EPHA2 as a novel target for OA associated with inflammation and chondrocyte hypertrophy. (A) The Venn diagram illustrates the genes related to the inflammatory response, genes that were differentially regulated in murine osteoarthritic cartilage (DMM vs sham) and genes differentially expressed in the murine growth plate (proliferative vs hypertrophic zone). The number of genes in each dataset [10, 11] is represented, together with those that overlapped. (B) List of 9 targets that overlapped in the three databases. (C) Target genes upregulated in human OA compared with healthy articular cartilage [12]. DEGs with a fold change greater than 3, and an adjusted p value lower than of 0.05, were considered for the analysis

EPHA2 triggers inflammatory markers and induces chondrocyte hypertrophy *in silico*

To evaluate the role of EPHA2 in the regulation of chondrocyte homeostasis, we used a computational model of articular chondrocyte regulatory pathways. This model enables the *in silico* screening of molecular targets in early stages of drug discovery [16]. This mechanistic model combines knowledge-based data of chondrocyte regulatory pathways, which consists of 60 biological components including growth factors, receptors, transcription factors,

extracellular matrix proteins and signaling molecules. They form a strongly interconnected network, regulated at the transcriptional and post-translational levels. EPHA2 was integrated into the network considering its previously reported interactions with the following components of the *in silico* model: Wntless and Int-1 (Wnt) [26], Dishevelled (DSH) [27], Nuclear factor kappa B (NFκB) [28], Protein kinase B (Akt) [29], extracellular signal-regulated kinase (Erk) 1/2 [30], phosphatidylinositol 3-kinase (Pi3k) [31, 32] and Rat sarcoma virus (Ras) [33] (Fig. 2A). Two mathematically stable states emerged from this model, that akin to previous versions of the model equated to two possible cellular states (i.e. chondrocyte phenotypes) [16]. Among the main characteristics of hypertrophic chondrocytes there is the upregulation of Matrix Metalloproteinase (*MMP13*), type 10 Collagen (*COL10A1*) and Runt-related transcription factor 2 (*RUNX2*) whereas healthy chondrocytes are characterized by the expression of type II collagen (*COL2A1*), Aggrecan (*ACAN*) and SRY-box transcription factor (*SOX9*) [34]. Based on the characteristic expression of these markers, we identified one stable state as ‘healthy’ and the other as ‘hypertrophic’ chondrocyte (Fig. 2A and supplementary figure 1), similar to what was observed in previous versions of the model [16]. The biological entities present in the model that relate to inflammation, specifically inflammatory cytokines, transforming growth factor-β-activated kinase (TAK) 1 and NFκB, were only active in the hypertrophic phenotype (see predicted hypertrophic activity profile in Fig. 2A), which aligns with the proposed close relationship between inflammation and hypertrophy. The variable representing EPHA2 was active in the hypertrophic while inactive in the healthy state (Fig 2A and supplementary figure 1). *In silico* experiments were performed to test the capacity of EPHA2 to induce inflammation and hypertrophy (Fig. 2B). Activation of EPHA2 triggered the transition of healthy articular chondrocytes towards the inflammatory hypertrophic state to a greater extent than the activation of the inflammatory cytokines and their receptors (9% and 5% for the conditions ‘EPHA2+’ and ‘Inflammation+’, respectively; Fig. 2C). As a result, both conditions initiated a decrease of anabolic markers (COL II, Aggrecan: blue vs orange and yellow bars; Fig. 2D) and an increase of hypertrophic and inflammatory markers (Fig. 2D, 2E). Activation of both EPHA2 and the inflammatory cytokines with their receptors had a robust synergistic effect, reaching 100% transition of healthy chondrocytes towards the inflammatory hypertrophic state (‘Inflammation+ EPHA2+’; Fig. 2C). Interestingly, this switching of cellular state was abolished when inhibiting EPHA2 (Inflammation+ EPHA2-; Fig. 2C) in this model, with a strong reduction of the activity of hypertrophic and inflammatory entities (green vs violet and yellow bars; Fig. 2 D & E). These *in silico* results support the hypertrophic and inflammatory role of EPHA2 in chondrocytes.

ALW-II-41-27 reduces human OA-derived chondrocyte inflammation

To explore whether pharmacological inhibition of EPHA2 could be used to reduce inflammation in OA, we used the tyrosine kinase inhibitor ALW-II-41-27 *in vitro* on TNF-α-treated human chondrocytes from OA donors (Fig. 3A). This small molecule is a type II kinase inhibitor with high selectivity for EPHA2 [35, 36]. Addition of ALW-II-41-27 effectively inhibited

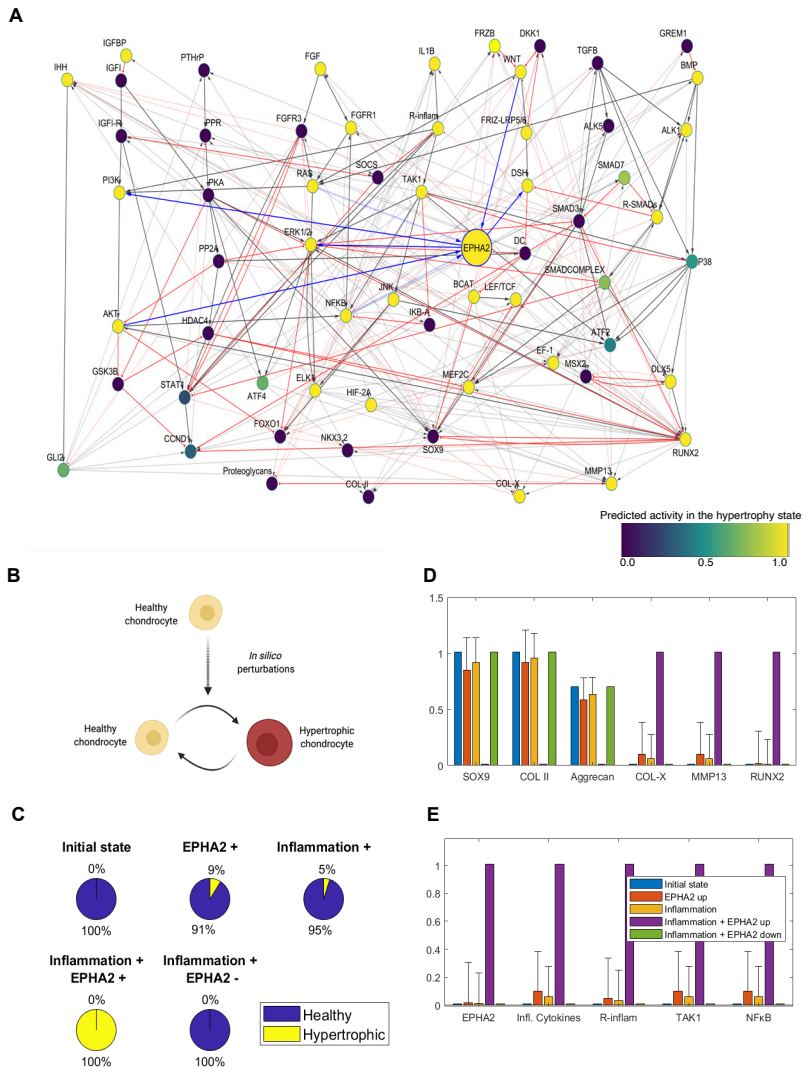


Figure 2 | EPHA2 activation induces chondrocyte hypertrophy and inflammation *in silico* (A) Integration of EPHA2 in the regulatory network of articular chondrocytes. Solid lines denote protein interaction while modulation at the gene level is in dotted lines. Activating interactions are in grey with delta arrows and inhibitory interactions are in red with a half circle. Connections with EPHA2 are denoted in blue. All components of the model are represented with a variable that is named with capital letters. The variable represents neither the protein activation level nor the gene expression but a product of both (global activity). The color of the nodes in the network denotes the global activity of the variables in the hypertrophic state, with dark blue being 0 and yellow being 1. (B) Scheme of the in silico experiment. (C) Activation of EPHA2 in the healthy state promotes the transition to a hypertrophic phenotype. Forced activation (+) or inhibition (-) of the entities from the initial healthy state is shown. Inflammation represents the activation of the variables related to inflammatory cytokines and their receptors, as input in the model. Pie charts represent the predicted percentage of perturbations leading to a transition to the hypertrophic phenotype or remaining in the healthy phenotype. (D) Average activity of the chondrogenic markers, being type II collagen, Aggrecan and SRY-box transcription factor (SOX9), and of hypertrophic markers, being Runt-related transcription factor 2 (RUNX2), Matrix Metalloproteinase (MMP13) and type 10 Collagen. (E) Average activity of EPHA2 and variables associated with inflammation. The bars represent the mean of the results of a hundred in silico experiments (+ standard deviations, +SD). There is no SD for the initial state (blue condition) as it denotes the starting point before the in silico perturbation is applied. Figure created with Cytoscape, MATLAB and Biorender.com

the TNF- α -induced inflammatory activity as shown by a 3-fold reduction in the secretion of nitric oxide metabolites (Fig. 3B). Likewise, administration of ALW-II-41-27 attenuated the TNF- α -induced expression of the inflammatory cytokine interleukin (IL)-6 at the gene (4-fold, Figure 2C) and protein level (5-fold, Figure 2D), known to be a downstream target gene of TNF- α via NF κ B [37]. Furthermore, ALW-II-41-27 treatment counteracted the TNF- α -induced upregulation of the cartilage matrix degrading enzymes *MMP1* (6-fold, Figure 3E) and *MMP13* (4-fold, Figure 3F). These results demonstrate the anti-inflammatory capacity of ALW-II-41-27 in TNF- α -stimulated OA chondrocytes.

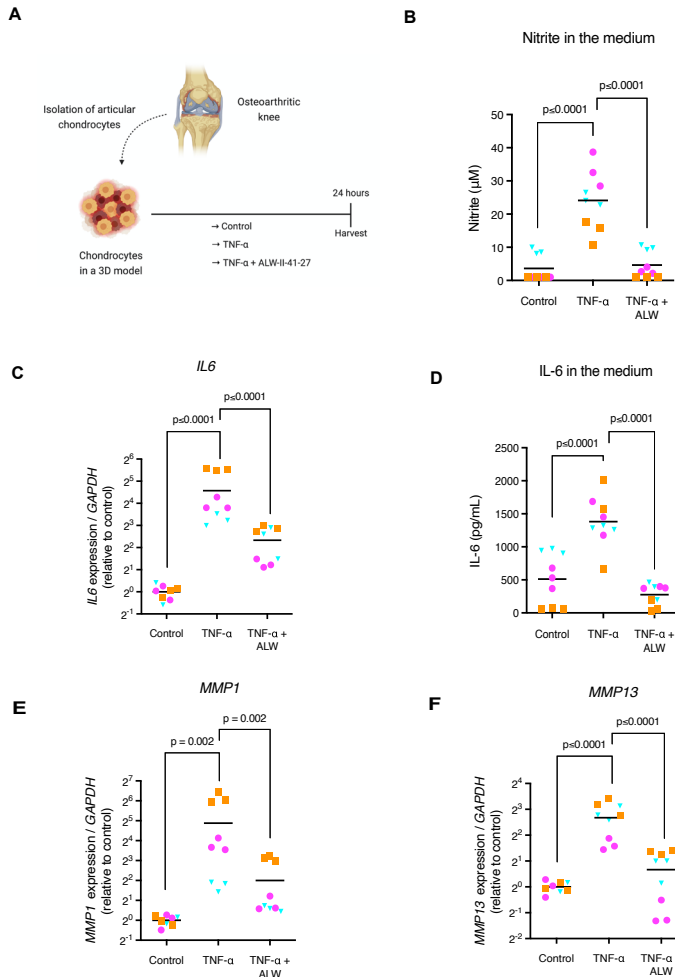


Figure 3 | ALW-II-41-27 decreases TNF- α induced catabolism and inflammation in human chondrocytes. (A) Experimental set-up to evaluate the anti-inflammatory capacity of ALW-II-41-27 (10 μ M) in human OA chondrocytes cultured with 10 ng/mL TNF- α . (B) Evaluation of nitrite in the medium as a marker for inflammatory activity as determined by Griess reagent. (C, E-F) Gene expression of IL6, MMP1 and MMP13 determined by qPCR. The average of control, per donor, is set to 1. (D) IL-6 in the medium determined by ELISA. Experiments were performed in triplicate, with cells from three donors. Donors are represented with different colors and symbols: violet circles (donor 1), blue triangles (donor 2) and orange squares (donor 3). The horizontal line in the graphs represents the mean. Data were analyzed with the linear mixed model with Bonferroni's multiple comparisons test. Figure created with Biorender.com

ALW-II-41-27 decreases chondrocyte hypertrophy

We then proceeded to evaluate whether pharmacological inhibition of EPHA2 with ALW-II-41-27 inhibits hypertrophy in human OA-derived articular chondrocytes (Fig. 4A). ALW-II-41-27 decreased *COL10A1* expression 2-fold (Fig. 4B), suggesting a reduction in

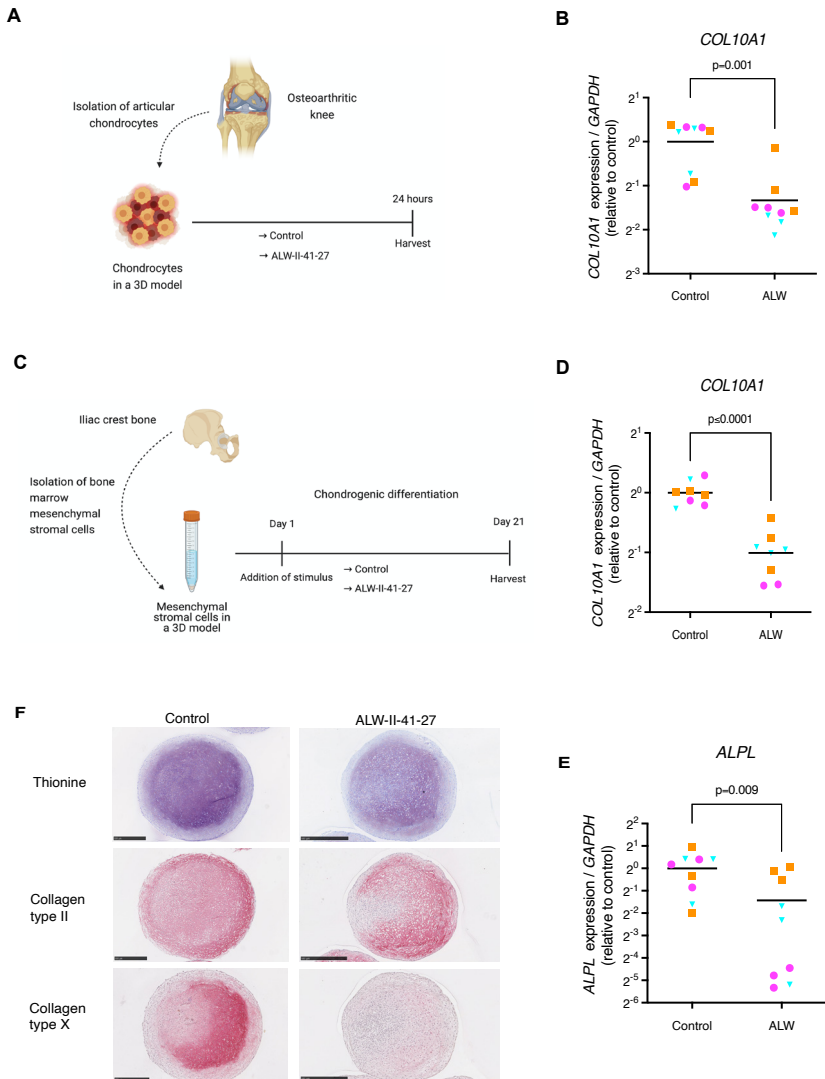


Figure 4 | ALW-II-41-27 decreases chondrocyte hypertrophy. (A) Experimental set-up to evaluate the capacity of ALW-II-41-27 (10 μ M) to modulate hypertrophy in human OA chondrocytes. (B) Gene expression of the hypertrophic marker *COL10A1* in cultured OA chondrocytes determined by qPCR. (C) Experimental set-up to evaluate how ALW-II-41-27 (100 nM) affects hypertrophy in tissue engineered cartilage from MSCs. (D, E) Gene expression of *COL10A1* and *ALPL* in MSC-generated cartilage determined by qPCR. (F) Histological analysis of tissue engineered cartilage derived from MSCs; Thionine staining showing glycosaminoglycans (violet), and immunohistochemistry of type II and type X collagen (red/pink). Experiments were performed with 3 replicates, for each of the three donors. Donors are represented with different colors and symbols: violet circles (donor 1), blue triangles (donor 2) and orange squares (donor 3). For gene expression analysis, the average of control replicates is set to 1 per donor. The horizontal line in the graphs represents the mean. For statistical analysis, the linear mixed model with Bonferroni's multiple comparisons test was performed.

hypertrophy. Since chondrocyte hypertrophy is a key process that hinders stable hyaline cartilage tissue engineering [38], we further investigated the effect of ALW-II-41-27 on cartilage tissue engineered constructs from mesenchymal stem cells (MSCs), well-known to become hypertrophic and prone to ossify when implanted *in vivo* [39-42] (Fig. 4C). Gene expression analysis revealed that the addition of ALW-II-41-27 attenuated the hypertrophic markers *COL10A1* and *ALPL* by a fold change of 2 and 3, respectively (Fig. 4D & E). Accordingly, when treated with ALW-II-41-27 the cells deposited less type X Collagen (Fig. 4F and supplementary figure 2). Interestingly, neither glycosaminoglycan nor type II Collagen deposition was reduced (Fig. 4F), suggesting that ALW-II-41-27 was mainly targeting hypertrophy.

ALW-II-41-27 treatment reduces joint inflammation and pathological endochondral ossification *in vivo*

EPHA2 inhibition reduced hypertrophy and inflammation *in silico* and its pharmacological inhibition with ALW-II-41-27 in cell culture *in vitro* confirmed these results. Therefore, we proceeded to evaluate whether ALW-II-41-27 could be an effective OA therapy *in vivo* using a mouse model of joint pain and degeneration following intra-articular injection of monoiodoacetate (MIA) [43]. ALW-II-41-27 was subcutaneously administered with a controlled delivery system (Fig. 5A). Total body weight was not affected by the administration of ALW-II-41-27 over the 14 days of the study, suggesting no significant effects of the treatment on the general health state of the animals (supplementary figure 3). Treatment with ALW-II-41-27 reduced the synovial membrane thickness (Fig. 5B, C & D) as well as synovitis (Fig. 5E) as compared to vehicle-treated mice. Synovitis is governed by macrophages, the crucial regulators of OA progression and primary mediators of the inflammatory response [44]. Macrophages were observed only in the synovial lining of vehicle-treated mice, indicating that ALW-II-41-27 effectively attenuated joint inflammation (Fig. 5F). Monocytes migrate from the circulation into tissues under inflammatory conditions and differentiate into macrophages [45, 46]. To investigate whether the observed decrease in local joint inflammation following ALW-II-41-27 administration was associated with a systemic effect on immune cells, we also examined potential effects on peripheral blood monocytes. At day 2 and 12, the levels of monocytes in blood were not altered compared to vehicle-treated mice (Fig. 5G), suggesting that the drug selectively decreased local joint inflammation.

Since joint pain is a major symptom in OA often associated with inflammation [47, 48], we investigated this parameter by evaluating distribution of weight between the limbs of the mice. However, no significant difference was detected between ALW-II-41-27-treated and vehicle-treated mice, suggesting no effect was apparent on pain (supplementary Figure 4).

Since cartilage damage and osteophyte formation are prominent pathophysiological features of OA, we next interrogated whether ALW-II-41-27 modulates cartilage damage and osteophytosis in the joint. Cartilage degeneration was observed by loss of proteoglycans and was exhibited in all mice regardless of the treatment with ALW-II-41-27 (Fig. 6 A&B), suggesting that ALW-II-41-27 was not able to rescue matrix degeneration *in vivo*. Histological

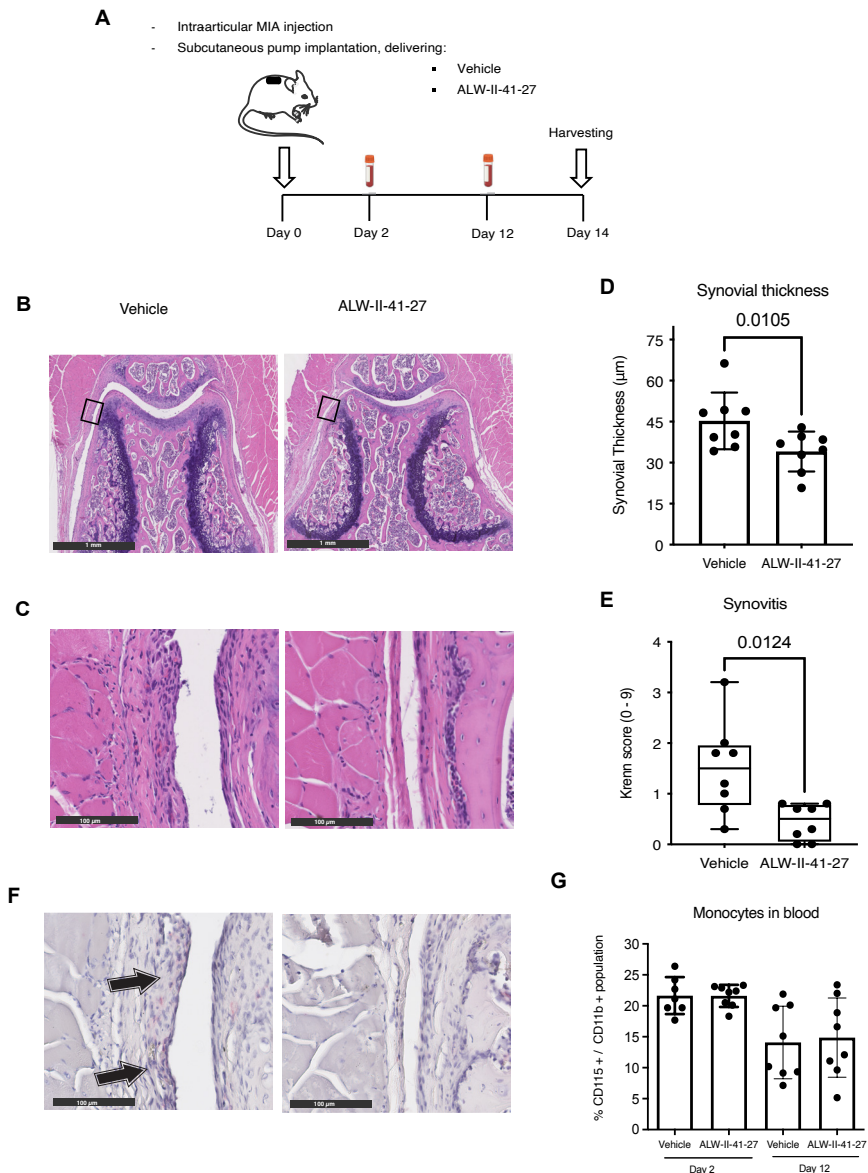


Figure 5 | ALW-II-41-27 treatment attenuates joint inflammation. (A) Experimental set-up of the *in vivo* experiment. Intra-articular injection of monoiodoacetate (MIA, 60 µg in 6 µl of saline) was applied to the right knee of mice for each experimental group (N=8) to induce OA. An osmotic pump was implanted on the back of the mice, slightly posterior to the scapulae, which continuously delivered vehicle or ALW-II-41-27 in a dose of 6.6 µg/ hour. At day 2 and 12 peripheral blood was harvested. At day 14 mice were euthanized to assess the effects of ALW-II-41-27 on the degenerated joint. (B) Hematoxylin and Eosin staining of knees (patellofemoral region) from vehicle-treated and ALW-II-41-27-treated mice. Black square indicates the region of magnification for the image below (C) showing the synovial lining where synovial thickness and Krenn score were determined. (D) Synovial thickness is represented by the mean ± SD. (E) Krenn score illustrated with box-and-whiskers plots, with line indicating the median and error bars spanning maximum to minimum values. (F) Immunohistochemistry of F4/80 (pink) showing macrophages in the synovial lining. Arrows indicate positive staining. (G) Percentage of monocytes present in the peripheral blood of mice at day 2 and 12, respect to the myeloid cell population. In all graphs, each dot represents data of an individual mouse (N=8). For statistical analysis, the linear mixed model with Bonferroni's multiple comparisons test was performed.

assessment of the knee joints showed that osteophytes, particularly present at the lateral side of the patella (Fig. 6C), were significantly smaller in ALW-II-41-27-treated mice (Fig. 6D). Accordingly, type X collagen deposition was decreased in the knees of ALW-II-41-27-treated mice (Fig. 6E). These results indicate that subcutaneous delivery of ALW-II-41-27 effectively targets endochondral ossification in the injured joint.

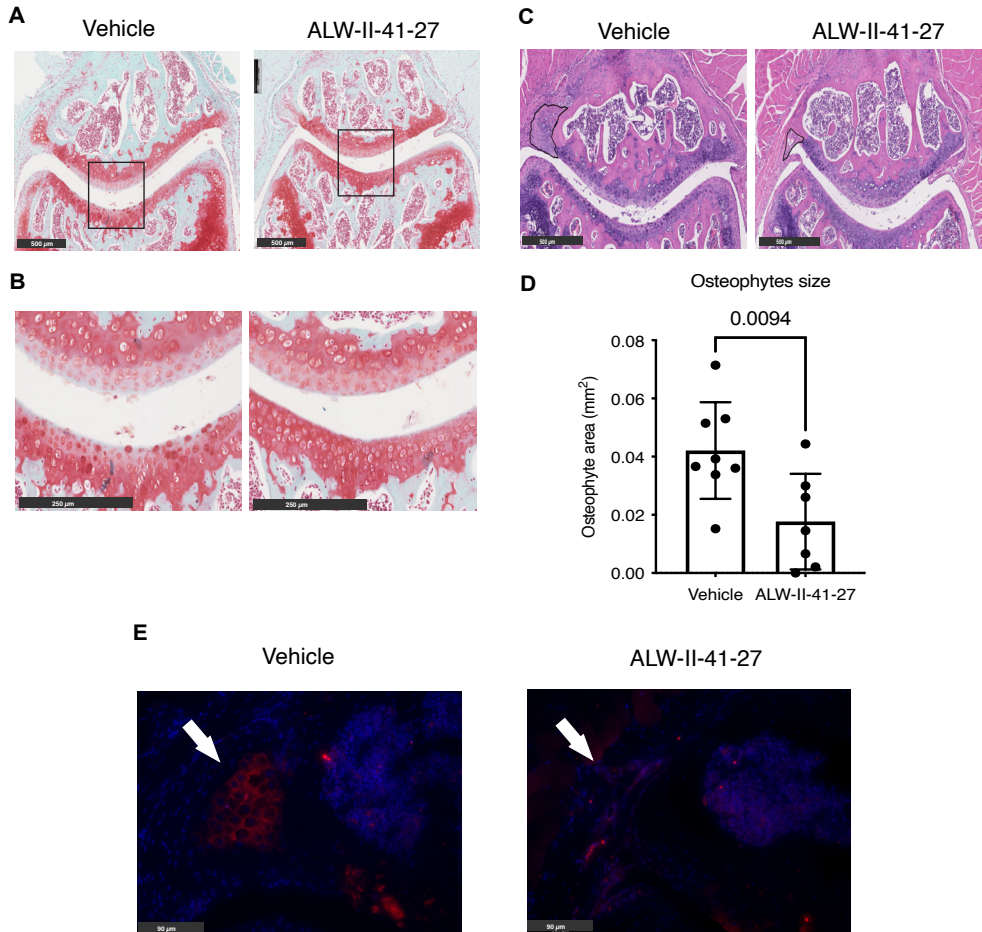


Figure 6 | ALW-II-41-27 treatment attenuates pathological endochondral ossification (A) Safranin-O / Fast Green staining of vehicle-treated and ALW-II-41-27-treated mice knees with magnification of the patellofemoral region. Black square indicates the region of magnification for the image below (B) showing the central part of the patellofemoral articular cartilage. (C) Hematoxylin and Eosin stain of vehicle-treated and ALW-II-41-27-treated mice knees with magnification of the patellofemoral region. Osteophyte's diameter is indicated with a black line in the lateral side of the patella. (D) Osteophyte area adjacent to the lateral side of the patella is represented by the mean \pm SD. Each dot represents data of an individual mouse (n=8). For statistical analysis, the linear mixed model with Bonferroni's multiple comparisons test was performed (E) Immunofluorescence of type X collagen (red) and DAPI (blue) in the lateral side of the patellofemoral region. Arrow indicates an osteophyte in the lateral side of the patella.

Discussion

There is an urgent unmet need for effective therapies for OA patients. Here, we show that EPHA2 is a promising drug target for OA and we report the small molecule ALW-II-41-27 as a disease-modifying OA drug (DMOAD), specifically targeting inflammation and pathological endochondral ossification (Fig. 7A). To find targets associated with inflammation and chondrocyte hypertrophy we have used a particular sequence of studies that involved *in silico*, *in vitro* and *in vivo* analyses (Fig. 7B). For the *in silico* analyses we leveraged previously published large gene expression dataset depositories and narrowed them down to one target of interest. The role of the identified target on inflammation and chondrocyte hypertrophy was further investigated through *in silico* experiments using a computational model of cellular signaling networks controlling chondrocyte phenotypes. These *in silico* studies served as the starting point for a series of *in vitro* experiments using different cell models, which were followed by an *in vivo* study. We demonstrate the effectiveness of this experimental approach to identify a new target for specific biological processes in osteoarthritis.

Whereas others have found EPHA2 as a main regulator in diseases such as cancer [49-52] and irritable bowel disease [53], this is the first study, to our knowledge, that highlights the influence of EPHA2 in OA. Other tyrosine kinases, such as fibroblast growth factor receptor (FGFR) 1, Fyn and vascular endothelial growth factor receptor (VEGFR), have been indicated to promote chondrocyte hypertrophy [54-57]. Here we show that the tyrosine kinase EPHA2 is not only involved in hypertrophy but also in inflammation, making it an attractive target to attenuate pathological drivers in OA.

The mechanism by which EPHA2 modulates chondrocyte hypertrophy and inflammation is not completely decrypted in our study. However, an insight of the signaling pathways is appreciated in the computational chondrocyte model. EPHA2 controls signaling pathways that are key regulators of chondrocyte hypertrophy and inflammation, namely WNT [58], RAS [59], and the PI3K-AKT axis [60]. The regulatory interactions, based on studies performed in other cell types [26-33], were input in the model and this led to the predictions suggesting the pro-hypertrophic and inflammatory role of EPHA2 in chondrocytes. Given that those predictions were further confirmed *in vitro* and *in vivo*, it supports the possible role of the aforementioned mechanistic interactions. Nevertheless, EPHA2 being still largely understudied in cartilage, it is likely that regulatory interactions with other entities of the chondrocyte regulatory network have been overlooked and should be investigated.

In this pre-clinical study, we identified a promising compound, ALW-II-41-27, which showed potential as a DMOAD since it attenuated inflammation and pathological endochondral ossification *in vitro* and *in vivo*. To date, a wide variety of DMOADs targeting chondrocyte hypertrophy have been tested in experimental studies *in vitro* and *in vivo* [61]. Pterostin B, an inhibitor of salt-inducible kinase (Sik) 3, modified OA by preventing chondrocyte hypertrophy [62]. In a similar manner, Paroxetine, a G protein-coupled receptor kinase

(GRK) 2 inhibitor, prevented cartilage degeneration targeting hypertrophy [63]. It is unclear, however, whether those agents have been subjected to further research. Regulatory agencies, such as the Food and Drug Administration (FDA) or the European Medicines Agency (EMA), have not yet approved any existing disease-modifying pharmacological intervention for OA [64]. Considering the pre-clinical data of ALW-II-41-27 to modulate OA pathogenesis and its extensive pharmacological analysis in other diseases [49-53], it is expected that clinical trials with this drug have a lower-risk with higher chance of success.

Next to cartilage hypertrophy, inflammation of the synovium is an important component of OA pathology [65]. Our data show that ALW-II-41-27 also exerts anti-inflammatory effects, which is in agreement with the previously reported anti-inflammatory effects of this molecule in colonic cells *in vitro* and in a model of irritable bowel syndrome *in vivo* [53]. EPHA2 is not only expressed in chondrocytes but also in other cells present in the synovium, such as fibroblasts [66], monocytes [67] and macrophages [68]. Therefore, the underlying anti-

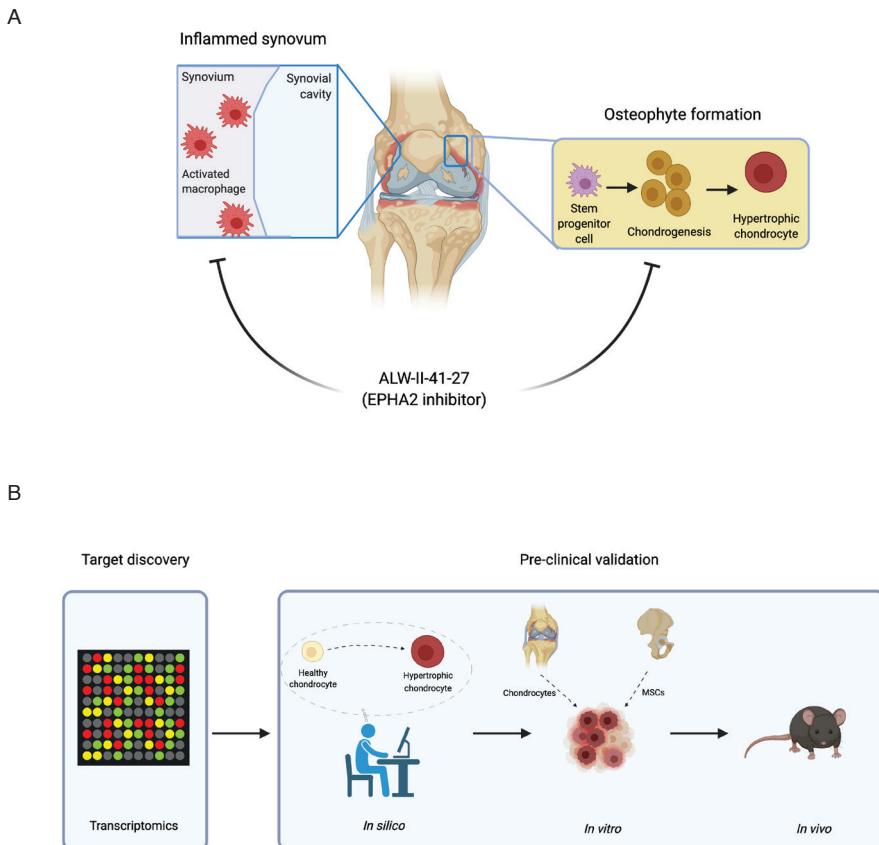


Figure 7 | Graphical representation of main findings and experimental approach. (A) ALW-II-41-27 attenuates synovitis and osteophyte formation. (B) Drug discovery pipeline combining transcriptomic datasets, *in silico*, *in vitro* and *in vivo* models

inflammatory mechanism observed in mice might also be associated with the action of ALW-II-41-27 on these cells.

Our study has some limitations. In this study we initiated treatment at the same time we induced OA, due to the progressive nature of the disease and the subsequent challenge faced by a DMOAD where extensive structural changes in the joint in end-stage OA might be impossible to reverse. Therefore, the pharmacological benefits of ALW-II-41-27 to attenuate inflammation and osteophytosis may be best achieved if applied in earlier stages of the disease. Our study failed to show that ALW-II-41-27 administration can prevent either the cartilage loss or pain produced in the MIA mouse model. Additional investigation in other experimental animal models may reveal whether ALW-II-41-27 specifically targets hypertrophy and inflammation, or whether its effect extend to preventing cartilage degeneration and alleviate pain. Moreover, investigation of the possible effect of ALW-II-41-27 on post-traumatic OA or other non-chemically induced forms of OA is needed.

In this study we have applied systemic delivery of the drug *in vivo*. This would be suitable to treat or prevent osteoarthritis development in multiple joints, so called polyarticular OA [69, 70]. Aiming for the clinical translation of the treatment, future studies should evaluate the efficacy of oral administration of ALW-II-41-27 to treat polyarticular OA. Toxicological assessment in mice have been reported for this small molecule, showing no significant histopathologic effects in the heart, liver, or kidney [50]. Therefore, ALW-II-41-27 possess promising characteristics to be translated to OA clinical trials. Of note, common adverse effects of clinically used tyrosine kinase inhibitors are diarrhea and anemia [71, 72], that might be attenuated by dose-escalation. For patients with OA in a single joint, local delivery of ALW-II-41-27 might offer advantages in maximizing the dose to the affected tissues while minimizing systemic side effects, as reported for the CDC-like kinase 2 (CLK2) and dual-specificity tyrosine phosphorylation-regulated kinase 1A (DYRK1A) inhibitor Lorecivivint, currently in clinical trials for OA [73].

In conclusion, we provide evidence that EPHA2 plays a pathogenic role in OA. Inhibition of EPHA2 with ALW-II-41-27 was effective in halting inflammation and pathological endochondral ossification in *in silico* models, *in vitro* models with human cells and a mouse model, which warrants further research on this candidate disease-modifying OA drug.

Supplementary Materials

Supplementary table 1 | List of regulatory interactions between EPHA2 and other components of the network. Each regulatory link is directed from the Source to the Target entity and the Sign indicates the type of influence (1 stands for activation). Literature references are provided to support the assumptions.

Protein signaling			
Source	Target	Sign	Reference
EPHA2	Dsh	1	2
EPHA2	ERK1/2	1	5
EPHA2	PI3K	1	6 and 7
AKT	EPHA2	1	4
WNT	EPHA2	1	1

Genetic regulation			
Source	Target	Sign	Reference
NFKB	EPHA2	1	3
RAS	EPHA2	1	8

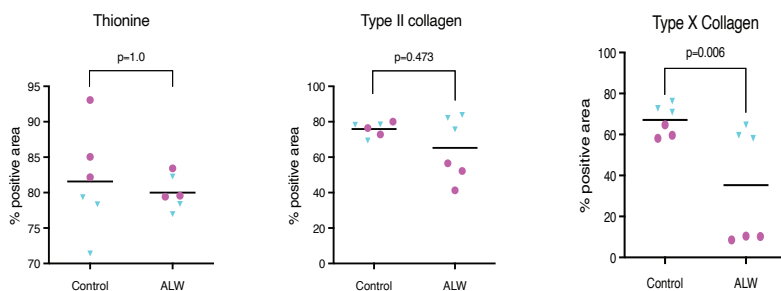
- 1 Peng Q, Chen L, Wu W, Wang J, Zheng X, Chen Z, et al. EPH receptor A2 governs a feedback loop that activates Wnt/beta-catenin signaling in gastric cancer. *Cell Death Dis.* 2018 Nov 19; 9(12):1146.
- 2 Li JY, Xiao T, Yi HM, Yi H, Feng J, Zhu JF, et al. S897 phosphorylation of EphA2 is indispensable for EphA2-dependent nasopharyngeal carcinoma cell invasion, metastasis and stem properties. *Cancer Lett.* 2019 Mar 1; 444:162-174.
- 3 Irie N, Takada Y, Watanabe Y, Matsuzaki Y, Naruse C, Asano M, et al. Bidirectional signaling through ephrinA2-EphA2 enhances osteoclastogenesis and suppresses osteoblastogenesis. *J Biol Chem.* 2009 May 22; 284(21):14637-14644.
- 4 Miao H, Li DQ, Mukherjee A, Guo H, Petty A, Cutter J, et al. EphA2 mediates ligand-dependent inhibition and ligand-independent promotion of cell migration and invasion via a reciprocal regulatory loop with Akt. *Cancer Cell.* 2009 Jul 7; 16(1):9-20.
- 5 Pratt RL, Kinch MS. Activation of the EphA2 tyrosine kinase stimulates the MAP/ERK kinase signaling cascade. *Oncogene.* 2002 Oct 31; 21(50):7690-7699.
- 6 Pandey A, Lazar DF, Saltiel AR, Dixit VM. Activation of the Eck receptor protein tyrosine kinase stimulates phosphatidylinositol 3-kinase activity. *J Biol Chem.* 1994 Dec 2; 269(48):30154-30157.
- 7 Kim HS, Won YJ, Shim JH, Kim HJ, Kim BS, Hong HN. Role of EphA2-PI3K signaling in vasculogenic mimicry induced by cancer-associated fibroblasts in gastric cancer cells. *Oncol Lett.* 2019 Sep; 18(3):3031-3038.
- 8 Macrae M, Neve RM, Rodriguez-Viciana P, Haqq C, Yeh J, Chen C, et al. A conditional feedback loop regulates Ras activity through EphA2. *Cancer Cell.* 2005 Aug; 8(2):111-118.

Supplementary table 2 | Flow cytometry antibodies used for markers of interest

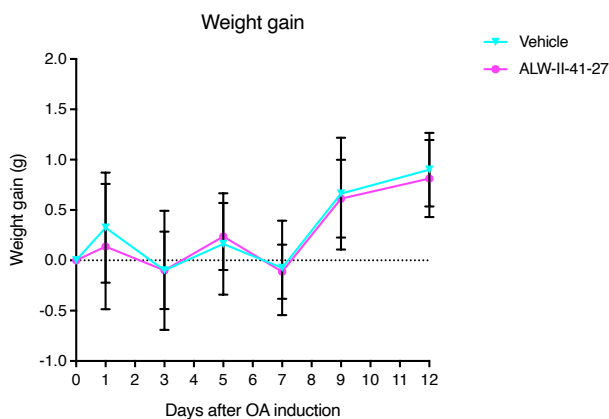
Antibody	Clone	Fluorophore
Anti-mouse/human CD11b	M1/70	PerCp-Cy5.5
Anti-mouse CD115	AFS98	PE
Anti-mouse Ly6C	HK1.4	FITC
Anti-mouse CD62L	MEL-14	APC
Anti-mouse Ly6G	1A8	PE-Cy7
Anti-mouse CD3	17A2	PE-Cy7
Anti-mouse NK1.1	PK136	PE-Cy7
Anti-mouse CD19	6D5	PE-Cy7
Anti-mouse F4/80	BM8	FITC
Anti-mouse CD86	GL-1	PE-Cy7
Anti-mouse CD206	C068C2	APC
Anti-mouse CD163	TNKUPJ	PE
Anti-mouse CD31	390	APC

	HP	No HP
WNT	1.00	0.00
BMP	0.92	0.00
WNT antagonist	0.00	0.92
BMP antagonist	0.00	1.00
FGF	1.00	0.00
IHH	1.00	0.59
PTHRP	0.00	0.96
IGF	0.00	0.72
TFGB	0.00	0.89
MAPK/ERK	0.88	0.11
RUNX2	1.00	0.00
MMP13	1.00	0.00
COL-X	1.00	0.00
COL-II	0.00	1.00
Proteoglycans	0.00	0.69
SOX9	0.00	1.00
NKX3.2	0.00	1.00
Inflammation	1.00	0.00
Infl. Inhibitors	0.00	0.29
EPHA2	1.00	0.00
CANALISATION	6%	94%

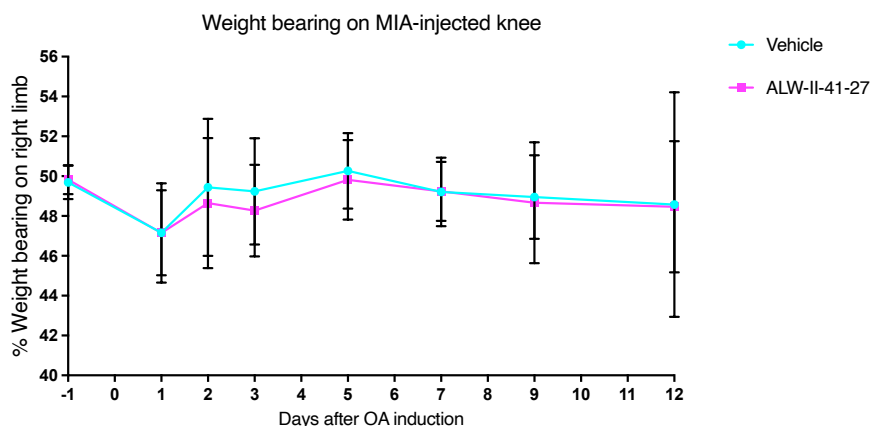
Supplementary figure 1 | Summary of global predicted activity profiles for the two stable states emerging from the random initialization (Monte Carlo). The canalization indicates the chance of occurrence in the unconstrained system (i.e. the percentage of initial states, among 10.000, reaching the final state). Bold labels are used when the average activity of the pathway is displayed while regular labels are used for specific single entities (i.e. variables). Values and colors reflect the global activity level, i.e. the product of the predicted gene expression and of the protein activation or repression level. HP= hypertrophic chondrocyte.



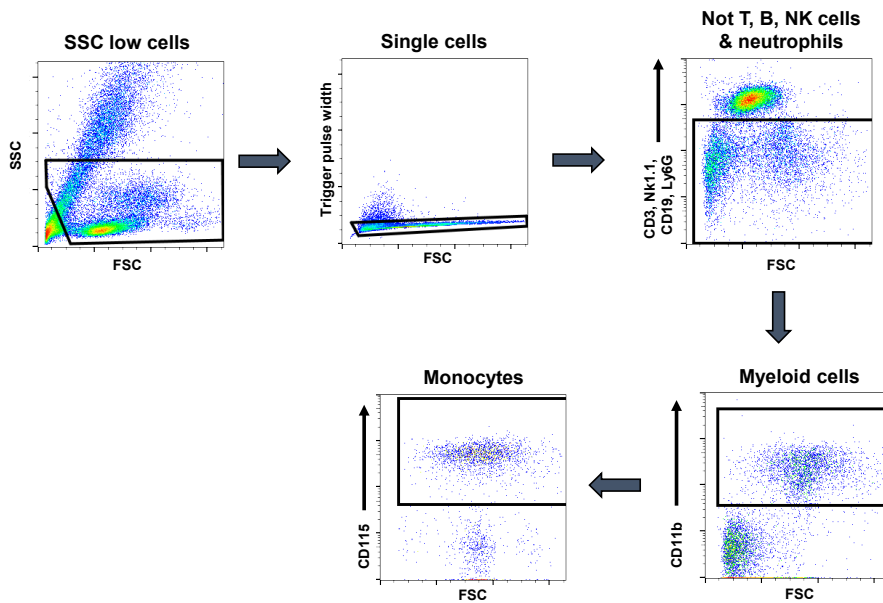
Supplementary figure 2 | ALW-II-41-27 decreases type X collagen deposition but did not affected type II collagen and glycosaminoglycans. Percentage of positive area of thionine, type II collagen and type X collagen of tissue engineered cartilage derived from MSCs. Donors are represented with different colors and symbols: violet circles (donor 1) and blue triangles (donor 2). The horizontal line in the graphs represents the mean. For statistical analysis, the linear mixed model with Bonferroni's multiple comparisons test was performed.



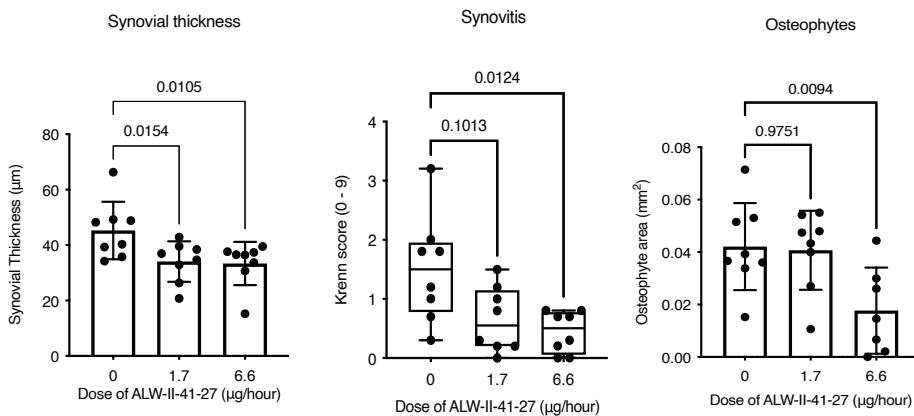
Supplementary figure 3 | Weight gain of mice. Total body weight of each mice was determined on day 0, 1, 3, 5, 7, 9 and 12 using a scale. The average weight of the experimental group, vehicle- or ALW-II-41-27-treated mice (n=8) is shown.



Supplementary figure 4 | Pain measurements with incapitance tester. Weight bearing between limbs along the study showed no differences between treated and vehicle group



Supplementary figure 5 | Gating strategy applied for blood monocytes analysis



Supplementary figure 6 | ALW-II-41-27 treatment attenuates synovitis and osteophytosis. Analysis of synovial thickness, Krenn score and osteophyte area adjacent to the lateral side of the patella in mice containing an osmotic pump with vehicle (dose 0 µg/ hour) or ALW-II-41-27 (dose 1.7 and 6.6 µg/ hour). The data for the vehicle and the dose 6.6 µg/ hour is already shown in figure 5 and 6. Each dot represents data of an individual mouse (n=8). For statistical analysis, the linear mixed model with Bonferroni's multiple comparisons test was performed

References

1. Cross, M., et al., The global burden of hip and knee osteoarthritis: estimates from the global burden of disease 2010 study. *Ann Rheum Dis*, 2014. 73(7): p. 1323-30.
2. Bacon, K., et al., Does cartilage loss cause pain in osteoarthritis and if so, how much? *Ann Rheum Dis*, 2020. 79(8): p. 1105-1110.
3. Loeser, R.F., et al., Osteoarthritis: a disease of the joint as an organ. *Arthritis Rheum*, 2012. 64(6): p. 1697-707.
4. van der Kraan, P.M. and W.B. van den Berg, Chondrocyte hypertrophy and osteoarthritis: role in initiation and progression of cartilage degeneration? *Osteoarthritis Cartilage*, 2012. 20(3): p. 223-32.
5. Roelofs, A.J., et al., Identification of the skeletal progenitor cells forming osteophytes in osteoarthritis. *Ann Rheum Dis*, 2020. 79(12): p. 1625-1634.
6. Smith, M.D., et al., Synovial membrane inflammation and cytokine production in patients with early osteoarthritis. *J Rheumatol*, 1997. 24(2): p. 365-71.
7. Benito, M.J., et al., Synovial tissue inflammation in early and late osteoarthritis. *Ann Rheum Dis*, 2005. 64(9): p. 1263-7.
8. Saito, T., et al., Transcriptional regulation of endochondral ossification by HIF-2alpha during skeletal growth and osteoarthritis development. *Nat Med*, 2010. 16(6): p. 678-86.
9. Ferrao Blanco, M.N., et al., Effect of Inflammatory Signaling on Human Articular Chondrocyte Hypertrophy: Potential Involvement of Tissue Repair Macrophages. *Cartilage*, 2021. 13(2_suppl): p. 168S-174S.
10. Belluoccio, D., et al., Sorting of growth plate chondrocytes allows the isolation and characterization of cells of a defined differentiation status. *J Bone Miner Res*, 2010. 25(6): p. 1267-81.
11. Bateman, J.F., et al., Transcriptomics of wild-type mice and mice lacking ADAMTS-5 activity identifies genes involved in osteoarthritis initiation and cartilage destruction. *Arthritis Rheum*, 2013. 65(6): p. 1547-60.
12. Karlsson, C., et al., Genome-wide expression profiling reveals new candidate genes associated with osteoarthritis. *Osteoarthritis Cartilage*, 2010. 18(4): p. 581-92.
13. Ashburner, M., et al., Gene ontology: tool for the unification of biology. The Gene Ontology Consortium. *Nat Genet*, 2000. 25(1): p. 25-9.
14. Gene Ontology, C., The Gene Ontology resource: enriching a Gold mine. *Nucleic Acids Res*, 2021. 49(D1): p. D325-D334.
15. Pathan, M., et al., FunRich: An open access standalone functional enrichment and interaction network analysis tool. *Proteomics*, 2015. 15(15): p. 2597-601.
16. Lesage, R., et al., An integrated in silico-in vitro approach for identification of therapeutic drug targets for osteoarthritis. *bioRxiv*, 2021: p. 2021.09.27.461207.
17. Kerkhofs, J., et al., A Qualitative Model of the Differentiation Network in Chondrocyte Maturation: A Holistic View of Chondrocyte Hypertrophy. *PLoS One*, 2016. 11(8): p. e0162052.
18. Kerkhofs, J. and L. Geris, A Semiquantitative Framework for Gene Regulatory Networks: Increasing the Time and Quantitative Resolution of Boolean Networks. *PLoS One*, 2015. 10(6): p.

eo130033.

19. Yaeger, P.C., et al., Synergistic action of transforming growth factor-beta and insulin-like growth factor-I induces expression of type II collagen and aggrecan genes in adult human articular chondrocytes. *Exp Cell Res*, 1997. 237(2): p. 318-25.
20. Mandl, E.W., et al., Multiplication of human chondrocytes with low seeding densities accelerates cell yield without losing redifferentiation capacity. *Tissue Eng*, 2004. 10(1-2): p. 109-18.
21. Ferrao Blanco, M.N., et al., Intra-articular injection of triamcinolone acetonide sustains macrophage levels and aggravates osteophytosis during degenerative joint disease in mice. *Br J Pharmacol*, 2021.
22. Glasson, S.S., et al., The OARSI histopathology initiative - recommendations for histological assessments of osteoarthritis in the mouse. *Osteoarthritis Cartilage*, 2010. 18 Suppl 3: p. S17-23.
23. Krenn, V., et al., Synovitis score: discrimination between chronic low-grade and high-grade synovitis. *Histopathology*, 2006. 49(4): p. 358-64.
24. Yuan, X.C., et al., Electroacupuncture potentiates peripheral CB2 receptor-inhibited chronic pain in a mouse model of knee osteoarthritis. *J Pain Res*, 2018. 11: p. 2797-2808.
25. Varela-Eirin, M., et al., Targeting of chondrocyte plasticity via connexin43 modulation attenuates cellular senescence and fosters a pro-regenerative environment in osteoarthritis. *Cell Death Dis*, 2018. 9(12): p. 1166.
26. Peng, Q., et al., EPH receptor A2 governs a feedback loop that activates Wnt/beta-catenin signaling in gastric cancer. *Cell Death Dis*, 2018. 9(12): p. 1146.
27. Li, J.Y., et al., S897 phosphorylation of EphA2 is indispensable for EphA2-dependent nasopharyngeal carcinoma cell invasion, metastasis and stem properties. *Cancer Lett*, 2019. 444: p. 162-174.
28. Irie, N., et al., Bidirectional signaling through ephrinA2-EphA2 enhances osteoclastogenesis and suppresses osteoblastogenesis. *J Biol Chem*, 2009. 284(21): p. 14637-44.
29. Miao, H., et al., EphA2 mediates ligand-dependent inhibition and ligand-independent promotion of cell migration and invasion via a reciprocal regulatory loop with Akt. *Cancer Cell*, 2009. 16(1): p. 9-20.
30. Pratt, R.L. and M.S. Kinch, Activation of the EphA2 tyrosine kinase stimulates the MAP/ERK kinase signaling cascade. *Oncogene*, 2002. 21(50): p. 7690-9.
31. Pandey, A., et al., Activation of the Eck receptor protein tyrosine kinase stimulates phosphatidylinositol 3-kinase activity. *J Biol Chem*, 1994. 269(48): p. 30154-7.
32. Kim, H.S., et al., Role of EphA2-PI3K signaling in vasculogenic mimicry induced by cancer-associated fibroblasts in gastric cancer cells. *Oncol Lett*, 2019. 18(3): p. 3031-3038.
33. Macrae, M., et al., A conditional feedback loop regulates Ras activity through EphA2. *Cancer Cell*, 2005. 8(2): p. 111-8.
34. Dreier, R., Hypertrophic differentiation of chondrocytes in osteoarthritis: the developmental aspect of degenerative joint disorders. *Arthritis Res Ther*, 2010. 12(5): p. 216.
35. Choi, Y., et al., Discovery and structural analysis of Eph receptor tyrosine kinase inhibitors. *Bioorg Med Chem Lett*, 2009. 19(15): p. 4467-70.

-
36. Moccia, M., et al., Identification of Novel Small Molecule Inhibitors of Oncogenic RET Kinase. *PLoS One*, 2015. 10(6): p. e0128364.
 37. Libermann, T.A. and D. Baltimore, Activation of interleukin-6 gene expression through the NF-kappa B transcription factor. *Mol Cell Biol*, 1990. 10(5): p. 2327-34.
 38. Mueller, M.B. and R.S. Tuan, Functional characterization of hypertrophy in chondrogenesis of human mesenchymal stem cells. *Arthritis Rheum*, 2008. 58(5): p. 1377-88.
 39. Farrell, E., et al., Chondrogenic priming of human bone marrow stromal cells: a better route to bone repair? *Tissue Eng Part C Methods*, 2009. 15(2): p. 285-95.
 40. Scotti, C., et al., Recapitulation of endochondral bone formation using human adult mesenchymal stem cells as a paradigm for developmental engineering. *Proc Natl Acad Sci U S A*, 2010. 107(16): p. 7251-6.
 41. Hellingman, C.A., et al., Fibroblast growth factor receptors in in vitro and in vivo chondrogenesis: relating tissue engineering using adult mesenchymal stem cells to embryonic development. *Tissue Eng Part A*, 2010. 16(2): p. 545-56.
 42. Narcisi, R., et al., Long-term expansion, enhanced chondrogenic potential, and suppression of endochondral ossification of adult human MSCs via WNT signaling modulation. *Stem Cell Reports*, 2015. 4(3): p. 459-72.
 43. van der Kraan, P.M., et al., Development of osteoarthritic lesions in mice by "metabolic" and "mechanical" alterations in the knee joints. *Am J Pathol*, 1989. 135(6): p. 1001-14.
 44. Zhang, H., D. Cai, and X. Bai, Macrophages regulate the progression of osteoarthritis. *Osteoarthritis Cartilage*, 2020. 28(5): p. 555-561.
 45. Sunderkotter, C., et al., Subpopulations of mouse blood monocytes differ in maturation stage and inflammatory response. *J Immunol*, 2004. 172(7): p. 4410-7.
 46. Geissmann, F., S. Jung, and D.R. Littman, Blood monocytes consist of two principal subsets with distinct migratory properties. *Immunity*, 2003. 19(1): p. 71-82.
 47. Scanzello, C.R. and S.R. Goldring, The role of synovitis in osteoarthritis pathogenesis. *Bone*, 2012. 51(2): p. 249-57.
 48. Miller, R.E., R.J. Miller, and A.M. Malfait, Osteoarthritis joint pain: the cytokine connection. *Cytokine*, 2014. 70(2): p. 185-93.
 49. Amato, K.R., et al., EPHA2 Blockade Overcomes Acquired Resistance to EGFR Kinase Inhibitors in Lung Cancer. *Cancer Res*, 2016. 76(2): p. 305-18.
 50. Amato, K.R., et al., Genetic and pharmacologic inhibition of EPHA2 promotes apoptosis in NSCLC. *J Clin Invest*, 2014. 124(5): p. 2037-49.
 51. Martini, G., et al., EPHA2 Is a Predictive Biomarker of Resistance and a Potential Therapeutic Target for Improving Antiepidermal Growth Factor Receptor Therapy in Colorectal Cancer. *Mol Cancer Ther*, 2019. 18(4): p. 845-855.
 52. Xiang, Y.P., et al., Y772 phosphorylation of EphA2 is responsible for EphA2-dependent NPC nasopharyngeal carcinoma growth by Shp2/Erk-1/2 signaling pathway. *Cell Death Dis*, 2020. 11(8): p. 709.
 53. Zeng, L., et al., A Novel EphA2 Inhibitor Exerts Beneficial Effects in PI-IBS in Vivo and in Vitro

Models via Nrf2 and NF-kappaB Signaling Pathways. *Front Pharmacol*, 2018. 9: p. 272.

54. Yan, D., et al., Fibroblast growth factor receptor 1 is principally responsible for fibroblast growth factor 2-induced catabolic activities in human articular chondrocytes. *Arthritis Res Ther*, 2011. 13(4): p. R130.
55. Li, K., et al., Tyrosine kinase Fyn promotes osteoarthritis by activating the beta-catenin pathway. *Ann Rheum Dis*, 2018. 77(6): p. 935-943.
56. Zhang, X., R. Crawford, and Y. Xiao, Inhibition of vascular endothelial growth factor with shRNA in chondrocytes ameliorates osteoarthritis. *J Mol Med (Berl)*, 2016. 94(7): p. 787-98.
57. Ferrao Blanco, M.N., et al., Tyrosine kinases regulate chondrocyte hypertrophy: promising drug targets for Osteoarthritis. *Osteoarthritis Cartilage*, 2021. 29(10): p. 1389-1398.
58. Guo, X., et al., The Wnt/beta-catenin pathway interacts differentially with PTHrP signaling to control chondrocyte hypertrophy and final maturation. *PLoS One*, 2009. 4(6): p. e6067.
59. Prasad, I., et al., ERK-1/2 and p38 in the regulation of hypertrophic changes of normal articular cartilage chondrocytes induced by osteoarthritic subchondral osteoblasts. *Arthritis Rheum*, 2010. 62(5): p. 1349-60.
60. Tang, Q., et al., Wogonoside inhibits IL-1beta induced catabolism and hypertrophy in mouse chondrocyte and ameliorates murine osteoarthritis. *Oncotarget*, 2017. 8(37): p. 61440-61456.
61. Hunter, D.J., Pharmacologic therapy for osteoarthritis--the era of disease modification. *Nat Rev Rheumatol*, 2011. 7(1): p. 13-22.
62. Yahara, Y., et al., Pterostilbene prevents chondrocyte hypertrophy and osteoarthritis in mice by inhibiting SIK3. *Nat Commun*, 2016. 7: p. 10959.
63. Carlson, E.L., et al., Paroxetine-mediated GRK2 inhibition is a disease-modifying treatment for osteoarthritis. *Sci Transl Med*, 2021. 13(580).
64. Roemer, F.W., et al., The role of radiography and MRI for eligibility assessment in DMOAD trials of knee OA. *Nat Rev Rheumatol*, 2018. 14(6): p. 372-380.
65. Sellam, J. and F. Berenbaum, The role of synovitis in pathophysiology and clinical symptoms of osteoarthritis. *Nat Rev Rheumatol*, 2010. 6(11): p. 625-35.
66. Hong, H.N., et al., Cancer-associated fibroblasts promote gastric tumorigenesis through EphA2 activation in a ligand-independent manner. *J Cancer Res Clin Oncol*, 2018. 144(9): p. 1649-1663.
67. Mukai, M., et al., EphA receptors and ephrin-A ligands are upregulated by monocytic differentiation/maturation and promote cell adhesion and protrusion formation in HL60 monocytes. *BMC Cell Biol*, 2017. 18(1): p. 28.
68. Finney, A.C., et al., EphA2 Expression Regulates Inflammation and Fibroproliferative Remodeling in Atherosclerosis. *Circulation*, 2017. 136(6): p. 566-582.
69. Huskisson, E.C., et al., Another look at osteoarthritis. *Ann Rheum Dis*, 1979. 38(5): p. 423-8.
70. Kellgren, J.H. and R. Moore, Generalized osteoarthritis and Heberden's nodes. *Br Med J*, 1952. 1(4751): p. 181-7.
71. Jackson, T.L., et al., Oral Tyrosine Kinase Inhibitor for Neovascular Age-Related Macular Degeneration: A Phase 1 Dose-Escalation Study. *JAMA Ophthalmol*, 2017. 135(7): p. 761-767.
72. Richeldi, L., et al., Efficacy and safety of nintedanib in idiopathic pulmonary fibrosis. *N Engl J*

Med, 2014. 370(22): p. 2071-82.

73. Yazici, Y., et al., A Phase 2b randomized trial of lorecivivint, a novel intra-articular CLK2/DYRK1A inhibitor and Wnt pathway modulator for knee osteoarthritis. *Osteoarthritis Cartilage*, 2021. 29(5): p. 654-666.

Chapter 6

Tyrosine kinases regulate chondrocyte hypertrophy: promising drug targets for osteoarthritis

Mauricio N. Ferrao Blanco ¹, Heura Domenech Garcia ¹, Laurence Legeai-Mallet ⁴, Gerjo J.V.M. van Osch ^{1,2,3}.

¹ Department of Orthopedics and Sports Medicine, Erasmus MC, University Medical Center Rotterdam, Rotterdam, The Netherlands

² Department of Otorhinolaryngology, Erasmus MC, University Medical Center Rotterdam, Rotterdam, The Netherlands

³ Department of Biomechanical Engineering, TU Delft, Delft, The Netherlands

⁴ Université de Paris, INSERM U1163, Institut Imagine, Paris, France

Osteoarthritis and Cartilage. 2021

DOI 10.1016/j.joca.2021.07.003

Summary

Osteoarthritis (OA) is a major health problem worldwide that affects the joints and causes severe disability. It is characterized by pain and low-grade inflammation. However, the exact pathogenesis remains unknown and the therapeutic options are limited. In OA articular chondrocytes undergo a phenotypic transition becoming hypertrophic, which leads to cartilage damage, aggravating the disease. Therefore, a therapeutic agent inhibiting hypertrophy would be a promising disease-modifying drug. The therapeutic use of tyrosine kinase inhibitors has been mainly focused on oncology, but the FDA approval of the Janus kinase inhibitor Tofacitinib in Rheumatoid Arthritis has broadened the applicability of these compounds to other diseases. Interestingly, tyrosine kinases have been associated with chondrocyte hypertrophy. In this review, we discuss the experimental evidence that implicates specific tyrosine kinases in signaling pathways promoting chondrocyte hypertrophy, highlighting their potential as therapeutic targets for OA.

Introduction

OA is a highly prevalent degenerative joint disorder worldwide [1]. OA is characterized by a slow-progressive degeneration of the articular cartilage, dysregulation of subchondral bone remodeling and synovial inflammation which ultimately lead to loss of joint function and chronic pain [2]. Despite the main risk factors for OA have been identified [3], there is still no effective disease-modifying treatment available.

Accumulating data suggest that articular chondrocytes undergo a phenotypic shift and become hypertrophic in OA [4]. This phenotypic change resembles the process of endochondral ossification, which naturally occurs in the growth plate for the elongation of long bones and lasts from early ante natal period until puberty. Within this process, the temporary cartilage found at the early embryonic stages of endochondral bones differentiates into hypertrophic cartilage and eventually enters apoptosis or differentiates to osteoblasts [5], leading to replacement by bone. However, this process should not occur in articular cartilage . Recent studies have confirmed by single cell RNA-seq that hypertrophic differentiation takes place in osteoarthritic articular cartilage [6, 7].

One of the main characteristics of hypertrophic chondrocytes is the upregulation of proteolytic enzymes, which drive the degradation of extracellular matrix (ECM) components such as type II Collagen and Aggrecan. These enzymes are mainly Matrix Metalloproteinase (MMP) 13 and ADAM Metalloproteinase with Thrombospondin Motif (ADAMTS) 4 and 5. In addition, hypertrophic chondrocytes produce Alkaline Phosphatase that enhances the calcification of the matrix and increase the expression of hypertrophic-related genes, such as type 10 Collagen (COL10A1) and Runt-related transcription factor 2 (RUNX2) [2]. Whereas, a healthy and proliferative chondrocyte is characterized by the expression of SRY-box transcription factor (SOX9) and type II collagen as well as Bagpipe homeobox homolog (BAPX1) (Figure1). Therefore, understanding the mechanisms that drive the terminal differentiation of hypertrophic chondrocyte and control the levels of ECM-degrading enzymes is important for developing effective therapies for OA.

Interestingly, recent insights into the field of OA pinpoint that tyrosine kinases may play an important role in regulating chondrocyte hypertrophy. These enzymes are highly involved in cellular differentiation and are the main regulators in several pathways [3]. However, there is no study that provides an overview of the tyrosine kinases associated with chondrocyte hypertrophy and the pathways that are involved in this phenotypic transition. To this end, this review aims to evaluate which tyrosine kinases have been related to chondrocyte hypertrophy during OA pathogenesis and provide a clear overview of the signaling pathways that they activate.

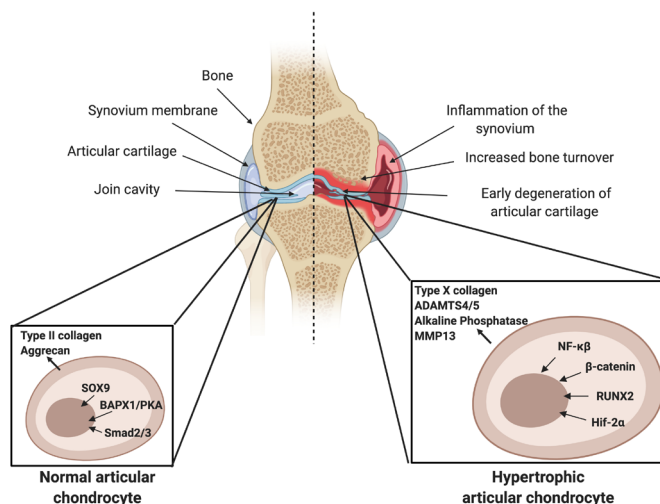


Figure 1 | Schematic representation of main characteristics of normal articular cartilage compared to an osteoarthritic cartilage. On the left, a normal articular chondrocyte is depicted together with the positive stimuli that induce chondrocyte homeostasis. Conversely, on the right a hypertrophic chondrocyte is shown, including the signaling and responses that occur during OA.

Main pathways driving chondrocyte phenotype

Various pathways have been associated with chondrocyte hypertrophy that takes place during bone development (Figure 2). Indian hedgehog (IHH) and parathyroid hormone-related protein (PTHrP) are known to generate a negative feedback loop, which allows to maintain chondrocyte homeostasis. Namely, IHH promotes hypertrophy while PTHrP blocks it [8]. Moreover, TGF- β has been shown to prevent hypertrophy via Smad2/3 signaling, through modulating the levels of main chondrocyte phenotype-determining transcriptional regulators such as SOX9 and RUNX2. Conversely, TGF- β might promote hypertrophy when it activates Smad1/5/9 phosphorylation [9]. Another pathway that contributes to chondrocyte hypertrophy is Wnt signaling. Wnt induces the stabilization of β -catenin in the cytoplasm, allowing its translocation to the nucleus and this eventually enables the transcription of RUNX2 [10]. Similarly, pro-inflammatory cytokines such as interleukin (IL)-1 β and tumor necrosis factor (TNF)- α , have also shown to upregulate the expression of hypertrophic markers and downregulate SOX9 by stabilizing nuclear factor kappa-light-chain-enhancer of activated B cells (NF- κ B) and hypoxia inducible factor 2 α (Hif-2 α) [3, 8]. Other pathways including MAP-kinases signaling, PI3K-AKT and JAK2-STAT, however, may lead to opposite responses depending on the ligand-receptor by which the transduction is initiated [2].

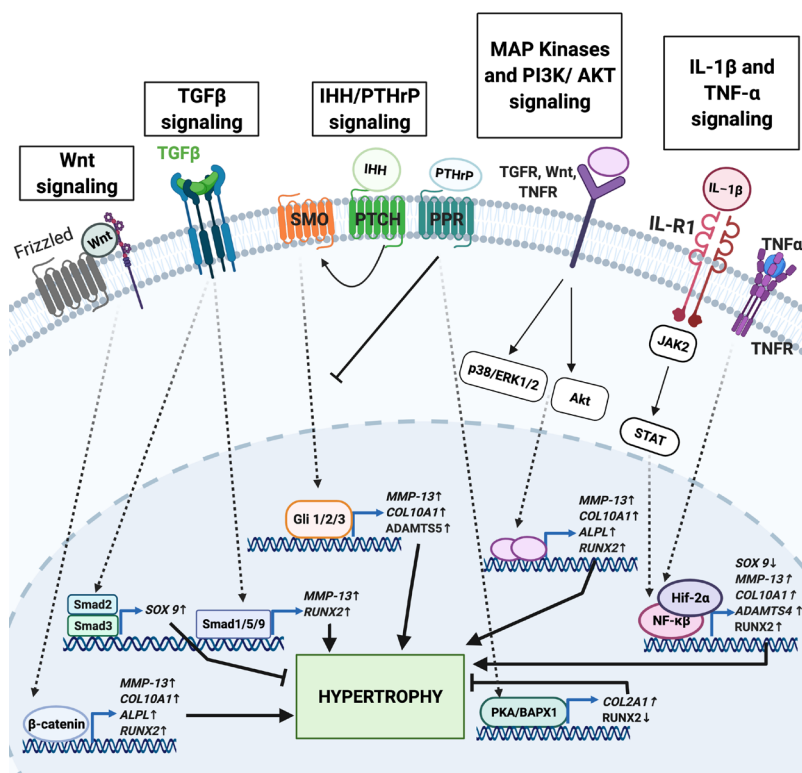


Figure 2 | Overview of the signaling pathways involved in the regulation of chondrocyte homeostasis and their relation to chondrocyte hypertrophy. The arrows and T-shaped lines signify positive and negative actions, respectively.

The involvement of tyrosine kinase members in driving chondrocyte hypertrophy

Tyrosine kinases (TKs) are a large subclass of protein kinases, which play a major role in cellular signaling. Through their ability to phosphorylate other proteins at their tyrosine residues, TKs are able to control most fundamental cellular processes such as cell proliferation and differentiation, cell metabolism as well as cellular survival [11]. Recent studies have entailed TKs as the most pursued targets in current pharmacological research [3, 12] and importantly, there are already several TK inhibitors that are FDA approved [13].

Current advances in the field of OA have suggested that both, receptor and non-receptor tyrosine kinases, are associated to articular chondrocyte catabolism (Table 1). Some TKs have been associated to the synthesis of inflammatory mediators, such as AXL and TYRO-3 [14], others have been shown to be increased in OA chondrocytes, such as ERBB4, IR, c-MET and VEGFR-3 [15-18], to inhibit catabolic factors such as EPHB4 [19], or to modulate cartilage degradation such as LYN, FRK, HCK and SYK [20, 21]. In spite of this information, the specific role of these TKs in the mechanisms underlying chondrocyte hypertrophy remains to be elucidated.

	Tyrosine Kinase	TK Family	Reference
Receptor	AXL	AXL	[14]
	TYRO-3		[14]
	DDR1	DDR	[22, 23]
	DDR2		[24-26]
	EGFR	EGFR	[27]
	ERBB4		[18]
	EPHB 4	EPH	[19]
	FGFR-1	FGFR	[1, 2, 14, 28]
	FGFR-3		[29-31]
	IGF1-R	INSR	[32, 33]
	IR		[34]
	c-MET	MET	[17]
	ROR2	ROR	[35]
	TRK-A	TRK	[8, 36, 37]
	VEGFR-1	VEGFR	[38, 39]
	VEGFR-2		[16, 36, 39]
VEGFR-3	[8, 16, 36, 37, 40]		
Non-receptor	FAK	FAK	[41, 42]
	JAK2	JAK	[43-45]
	FRK	FRK	[20]
	FYN	SRC	[3, 14]
	HCK		[20]
	LYN		[20]
SYK	SYK	[21]	

Table 1 | Overview of the receptor and non-receptor tyrosine kinases that have been associated to chondrocyte catabolism.

Receptor tyrosine kinases

Receptor tyrosine kinases (RTK) are the major subgroup of the tyrosine kinase family and are essential components of signal transduction pathways that participate in intercellular communication. Out of 58 types of RTKs that are found in the human genome [46], ten have been associated to chondrocyte hypertrophy and are described below.

Fibroblast growth factor receptor 1 and 3

Fibroblast growth factor receptors (FGFRs) are ubiquitous regulators of development involved in wound healing, angiogenesis and cartilage homeostasis [1, 47]. Mutations of FGFR genes are the basis of a broad range of skeletal developmental disorders such as craniosynostoses and chondrodysplasia [29]. FGFRs are activated through binding of fibroblast growth factors (FGFs) ligand and co receptor heparan sulfate to the extracellular domain of the receptor, which induces FGFR dimerization and transphosphorylation of tyrosine residues. Stimulation of the tyrosine kinase domain leads to activation of various downstream signaling proteins either from MAP kinases or PI3K/AKT pathway [47]. So far, four signaling members of FGFRs have been reported FGFR1, FGFR2, FGFR3 and FGFR4 [48]. FGFR-1 and FGFR-3 thoroughly

investigated in clinical trials as drug targets for various cancers and skeletal dysplasia [49, 50], have shown to be the most predominant receptors expressed in human cartilage [28]. Thus, they are suggested to play essential roles in cartilage upon interaction with the FGF-2 and FGF-18 ligands [1, 2, 51, 52]. It has been consistently shown that the ratio of FGFR-3 to FGFR-1 is significantly reduced in OA, and that this is mediated by the upregulation of FGF-2 [1, 2]. Hence, suggesting these FGFRs mediate opposing effects in human chondrocytes [28]. Suppression of FGFR-1 by G141, a non-ATP-competitive FGFR-1 inhibitor, impaired the expression of MMP13, ADAMTS5 and COL10A1 as well as reduced the loss of aggrecan in FGF-2 treated human chondrocytes. Additionally, G141 could delay the progression of cartilage degradation in a mouse model of OA [1]. Similarly, inhibition of components of the FGFR-1 signaling pathway, specifically FGFR-1 and ERK, abolished FGF-2 driven catabolic events in chondrocytes in vitro [2]. Similar effects were observed using Fgfr-1 conditional knock out mice [28]. Another morphogen that is overexpressed in OA-chondrocytes, FGF-23, can also activate FGFR-1. The addition of FGF-23 to healthy articular chondrocytes led to increased RUNX2 expression and downregulation of SOX9, which is indicative of a hypertrophic phenotype [51].

On the other hand, FGFR-3 is essential for cartilage protection and inhibition of hypertrophic phenotype. In fact, Fgfr-3 (-/-) mice develop spontaneous OA, evidenced by an accelerated degradation of cartilage in association with an upregulation of Mmp13 and Col10a1 [1, 52]. Further evidence demonstrated that Fgfr-3 levels were reduced in mtorc1 knockout mice that displayed cartilage degradation and chondrocyte hypertrophy [53]. Interestingly, exogenous stimulation of FGFR-3 by fibroblast growth factor 18 (FGF-18) was able to ameliorate OA [31]. Of note, in a randomized phase II clinical trial the intra-articular injection of FGF-18 increased cartilage thickness, and substantially reduced cartilage loss [54]. Taken together, recent advances have shown that FGFR-1 induces chondrocyte hypertrophy while FGFR-3 prevents it.

Discoidin domain receptor 1 and 2

The discoidin domain receptors (DDRs) family comprises two members, DDR1 and DDR2, and are the only type I transmembrane receptor TKs that specifically bind to and are activated by collagen [55]. DDRs mediate cell-collagen interactions under both, normal and pathological conditions. Of note, DDRs regulate cell proliferation, migration, adhesion and tumor metastasis [56]. DDRs can be activated by different types of collagen and each receptor has different affinities for each one. Namely, only DDR1 binds to collagen IV [55, 57], whereas DDR2 preferentially binds collagen II [58] and X [59]. Both DDRs activate signaling pathways including PI3K/AKT and RAS/ERK/p38 [60-64].

Provided the affinity of DDR2 for collagen type II and X, it was previously believed that this was the only DDR receptor involved in OA pathogenesis [65]. Several in vitro studies investigating the role of DDR2 in OA suggested that cumulative injuries in joint tissues lead to increased collagen II cleavage that results in DDR2 activation by tyrosine autophosphorylation [24-26].

DDR2 signaling induce overexpression of hypertrophic markers such as *Mmp13*, *Alpl* and *Col10a1* in vivo [66]. OA severity was attenuated in *Ddr2*-deficient mutant mice [67]. A recent publication has highlighted that inhibition of DDR1 in OA-mice models decreased expression of *Mmp13* and *Col10a1* [22]. In the light of these findings, it can be elucidated that both DDRs may be involved in promoting chondrocyte hypertrophy.

Insulin-like growth factor 1 receptor

Insulin-like growth factor receptor 1 (IGF1-R), along with insulin receptor (IR) and IGF2-R, is a member of the IGF signaling pathway that is essential for cell growth and tissue differentiation [68]. Interestingly, a number of clinical trials involving IGF1-R inhibition in breast cancer patients have been published [69-71]. This receptor mainly mediates the effect of insulin-like growth factor 1 (IGF1) and IGF2. Ligand-activated IGF1-R subsequently recruits and activates signaling intermediates, that include members of the insulin-receptor substrate (IRS) family and Shc. Activation of IRs induces activation of the PI3K/AKT pathway. Conversely, Shc leads to activation of the MAPK/ERK pathway [72]. Besides tumorigenesis, IGF1-R is thought to be involved in the regulation of articular cartilage metabolism via IGF-1 binding [33]. Namely, stimulation of IGF-1R by IGF-1 impaired interleukin (IL)-1 β induced NF- κ B activation in human chondrocytes. Consequently, hypertrophic differentiation was prevented [32]. Together these findings suggest a protective role of IGF1-R in OA progression.

Epidermal growth factor receptor

The epidermal growth factor receptor (EGFR, ErbB1) is a member of the ErbB family of receptors, which also includes ErbB2, ErbB3 and ErbB4. EGFR is crucial for the development of several organs during embryonic and postnatal stages [73]. Through its interaction with its growth factor ligands, transforming growth factor (TGF)- α and EGF, EGFR undergoes a transition from monomeric to an active homodimer. Subsequent dimerization leads to protein autophosphorylation and downstream activation of MAPK, AKT and JNK pathways. Importantly, EGFR has shown to promote inflammatory processes upon TGF- α binding [74]. Overexpression of EGFR has been so far related to cancer, fibrosis and inflammatory diseases . Current literature on the field of OA, suggests that TGF- α and EGFR are involved in the molecular events that influence joint cartilage degeneration, since overexpression of both proteins was observed in degenerating cartilage in experimental knee OA [74]. Moreover, levels of anabolic genes such as *Acan* and *Col2a1* were reduced, whereas *Mmp13* levels were increased in articular chondrocytes in response to TGF- α [74]. Particularly, EGFR signaling is thought to drive ECM degradation through the activation of MAPK pathways, which involves the phosphorylation of p38 and ERK kinases. This latter event is essential for the translocation of β -catenin into the nucleus and the expression of catabolic genes . Moreover, downregulation of EGFR prevents thrombin-induced *Mmp-13* expression in human chondrocytes via PI3K/AKT [27]. Clinical studies specifically targeting EGFR in OA have not hitherto been reported, albeit it could be of interest provided the participation of EGFR in the regulation of

hypertrophic markers.

Vascular endothelial growth factor receptor 1 and 2

Vascular endothelial growth factor receptors (VEGFRs) are responsible for binding with their ligands VEGFs to promote angiogenesis and vasculogenesis during development, wound healing and endochondral ossification. Pathophysiological effects of VEGF/VEGFR signaling have been described in diseases such as cancer and rheumatoid arthritis [75, 76]. In fact, VEGFR inhibitors have been used in clinical trials and were approved by FDA as drug targets for the treatment of cancer, pulmonary fibrosis and macular degeneration [77, 78]. There are three subtypes of VEGF receptors, including VEGFR-1, VEGFR-2 and VEGFR-3, which can be activated by diverse structurally related VEGFs. Binding of VEGF to its receptor leads to protein homo- or heterodimerization, consequently inducing auto-phosphorylation of the tyrosine residues of the receptor and phosphorylation of downstream signal mediators that mainly participate in MAPK or PI3K/AKT pathways [79]. Besides their involvement in cancer progression, all VEGFRs have also appeared to be highly expressed in OA chondrocytes [16, 38]. However, only the role of VEGF-A and its receptors VEGFR-1/-2 have been extensively studied in the pathophysiology of OA. Both receptor TKs are thought to drive vascular invasion of articular cartilage upon secretion of VEGF-A, a phenomena that is more pronounced in sever OA cartilage [39, 80]. Both, *in vitro* and *in vivo* studies, showed that shRNA -mediated knockdown of VEGF-A was able to ameliorate OA. Namely, VEGF-A inhibition protected cartilage from hypertrophy by decreasing *Mmp13*, *Runx2* and *Col10a1* [39]. Inhibition of VEGF-A in an OA animal model reduced articular cartilage degradation. In contrast to healthy chondrocytes, VEGF-A downregulation increased expression of *Acan* and *Col2a1* and reduced *Mmp-13* and *Adamts5* levels . Since VEGF-A can bind to both VEGFR-1 and -2, further studies investigating the specific roles of these receptors and their targeted inhibition in OA progression would be of interest.

Tropomyosin receptor kinase A

Tropomyosin receptor kinase A (TrkA), also recognized as high affinity nerve growth factor (NGF) receptor, is a member of the neurotrophic tyrosine kinase receptor (NTRK) family. Two other members constitute this family and are designated TrkB and TrkC. As a kinase, TrkA is responsible for functional NGF signal transduction to promote neuronal differentiation and proliferation, nociceptor response and avoidance of apoptosis. Precisely, the NGF-activated TrkA undergoes dimerization and autophosphorylation at multiple tyrosine residues, leading to the activation of diverse intracellular pathways such as PI3K/AKT and MAPK signaling. In many occasions, the NGF-TrkA complex is internalized via endocytosis and subsequently activates several signaling pathways, [81]. NGF-TrkA signaling play a role in the pathophysiology of cancer and OA. Indeed, NGF and TrkA were found to be expressed in human articular chondrocytes and they were upregulated in osteoarthritic chondrocytes in accordance with the degree of tissue injury [82]. Besides the involvement of NGF-TrkA

signaling in neuropathic pain in OA, this pathway was suggested to participate in chondrocyte homeostasis and hypertrophy [83]. Namely, it was found that the expression of an agonist of NGF and TrkA in human articular chondrocytes promoted chondrocyte hypertrophy. Conversely, inhibition of NGF receptor could also downregulate *SOX-9* and increase the expression of hypertrophy-related genes, including *ALPL* and *RUNX2*. The fact that both, over-activation and inactivation, of NGF-TrkA pathway give similar outcomes might be explained by the disruption of the feedback loop between IHH and PTHrP, two factors involved in regulating the homeostasis of articular chondrocytes [8]. Since 2015, a number of randomized clinical trials have been performed to evaluate the efficacy of TrkA inhibitors GZ389988, ASP7962 and ONO-4474 as treatment for OA knee pain and physical function. Whereas ASP7962 was unable to ameliorate pain and physical function, GZ389988 and ONO-4474 were able to safely reduce pain and gain physical function [36, 37, 40]. However, no structural changes were measured that could be associated with hypertrophy. Further research is required to decipher whether TrkA inhibition is a disease-modifying OA drug

Receptor tyrosine kinase-like orphan receptor 2

Receptor tyrosine kinase-like orphan receptor (ROR) family consists of two members, ROR1 and ROR2, which are essential for regulating skeletal and neuronal development, cell polarity and migration [84]. The RORs are single-pass transmembrane receptors, with the unique feature that their cysteine-like rich domain resembles that of the Frizzled receptors and thus, non-canonical WNT ligands can bind to the receptor. Interaction of a non- canonical WNT ligand (WNT5A) with ROR triggers the association of ROR with other WNT co-receptors and subsequent RTK activation occurs. The signal is then transduced to downstream pathways such as WNT, PI3K/AKT, MAPK/ERK and Rho/YAP, which leads to the expression of genes related with cell proliferation and survival [85]. Since RORs are involved in cell proliferation and they are rarely expressed in adult tissues, they have become an attractive target for cancer therapy [86, 87]. Nonetheless, a recent study showed that specifically ROR2 signaling was upregulated in OA cartilage and impaired chondrocyte differentiation via Rho/YAP pathway. ROR2 inhibition in primary human chondrocytes suppressed expression of *ADAMTS4/5* and increased *SOX9*. Furthermore, blocking ROR2 in a mouse OA model reduce pain and cartilage damage [35]. This study suggests that ROR2 is associated with WNT5A and hypertrophy and thus, ROR2 could also be a potential target for OA.

Cytoplasmic non-receptor tyrosine kinases

Non-receptor tyrosine kinases (NRTKs) are enzymes that are involved in the transduction of signals initiating from extracellular clues and which often interact with transmembrane receptors [88]. Three members (JAKs, FAK, Fyn) have been described to play a role in chondrocyte hypertrophy.

Janus kinase 2

Janus kinases (JAKs) family is constituted by four members, including JAK1, JAK2, JAK3 and Tyrosine kinase 2 (Tyk2), which are crucial components of various signal transduction pathways that control cellular survival and differentiation, among others. Janus kinases can be activated by either cytokines/interferons or growth factors. Upon the activation of JAKs by ligand-induced receptor oligomerization, these enzymes then phosphorylate the receptor that initiated the signal transduction and create docking sites for signaling molecules, especially members of the signal transducer and activator of transcription (STAT) family. Subsequently, the phosphorylated STATs form homo- or heterodimers that translocate into the nucleus to induce transcription of specific gene targets [89]. One of the members of the JAK family that is well-known to promote cell proliferation, JAK2, has recently been found to be activated in OA chondrocytes [90]. IL-1 β highly increases JAK2/STAT3 phosphorylation in rat chondrocytes *in vitro*. Namely, the inhibition of JAK2/STAT3 pathway by JAK2 inhibitors such as AG490, prevented *Mmp-13* overexpression and the degradation of type II collagen [45]. Conversely, other studies have found JAK2 to present a protective role in OA. In fact, JAK2/STAT3 inhibition by miR-375 resulted in upregulation of *Adamts5* and *Mmp13* and downregulation of *Col2a1* and *Acan* in mouse chondrocytes [44]. Moreover, JAK2/STAT1 signaling could lead to the inhibition of hypertrophy in rat chondrocytes via PTH/PTHrP receptor downregulation upon FGFR3 activation [43]. In summary, JAK2 has a pivotal role in chondrocyte hypertrophy.

Focal adhesion kinase

Focal adhesion kinase (FAK) is a non-receptor tyrosine kinase that belongs to the FAK family, which also includes proline-rich tyrosine kinase 2 (PYK2). FAK has been suggested to play an essential role in integrin-mediated signal transductions and is important for early stages of cell migration and angiogenesis [91]. Activation of FAK occurs by disruption of an auto-inhibitory molecular interaction between the amino terminal FERM domain and the central kinase domain. Upon activation, FAK associates with Src family kinases to initiate several signaling pathways including PI3K/AKT and MAPK. A number of studies *in vitro* suggested a critical role of FAK in angiogenesis during cancer progression [92]. On the other hand, FAK was also found to be involved in the pathophysiology of OA. Specifically, FAK could induce chondrocyte hypertrophic differentiation in response to factor XIIIa (FXIIIa) and transglutaminase 2 (TG2). Both transglutaminases are known to undergo physiologic upregulation in OA cartilage. In particular, TG2 mobilization to the cell surface is mediated by FXIIIa, upon its interaction with $\alpha 1\beta 1$ integrin and thus, results in the phosphorylation of FAK and p38 MAP kinase. The activation of these protein kinases then led to increased levels of *COL10A1* in bovine articular chondrocytes [93]. FAK may act as a positive regulator of chondrocyte hypertrophy since FAK is able to activate PI3K, which in turns inhibits BAPX1 and that allows the transcription of *Col10a1* and *Mmp13* [41]. In spite of these findings further studies investigating the association between FAK and hypertrophy are required.

Fyn

Fyn is one of the nine members of the Src family, well-known proto-oncogenes that regulate cell growth and are frequently mutated in cancer [94]. Fyn is a tyrosine-specific phosphotransferase activated by autophosphorylation at Tyr416, upon stimulation of diverse transmembrane receptors including RTKs, G protein-coupled receptors, integrins and cytokine receptors [95]. Thus, Fyn mediates multiple signal transduction pathways such as PKC δ /MAPK/NF- κ B, STAT3 or mTORC1, which regulate a large spectrum of biological processes involved in inflammation, fibrosis and cellular survival, respectively [96]. Recently, Fyn has been found to accumulate in human OA cartilage, thereby suggesting a potential role of Fyn also in the pathogenesis of OA [3]. Concretely, Fyn deficiency in mice protected against age-related or trauma-induced cartilage degradation and the development of OA. Furthermore, they revealed that Fyn phosphorylation led to the increased expression of hypertrophic markers such as *COL10A1*, *MMP13* and *ADAMTS5* in mice and human chondrocytes, through the stabilization of β -catenin in a Wnt-independent manner. Given the close relation between Fyn and hypertrophy of articular chondrocytes [3], more pre-clinical studies about Fyn role in OA pathophysiology would be of high interest.

Drug	Target Tyrosine kinase	Target Disease	Side effects
Fedratinib	JAK2	Myelofibrosis	Anemia Diarrhea Fatigue
Ruxolitinib	JAK2	Myelofibrosis	Anemia Thrombocytopenia
Nintedanib	VEGFRs, FGFR1-3 and PDGFRs	Pulmonary fibrosis	Diarrhea

Table 2 | Overview of FDA-approved tyrosine kinase inhibitors with potential interest for osteoarthritis

Discussion

In recent years, there has been increasing interest in the roles of tyrosine kinases in the pathophysiology of various diseases, since these are essential players in cellular signaling processes [3]. In this review it was highlighted that some members of the tyrosine kinase family, including FGFR-1, DDR1, DDR2, EGFR, VEGFR, TrkA, ROR2, FAK and Fyn, have been found to induce chondrocyte hypertrophy in articular cartilage (Figure 3) [2, 8, 39, 41, 67, 97]. Thus, the use of inhibitors that impair the activity of these tyrosine kinases could be considered as a potential treatment for OA. On this regard, repositioning drugs is an attractive alternative to lower development costs and shorten bench to bedside timeline. Three molecules that have been approved for clinical use for the treatment of Myelofibrosis and Pulmonary fibrosis (Table 2) might be interesting for drug repurposing as disease-modifying osteoarthritic drugs. Nintedanib is an oral tyrosine kinase inhibitor with specificity against VEGFRs, FGFRs and PDGFRs. Fedratinib and Ruxolitinib, both orally bioavailable, selectively inhibit JAK2, however, considering the pivotal role of JAK2 in chondrocyte hypertrophy, caution should be taken. Of note, the adverse effects associated with these medications are often related to systemic application and could be decreased by dose-scalation or by intra-articular injection. The tyrosine kinases FGFR-3 and IGF-1 receptor may be playing a protective role in cartilage homeostasis, therefore, its inhibition could lead to hypertrophy in articular chondrocytes (Figure 3) [32, 52] Currently, some companies are working on agonist against FGFR-3 due to their potentiality to treat OA in an efficient manner.

Despite these findings, a limitation of this review is that only few studies exist for each of these proteins. Moreover, some of these studies used growth plate chondrocytes which may behave differently from articular chondrocytes [98]. Hence, it would be interesting to further study the role of tyrosine kinases in human articular chondrocytes. Furthermore, since tyrosine kinase inhibition could affect other joint structures, such as the synovium and the subchondral bone, the role of TK in these tissues should also be evaluated. To improve the specificity of the treatment, the use of non-competitive inhibitors is recommended since these molecules do not target the active site of the TKs and thereby have less promiscuity in binding [99]. Since TKs do not only modulate chondrocyte hypertrophy but also play a role in inflammation and autophagy [100], TKs inhibitors could significantly help in elaborating treatments that can hinder the progression of OA.

In conclusion, articular cartilage homeostasis is highly susceptible by changes in signaling pathways regulated by TKs that, when dysregulated, lead to chondrocyte hypertrophy. Unrevealing the mechanisms by which TKs influence cartilage hypertrophy could further provide new pharmacological targets for the elaboration of more effective treatments.

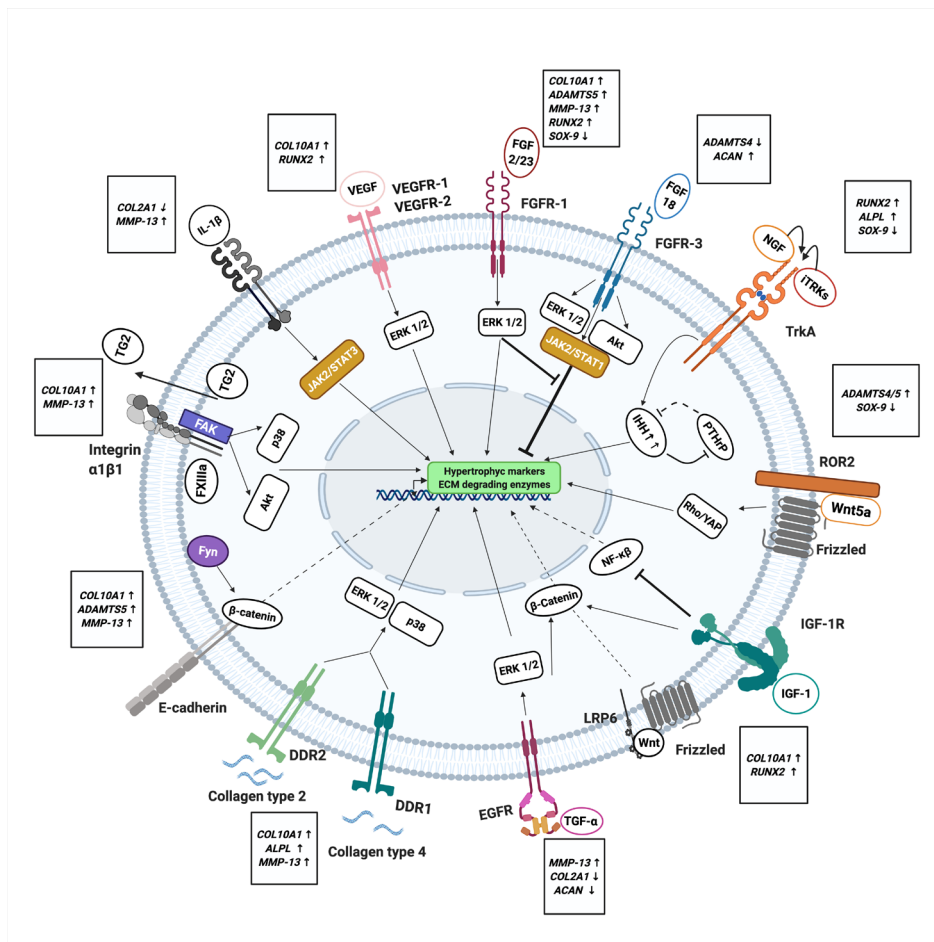


Figure 3 | Overview of the receptor and non-receptor tyrosine kinases that have been associated with osteoarthritis and the pathways through which they regulate chondrocyte hypertrophy. In red, the inhibitory relations are depicted; the black dashed arrows indicate the translocation of the factors to the nucleus and the non-dashed arrows indicate the positive relations for each pathway. In white text-boxes there is written the genes that either are being upregulated or downregulated.

References

1. Xu W, Xie Y, Wang Q, Wang X, Luo F, Zhou S, et al. A novel fibroblast growth factor receptor 1 inhibitor protects against cartilage degradation in a murine model of osteoarthritis. *Sci Rep* 2016; 6: 24042.
2. Yan D, Chen D, Cool SM, van Wijnen AJ, Mikecz K, Murphy G, et al. Fibroblast growth factor receptor 1 is principally responsible for fibroblast growth factor 2-induced catabolic activities in human articular chondrocytes. *Arthritis Res Ther* 2011; 13: R130.
3. Li K, Zhang Y, Zhang Y, Jiang W, Shen J, Xu S, et al. Tyrosine kinase Fyn promotes osteoarthritis by activating the beta-catenin pathway. *Ann Rheum Dis* 2018; 77: 935-943.
4. Aigner T, Dietz U, Stoss H, von der Mark K. Differential expression of collagen types I, II, III, and X in human osteophytes. *Lab Invest* 1995; 73: 236-243.
5. Yang L, Tsang KY, Tang HC, Chan D, Cheah KS. Hypertrophic chondrocytes can become osteoblasts and osteocytes in endochondral bone formation. *Proc Natl Acad Sci U S A* 2014; 111: 12097-12102.
6. Ji Q, Zheng Y, Zhang G, Hu Y, Fan X, Hou Y, et al. Single-cell RNA-seq analysis reveals the progression of human osteoarthritis. *Ann Rheum Dis* 2019; 78: 100-110.
7. Chou CH, Jain V, Gibson J, Attarian DE, Haraden CA, Yohn CB, et al. Synovial cell cross-talk with cartilage plays a major role in the pathogenesis of osteoarthritis. *Sci Rep* 2020; 10: 10868.
8. Jiang Y, Tuan RS. Role of NGF-TrkA signaling in calcification of articular chondrocytes. *Faseb j* 2019; 33: 10231-10239.
9. Blaney Davidson EN, Remst DF, Vitters EL, van Beuningen HM, Blom AB, Goumans MJ, et al. Increase in ALK1/ALK5 ratio as a cause for elevated MMP-13 expression in osteoarthritis in humans and mice. *J Immunol* 2009; 182: 7937-7945.
10. Day TF, Guo X, Garrett-Beal L, Yang Y. Wnt/beta-catenin signaling in mesenchymal progenitors controls osteoblast and chondrocyte differentiation during vertebrate skeletogenesis. *Dev Cell* 2005; 8: 739-750.
11. Islam S, Kermode T, Sultana D, Moskowitz RW, Mukhtar H, Malemud CJ, et al. Expression profile of protein tyrosine kinase genes in human osteoarthritis chondrocytes. *Osteoarthritis Cartilage* 2001; 9: 684-693.
12. Murthy RK, Loi S, Okines A, Paplomata E, Hamilton E, Hurvitz SA, et al. Tucatinib, Trastuzumab, and Capecitabine for HER2-Positive Metastatic Breast Cancer. *N Engl J Med* 2020; 382: 597-609.
13. Solassol I, Pinguet F, Quantin X. FDA- and EMA-Approved Tyrosine Kinase Inhibitors in Advanced EGFR-Mutated Non-Small Cell Lung Cancer: Safety, Tolerability, Plasma Concentration Monitoring, and Management. *Biomolecules* 2019; 9.
14. Daouti S, Latario B, Nagulapalli S, Buxton F, Uziel-Fusi S, Chirn GW, et al. Development of comprehensive functional genomic screens to identify novel mediators of osteoarthritis. *Osteoarthritis Cartilage* 2005; 13: 508-518.
15. Claassen H, Schicht M, Brandt J, Reuse K, Schädlich R, Goldring MB, et al. C-28/I2 and T/C-

28a2 chondrocytes as well as human primary articular chondrocytes express sex hormone and insulin receptors--Useful cells in study of cartilage metabolism. *Ann Anat* 2011; 193: 23-29.

16. Shakibaei M, Schulze-Tanzil G, Mobasheri A, Beichler T, Dressler J, Schwab W. Expression of the VEGF receptor-3 in osteoarthritic chondrocytes: stimulation by interleukin-1 beta and association with beta 1-integrins. *Histochem Cell Biol* 2003; 120: 235-241.

17. Pfander D, Cramer T, Weseloh G, Pullig O, Schuppan D, Bauer M, et al. Hepatocyte growth factor in human osteoarthritic cartilage. *Osteoarthritis Cartilage* 1999; 7: 548-559.

18. Nawachi K, Inoue M, Kubota S, Nishida T, Yosimichi G, Nakanishi T, et al. Tyrosine kinase-type receptor ErbB4 in chondrocytes: interaction with connective tissue growth factor and distribution in cartilage. *FEBS Lett* 2002; 528: 109-113.

19. Kwan Tat S, Pelletier JP, Amiable N, Boileau C, Lavigne M, Martel-Pelletier J. Treatment with ephrin B2 positively impacts the abnormal metabolism of human osteoarthritic chondrocytes. *Arthritis Res Ther* 2009; 11: R119.

20. Bursell L, Woods A, James CG, Pala D, Leask A, Beier F. Src kinase inhibition promotes the chondrocyte phenotype. *Arthritis Res Ther* 2007; 9: R105.

21. Kjelgaard-Petersen CF, Sharma N, Kayed A, Karsdal MA, Mobasheri A, Hägglund P, et al. Tofacitinib and TPCA-1 exert chondroprotective effects on extracellular matrix turnover in bovine articular cartilage ex vivo. *Biochem Pharmacol* 2019; 165: 91-98.

22. Chou HC, Chen CH, Chou LY, Cheng TL, Kang L, Chuang SC, et al. Discoidin Domain Receptors 1 Inhibition Alleviates Osteoarthritis via Enhancing Autophagy. *Int J Mol Sci* 2020; 21.

23. Schminke B, Muhammad H, Bode C, Sadowski B, Gerter R, Gersdorff N, et al. A discoidin domain receptor 1 knock-out mouse as a novel model for osteoarthritis of the temporomandibular joint. *Cell Mol Life Sci* 2014; 71: 1081-1096.

24. Zhang S, Zhong Y, Li R, Wang W, Zeng L, Wang Z, et al. Experimental chondrocyte hypertrophy is promoted by the activation of discoidin domain receptor 2. *Mol Med Rep* 2014; 10: 1543-1548.

25. Sunk IG, Bobacz K, Hofstaetter JG, Amoyo L, Soleiman A, Smolen J, et al. Increased expression of discoidin domain receptor 2 is linked to the degree of cartilage damage in human knee joints: a potential role in osteoarthritis pathogenesis. *Arthritis Rheum* 2007; 56: 3685-3692.

26. Xu L, Peng H, Glasson S, Lee PL, Hu K, Ijiri K, et al. Increased expression of the collagen receptor discoidin domain receptor 2 in articular cartilage as a key event in the pathogenesis of osteoarthritis. *Arthritis Rheum* 2007; 56: 2663-2673.

27. Huang CY, Lin HJ, Chen HS, Cheng SY, Hsu HC, Tang CH. Thrombin promotes matrix metalloproteinase-13 expression through the PKC δ c-Src/EGFR/PI3K/Akt/AP-1 signaling pathway in human chondrocytes. *Mediators Inflamm* 2013; 2013: 326041.

28. Weng T, Yi L, Huang J, Luo F, Wen X, Du X, et al. Genetic inhibition of fibroblast growth factor receptor 1 in knee cartilage attenuates the degeneration of articular cartilage in adult mice. *Arthritis Rheum* 2012; 64: 3982-3992.

29. Tang J, Su N, Zhou S, Xie Y, Huang J, Wen X, et al. Fibroblast Growth Factor Receptor 3 Inhibits Osteoarthritis Progression in the Knee Joints of Adult Mice. *Arthritis Rheumatol* 2016; 68: 2432-2443.

-
30. Valverde-Franco G, Binette JS, Li W, Wang H, Chai S, Laflamme F, et al. Defects in articular cartilage metabolism and early arthritis in fibroblast growth factor receptor 3 deficient mice. *Hum Mol Genet* 2006; 15: 1783-1792.
31. Davidson D, Blanc A, Filion D, Wang H, Plut P, Pfeffer G, et al. Fibroblast growth factor (FGF) 18 signals through FGF receptor 3 to promote chondrogenesis. *J Biol Chem* 2005; 280: 20509-20515.
32. Montaseri A, Busch F, Mobasheri A, Buhrmann C, Aldinger C, Rad JS, et al. IGF-1 and PDGF-bb suppress IL-1 β -induced cartilage degradation through down-regulation of NF- κ B signaling: involvement of Src/PI-3K/AKT pathway. *PLoS One* 2011; 6: e28663.
33. Shakibaei M, Seifarth C, John T, Rahmzadeh M, Mobasheri A. Igf-I extends the chondrogenic potential of human articular chondrocytes in vitro: molecular association between Sox9 and Erk1/2. *Biochem Pharmacol* 2006; 72: 1382-1395.
34. Rosa SC, Rufino AT, Judas F, Tenreiro C, Lopes MC, Mendes AF. Expression and function of the insulin receptor in normal and osteoarthritic human chondrocytes: modulation of anabolic gene expression, glucose transport and GLUT-1 content by insulin. *Osteoarthritis Cartilage* 2011; 19: 719-727.
35. Thorup AS, Strachan D, Caxaria S, Poulet B, Thomas BL, Eldridge SE, et al. ROR2 blockade as a therapy for osteoarthritis. *Sci Transl Med* 2020; 12.
36. Krupka E, Jiang GL, Jan C. Efficacy and safety of intra-articular injection of tropomyosin receptor kinase A inhibitor in painful knee osteoarthritis: a randomized, double-blind and placebo-controlled study. *Osteoarthritis Cartilage* 2019; 27: 1599-1607.
37. Watt FE, Blauwet MB, Fakhoury A, Jacobs H, Smulders R, Lane NE. Tropomyosin-related kinase A (TrkA) inhibition for the treatment of painful knee osteoarthritis: results from a randomized controlled phase 2a trial. *Osteoarthritis Cartilage* 2019; 27: 1590-1598.
38. Shen P, Jiao Z, Zheng JS, Xu WF, Zhang SY, Qin A, et al. Injecting vascular endothelial growth factor into the temporomandibular joint induces osteoarthritis in mice. *Sci Rep* 2015; 5: 16244.
39. Zhang X, Crawford R, Xiao Y. Inhibition of vascular endothelial growth factor with shRNA in chondrocytes ameliorates osteoarthritis. *J Mol Med (Berl)* 2016; 94: 787-798.
40. Ishiguro N, Oyama S, Higashi R, Yanagida K. Efficacy, Safety, and Tolerability of ONO-4474, an Orally Available Pan-Tropomyosin Receptor Kinase Inhibitor, in Japanese Patients With Moderate to Severe Osteoarthritis of the Knee: A Randomized, Placebo-Controlled, Double-Blind, Parallel-Group Comparative Study. *J Clin Pharmacol* 2020; 60: 28-36.
41. Cao Z, Dou C, Li J, Tang X, Xiang J, Zhao C, et al. Cordycepin inhibits chondrocyte hypertrophy of mesenchymal stem cells through PI3K/Bapx1 and Notch signaling pathway. *BMB Rep* 2016; 49: 548-553.
42. Johnson KA, Rose DM, Terkeltaub RA. Factor XIIIa mobilizes transglutaminase 2 to induce chondrocyte hypertrophic differentiation. *J Cell Sci* 2008; 121: 2256-2264.
43. Li M, Seki Y, Freitas PH, Nagata M, Kojima T, Sultana S, et al. FGFR3 down-regulates PTH/PTHrP receptor gene expression by mediating JAK/STAT signaling in chondrocytic cell line. *J Electron Microsc (Tokyo)* 2010; 59: 227-236.
44. Zou LX, Yu L, Zhao XM, Liu J, Lu HG, Liu GW, et al. MiR-375 Mediates Chondrocyte Metabolism and Oxidative Stress in Osteoarthritis Mouse Models through the JAK2/STAT3 Signaling Pathway. *Cells*

Tissues Organs 2019; 208: 13-24.

45. Yao ZZ, Hu AX, Liu XS. DUSP19 regulates IL-1 β -induced apoptosis and MMPs expression in rat chondrocytes through JAK2/STAT3 signaling pathway. *Biomed Pharmacother* 2017; 96: 1209-1215.
46. Lemmon MA, Schlessinger J. Cell signaling by receptor tyrosine kinases. *Cell* 2010; 141: 1117-1134.
47. Oladipupo SS, Smith C, Santeford A, Park C, Sene A, Wiley LA, et al. Endothelial cell FGF signaling is required for injury response but not for vascular homeostasis. *Proc Natl Acad Sci U S A* 2014; 111: 13379-13384.
48. Xie Y, Su N, Yang J, Tan Q, Huang S, Jin M, et al. FGF/FGFR signaling in health and disease. *Signal Transduct Target Ther* 2020; 5: 181.
49. Wu YM, Su F, Kalyana-Sundaram S, Khazanov N, Ateeq B, Cao X, et al. Identification of targetable FGFR gene fusions in diverse cancers. *Cancer Discov* 2013; 3: 636-647.
50. Brodie SG, Kitoh H, Lachman RS, Nolasco LM, Mekikian PB, Wilcox WR. Platypondylic lethal skeletal dysplasia, San Diego type, is caused by FGFR3 mutations. *Am J Med Genet* 1999; 84: 476-480.
51. Bianchi A, Guibert M, Cailotto F, Gasser A, Presle N, Mainard D, et al. Fibroblast Growth Factor 23 drives MMP13 expression in human osteoarthritic chondrocytes in a Klotho-independent manner. *Osteoarthritis Cartilage* 2016; 24: 1961-1969.
52. Valverde-Franco G, Binette JS, Li W, Wang H, Chai S, Laflamme F, et al. Defects in articular cartilage metabolism and early arthritis in fibroblast growth factor receptor 3 deficient mice. *Human Molecular Genetics* 2006; 15: 1783-1792.
53. Zhang H, Wang H, Zeng C, Yan B, Ouyang J, Liu X, et al. mTORC1 activation downregulates FGFR3 and PTH/PTHrP receptor in articular chondrocytes to initiate osteoarthritis. *Osteoarthritis Cartilage* 2017; 25: 952-963.
54. Eckstein F, Kraines JL, Aydemir A, Wirth W, Maschek S, Hochberg MC. Intra-articular sprifermin reduces cartilage loss in addition to increasing cartilage gain independent of location in the femorotibial joint: post-hoc analysis of a randomised, placebo-controlled phase II clinical trial. *Ann Rheum Dis* 2020; 79: 525-528.
55. Vogel W, Gish GD, Alves F, Pawson T. The discoidin domain receptor tyrosine kinases are activated by collagen. *Mol Cell* 1997; 1: 13-23.
56. Labrador JP, Azcoitia V, Tuckermann J, Lin C, Olaso E, Mañes S, et al. The collagen receptor DDR2 regulates proliferation and its elimination leads to dwarfism. *EMBO Rep* 2001; 2: 446-452.
57. Shrivastava A, Radziejewski C, Campbell E, Kovac L, McGlynn M, Ryan TE, et al. An orphan receptor tyrosine kinase family whose members serve as nonintegrin collagen receptors. *Mol Cell* 1997; 1: 25-34.
58. Leitinger B, Steplewski A, Fertala A. The D2 period of collagen II contains a specific binding site for the human discoidin domain receptor, DDR2. *J Mol Biol* 2004; 344: 993-1003.
59. Leitinger B, Kwan AP. The discoidin domain receptor DDR2 is a receptor for type X collagen. *Matrix Biol* 2006; 25: 355-364.
60. Reel B, Korkmaz CG, Arun MZ, Yildirim G, Ogut D, Kaymak A, et al. The Regulation of Matrix Metalloproteinase Expression and the Role of Discoidin Domain Receptor 1/2 Signalling in Zoledronate-

treated PC3 Cells. *J Cancer* 2015; 6: 1020-1029.

61. Zhang Y, Su J, Yu J, Bu X, Ren T, Liu X, et al. An essential role of discoidin domain receptor 2 (DDR2) in osteoblast differentiation and chondrocyte maturation via modulation of Runx2 activation. *J Bone Miner Res* 2011; 26: 604-617.
62. Lin KL, Chou CH, Hsieh SC, Hwa SY, Lee MT, Wang FF. Transcriptional upregulation of DDR2 by ATF4 facilitates osteoblastic differentiation through p38 MAPK-mediated Runx2 activation. *J Bone Miner Res* 2010; 25: 2489-2503.
63. Suh HN, Han HJ. Collagen I regulates the self-renewal of mouse embryonic stem cells through $\alpha 2\beta 1$ integrin- and DDR1-dependent Bmi-1. *J Cell Physiol* 2011; 226: 3422-3432.
64. Lu KK, Trcka D, Bendeck MP. Collagen stimulates discoidin domain receptor 1-mediated migration of smooth muscle cells through Src. *Cardiovasc Pathol* 2011; 20: 71-76.
65. Xiao L, Liu C, Wang B, Fei W, Mu Y, Xu L, et al. Targeting Discoidin Domain Receptor 2 for the Development of Disease-Modifying Osteoarthritis Drugs. *Cartilage* 2019: 1947603519852401.
66. Xu L, Peng H, Wu D, Hu K, Goldring MB, Olsen BR, et al. Activation of the discoidin domain receptor 2 induces expression of matrix metalloproteinase 13 associated with osteoarthritis in mice. *J Biol Chem* 2005; 280: 548-555.
67. Xu L, Servais J, Polur I, Kim D, Lee PL, Chung K, et al. Attenuation of osteoarthritis progression by reduction of discoidin domain receptor 2 in mice. *Arthritis Rheum* 2010; 62: 2736-2744.
68. Brown J, Delaine C, Zaccaro OJ, Siebold C, Gilbert RJ, van Boxel G, et al. Structure and functional analysis of the IGF-II/IGF2R interaction. *Embo j* 2008; 27: 265-276.
69. Gao J, Chesebrough JW, Cartlidge SA, Ricketts SA, Incognito L, Veldman-Jones M, et al. Dual IGF-I/II-neutralizing antibody MEDI-573 potently inhibits IGF signaling and tumor growth. *Cancer Res* 2011; 71: 1029-1040.
70. Hidalgo M, Gomez MT, Lewis N, Vuky JL, Taylor G, Hayburn JL, et al. A phase I study of MK-0646, a humanized monoclonal antibody against the insulin-like growth factor receptor type 1 (IGF1R) in advanced solid tumor patients in a q2 wk schedule. *Journal of Clinical Oncology* 2008; 26: 3520-3520.
71. Higano CS, Yu EY, Whiting SH, Gordon MS, LoRusso P, Fox F, et al. A phase I, first in man study of weekly IMC-A12, a fully human insulin like growth factor-I receptor IgG1 monoclonal antibody, in patients with advanced solid tumors. *Journal of Clinical Oncology* 2007; 25: 3505-3505.
72. Yin W, Park JI, Loeser RF. Oxidative stress inhibits insulin-like growth factor-I induction of chondrocyte proteoglycan synthesis through differential regulation of phosphatidylinositol 3-Kinase-Akt and MEK-ERK MAPK signaling pathways. *J Biol Chem* 2009; 284: 31972-31981.
73. Wieduwilt MJ, Moasser MM. The epidermal growth factor receptor family: biology driving targeted therapeutics. *Cell Mol Life Sci* 2008; 65: 1566-1584.
74. Appleton CTG, Usmani SE, Bernier SM, Aigner T, Beier F. Transforming growth factor α suppression of articular chondrocyte phenotype and Sox9 expression in a rat model of osteoarthritis. *Arthritis & Rheumatism* 2007; 56: 3693-3705.
75. Molina AM, Hutson TE, Nosov D, Tomczak P, Lipatov O, Sternberg CN, et al. Efficacy of tivozanib treatment after sorafenib in patients with advanced renal cell carcinoma: crossover of a phase 3 study. *Eur J Cancer* 2018; 94: 87-94.

76. Kong X, Zhang Y, Liu C, Guo W, Li X, Su X, et al. Anti-angiogenic effect of triptolide in rheumatoid arthritis by targeting angiogenic cascade. *PLoS One* 2013; 8: e77513.
77. Richeldi L, du Bois RM, Raghu G, Azuma A, Brown KK, Costabel U, et al. Efficacy and safety of nintedanib in idiopathic pulmonary fibrosis. *N Engl J Med* 2014; 370: 2071-2082.
78. Jackson TL, Boyer D, Brown DM, Chaudhry N, Elman M, Liang C, et al. Oral Tyrosine Kinase Inhibitor for Neovascular Age-Related Macular Degeneration: A Phase 1 Dose-Escalation Study. *JAMA Ophthalmol* 2017; 135: 761-767.
79. Koch S, Tugues S, Li X, Gualandi L, Claesson-Welsh L. Signal transduction by vascular endothelial growth factor receptors. *Biochem J* 2011; 437: 169-183.
80. Walsh DA, McWilliams DF, Turley MJ, Dixon MR, Fransès RE, Mapp PI, et al. Angiogenesis and nerve growth factor at the osteochondral junction in rheumatoid arthritis and osteoarthritis. *Rheumatology (Oxford)* 2010; 49: 1852-1861.
81. Huang EJ, Reichardt LF. Trk receptors: roles in neuronal signal transduction. *Annu Rev Biochem* 2003; 72: 609-642.
82. Iannone F, De Bari C, Dell'Accio F, Covelli M, Patella V, Lo Bianco G, et al. Increased expression of nerve growth factor (NGF) and high affinity NGF receptor (p140 TrkA) in human osteoarthritic chondrocytes. *Rheumatology* 2002; 41: 1413-1418.
83. Driscoll C, Chanalaris A, Knights C, Ismail H, Sacitharan PK, Gentry C, et al. Nociceptive Sensitizers Are Regulated in Damaged Joint Tissues, Including Articular Cartilage, When Osteoarthritic Mice Display Pain Behavior. *Arthritis Rheumatol* 2016; 68: 857-867.
84. Masiakowski P, Carroll RD. A novel family of cell surface receptors with tyrosine kinase-like domain. *J Biol Chem* 1992; 267: 26181-26190.
85. Yu J, Chen L, Cui B, Widhopf GF, 2nd, Shen Z, Wu R, et al. Wnt5a induces ROR1/ROR2 heterooligomerization to enhance leukemia chemotaxis and proliferation. *J Clin Invest* 2016; 126: 585-598.
86. Chien HP, Ueng SH, Chen SC, Chang YS, Lin YC, Lo YF, et al. Expression of ROR1 has prognostic significance in triple negative breast cancer. *Virchows Arch* 2016; 468: 589-595.
87. Guo M, Ma G, Zhang X, Tang W, Shi J, Wang Q, et al. ROR2 knockdown suppresses breast cancer growth through PI3K/ATK signaling. *Aging (Albany NY)* 2020; 12: 13115-13127.
88. Gocek E, Moulas AN, Studzinski GP. Non-receptor protein tyrosine kinases signaling pathways in normal and cancer cells. *Crit Rev Clin Lab Sci* 2014; 51: 125-137.
89. Berry DC, Jin H, Majumdar A, Noy N. Signaling by vitamin A and retinol-binding protein regulates gene expression to inhibit insulin responses. *Proc Natl Acad Sci U S A* 2011; 108: 4340-4345.
90. Brooks AJ, Dai W, O'Mara ML, Abankwa D, Chhabra Y, Pelekanos RA, et al. Mechanism of activation of protein kinase JAK2 by the growth hormone receptor. *Science* 2014; 344: 1249783.
91. Polte TR, Naftilan AJ, Hanks SK. Focal adhesion kinase is abundant in developing blood vessels and elevation of its phosphotyrosine content in vascular smooth muscle cells is a rapid response to angiotensin II. *J Cell Biochem* 1994; 55: 106-119.
92. Shi Q, Hjelmeland AB, Keir ST, Song L, Wickman S, Jackson D, et al. A novel low-molecular weight inhibitor of focal adhesion kinase, TAE226, inhibits glioma growth. *Mol Carcinog* 2007; 46: 488-

496.

93. Johnson KA, Rose DM, Terkeltaub RA. Factor XIIIa mobilizes transglutaminase 2 to induce chondrocyte hypertrophic differentiation. *Journal of Cell Science* 2008; 121: 2256-2264.
94. Parsons SJ, Parsons JT. Src family kinases, key regulators of signal transduction. *Oncogene* 2004; 23: 7906-7909.
95. Jelić D, Mildner B, Kostrun S, Nujić K, Verbanac D, Culić O, et al. Homology modeling of human Fyn kinase structure: discovery of rosmarinic acid as a new Fyn kinase inhibitor and in silico study of its possible binding modes. *J Med Chem* 2007; 50: 1090-1100.
96. Seo HY, Jeon JH, Jung YA, Jung GS, Lee EJ, Choi YK, et al. Fyn deficiency attenuates renal fibrosis by inhibition of phospho-STAT3. *Kidney Int* 2016; 90: 1285-1297.
97. Li XS, Chen H, Zhen P, Li SS, Zhou SH, Tian Q, et al. [JAK2/STAT3 signal pathway mediating curcumin in cartilage cell metabolism of osteoarthritis]. *Zhongguo Gu Shang* 2016; 29: 1104-1109.
98. Wang L, Shao YY, Ballock RT. Thyroid hormone-mediated growth and differentiation of growth plate chondrocytes involves IGF-1 modulation of beta-catenin signaling. *J Bone Miner Res* 2010; 25: 1138-1146.
99. Kirkland LO, McInnes C. Non-ATP competitive protein kinase inhibitors as anti-tumor therapeutics. *Biochem Pharmacol* 2009; 77: 1561-1571.
100. Domigan CK, Warren CM, Antanesian V, Happel K, Ziyad S, Lee S, et al. Autocrine VEGF maintains endothelial survival through regulation of metabolism and autophagy. *J Cell Sci* 2015; 128: 2236-2248.

Chapter 7

General discussion

Discussion

The prevalence of osteoarthritis (OA) is steadily increasing worldwide, representing a major public health challenge [1]. This is emphasized by the lack of specific therapies which makes OA a serious disease with an unmet medical need. Advances in the understanding of OA have enabled the identification of key pathophysiological processes. Early in the disease, articular chondrocytes lose their phenotypic stability and display a transcriptomic fingerprint similar to hypertrophic chondrocytes in the growth plate [2]. Chondrocyte hypertrophy is characterized by molecular changes that trigger the degradation of the cartilage extracellular matrix, which ultimately leads to the transition of cartilage to bone [3]. Therefore, hypertrophic differentiation of articular chondrocytes is considered a main driver of OA progression [4]. OA does not only affect the cartilage but is a disease of the entire joint, including osteophytosis, subchondral bone changes and synovitis [5]. In a similar way to articular chondrocyte hypertrophy, the formation of osteophytes is governed by pathological endochondral ossification [6]. Synovitis, on the other hand, is characterized by the presence of activated macrophages in the joint lining which increase the production of cytokines and catabolic enzymes, leading to chronic inflammation [7]. Given the occurrence of chondrocyte hypertrophy and inflammation in early stages of OA, targeting these processes are expected to considerably reshape the landscape of OA management, moving on from palliative care to disease-modifying OA drugs (DMOADs). In this context, in this thesis I aim to acquire new knowledge on how chondrocyte hypertrophy and inflammation orchestrate joint degeneration and further identify specific targeted therapies that could lead to a DMOAD.

How does the articular microenvironment orchestrate joint degeneration?

Increasing our understanding of disease mechanisms in OA are crucial to develop treatments to attenuate disease progression. In this perspective, transcriptomic changes in articular cartilage have been reported in human and animal models, highlighting the presence of a hypertrophic-like chondrocyte gene expression in OA articular cartilage [8, 9]. This is observed by the upregulation of a set of genes also upregulated in the hypertrophic zone of the growth plate, such as alkaline phosphatase (*ALPL*), type X collagen (*COL10A1*), matrix metalloproteinase 13 (*MMP13*) and runt-related transcription factor 2 (*RUNX2*) [10, 11]. Articular chondrocytes are responsible for maintaining the balance between catabolic and anabolic processes in the cartilage but in OA the acquisition of this hypertrophic-like chondrocyte fingerprint catalyzes the degradation of the articular cartilage, leading to joint degeneration [12-14]. Single cell transcriptomics have recently proven the presence of cells with different phenotypes in osteoarthritic cartilage, including hypertrophic chondrocytes, even when the cartilage is macroscopically intact [2, 15]. These findings highlight the presence of chondrocyte hypertrophy in early stages of the disease. Hence, identification of triggers

of chondrocyte hypertrophy is an interesting approach to develop effective OA treatments that halt disease progression. In chapter 4, in collaboration with the University of Leuven we developed a *in silico* model of articular chondrocyte phenotype that facilitates the identification of such signals. Based on our *in silico* experiments, activation of fibroblast growth factor receptor (FGFR) 1 was shown to be a potent inducer of chondrocyte hypertrophy. Previous reports indicate that inhibition of FGFR1 in human chondrocytes impaired the expression of *MMP13* and *COL10A1* [16]. FGFR1 is a tyrosine kinase receptor which is activated through binding of fibroblast growth factors (FGFs) ligands, FGF-2, FGF-18 and FGF-23 [16, 17]. Stimulation by these growth factors leads to the activation of various downstream signaling pathways, such as ERK1/2 and PI3K/AKT [17, 18]. Interestingly, our results using the *in silico* articular chondrocyte in chapter 4, identified ERK1/2 and AKT as hypertrophic triggers, which are intrinsically associated with inflammatory signaling cues as well. Inflammation have been shown to induce chondrocyte hypertrophy, though current studies mainly used mouse chondrocytes [19-21]. The experiments in chapter 2, demonstrate that pro-inflammatory cytokines did not mediate the hypertrophic differentiation of human articular chondrocytes. In contrast to these results, in chapter 4 we found that inflammatory signaling activation triggers a hypertrophic switch in chondrocytes *in silico*. This discrepancy might be explained considering that the inflammatory processes in OA are driven by a broad spectrum of cytokines and immune factors that might have been differently recapitulated in the *in silico* than *in vitro* models. To accomplish this, in chapter 2 we used the secretome of *in vitro* polarized macrophages which represents better the complex inflammatory microenvironment in an osteoarthritic joint. Secreted products of pro-inflammatory M(IFN γ +TNF α), tissue repair M(IL4) and anti-inflammatory M(IL10) polarized macrophages were cultured with cartilage explants of knee OA patients. Based on changes in gene expression levels, it was shown that the secreted products of M(IFN γ +TNF α), enhanced catabolism, as previously reported [22], while we reported that tissue repair macrophages M(IL4) induced chondrocyte hypertrophy. Interestingly, this macrophage subset secretes the pleiotropic cytokine transforming growth factor beta (TGF β), which can lead to chondrocyte hypertrophy via the activation of activin receptor-like kinase 1 (ALK1) in aging cartilage [23]. In chapter 4, we showed that TGF β induced hypertrophic differentiation in chondrocytes with an increase ratio of the TGF β receptors ALK1/ALK5 *in silico*, in accordance with previous work [24]. Tissue repair macrophages also secrete FGF-2 [25], which can activate FGFR1 and leads to chondrocyte hypertrophy, as discussed above. Therefore, inflammatory signals can drive hypertrophic differentiation of articular chondrocytes, hence leading to joint degeneration. In this perspective, in chapter 3, we aimed to investigate whether an anti-inflammatory drug could attenuate joint degeneration in a mice model of OA. However, instead of decreasing inflammation, the intra-articular injection of triamcinolone acetonide (TAA) accentuated synovial macrophages in the joint with a pro-inflammatory phenotype. Multiple mechanisms normally ensure the resolution of inflammation after tissue damage, though an abnormal inflammatory response can lead to a non-resolving state [26]. The modulation of inflammation by TAA might therefore dysregulate

the normal resolution process in the pathological articular microenvironment, contributing to a loss of homeostasis during repair. The formation of osteophytes is governed by the process of endochondral ossification, where chondrocyte hypertrophy is a major driver. In accordance with the results of chapter 2 and chapter 4 linking inflammation with hypertrophy, here we observed that increased synovial inflammation was accompanied by exacerbated osteophyte formation. Corticoids are potent molecules influencing a wide array of physiological processes such as metabolism, inflammation and immunity [27, 28]. Considering their broad mechanism of action, a more targeted therapy should be developed to attenuate inflammation and chondrocyte hypertrophy in the context of OA. In this view, in chapter 5, we identified EPHA2 as a main regulator of inflammation and chondrocyte hypertrophy in OA, using the *in silico* model described in chapter 4, in combination with *in vitro* models. Inhibition of EPHA2 in mice attenuated osteophytosis and synovitis, providing further evidence that chondrocyte hypertrophy and inflammation orchestrate joint degeneration. Moreover, as described in chapter 6, other members of the tyrosine kinase family, including FGFR1, are key regulators of chondrocyte hypertrophy and therefore enhance joint degeneration. Interestingly, these enzymes play a role in signaling cascades activated by inflammatory stimuli [29], therefore, enhancing the cross-talk between inflammatory pathways and chondrocyte hypertrophy as main drivers in orchestrating joint degeneration in OA.

What are the challenges in OA pharmacology?

Current pharmaceutical treatments in OA aim to reduce the burden of the disease by relieving the symptoms, though these therapeutics have minimal or low effect in stopping the biological processes underlying tissue damage. Yet the available drugs recommended by international guidelines to treat OA have relatively small effect sizes and uncertainty around their long-term efficacy [30-32]. Moreover, commonly used analgesics, such as non-steroidal anti-inflammatory drugs (NSAIDs) have raised concerns about their safety, especially for patients with cardiovascular comorbidities as they are associated with a heightened cardiovascular risk [33, 34]. Glucocorticoids are widely used anti-inflammatory agents in OA associated with short-term analgesic benefits and knee function [35, 36]. Using intra-articular administration offers the opportunity to target inflammation locally, therefore reducing systemic exposure to the drug and its associated complications [37]. However, concerns exist about a possible detrimental effect in the joint. In this perspective, our results from chapter 3, contributed to this topic by showing that early intervention with short-term triamcinolone acetonide aggravates osteophytosis and exacerbate long-term synovial macrophages in mice. These findings do not support the use of triamcinolone acetonide as OA treatment, which is in accordance with clinical trials that report an association of intra-articular corticosteroid treatment with accelerated structural progression of OA [38]. Thus, alternative therapeutics are needed for the treatment of OA.

Advances in the understanding of OA pathophysiology have identified a variety of molecular

processes that might trigger disease onset and progression, such as inflammation, cellular senescence, catabolism and chondrocyte hypertrophy [39], leading to a large list of possible pharmacological targets. To evaluate the efficacy of these targets, computer modelling and simulation is a powerful tool in biomedical research, augmenting experimental research through detailed mechanistic investigations which are impossible with other means [40]. In this context, in chapter 4 we developed an *in silico* model that enables the screening of several targets in a less time-consuming manner than in the wet lab. We used this approach on chapter 5, in the early stages of drug target discovery, to evaluate the efficacy of EPHA2. The capacity of EPHA2 to attenuate chondrocyte hypertrophy and inflammation was confirmed *in vitro* and *in vivo*, validating the strategy of using the *in silico* model in the drug discovery pipeline of a DMOAD. Therefore, the computational model described in chapter 4, opens the possibility to accelerate the drug discovery field in OA, dramatically decreasing the time from discovery to implementation in the clinics.

Regulatory agencies, such as the U.S. Food and Drug Administration (FDA) and the European Medicines Agency (EMA) generally approve drugs based upon measurements on how a patient feels, functions, or survives. In the case of OA, this translates to patient-reported outcomes of pain and function as trial endpoints, though not considering structural joint features [41]. This requirement has been problematic for approval of disease modifying medications because changes in structure do not translate immediately to changes in symptoms, but instead give rise to symptom reduction after years [30, 42, 43]. Therefore, regulatory agencies have recently considered OA as a serious disease which allows to use imaging or molecular biomarkers associated with joint degeneration as primary outcomes for clinical trials [44]. These considerations are supposed to also influence the development of DMOADs in pre-clinical studies. In this perspective, the molecule studied in chapter 5 showed to attenuate joint degeneration in mice based upon evidence on synovial inflammation and osteophyte formation, but did not reduce pain at the short term. Clinical studies report that synovitis and osteophytosis are surrogate endpoints, measures that do not themselves represent clinical benefits but have been shown to predict clinical benefit based on studies considering patient-reported pain and function [45-47]. This also applies to emerging therapies for OA that are currently in clinical trials [48]. One of these promising DMOADs is Lorecivint, a WNT signaling inhibitor, that has been shown to induce chondrogenesis of mesenchymal stromal cells *in vitro* and inhibited joint degeneration in a rat model of OA [49]. These results are comparable to our results found with the molecule described in chapter 5. Further clinical trials revealed that a single intra-articular injection of Lorecivint attenuates radiographic joint space narrowing over 24 weeks [50]. However, the drug itself has not yet been shown to reduce pain during the time-frames of the existing studies [51]. To ensure precise bench-to-bedside translation, pharmaceutical companies have rigorously prioritized the identification of the right biological target for the right patient population, since early stages of drug development [52]. Selectively targeting some phenotypes of patients with OA may enable the development of DMOADs based on personalized medicine [53]. New tools are needed to

support the prediction of the patients best suited for a given DMOAD, and should allow for a better response to a specific treatment [54]. In chapter 2, we found that macroscopically intact cartilage from OA patients undergoing total knee replacement expressed characteristic chondrocyte hypertrophy markers, mainly type X collagen (*COL10A1*). Even though *COL10A1* was detected in the cartilage of most OA donors, there were certain donors that had no detectable *COL10A1*. This suggests that chondrocyte hypertrophy might not be present in all OA patients. In this context, type X collagen in serum has been reported as a diagnostic biomarker in a subset of patients with inflammatory OA [14, 55]. Moreover, studies have shown that drug development programs that can rely on biomarkers correlating with efficacy have a higher chance of success [56, 57]. Therefore, the selection of patients to evaluate the clinical efficacy of a DMOAD targeting chondrocyte hypertrophy, as Lorecivint and the EPHA2 inhibitor ALW-II-41-27 described in chapter 5, should consider this cohort of patients to decrease the risk of the clinical trial, guaranteeing higher chances of success.

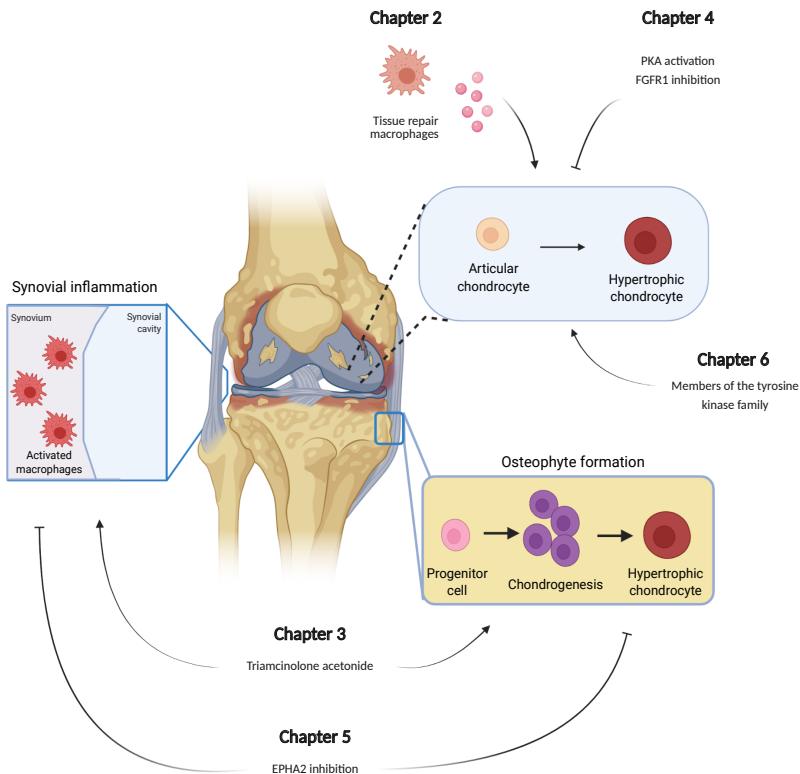


Figure 1 | Schematic representation of the main results of this thesis

Future perspectives

Developing disease modifying OA drugs (DMOADs) remains challenging. One of the challenges is the late diagnosis of the disease, when a chronic mechanism of joint degeneration is already established [58]. However, in the past years more sensitive techniques have been developed allowing the identification of molecular and imaging biomarkers that facilitate the detection of the disease in an early stage [59-61]. This increases the chance for a treatment to stop disease progression. OA includes multiple phenotypes and subgroups. Identification of phenotypes will accelerate the development of approaches to pharmacological therapies as well as distinguish individuals who are at higher risk of progression. Screening of patients with early OA will be extremely useful to guide clinical decision-making and help to advance towards precision medicine, allowing to distinguish the responders from the non-responders of a given therapy. This knowledge can nourish the pre-clinical development of drugs, designing molecules for a specific group of patients.

One extra challenge is the long-term natural course of the disease, which means that clinical trials require very long follow-up periods to detect an effect on joint pathology. Keeping the study participants in trials for several years is resource intensive for the pharma industry and also challenging for participants that may try a range of concomitant therapies, blunting the effect of the drug, or stop the treatment. This challenge will require careful collaboration among patients and the OA researchers.

It is now the time to move this therapeutic field forward. New technologies are available that allow us to take steps towards personalized medicine, predict which patients are best suited for a given DMOAD, and tackle disease progression with a specific treatment. These advances in OA drug discovery are expected to reshape the landscape of OA management over the next few years.

References

1. Diseases, G.B.D. and C. Injuries, Global burden of 369 diseases and injuries in 204 countries and territories, 1990-2019: a systematic analysis for the Global Burden of Disease Study 2019. *Lancet*, 2020. 396(10258): p. 1204-1222.
2. Ji, Q., et al., Single-cell RNA-seq analysis reveals the progression of human osteoarthritis. *Ann Rheum Dis*, 2019. 78(1): p. 100-110.
3. Singh, P., et al., Phenotypic instability of chondrocytes in osteoarthritis: on a path to hypertrophy. *Ann N Y Acad Sci*, 2019. 1442(1): p. 17-34.
4. van der Kraan, P.M. and W.B. van den Berg, Chondrocyte hypertrophy and osteoarthritis: role in initiation and progression of cartilage degeneration? *Osteoarthritis Cartilage*, 2012. 20(3): p. 223-32.
5. Martel-Pelletier, J., et al., Osteoarthritis. *Nat Rev Dis Primers*, 2016. 2: p. 16072.
6. Gelse, K., et al., Osteophyte development--molecular characterization of differentiation stages. *Osteoarthritis Cartilage*, 2003. 11(2): p. 141-8.
7. Robinson, W.H., et al., Low-grade inflammation as a key mediator of the pathogenesis of osteoarthritis. *Nat Rev Rheumatol*, 2016. 12(10): p. 580-92.
8. Sato, T., et al., Comparative analysis of gene expression profiles in intact and damaged regions of human osteoarthritic cartilage. *Arthritis Rheum*, 2006. 54(3): p. 808-17.
9. Bateman, J.F., et al., Transcriptomics of wild-type mice and mice lacking ADAMTS-5 activity identifies genes involved in osteoarthritis initiation and cartilage destruction. *Arthritis Rheum*, 2013. 65(6): p. 1547-60.
10. K. Von Der Mark, A.N., A. Kuss, G. Weseloh, K. Glückert, H. Stöss, Type X collagen synthesis in human osteoarthritic cartilage. Indication of chondrocyte hypertrophy. *Arthritis Rheum*, 1992. 35.
11. Aigner, T., et al., Type X collagen expression in osteoarthritic and rheumatoid articular cartilage. *Virchows Arch B Cell Pathol Incl Mol Pathol*, 1993. 63(4): p. 205-11.
12. Ripmeester, E.G.J., et al., Recent Insights into the Contribution of the Changing Hypertrophic Chondrocyte Phenotype in the Development and Progression of Osteoarthritis. *Front Bioeng Biotechnol*, 2018. 6: p. 18.
13. Pesesse, L., et al., Consequences of chondrocyte hypertrophy on osteoarthritic cartilage: potential effect on angiogenesis. *Osteoarthritis Cartilage*, 2013. 21(12): p. 1913-23.
14. He, Y., et al., Type X collagen levels are elevated in serum from human osteoarthritis patients and associated with biomarkers of cartilage degradation and inflammation. *BMC Musculoskelet Disord*, 2014. 15: p. 309.
15. Chou, C.H., et al., Synovial cell cross-talk with cartilage plays a major role in the pathogenesis of osteoarthritis. *Sci Rep*, 2020. 10(1): p. 10868.
16. Xu, W., et al., A novel fibroblast growth factor receptor 1 inhibitor protects against cartilage degradation in a murine model of osteoarthritis. *Sci Rep*, 2016. 6: p. 24042.
17. Yan, D., et al., Fibroblast growth factor receptor 1 is principally responsible for fibroblast growth factor 2-induced catabolic activities in human articular chondrocytes. *Arthritis Res Ther*, 2011. 13(4): p. R130.

18. Oladipupo, S.S., et al., Endothelial cell FGF signaling is required for injury response but not for vascular homeostasis. *Proc Natl Acad Sci U S A*, 2014. 111(37): p. 13379-84.
19. Saito, T., et al., Transcriptional regulation of endochondral ossification by HIF-2 α during skeletal growth and osteoarthritis development. *Nat Med*, 2010. 16(6): p. 678-86.
20. Yang, S., et al., Hypoxia-inducible factor-2 α is a catabolic regulator of osteoarthritic cartilage destruction. *Nat Med*, 2010. 16(6): p. 687-93.
21. Zhang, H., et al., Synovial macrophage M1 polarisation exacerbates experimental osteoarthritis partially through R-spondin-2. *Ann Rheum Dis*, 2018. 77(10): p. 1524-1534.
22. Utomo, L., et al., Cartilage inflammation and degeneration is enhanced by pro-inflammatory (M1) macrophages in vitro, but not inhibited directly by anti-inflammatory (M2) macrophages. *Osteoarthritis Cartilage*, 2016. 24(12): p. 2162-2170.
23. van der Kraan, P.M., et al., Age-dependent alteration of TGF- β signalling in osteoarthritis. *Cell Tissue Res*, 2012. 347(1): p. 257-65.
24. Narcisi, R., et al., TGF β -1 administration during ex vivo expansion of human articular chondrocytes in a serum-free medium redirects the cell phenotype toward hypertrophy. *J Cell Physiol*, 2012. 227(9): p. 3282-90.
25. Jetten, N., et al., Anti-inflammatory M2, but not pro-inflammatory M1 macrophages promote angiogenesis in vivo. *Angiogenesis*, 2014. 17(1): p. 109-18.
26. Buckley, C.D., et al., The resolution of inflammation. *Nat Rev Immunol*, 2013. 13(1): p. 59-66.
27. Reichardt, S.D., et al., The Role of Glucocorticoids in Inflammatory Diseases. *Cells*, 2021. 10(11).
28. Cain, D.W. and J.A. Cidlowski, Immune regulation by glucocorticoids. *Nat Rev Immunol*, 2017. 17(4): p. 233-247.
29. Page, T.H., et al., Tyrosine kinases and inflammatory signalling. *Curr Mol Med*, 2009. 9(1): p. 69-85.
30. Gregori, D., et al., Association of Pharmacological Treatments With Long-term Pain Control in Patients With Knee Osteoarthritis: A Systematic Review and Meta-analysis. *JAMA*, 2018. 320(24): p. 2564-2579.
31. Kolasinski, S.L., et al., 2019 American College of Rheumatology/Arthritis Foundation Guideline for the Management of Osteoarthritis of the Hand, Hip, and Knee. *Arthritis Rheumatol*, 2020. 72(2): p. 220-233.
32. Bannuru, R.R., et al., OARSI guidelines for the non-surgical management of knee, hip, and polyarticular osteoarthritis. *Osteoarthritis Cartilage*, 2019. 27(11): p. 1578-1589.
33. Mukherjee, D., S.E. Nissen, and E.J. Topol, Risk of cardiovascular events associated with selective COX-2 inhibitors. *JAMA*, 2001. 286(8): p. 954-9.
34. Trelle, S., et al., Cardiovascular safety of non-steroidal anti-inflammatory drugs: network meta-analysis. *BMJ*, 2011. 342: p. c7086.
35. Juni, P., et al., Intra-articular corticosteroid for knee osteoarthritis. *Cochrane Database Syst Rev*, 2015(10): p. CD005328.
36. Zeng, C., et al., Intra-articular corticosteroids and the risk of knee osteoarthritis progression:

results from the Osteoarthritis Initiative. *Osteoarthritis Cartilage*, 2019. 27(6): p. 855-862.

37. Oray, M., et al., Long-term side effects of glucocorticoids. *Expert Opin Drug Saf*, 2016. 15(4): p. 457-65.
38. McAlindon, T.E., et al., Effect of Intra-articular Triamcinolone vs Saline on Knee Cartilage Volume and Pain in Patients With Knee Osteoarthritis: A Randomized Clinical Trial. *JAMA*, 2017. 317(19): p. 1967-1975.
39. Sherwood, J., Osteoarthritis year in review 2018: biology. *Osteoarthritis Cartilage*, 2019. 27(3): p. 365-370.
40. Musuamba, F.T., et al., Scientific and regulatory evaluation of mechanistic in silico drug and disease models in drug development: Building model credibility. *CPT Pharmacometrics Syst Pharmacol*, 2021. 10(8): p. 804-825.
41. Cho, Y., et al., Disease-modifying therapeutic strategies in osteoarthritis: current status and future directions. *Exp Mol Med*, 2021. 53(11): p. 1689-1696.
42. Eckstein, F., et al., Brief Report: Cartilage Thickness Change as an Imaging Biomarker of Knee Osteoarthritis Progression: Data From the Foundation for the National Institutes of Health Osteoarthritis Biomarkers Consortium. *Arthritis Rheumatol*, 2015. 67(12): p. 3184-9.
43. Hunter, D., et al., Longitudinal validation of periarticular bone area and 3D shape as biomarkers for knee OA progression? Data from the FNIH OA Biomarkers Consortium. *Ann Rheum Dis*, 2016. 75(9): p. 1607-14.
44. Kraus, V.B., et al., Proposed study designs for approval based on a surrogate endpoint and a post-marketing confirmatory study under FDA's accelerated approval regulations for disease modifying osteoarthritis drugs. *Osteoarthritis Cartilage*, 2019. 27(4): p. 571-579.
45. Fjellstad, C.M., et al., Associations Between Ultrasound-Detected Synovitis, Pain, and Function in Interphalangeal and Thumb Base Osteoarthritis: Data From the Nor-Hand Cohort. *Arthritis Care Res (Hoboken)*, 2020. 72(11): p. 1530-1535.
46. Obotiba, A.D., et al., Synovitis and bone marrow lesions associate with symptoms and radiographic progression in hand osteoarthritis: a systematic review and meta-analysis of observational studies. *Osteoarthritis Cartilage*, 2021. 29(7): p. 946-955.
47. Stefanik, J.J., et al., The relation of MRI-detected structural damage in the medial and lateral patellofemoral joint to knee pain: the Multicenter and Framingham Osteoarthritis Studies. *Osteoarthritis Cartilage*, 2015. 23(4): p. 565-70.
48. Latourte, A., M. Kloppenburg, and P. Richette, Emerging pharmaceutical therapies for osteoarthritis. *Nat Rev Rheumatol*, 2020. 16(12): p. 673-688.
49. Deshmukh, V., et al., A small-molecule inhibitor of the Wnt pathway (SMO4690) as a potential disease modifying agent for the treatment of osteoarthritis of the knee. *Osteoarthritis Cartilage*, 2018. 26(1): p. 18-27.
50. Yazici, Y., et al., A novel Wnt pathway inhibitor, SMO4690, for the treatment of moderate to severe osteoarthritis of the knee: results of a 24-week, randomized, controlled, phase 1 study. *Osteoarthritis Cartilage*, 2017. 25(10): p. 1598-1606.
51. Yazici, Y., et al., Lorecivivint, a Novel Intraarticular CDC-like Kinase 2 and Dual-Specificity

Tyrosine Phosphorylation-Regulated Kinase 1A Inhibitor and Wnt Pathway Modulator for the Treatment of Knee Osteoarthritis: A Phase II Randomized Trial. *Arthritis Rheumatol*, 2020. 72(10): p. 1694-1706.

52. Dolgos, H., et al., Translational Medicine Guide transforms drug development processes: the recent Merck experience. *Drug Discov Today*, 2016. 21(3): p. 517-26.

53. Arden, N., et al., Can We Identify Patients with High Risk of Osteoarthritis Progression Who Will Respond to Treatment? A Focus on Biomarkers and Frailty. *Drugs Aging*, 2015. 32(7): p. 525-35.

54. Cooper, C., et al., How to define responders in osteoarthritis. *Curr Med Res Opin*, 2013. 29(6): p. 719-29.

55. He, Y., et al., Potential diagnostic value of a type X collagen neo-epitope biomarker for knee osteoarthritis. *Osteoarthritis Cartilage*, 2019. 27(4): p. 611-620.

56. Plenge, R.M., Disciplined approach to drug discovery and early development. *Sci Transl Med*, 2016. 8(349): p. 349ps15.

57. Heatherington, A.C., S. Kasichayanula, and K. Venkatakrishnan, How Well Are We Applying Quantitative Methods to Reverse Translation to Inform Early Clinical Development? *Clin Pharmacol Ther*, 2018. 103(2): p. 174-176.

58. Loeser, R.F., et al., Osteoarthritis: a disease of the joint as an organ. *Arthritis Rheum*, 2012. 64(6): p. 1697-707.

59. Kijowski, R., et al., Osteoarthritis year in review 2019: imaging. *Osteoarthritis Cartilage*, 2020. 28(3): p. 285-295.

60. Mahmoudian, A., et al., Early-stage symptomatic osteoarthritis of the knee - time for action. *Nat Rev Rheumatol*, 2021. 17(10): p. 621-632.

61. Convill, J.G., et al., Clinically Relevant Molecular Biomarkers for Use in Human Knee Osteoarthritis: A Systematic Review. *Cartilage*, 2021. 13(1_suppl): p. 1511S-1531S.

Chapter 8

Summary

Summary

Osteoarthritis (OA) is a disabling disease of the locomotor system that has no available cure. It has been identified as a serious disease determining morbidity, affecting more than 300 million people worldwide. OA is characterized by articular joint degeneration, where inflammation and loss of cartilage play an important role. In osteoarthritis, the cartilage cells, called chondrocytes, change their phenotype leading to cartilage damage. Factors secreted by inflammatory cells residing in the joint microenvironment, mainly macrophages, promote inflammation and further accelerate disease progression. Therefore, to develop an effective pharmacological treatment, we need to intervene in these key processes early in the disease, targeting chondrocyte phenotypical changes (hypertrophy) and inflammation. In this thesis I aimed to identify pharmacological targets for OA, targeting chondrocyte hypertrophy and inflammation.

Chondrocyte hypertrophy triggers the degradation of the cartilage extracellular matrix. However, whether the inflammatory microenvironment in the joint influences hypertrophic differentiation of human articular chondrocytes is not clear. Therefore, in Chapter 2 we evaluated how inflammatory signaling cues modulate chondrocyte hypertrophy. Using cartilage explants and articular chondrocytes from human patients undergoing total knee replacement, we used 3D *in vitro* culture models to study the capacity of inflammatory cytokines and different macrophage subsets to stimulate hypertrophy. We found that inflammatory signaling activation is not involved in hypertrophic differentiation of human articular chondrocytes. However, macrophages with a tissue repair phenotype are able to trigger this detrimental phenotype in human osteoarthritic cartilage. Therefore, targeting the inflammatory microenvironment in the joint might lead to decrease chondrocyte hypertrophy. Corticosteroids are potent anti-inflammatory drugs currently used in clinical practice to relieve pain in OA patients, and therefore interesting candidates. However, how these drugs modulate inflammation and chondrocyte hypertrophy is controversial. In Chapter 3 we investigated how intra-articular injection of the corticosteroid Triamcinolone Acetonide (TAA) modulates inflammation and pathological endochondral ossification during OA progression in a mouse model of OA. Unexpectedly, we found that the intra-articular injection of TAA sustained synovial macrophages in the joint with a pro-inflammatory phenotype, also leading to exacerbated osteophyte formation. Osteophytes are ectopic bone formations generated via a process called endochondral ossification, where chondrocyte hypertrophy is a major driver. These results are in accordance with our previous results linking inflammation with hypertrophy. Considering the broad mechanism of action of corticosteroids, a more targeted therapy should be developed to attenuate inflammation and chondrocyte hypertrophy in the context of OA. Therefore, we then focus on the discovery of novel pharmacological targets that could target inflammation and chondrocyte hypertrophy. In Chapter 4, we develop a computational model of articular chondrocyte phenotype, that enables the high throughput testing of promising drug targets. By using this signal transduction network model, we

identified a synergistic effect between the Protein Kinase A and the Fibroblast Growth Factor Receptor 1, which was confirmed to attenuate hypertrophy also *in vitro*. In chapter 5, we identified EPHA2 as a main regulator of inflammation and chondrocyte hypertrophy in OA, using transcriptomic datasets. We then tested the capacity of EPHA2 to modulate chondrocyte hypertrophy and inflammation in the *in silico* chondrocyte developed in chapter 4, confirming these effects. Pharmacological inhibition of EPHA2 decreased hypertrophic differentiation of mesenchymal stromal cells and articular chondrocytes, as well as TNF α -induced catabolism *in vitro*. In a mouse model of OA, EPHA2 inhibition attenuated joint degeneration by decreasing synovitis and pathological endochondral ossification. Therefore, EPHA2 inhibition is a promising drug target for OA. In chapter 6, we reviewed whether other members of the tyrosine kinase family modulate chondrocyte hypertrophy. Here we described how 9 tyrosine kinases orchestrate chondrocyte hypertrophy. Interestingly, these enzymes play a role in signaling cascades activated by inflammatory stimuli, hence, enhancing joint degeneration. Thus, tyrosine kinases might orchestrate OA pathology, being promising targets to halt disease progression.

In conclusion, in this thesis I have generated knowledge on how articular chondrocyte hypertrophy is regulated by the inflammatory microenvironment in the joint. We have boosted the discovery of new pharmacological treatments by making use of computational models, patient-derived cell models and *in vivo* disease models, identifying a new drug target for OA. The results described on this thesis refine a drug discovery pipeline which I expect will pave the path for effective treatments for osteoarthritis.

Chapter 9

Appendices

Nederlandse samenvatting

PhD portfolio

List of publications

Curriculum Vitae

Acknowledgements

Nederlandse samenvatting

Artrose is een aandoening van het bewegingsapparaat die pijn en bewegingsbeperking geeft. Deze ernstige ziekte treft wereldwijd meer dan 300 miljoen mensen. Artrose wordt gekenmerkt door gewrichtsdegeneratie, waarbij verlies van het kraakbeen en ontsteking een belangrijke rol spelen. Bij artrose verandert het gedrag van de kraakbeencellen, chondrocyten genaamd, wat leidt tot kraakbeenschade. Verder scheiden ontstekingscellen, voornamelijk macrofagen die zich in de gewrichtsmicro-omgeving bevinden, factoren uit die ontsteking bevorderen en het ziekteproces verder versnellen. Om een effectieve farmacologische behandeling voor deze ziekte te ontwikkelen, moeten we vroegtijdig ingrijpen in de bovengenoemde processen. In dit proefschrift zocht ik naar manieren om artrose farmacologisch te behandelen, gericht op het remmen van fenotypische veranderingen (hypertrofie) van kraakbeencellen en ontsteking. Kraakbeencelhypertrofiespeelt een rol in de afbraak van het kraakbeen. Het is echter niet duidelijk of de ontstoken micro-omgeving in het gewricht de ontwikkeling van hypertrofie in menselijke gewrichtskraakbeencellen beïnvloedt. Daarom hebben we dit in Hoofdstuk 2 geëvalueerd met behulp van stukjes gewrichtskraakbeen van patiënten die een operatie ondergingen waarbij de knie met artrose werd vervangen door een prothese. De stukjes kraakbeen of de cellen die we daaruit geïsoleerd hadden, gebruikten we als 3D kweekmodellen in het laboratorium om het vermogen te bestuderen van ontstekingscellen en verschillende typen macrofagen om hypertrofie te stimuleren. We ontdekten dat activering van ontstekings-signalering niet betrokken is bij de ontwikkeling van hypertrofe gewrichtskraakbeencellen. Macrofagen met een weefselherstelfenotype zijn echter wel in staat om dit schadelijke fenotype in artrotisch kraakbeen te activeren. Daarom kan een behandeling gericht op deze ontstekingscellen in het gewricht, leiden tot een afname van de hypertrofie van kraakbeencellen. Corticosteroiden zijn krachtige ontstekingsremmende geneesmiddelen die momenteel in de klinische praktijk worden gebruikt om pijn bij artrosepatiënten te verlichten. Hoe deze medicijnen ontstekingen en hypertrofie van kraakbeencellen beïnvloeden, is echter controversieel. In Hoofdstuk 3 hebben we onderzocht hoe een injectie in het gewricht met het corticosteroid Triamcinolon Acetonide (TAA) artrose beïnvloedt in een muizenmodel. Onverwacht vonden we dat de injectie met TAA ervoor zorgde dat synoviale macrofagen in het gewricht langer een pro-ontstekingsfenotype hielden. Bovendien was er meer botvorming aan de randen van het gewricht, de zogenaamde osteofyten die worden gegenereerd via hypertrofe kraakbeencellen in een proces dat endochondrale verbening wordt genoemd. Deze resultaten uit Hoofdstuk 2 en 3, koppelen ontsteking aan hypertrofie van kraakbeencellen. Gezien het brede mechanisme van corticosteroiden, moet een meer gerichte therapie worden ontwikkeld om ontsteking en kraakbeencelhypertrofie in artrose te verminderen. Daarom hebben we in Hoofdstuk 4 een computermodel ontwikkeld van een gewrichtskraakbeencel tijdens hypertrofie, waarmee het mogelijk is om sneller veelbelovende strategieën voor medicijnontwikkeling te identificeren. Door dit “signaaltransductienetwerkmodel” van de kraakbeencel te gebruiken, identificeerden we een synergetisch effect tussen de Protein Kinase A en de Fibroblast

Growth Factor Receptor 1, en experimenten in het laboratorium konden dat bevestigen. In Hoofdstuk 5 hebben we de receptor EPHA2 geïdentificeerd als een belangrijke regulator van zowel ontsteking als hypertrofie van kraakbeencellen bij artrose, door combinatie van een aantal bestaande genexpressie datasets. Vervolgens hebben we met het computermodel van de kraakbeencel dat we ontwikkeld hebben in Hoofdstuk 4, het vermogen van EPHA2 om hypertrofie en ontsteking te beïnvloeden bevestigd. In het laboratorium toonden we vervolgens aan dat farmacologische remming van EPHA2 ontsteking, kraakbeencelhypertrofie en osteofytvorming kan verminderen in celkweken en in muizen met artrose. Daarom is EPHA2-remming een veelbelovende kandidaat voor het ontwikkelen van een behandeling voor artrose. In Hoofdstuk 6 hebben we in de literatuur gezocht of naast EPHA2 ook andere leden van de tyrosinekinasefamilie hypertrofie van kraakbeencellen beïnvloeden. Hier hebben we van 9 tyrosinekinasen beschreven hoe deze enzymen een rol spelen bij het signaleren van cascades die worden geactiveerd door ontsteking, waardoor de gewrichtsdegeneratie wordt versterkt. Dus tyrosinekinasen kunnen artrose orkestreren, en zijn veelbelovende doelen voor geneesmiddelen om ziekteprogressie te stoppen.

Concluderend heb ik in dit proefschrift kennis gegeneerd over hoe hypertrofie van de gewrichtskraakbeencel wordt gereguleerd door de ontsteking in de micro-omgeving in het gewricht. Door gebruik te maken van computermodellen, van laboratoriummodellen met weefsels en cellen van patiënten en dierexperimentele ziektemodellen, hebben we een nieuw aangrijppunt voor een farmacologische behandeling voor artrose geïdentificeerd. De aanpak die in dit proefschrift wordt beschreven, is een verfijning van het pad voor het ontdekken van geneesmiddelen waarvan ik verwacht dat het uiteindelijk zal leiden tot een effectieve behandelingen van artrose.

PhD portfolio

Year	Courses/Workshop	Workload (ECTS)
2017	Biomedical research techniques	1.5
2017	Monocytes: origins, destinations, functions and diagnostic targets	0.2
2018	Scientific Integrity	0.3
2019	FELASA C. Laboratory animal science.	4.0
2021	Gene expression data analysis using R	2.0

Year	Conferences	Workload (ECTS)
2018	NVMB conference. Poster presentation	1.0
2019	Molecular Medicine Day. Poster presentation	0.5
2019	NVMB conference. Oral presentation	1.0
2021	OARSI conference. Poster presentation	1.0

Year	Department and Consortium Meetings	Workload (ECTS)
2017-2022	Research department meetings (weekly) Orthopaedics	2.0
2017-2022	Research department meetings Internal medicine, Oral and Maxillofacial Surgery and Orthopaedics	2.0
2017-2022	Orthopaedics science day (annually)	1.0
2018-2021	CARBON consortium meetings (biannually)	2.0

Year	Internships	Workload (ECTS)
2019	Visiting PhD student at Maastricht university medical centre	5.0
2019	Visiting PhD student at KU Leuven	5.0

Year	Student supervision	Workload (ECTS)
2019	Supervision master student Erasmus – China Internship (Samson Chen)	0.5
2020	Supervision MolMed master student Literautre Review course (Heura Domenech Garcia)	0.5
2020	Supervision MolMed master student thesis (Fjodor Bekedam)	2.0
2021	Supervision master student Erasmus – Greece Internship (Athina Chavli)	0.5

Total ECTS: 32

List of publications

Ferrao Blanco MN, Bastiaansen-Jenniskens YM, Chambers MG, Pitsillides AA, Narcisi R, van Osch GJVM. Effect of Inflammatory Signaling on Human Articular Chondrocyte Hypertrophy: Potential Involvement of Tissue Repair Macrophages. *Cartilage*. 2021 Dec;13(2_suppl):168S-174S. doi: 10.1177/19476035211021907. Epub 2021 Jun 24. PMID: 34165367.

Ferrao Blanco MN, Domenech Garcia H, Legeai-Mallet L, van Osch GJVM. Tyrosine kinases regulate chondrocyte hypertrophy: promising drug targets for Osteoarthritis. *Osteoarthritis Cartilage*. 2021 Oct;29(10):1389-1398. doi: 10.1016/j.joca.2021.07.003. Epub 2021 Jul 17. PMID: 34284112.

Ferrao Blanco MN, Bastiaansen Jenniskens YM, Kops N, Chavli A, Narcisi R, Botter SM, Leenen PJM, van Osch GJVM, Fahy N. Intra-articular injection of triamcinolone acetonide sustains macrophage levels and aggravates osteophytosis during degenerative joint disease in mice. *Br J Pharmacol*. 2022 Jun;179(11):2771-2784. doi: 10.1111/bph.15780. Epub 2022 Jan 26. PMID: 34907535.

Ferrao Blanco MN, Lesage R, Kops N, et al. Pharmacologic inhibition of EPHA2 decreases inflammation and pathological endochondral ossification in osteoarthritis. *bioRxiv*; 2022. DOI: 10.1101/2022.06.12.495737.

Lesage R, **Ferrao Blanco MN**, Narcisi R, et al. An integrated in silico - in vitro approach for identification of therapeutic drug targets for osteoarthritis. *bioRxiv*; 2021. DOI: 10.1101/2021.09.27.461207.

Curriculum Vitae

Mauricio Nicolás Ferrao Blanco was born on 22nd September 1990 in Salto, Uruguay. At the age of 15, he enrolled to the Chemistry Olympiad and won the gold medal in his state and in the national competition. He travelled to Costa Rica to represent his country in the Iberoamerican Chemistry Olympiad where he won the bronze medal. At the age of 17, he won a fellowship from the Department of State of the United States which allowed him to visit Washington D.C. and Minnesota. He studied Pharmaceutical Chemistry at the Universidad de la República in Montevideo, Uruguay. During his studies, he was awarded a fellowship to study for a semester in the Universidade Estadual de Campinas in São Paulo, Brazil. After culminating his studies, he worked in the Technological Laboratory of Uruguay and subsequently, in the Research & Development Department of Eurofarma, a pharmaceutical company in Montevideo. In 2016, he was awarded a fellowship to study a Master in Biomedicine in the Universidad de Córdoba, Spain. He pursued his PhD studies in the lab of Professor Gerjo van Osch in the Department of Orthopedics and Sports Medicine at Erasmus Medical Center, the Netherlands. Subsequently, he worked as a postdoctoral researcher in the same lab on a project in collaboration with the pharmaceutical company Galapagos. Since May 2022, Mauricio is enrolled as a postdoctoral researcher in the Princess Máxima Centrum in Utrecht. Mauricio's research interests lie in understanding the communication network of stromal cells and their progeny with the microenvironment, to boost the discovery of pharmacological treatments.

Acknowledgements

Often times in life it is extremely easy to forget about all the people that have supported you and pushed you to better yourself. This is my letter of gratitude to each and every single person that has supported me along the way during this journey. To my friends and family, co-workers and teachers for all the support they have brought into my life. People present in my life or from the past, or even people that I do not remember their names. Thank you. For the education that I was fortunate to receive, the opportunities that I have had, to the places I have travelled. Thank you. For the challenges I have faced, that have brought me to this moment in time and have nourished the resilience inside of me. Thank you.

To the persons that gave me the possibility to start the PhD journey. Prof. dr. Gerjo van Osch and Dr. Yvonne Bastiaansen-Jenniskens, thanks for believing in me since the beginning. Gerjo, your passion and determination are admirable. I feel enormously grateful to have learnt from one of the best researchers and teachers. Yvonne, your trust and support has stimulated me to grow. You transmit joy and a 'alles komt goed' feeling that made our meetings the best ever. Life changes, and so was my PhD journey. Thanks Dr. Roberto Narcisi for your scientific input.

To all the lab members and interns with whom I have shared moments in these years, thank you all. Nicole, you're the best technician ever. Thanks for all the beautiful histological images you generated, your help with the *in vivo*'s and your gezelligheid. I loved working with you. Wendy and Janneke, thanks for your kind assistance every time I needed you. Sandra, thanks for your help with the forms and documentation. Thanks to Andrea, Niamh, Kavitha, Sohrab, Pedro, Shorouk, Tim, Encheng, Jietao, Lizette, Amaia, Chantal, Virginia, Enrique and Yannick for all the lab meetings, lab days and drinks. Thanks Niamh for the great talks during the buffy coat afternoons, those days working in the ML2 listening to Britney and singing along were fabulous. Yannick, my best german friend! I have great memories with you. Eric, it was a pleasure to work with you, I value the insights and guidance you provide.

To the CarBon consortium members. I'm grateful that I could join the team as the number 13 early-stage researcher in this extraordinary Marie Slodowska-Curie ITN. Traveling around Europe to discuss science and enjoy the company of you was amazing, Cansu, Claudio, Dionysia, Enrique, Farhad, Kathi, Martina, Mengjie, Nicolás, Raphaëlle, Satanik, Soraia and Yannick. Raphaëlle, what nice adventures we have experienced together! We have shared many fun moments in the lab with Benoit in Rotterdam, Maastricht and Leuven. Thanks to all principal investigators for their contributions in our meetings and for stimulating young researchers in their careers. A special acknowledge to Prof. dr. Liesbet Geris and Prof. dr. Andrew Pitsillides, two great mentors and source of inspiration.

To my master students, one of the best part of this PhD was to work together with you. Athina, you're one of the sweetest person I met, a Greek goddess. Fjodor thanks for reminding me that 'ik een beetje apart ben'. Heura, it was fun working with you. Judith, with you I have learnt not only science but also Dutch.

Thanks to all co-authors Prof. dr. Liesbet Geris, Prof. dr. Andrew Pitsillides, Dr. Mark .G. Chambers, Dr. Yvonne .M. Bastiaansen-Jenniskens, Dr. Roberto Narcisi, Prof. dr. Gerjo .J.V.M. van Osch, Nicole Kops, Athina Chavli, Dr. Sander M. Botter, Dr. Pieter J.M. Leenen, Dr. Niamh Fahy, Dr. Raphaëlle Lesage, Prof. dr. Tim Welting, Fjodor T. Bekedam, Heura Domenech Garcia, Prof. dr. Laurence Legeai-Mallet. I would also like to acknowledge the members of the animal facility in Erasmus MC for the assistance in the experiments.

To the members of the Orthopedics and Sports Medicine department, thanks for collecting the patient tissues that were so useful for our research. Prof. dr. Sita Bierma-Zeinstra and Dr. Koen Bos, thanks for your input and interest in my research every time I presented my work.

To the members of the committee, Prof. dr. R.W. Hendriks, Prof. dr. P.M. van der Kraan, Dr. J.N. Post, Prof. dr. R.J.E.M. Dolhain and Dr. K. Sivasubramaniyan thanks for accepting the invitation and taking the time for my dissertation.

To my beautiful paranympths, Chantal and Virginia. The perfect combination of personalities to have the best friends at work. Chanti, you are amazing! You have helped me to see things in a completely different perspective and you are one of the reasons why I feel at home in the Netherlands. Virginia, your passionate heart nourishes me every time we are together. I could not imagine these years in the Erasmus MC without you. Thanks for being there every time I needed you.

Al café español, Enrique, Virginia, Ana. Thanks for bringing a piece of Spain to the Netherlands. I really enjoyed our eternal lunch breaks and the paellas, salmorejos, jamón and quesos we ate in house parties.

And back to where this all began. A mis padres, mi hinchas favoritos, los que siempre han creído en mi y me han dado alas para salir tras mis sueños. Ma, gracias por tus lecciones de vida y amor incondicional que me han servido de guia para hacer mi camino. Pa, gracias por enseñarme a luchar por lo que quiero y no bajar los brazos. Tita, gracias por ser siempre una fuente de amor, mi segunda madre. Marce, gracias por siempre estar. A mis sobrinas, Renata y Naiara, gracias por todas las sonrisas. Vale, Ana, Tia Zulma, Tio Carlos, Tio Galli, Tia Angellita, Negrita, Abuela Celica y Abuela Claudelina, mismo a la distancia, se que siempre están a mi lado. Marisel, Mariela, Tío Beto y Tía Teresa gracias por la alegría y los hermosos momentos en Artigas y Montevideo.

A mis amigos en Uruguay, mis hermanos del corazón, en Salto y en Montevideo. En especial, Lucy, Ana, Luciana, Maika, Shelley, Flor, Gaby, Dani siempre las recuerdo. Luba, Anita, Carla, Vittoria, Maria Victoria, Vale, Flor, Estefa, Vania gracias por las videollamadas y siempre hacerme reír. Tero, mil recuerdos juntos. A toda/os los amo.

Vervolgens wil ik graag mijn vrienden hier in Nederland bedanken. Lieve Marcella, je bent één van de mooiste cadeautjes die ik in dit land heb gekregen. Chanti, Yannick, Virginia, Athina, Nikkie, ik vind het zo fijn dat wij zo een mooie vriendschap hebben opgebouwd.

Lieve Thijs, met jou voel ik mij altijd in evenwicht. Jij bent mijn soulmate, ik hou zo veel van jou. Verder wil ik graag de familie Nell – Koopmanschap bedanken voor hun steun en gezelligheid.

To the practice of yoga and all the fabulous instructors. Thanks for helping me to live a life true to myself.

Soy porque somos, I am because we are, Ik ben omdat wij zijn.

Gracias. Thank you. Merci. Bedankt. Obrigado

